PROCEEDINGS
of the

Eleventh
International Tissue Elasticity Conference™

Deauville, Normandy, France
October 2 – 5, 2012

PROCEEDINGS

of the

Eleventh International Tissue Elasticity ConferenceTM

Deauville, Normandy, France
October 2–5, 2012

Table of Contents

Welcome

Dear Conference Delegate:

Welcome to the 11th ITEC Conference and, in particular, to the beautiful city of Deauville, Normandy, France. We are very glad that ITEC's choice fell on France, but at the same time we are sad that Jonathan and Karen will not be able to attend this year. However, with the aid of Skype they will, nonetheless, be able to attend selective Conference events – which deprives them hence of only ½ of a Conference Attendee point ☺. [Editor's Note: We'll see about that!]

We started planning this Conference back in 2007 at Santa Fe. Organizing a Conference was a first for me, and I would like to thank Karen and Jonathan for their expertise, guidance and constant help; our local organizing committee, consisting of Sabrina Doblas, Philippe Garteiser and Simon Chatelin deserve much credit for their untiring efforts. With such a great team, it is truly a pleasure to prepare and organize such an event. I would likewise to acknowledge the tremendous contributions of INSERM (Ms. Margot Sauvadet) and our 3rd year volunteer, Ms. Charlene Waldron from Seattle, Washington, USA.

This year we have the distinct pleasure to welcome John Waterton from AstraZeneca (UK) and Jens Würfel from the Universities of Göttingen, Lübeck and Berlin (Germany) as plenary speakers. The intention, which motivated us for this particular constellation, was to provide new perspectives and challenges to the elasticity imaging community: Does the pharmaceutical industry see a place for elasticity imaging in their armament of imaging biomarkers, and does elasticity imaging provide new potentials in the neuro-domain when considering diseases such as MS or Alzheimer's?

The Organizing Committee hopes that you will listen to inspiring presentations and fruitful discussions during the Conference, enjoy the Riviera atmosphere of Deauville and the great hospitality of the Amirauté Hôtel, and plan to spend a memorable evening at the Normandy Hotel during our Conference dinner on Wednesday.

Ralph Sinkus
Chair of the Local Organizing Team
2 October 2012

A Personal Note:

We will regretfully not be able to participate in person in this year's Conference events due to circumstances beyond our control. We will miss meeting all the colleagues and friends again, but we trust that with Ralph's remarkable enthusiasm and Kevin's support, the Conference will be as good or better than ever.

We will be at the Registration Desk and elsewhere on Skype. Please come by and say "Hello"!

Karen and Jonathan

FOREWORD

Dear Conference Delegate:

On behalf of the US oraganizing team, welcome to the 11th annual International Tissue Elasticity Conference™!

In the 1990s we saw a remarkable development of technologies and approaches for imaging various elastic properties of tissues. In more recent years we have seen a continuation of innovative approaches, with the addition of a major step. That important step was the creation of specialized scanners for conducting clinical research on thousands of patients in some of the most highly respected medical centers around the world. In retrospect, the evolution of the field is a superb case study of translational research, developing from "bench to bedside." This Conference series has, by design, served as the place where researchers, clinicians, industry leaders and students from around the world could trade ideas and discuss the latest advances, while creating an archival record of their progress. The international participation in the Conference now includes virtually all global entities engaged in research, development, commercialization and practice in the field.

In this year's tutorial series, we are pleased that Drs. John Waterton from AstraZeneca (UK) and Jens Würfel from the Universities of Göttingen, Lübeck and Berlin (DE) agreed to present this year's exciting tutorials on potential new frontiers and opportunities for imaging the elastic properties of tissues. We are also continuing the popular format of the formal Poster Session, where each presenter has the opportunity to give a brief oral summary of his/her poster, and we thank Drs. Rémi Souchon, (FR) and Michael Richards (US) for their enthusiastic leadership in conducting this event.

We continue to attract a growing number of cutting-edge clinical papers in three clinical sessions and two cardiovascular sessions. This year we have also added a new commercial session where some of the corporate leaders in the field have been invited to present their various technological approaches.

The Student Best Paper Presentations and Awards session continues to be most popular. This year, the Conference is funding the Student Best Paper certificates and cash awards to the authors of papers that have been judged as most meritorious through independent review cycles. On Tuesday afternoon, we will have a special session in which the eight finalists will present their abstracts. The final awardees will be announced during Thursday's Lunch in the Pymarid.

We thank The University of Texas Medical School at Houston, Diagnostic & Interventional Imaging Department (US), which is a Gold sponsor of the Conference again this year. Additional sponsors this year are: Université Paris Diderot, Sorbonne Paris Cité, CRB3, UMR 773, INSERM as a Bronze Sponsor, CRC Press Taylor and Francis Group and Rochester Center for Biomedical Ultrasound, The University of Rochester as General Sponsors.

This year we welcome Versaonics, Inc. (US) as first time exhibitors at the Conference.

We would like to thank all the new and returning delegates, reviewers and session chairs for their continuing support of the Conference. Special thanks are in order to our enthusiastic support staff that has worked above and beyond. The local organizing committee from the Université Paris Diderot, comprising Drs. Philippe Gertesier (FR), Sabrina Doblas (FR) and Simon Chatelin (FR), and headed by Dr. Ralph Sinkus (FR), has worked for more than a year to put together this year's outstanding event, and we think you will agree that the results are superb. Ms. Karen Ophir (US) volunteered to design the Conference's artwork, publications and web site, organize the scientific program and edit all abstracts and publish the Conference Proceedings. Ms. Charlene Waldron (US) volunteered with correspondence and financial aspects of the Conference and will stand in for Karen at the registration this year; Ms. Cheryl Taylor (UK) helped with the Registration Desk and on-site organization; and Drs. Reza Zahiri Azar (CA) and Vladimir Egorov (US) as our official Conference photographer and videographer, respectively, again this year.

The Conference is conducted under the joint auspices of the University of Rochester Center for Biomedical Ultrasound and the Ultrasonics and Elastographics Laboratory in the Department of Diagnostic and Interventional Imaging at the University of Texas Health Science Center at Houston. Most direct funding for the Conference is derived from registration fees, and, with your continued support in abstract submissions and attendance, we are committed to improve and expand the Conference in the years to come. We appreciate your written and oral feedback that always helps us in planning for future Conferences.

We hope that you will enjoy this year's scientific and social programs as well as Deauville's unique venue and hospitality. We hope to see you again at the 12th ITEC next year!

J. Ophir and K.J. Parker, Conference Organizers
Deauville, Normandy, France
October 2nd, 2012

CONFERENCE–AT–A–GLANCE

Eleventh International Tissue Elasticity Conference™

The Amirauté Hôtel – Deauville, Normandy, France October 2–5, 2012

Tuesday, October 2		**9:00A – 8:00P**	
9:00A – 12:00P	**Set Up:**	Oral Presenters load presentations (CD or jump drive)	Marco Polo
		Poster Presenters set up presentations	Bar de l'Amphithéâtre
		Exhibitors set up exhibits	Bar de l'Amphithéâtre
9:00A – 8:00P		Registration Desk Open	Bar de l'Amphithéâtre
11:00A – 8:00P	**Session EEX:**	Equipment Exhibit *(during breaks & Reception)*	Bar de l'Amphithéâtre
12:00P – 2:00P	**Session TUT:**	**Tutorials**	Marco Polo
2:00P – 2:30P		*Coffee Break*	Bar de l'Amphithéâtre
2:30P – 4:30P	**Session SAS:**	**Oral Presentations of Finalists for Student Awards Session**	Marco Polo
4:30P – 5:00P		*Recess*	
5:00P – 6:00P	**Session POS:**	**Poster Session – Live Oral Summaries**	Bar de l'Amphithéâtre
6:00P – 8:00P		*Opening Reception*	Bar de l'Amphithéâtre
Wednesday, October 3		**8:00A – 11:30P**	
8:00A – 5:30P		Registration Desk Open	Bar de l'Amphithéâtre
8:00A – 5:30P	**Session POS:**	Posters	Bar de l'Amphithéâtre
8:00A – 5:30P	**Session EEX:**	Equipment Exhibit	Bar de l'Amphithéâtre
7:45A – 8:00A		Opening Remarks	Marco Polo
8:00A – 10:00A	**Session CAA-1:**	**Clinical and Animal Applications – I**	Marco Polo
10:00A – 10:30A		*Coffee Break*	Bar de l'Amphithéâtre
10:30A – 12:00P	**Session MIP–1:**	**Methods for Imaging Elastic Tissue Properties – I**	Marco Polo
12:00P – 1:30P		*Group Lunch*	The Pyramid
1:30P – 2:45P	**Session FIP:**	**Forward and Inverse Problems**	Marco Polo
2:45P – 4:00P	**Session CVE–1:**	**Cardiovascular Elasticity – I**	Marco Polo
4:00P – 4:30P		*Coffee Break*	Bar de l'Amphithéâtre
4:30P – 5:45P	**Session MPT–1:**	**Mechanical Properties of Tissues – I**	Marco Polo
5:45P – 6:15P		*Wine Bar & ITEC Cup Distribution*	Bar de l'Amphithéâtre
7:00P – 8:00P		Buses to the Hôtel Normandy Barrière	TBA
8:00P – 11:00P		*Conference Dinner*	La Belle Epoque / Hôtel Normandy Barrière
10:30P – 11:30P		Buses to the Amirauté Hôtel	TBA
Thursday, October 4		**8:00A – 7:15P**	
8:00A – 5:30P		Registration Desk Open	Bar de l'Amphithéâtre
8:00A – 5:30P	**Session POS:**	Posters	Bar de l'Amphithéâtre
8:00A – 5:30P	**Session EEX:**	Equipment Exhibit	Bar de l'Amphithéâtre
8:00A – 10:00A	**Session IND:**	**Industrial Presentations**	Marco Polo
10:00A – 10:30A		*Coffee Break*	Bar de l'Amphithéâtre
10:30A – 12:00P	**Session MIP–2:**	**Methods for Imaging Elastic Tissue Properties – II**	Marco Polo
12:00P – 2:00P		*Group Lunch*	The Pyramid
		ITEC Announcements *inclg* ***Student Best Paper Award Recipients***	
2:00P – 4:15P	**Session CAA–2:**	**Clinical and Animal Applications – II**	Marco Polo
4:15P – 4:45P		*Coffee Break*	Bar de l'Amphithéâtre
4:45P – 5:45P	**Session MPT–2:**	**Mechanical Properties of Tissues – II**	Marco Polo
5:45P – 6:45P		*Group Photo*	TBA
6:45P – 7:15P		*Wine Bar*	Bar de l'Amphithéâtre
Friday, October 5		**8:00A – 10:00P**	
8:00A – 4:15P		Registration Desk Open	Bar de l'Amphithéâtre
8:00A – 4:15P	**Session POS:**	Posters	Bar de l'Amphithéâtre
8:00A – 4:15P	**Session EEX:**	Equipment Exhibit	Bar de l'Amphithéâtre
8:00A – 10:00A	**Session SIP:**	**Signal and Image Processing**	Marco Polo
10:00A – 10:30A		*Coffee Break*	Bar de l'Amphithéâtre
10:30A – 12:00P	**Session MIP–3:**	**Methods for Imaging Elastic Tissue Properties – III**	Marco Polo
12:00P – 1:30P		*Group Lunch*	The Pyramid
1:30P – 3:00P	**Session CVE–2:**	**Cardiovascular Elasticity – II**	Marco Polo
3:00P – 3:45P	**Session CAA–3:**	**Clinical and Animal Applications – III**	Marco Polo
3:45P – 4:15P		*Coffee Break*	Bar de l'Amphithéâtre
4:15P – 5:30P	**Session MMT:**	**Mechanical Measurement Techniques for Tissues**	Marco Polo
5:30P – 6:00P		*Wine Bar*	Bar de l'Amphithéâtre
7:30P – 10:00P		*Crêpe Dinner Closing Reception (Proceedings Book Signing)*	The Pyramid

PROGRAM

Eleventh International Tissue Elasticity ConferenceTM

Deauville, Normandy, France
October 2 – 5, 2012

Tuesday, October 2 9:00A – 8:00P

9:00A – 12:00P Presentation & Exhibit Set Up

All Oral Presenters load presentations onto Conference computers — Marco Polo
Poster Presenters set up presentations — Bar de l'Amphithéâtre
Exhibitors set up exhibits — Bar de l'Amphithéâtre

9:00A – 8:00P

Registration Desk Open — Bar de l'Amphithéâtre

11:00A – 12:00P 2:00P – 2:30P 4:30P – 5:00P 6:00P – 8:00P
Session EEX: Equipment Exhibit — Bar de l'Amphithéâtre

Tuesday 12:00P – 2:00P
Session TUT: Tutorials: New Perspectives and Challenges to the Elasticity Imaging Community

Chair: R Sinkus, France *Co-Chair: TJ Hall, USA* Marco Polo

Page No.

12:00P – 12:45P

095 HOW AN INGENIOUS BIOPHYSICAL MEASUREMENT BECOMES A DECISION–MAKING BIOMARKER: THE ARDUOUS JOURNEY FROM IDEA TO IMPACT. 24
JC Waterton[1,2].*
[1]AstraZeneca, Macclesfield, Cheshire, England, UK; [2]University of Manchester, Manchester, England, UK.

12:45P – 1:00P Discussion

1:00P – 1:45P

096 MIND SHAKING – A NEUROLOGIST'S PERSPECTIVE ON CEREBRAL MAGNETIC RESONANCE ELASTOGRAPHY. 25
J Würfel[1].*
[1]University Medicine Goettingen, Goettingen, GERMANY.

1:45P – 2:00P Discussion

2:00P – 2:30P

COFFEE BREAK — Bar de l'Amphithéâtre

Tuesday 2:30P – 4:30P
Session SAS: Oral Presentations of Finalists for Student Awards Session

Chair: JF Greenleaf, USA *Co-Chair: E Brusseau, France* Marco Polo

Page No.

2:30P – 2:45P

011 ELECTROMECHANICAL WAVE IMAGING OF BIOLOGICAL AND ELECTRONIC PACEMAKERS IN CONSCIOUS DOGS *IN VIVO.* 26
A Costet[1] J Provost[1], A Gambhir[1], Y Bobkov[1], G Boink[1], P Danilo[1], M Rosen[1], EE Konofagou[1].*
[1]Columbia University, New York, NY, USA.

(Session SAS continues on next page)

(Session SAS continued from previous page)

2:45P – 3:00P

021 A NOVEL TECHNIQUE OF DETECTING MAGNETIC RESONANCE IMAGING (MRI)–NEGATIVE EPILEPTOGENIC LESIONS IN FOCAL SYMPTOMATIC EPILEPSY: A CASE REPORT USING INTRAOPERATIVE SHEAR WAVE ELASTOGRAPHY. 27

HW Chan[1,3], A Chakraborty[2], CE Uff[1], NL Dorward[1], JC Bamber[3], W Harkness[2].*
[1]Royal Free Hospital, London, England, UK; [2]Great Ormond Street Hospital, London, England, UK; [3]Institute of Cancer Research and Royal Marsden Hospital, Sutton, Surrey, England, UK.

3:00P – 3:15P

036 3D RECONSTRUCTION OF *IN VIVO* ARFI AND SWEI IMAGES OF THE PROSTATE. 28

S Rosenzweig[1], ML Palmeri[1], T Polascik[2], KR Nightingale[1].*
[1]Duke University, Durham, NC, USA; [2]Duke University Medical Center, Durham, NC, USA.

3:15P – 3:30P

046 ASSESSMENT OF THERAPY–INDUCED TUMOUR NECROSIS WITH MAGNETIC RESONANCE ELASTOGRAPHY. 29

J Li[1], Y Jamin[1], C Cummings[1], JC Waterton[2], J Ulloa[2], R Sinkus[3], JC Bamber[1], SP Robinson[1].*
[1]The Institute of Cancer Research and Royal Marsden NHS Trust, Sutton, Surrey, England, UK; [2]AstraZeneca, Macclesfield, Cheshire, England, UK; [3]Centre de Recherche Biomedicale Bichat–Beaujon, Clichy, FRANCE.

3:30P – 3:45P

057 THE ACCUMULATION OF DISPLACEMENT ESTIMATION ERROR OVER LARGE DEFORMATIONS. 30

MA Bayer[1], TJ Hall[1].*
[1]University of Wisconsin–Madison, Madison, WI, USA.

3:45P – 4:00P

067 MULTI–PARAMETRIC MONITORING OF VISCOELASTIC PROPERTY CHANGES DURING HIFU TREATMENT USING HMIFU *EX VIVO*. 31

GY Hou[1], D Shahmirzadi[1], F Marquet[1], EE Konofagou[1].*
[1]Columbia University, New York, NY, USA.

4:00P – 4:15P

080 SHEAR MODULUS RECONSTRUCTION WITHOUT HOMOGENEITY ASSUMPTIONS: A NEW CURL–BASED FINITE ELEMENT FORMULATION. 32

M Honarvar[1], RS Sahebjavaher[1], R Rohling[1], SE Salcudean[1], R Sinkus[2].*
[1]University of British Columbia, Vancouver, CANADA; [2]INSERM UMR 773, Paris, FRANCE.

4:15P – 4:30P

083 IMAGING THE MECHANICAL PROPERTIES OF CELLS. 33

DT Seidl[1], E Canović[1], AA Oberai[2], PE Barbone[1], D Stamenović[1], ML Smith[1].*
[1]Boston University, Boston, MA, USA; [2]Rensselaer Polytechnic Institute, Troy, NY, USA.

4:30P – 5:00P

Recess

Tuesday 5:00P – 6:00P

(Posters will be available for viewing and Coffee Break Discussion through the afternoon Coffee Break, Friday, October 5)

Session POS: Poster Session – Live Oral Summaries

Chair: R Souchon, France *Co-Chair: MS Richards, USA* Bar de l'Amphithéâtre

5:00P – 5:02P

001 MEASURING STRAIN USING THE INVERSE SQUARE RELATION OF RADIATION INTENSITY AND DISTANCE. 34

T Alrefae[1].*
[1]Kuwait University, Khaldia, KUWAIT.

5:02P – 5:04P

5:04P – 5:06P

5:06P – 5:08P

5:08P – 5:10P

5:10P – 5:12P

5:12P – 5:14P

5:14P – 5:16P

5:16P – 6:00P **Discussion**

Tuesday 6:00P – 8:00P
Opening Reception

Bar de l'Amphithéâtre

Wednesday, October 3 8:00A – 11:30P

8:00A – 5:30P

Registration Desk Open — Bar de l'Amphithéâtre

8:00A – 5:30P **Session POS: Posters** — Bar de l'Amphithéâtre

Session EEX: Equipment Exhibit — Bar de l'Amphithéâtre

Wednesday 7:45A – 8:00A
OPENING REMARKS

KJ Parker, R Sinkus Marco Polo

Wednesday 8:00A – 10:00A
Session CAA–1: Clinical and Animal Applications – I

Chair: JM Rubin, USA *Co-Chair: DO Cosgrove, UK* Marco Polo

Page No.

8:00A – 8:30A Invited Presentation

091 EMERGING APPROACHES TO QUANTITATIVE EVALUATION OF THE CERVIX FOR PRETERM BIRTH PREDICTION. 42

H Feltovich[1,2].*

[1]Intermountain Healthcare, Provo, UT, USA; [2]University of Wisconsin–Madison, Madison, WI, USA.

8:30A – 8:45A

025 SHEARWAVE™ ELASTOGRAPHY BE1 MULTINATIONAL BREAST STUDY: ADDITIONAL SWE™ FEATURES SUPPORT POTENTIAL TO DOWNGRADE BI–RADS® 3 LESIONS. 43

FKW Schäfer[1], J Gay[2], C Cohen–Bacrie[2] and DO Cosgrove[3].*

[1]University Hospital, Kiel, GERMANY; [2] Supersonic Imagine, Aix–en–Provence, FRANCE; [3] Imperial College, London, England, UK.

8:45A – 9:00A

064 ELASTOGRAPHIC FINDINGS COMPARISON OF CANCEROUS BREAST LESIONS OBSERVED *IN VIVO*. 44

E Brusseau[1], V Detti[1], A Coulon[2], E Maissiat[2], M Devouassoux–Shisheboran[2], N Boublay[3], L Boussel[1,2], J Fromageau[4], N Bush[4], JC Bamber[4].*

[1]CREATIS, Université Lyon 1, Villeurbanne, FRANCE; [2]Hôpital de la Croix–Rousse, Lyon, FRANCE; [3]Hospices Civils de Lyon, Université Lyon 1, Lyon, FRANCE; [4]Institute of Cancer Research and Royal Marsden Hospital, Sutton, Surrey, England, UK.

9:00A – 9:15A

086 COMPARISON OF STRAIN ELASTOGRAPHY, SHEARWAVE ELASTOGRAPHY AND SHEARWAVE ELASTOGRAPHY WITH A QUALITY MEASURE IN EVALUATION OF BREAST MASSES. 45

RG Barr[1,2] – Presented by A Milkowski.*

[1]Northeastern Ohio Medical College, Rootstown, Ohio, USA; [2]Radiology Consultants Inc., Youngstown, Ohio, USA.

9:15A – 9:30A

088 TISSUE ELASTICITY AS A MARKER OF PELVIC FLOOR CONDITIONS: CLINICAL RESULTS. 46

H van Raalte[1], V Egorov[2], V Lucente[3].*

[1]Princeton Urogynecology, Princeton, NJ, USA, [2]Artann Laboratories, Trenton, NJ, USA, [3]The Institute for Female Pelvic Medicine & Reconstructive Surgery, Allentown, PA, USA.

9:30A – 9:45A

008 QUANTITATIVE SHEAR WAVE ELASTOGRAPHY OF THE PROSTATE: CORRELATION TO SEXTANT AND TARGETED BIOPSIES. 47

JM Correas[1], A Khairoune[1], AM Tissier[1], A Criton[2], V Vassiliu[1], A Méjean[3], O Hélénon[1].*

[1]Necker Hospital, Paris, FRANCE; [2]SuperSonic Imagine, Aix–en–Provence, FRANCE; [3]HEGP Hospital, Paris, FRANCE.

9:45A – 10:00A

079 REAL–TIME STRAIN IMAGING OF THE PROSTATE USING THE ABLATHERM® HIFU DEVICE. 48

L Brasset[1], R Souchon[1], S Catheline[1], JY Chapelon[1], A Gelet[2], O Rouviere[2].*

[1]INSERM (LabTAU), Lyon, FRANCE; [2]Hospices Civils de Lyon, Edouard Herriot Hospital, Lyon, FRANCE.

10:00A – 10:30A

COFFEE BREAK Bar de l'Amphithéâtre

Wednesday 10:30A – 12:00P
Session MIP–1: Methods for Imaging Elastic Tissue Properties – I

Chair: V Egorov, USA *Co-Chair: J Bercoff, France* Marco Polo

Page No.

10:30A – 10:45A

006 RHEOLOGICAL STUDY OF A POLYMER SPHERE USING A 3–D SHEAR WAVE SCATTERING MODEL IN DYNAMIC ELASTOGRAPHY. 49

E Montagnon[1,2], A Hadj–Henni[3], C Schmitt[3], G Cloutier[1,2].*

[1]Université de Montréal Hospital Research Center (CRCHUM), Montréal, Québec, CANADA; [2]Université de Montréal, Montréal, Québec, CANADA; [3]Rheolution Inc., Montréal, Québec, CANADA.

10:45A – 11:00A

015 ON THE ADVANTAGES OF IMAGING THE AXIAL–SHEAR STRAIN COMPONENT OF THE TOTAL SHEAR STRAIN IN BREAST TUMORS. 50

AK Thittai[1], B Galaz[1,2], J Ophir[1].*

[1]The University of Texas Medical School, Houston, TX, USA; [2]Universidad de Santiago de Chile (USACH), Santiago, CHILE.

11:00A – 11:15A

018 INVESTIGATING DIFFERENCES IN SHEAR WAVE SPEEDS IN MOUSE TUMORS WITH DIFFERENT COLLAGEN CONTENT. 51

V Rotemberg[1], T Jordan[1], X Cao[1], ML Palmeri[1,2], F Yuan[1], KR Nightingale[1].*

[1]Duke University, Durham, NC, USA; [2]Duke Medical Center, Durham, NC, USA.

11:15A – 11:30A

019 FULLY AUTOMATED BREAST ULTRASOUND ELASTOGRAPHY SYSTEM. 52

R Zahiri Azar[1,2], C Leung[1], T Chen[1], K Dickie[1], J Dixon[1], KK Chan[1], L Pelissier[1].*

[1]Ultrasonix Medical Corporation, Richmond, BC, CANADA. [2]University of British Columbia, Vancouver, BC, CANADA.

11:30A – 11:45A

047 *IN VIVO* MEASUREMENT OF VOLUMETRIC STRAIN FOR THE ASSESSMENT OF INTRAHEPATIC PRESSURE ALTERATIONS. 53

S Hirsch[1], TJ Kroencke[1], J Guo[1], R Reiter[1], S Papazoglou[1], I Sack[1], J Braun[1].*

[1]Charité – University Medicine Berlin, Berlin, GERMANY.

11:45A – 12:00P

048 COMPRESSION SENSITIVE MAGNETIC RESONANCE ELASTOGRAPHY. 54

S Hirsch[1], F Beyer[1], J Guo[1], S Papazoglou[1], H Tzschätzsch[1], A Fehlner[1], I Sack[1], J Braun[1].*

[1]Charité – University Medicine Berlin, Berlin, GERMANY.

12:00P – 1:30P

GROUP LUNCH The Pyramid

Wednesday 1:30P – 2:30P
Session FIP: Forward and Inverse Problems

Chair: A Oberai, USA *Co-Chair: T Alrefae, Kuwait* Marco Polo

Page No.

1:30P – 1:45P

007 ELASTICITY IMAGE CALCULATION FROM X–RAY TOMOSYNTHESIS IMAGES UNDER COMPRESSION. 55

JG Kim[1], JH Shin[1], SY Lee[1].*

[1]Kyung Hee University, Yongin–si, Gyeonggi–do, KOREA.

(Session FIP continues on next page)

(Session FIP continued from previous page)

1:45P – 2:00P

027 ELASTIC MODULUS RECONSTRUCTION FOR TRANSVERSE VASCULAR CROSS–SECTIONS WITH AND WITHOUT COMPOUND STRAIN IMAGING. 56

HHG Hansen[1], MS Richards[2], MM Doyley[2], CL de Korte[1].*
[1]Radboud University Nijmegen Medical Center, Nijmegen, The NETHERLANDS; [2]University of Rochester, Rochester, NY, USA.

2:00P – 2:15P

055 MULTI–SCALE COMPRESSION–BASED QUANTITATIVE ELASTOGRAPHY AND ITS APPLICATION TO BLOOD PRESSURE ESTIMATION. 57

AM Zakrzewski[1], SY Sun[1], M Gilbertson[1], B Vannah[1], L Chai[1], J Ramos[1], BW Anthony[1].*
[1]Massachusetts Institute of Technology, Cambridge, MA, USA.

2:15P – 2:30P

056 RECONSTRUCTING THE MECHANICAL PROPERTIES OF CORONARY ARTERIES FROM DISPLACEMENTS MEASURED WITH A SYNTHETIC APERTURE ULTRASOUND IMAGING SYSTEM. 58

SJ Huntzicker[1], S Korukonda[1], MM Doyley[1].*
[1]University of Rochester, Rochester, NY, USA.

2:30P – 2:45P

063 THE ADJOINT WEIGHTED EQUATION (AWE) METHOD FOR THE SOLUTION OF INVERSE PROBLEMS OF INCOMPRESSIBLE ISOTROPIC ELASTICITY. 59

U Albocher[1], I Harari[1], PE Barbone[2], AA Oberai[3].*
[1]Tel Aviv University, Tel Aviv, ISRAEL; [2]Boston University, Boston, MA, USA; [3]Rensselaer Polytechnic Institute, Troy, NY, USA.

Wednesday 2:45P – 4:00P
Session CVE–1: Cardiovascular Elasticity – I

Chair: CL de Korte, The Netherlands *Co-Chair: J Vappou, France* Marco Polo

Page No.

2:45P – 3:00P

020 MULTI–BAND CONFIDENCE PROCESSING FOR TWO–PASS SPECKLE TRACKING IN ECHOCARDIOGRAPHY. 60

EY Wong[1], CB Compas[2], BA Lin[2], AJ Sinusas[2], JS Duncan[2], M O'Donnell[1].*
[1]University of Washington, Seattle, WA, USA; [2]Yale University, New Haven, CT, USA.

3:00P – 3:15P

034 A FEASIBILITY STUDY OF ULTRASOUND STRAIN IMAGING FOR RISK ASSESSMENT OF CAROTID ATHEROSCLEROTIC PLAQUES VALIDATED BY MAGNETIC RESONANCE IMAGING. 61

S Tao[1], L Huang[2], M Huang[3], X Pan[1], X Zhao[1], L He[1], J Luo[1], J Bai[1], C Yuan[1,4].*
[1]Tsinghua University, Beijing, CHINA; [2]Philips Research Asia, Shanghai, CHINA; [3]China Meitan General Hospital, Beijing, CHINA; [4]University of Washington, Seattle, WA, USA.

3:15P – 3:30P

039 IMAGING VULNERABLE PLAQUES WITH ACOUSTIC RADIATION FORCE IMPULSE (ARFI) IMAGING: FEM SIMULATION RESULTS. 62

JR Doherty[1], GE Trahey[1], ML Palmeri[1].*
[1]Duke University, Durham, NC, USA.

3:30P – 3:45P

058 TOWARDS THE QUANTIFICATION AND IMAGING OF STRESS USING MODEL–BASED INTRAVASCULAR ULTRASOUND ELASTOGRAPHY. 63

MS Richards[1], R Perucchio[1], MM Doyley[1].*
[1]University of Rochester, Rochester, NY, USA.

3:45P – 4:00P

059 EFFECTS OF THE WALL INCLUSION SIZE AND MODULUS CONTRAST ON THE REGIONAL PULSE WAVE PROPAGATION ALONG THE ARTERIAL WALL *IN SILICO*. 64
D Shahmirzadi[1], EE Konofagou[1] – Presented by RX Li[1].*
[1]Columbia University, New York, NY, USA.

4:00P – 4:30P

COFFEE BREAK Bar de l'Amphithéâtre

Wednesday 4:30P – 5:45P
Session MPT–1: Mechanical Properties of Tissues – I

Chair: B Guzina, USA *Co-Chair: S Doblas, France* Marco Polo

4:30P – 4:45P

005 ACUTE EFFECTS OF CANNABINOÏD RECEPTORS ACTIVATION ON BRAIN MECHANICAL PROPERTIES AND CEREBRAL BLOOD FLOW IN THE JUVENILE RAT HIPPOCAMPUS. 65
S Chatelin[1], M Humbert–Claude[2], P Garteiser[1], V Vilgrain[1], BE Van Beers[1], Z Lenkei[2], R Sinkus[1].*
[1]Paris Diderot University, Paris, FRANCE; [2]ESPCI–CNRS, UMR7637, Paris, FRANCE.

4:45P – 5:00P

023 *IN VIVO* HEEL PAD ELASTICITY INVESTIGATION: COMPARING MALES TO FEMALES. 66
S Matteoli[1,2], MM Madsen[1], A Virga[2], JE Wilhjelm[1], A Corvi[2], ST Torp–Pedersen[3].*
[1]Technical University of Denmark, Lyngby, DENMARK; [2]University of Florence, Florence, ITALY; [3]Frederiksberg Hospital, Frederiksberg, DENMARK.

5:00P – 5:15P

031 MULTIFREQUENCY VS MONOFREQUENCY MR ELASTOGRAPHY FOR THE CHARACTERIZATION OF LIVER FIBROSIS AND INFLAMMATION. 67
P Garteiser[12], G D'Assignies[1,2], H Leitao[1,2,3], RS Sahebjavaher[1,2,4], SA Lambert[1,2], F Mouri[1,2], V Vilgrain[1,2], BE Van Beers[1,2], R Sinkus[1,2].*
[1]INSERM, U773, Paris, FRANCE; [2]University Paris Diderot, Sorbonne Paris Cité, Paris, FRANCE; [3]University of Coimbra, Coimbra, PORTUGAL; [4]University of British Columbia, Vancouver, CANADA.

5:15P – 5:30P

038 DYNAMIC SHEAR ELASTICITY PROPERTIES OF BLOOD COAGULATION ASSESSED BY SHEAR WAVE IMAGING AND CLASSIC RHEOLOGY. 68
M Bernal[1], JL Gennisson[1], M Fink[1], P Flaud[2], M Tanter[1].*
[1]Institut Langevin–Ondes et Images, Paris, FRANCE; [2]Université Paris VII Denis Diderot, Paris, FRANCE.

5:30P – 5:45P

050 SHEAR WAVE DISPERSION MEASURES FAT CONCENTRATION IN A MOUSE LIVER MODEL. 69
Z Hah[1], A Partin[1], G Zimmerman[1], CT Barry[2], RA Mooney[2], DJ Rubens[2], KJ Parker[1].*
[1]University of Rochester, Rochester, NY, USA; [2]University of Rochester Medical Center, Rochester, NY, USA.

5:45P – 6:15P

WINE BAR – Wine and Light Snacks Bar de l'Amphithéâtre

ITEC CUP DISTRIBUTION

7:00P – 8:00P Buses to the Hôtel Normandy Barrière TBA

Wednesday 8:00P – 11:00P
Conference Dinner

La Belle Epoque at the Hôtel Normandy Barrière
Casual Business to Formal Attire *Proceedings Book Signing*

From the china and woodwork to the 200 Mahogany armchairs covered and cushioned with wine–colored velvet, the ITEC 2012 Conference Dinner at La Belle Epoque in the Hôtel Normandy Barrière will be an experience one can have only in France! We will dine in the same room where President Barack Obama hosted the 2011 G8 Summit dinner!

10:30P – 11:30P Buses to the Amirauté Hôtel TBA

Thursday, October 4 8:00A – 7:15P

8:00A – 5:30P
Registration Desk Open Bar de l'Amphithéâtre
8:00A – 5:30P **Session POS: Posters** Bar de l'Amphithéâtre
Session EEX: Equipment Exhibit Bar de l'Amphithéâtre

Thursday 8:00A – 10:00A
Session IND: Industrial Presentations

Chair: JC Bamber, UK *Co-Chair: R Daigle, USA* Marco Polo

Page No.

8:00A – 8:30A **Invited Presentation**

097 LIVER STIFFNESS MEASUREMENT USING VIBRATION–CONTROLLED TRANSIENT ELASTOGRAPHY: ROLE IN THE MANAGEMENT OF PATIENTS WITH CHRONIC LIVER DISEASES. 70
L Sandrin[1].*
[1]Echosens, Paris, FRANCE.

8:30A – 9:00A **Invited Presentation**

098 HAS THE QUANTITATIVE STRAIN METHOD OF SHEAR WAVE SPEED REACHED CLINICAL MATURITY? AN ANALYSIS USING HYPE AND TECHNOLOGY ADOPTION MODELS. 71
A Milkowski[1].*
[1]Siemens Medical Solutions USA, Inc., Issaquah, WA, USA.

9:00A – 9:30A **Invited Presentation**

099 THE MODERN ULTRASOUND RESEARCH INTERFACE. 72
R Zahiri Azar[1], C Leung[1], K Dickie[1], L Pelissier[1].*
[1]Ultrasonix Medical Corporation, Richmond, BC, CANADA.

9:30A – 10:00A **Invited Presentation**

100 A NEW PARADIGM IN ULTRASOUND IMAGING. 73
J Souquet[1], J Bercoff[1].*
[1]Supersonic Imagine, Aix–en–Provence, FRANCE.

10:00A – 10:30A
COFFEE BREAK Bar de l'Amphithéâtre

** indicates Presenter*

Thursday 10:30A – 12:15P
Session MIP–2: Methods for Imaging Elastic Tissue Properties – II

Chair: L Sandrin, France *Co-Chair: T Shiina, Japan* Marco Polo

Page No.

10:30A – 10:45A

051 SHEAR WAVE IMAGING WITH A CONVENTIONAL SCANNER: THE PASSIVE ELASTOGRAPHY APPROACH. 74

S Catheline[1], R Souchon[1], JY Chapelon[1].*

[1]INSERM U1032, University of Lyon, Lyon, FRANCE.

10:45A – 11:00A

093 VISCOELASTIC STRESS RELAXATION (ViSR) INDEPENDENCE FROM MUSCLE FIBER ORIENTATION WITH LARGE FOCAL CONFIGURATION. 75

MR Scola[1], CM Gallippi[1].*

[1]The University of North Carolina at Chapel Hill, Chapel Hill, NC, USA.

11:00A – 11:15A

065 NON–INVASIVE MECHANICAL STRENGTH MONITORING OF VASCULAR GRAFT DURING BABOON CELL CO–CULTURE USING ULTRASOUND ELASTICITY IMAGING. 76

D Dutta[1], KW Lee[2], RA Allen[2], Y Wang[2], J Brigham[2], K Kim[1,2] – Presented by JM Rubin.*

[1]University of Pittsburgh Medical Center, Pittsburgh, PA, USA; [2]University of Pittsburgh, Pittsburgh, PA, USA.

11:15A – 11:30A

070 MEASURING BLADDER VISCOELASTICITY USING ULTRASOUND. 77

IZ Nenadic[1], B Qiang[1], MW Urban[1], A Nabavizadeh[1], JF Greenleaf[1], M Fatemi[1].*

[1]Mayo Clinic College of Medicine, Rochester, MN, USA.

11:30A – 11:45A

072 INFERRING TISSUE MICROSTUCTURE USING ELASICITY IMAGING. 78

AA Oberai[1], E Rodrigues–Ferreira[1,2], PE Barbone[3], TJ. Hall[4].*

[1]Rensselaer Polytechnic Institute, Troy, NY, USA; [2]Université Libre de Bruxelles, Bruxelles, BELGIUM; [3]Boston University, Boston, MA, USA; [4]University of Wisconsin–Madison, Madison, WI, USA.

11:45A – 12:00P

076 HIGH FREQUENCY RHEOLOGY USING ULTRASOUND TRANSIENT ELASTOGRAPHY ON HYDROGEL. 79

JL Gennisson[1], A Marcellan[2], A Dizeux[1], M Tanter[1].*

[1]Institut Langevin – Ondes et Images, ESPCI ParisTech, Paris, France; [2]Université Pierre et Marie Curie, Paris, FRANCE.

12:00P – 2:00P

GROUP LUNCH The Pyramid

ITEC Announcements *including the* ***Student Best Paper Award Recipients***

Thursday 2:00P – 4:15P
Session CAA–2: Clinical and Animal Applications – II

Chair: W Svensson, UK *Co-Chair: H Feltovich, USA* Marco Polo

Page No.

2:00P – 2:15P Special Topic

024 EFSUMB GUIDELINES ON THE CLINICAL USE OF ELASTOGRAPHY. 80

DO Cosgrove[1], F Piscaglia[2], C Dietrich[3].*

[1]Imperial College, London, England, UK; [2]Hospital S.Orsola–Malpighi, Bologna, ITALY; [3]Caritas Krankenhaus, Bad Mergentheim, GERMANY.

(Session CAA–2 continues on next page)

2:15P – 2:30P Special Topic

101 THE RADIOLOGICAL SOCIETY OF NORTH AMERICA'S QUANTITATIVE IMAGING BIOMARKER ALLIANCE EFFORT TO DEVELOP AND VALIDATE CROSS–SYSTEM SHEAR WAVE SPEED MEASUREMENTS FOR STAGING LIVER FIBROSIS. 81

TJ Hall[1], BS Garra[2,3], A Milkwoski[4], PL Carson[5], D Sullivan[6], D Cosgrove[7], A Samir[8], C Cohen–Bacrie[9], KA Wear[3], ML Palmeri[6].*

[1]University of Wisconsin–Madison, Madison, WI, USA; [2]Washington DC VA Medical Center, Washington, DC, USA; [3]US Food and Drug Administration, Silver Spring, MD, USA; [4]Ultrasound, Siemens Healthcare, Mountain View, CA, USA; [5]University of Michigan, Ann Arbor, MI, USA; [6]Duke University, Durham, NC, USA; [7]Imperial College, London, England, UK; [8]Massachusetts General Hospital, Boston, MA, USA; [9]Supersonic Imagine, Aix–en–Provence, FRANCE.

2:30P – 2:45P

009 *IN VITRO* COMPARISON OF ULTRASOUND BASED ELASTOGRAPHY TECHNIQUES. 82

S Franchi–Abella[1], C Ellie[2], JM Correas[2].*

[1]Kremlin–Bicêtre Hospital, Le Kremlin–Bicêtre, FRANCE; [2]Necker Hospital, Paris, FRANCE.

2:45P – 3:00P

010 MONITORING SURGICAL RESECTION OF TUMORS WITH ULTRASOUND STRAIN IMAGING. 83

TS Pheiffer[1], BC Byram[3], MI Miga[1,2].*

[1]Vanderbilt University, Nashville, TN, USA; [2]Vanderbilt University Medical Center, Nashville, TN, USA; [3]Duke University, Durham, NC, USA.

3:00P – 3:15P

040 MONITORING CRYOABLATION LESIONS WITH QUANTITATIVE ULTRASOUND ELASTOGRAPHY: A FEASIBILITY STUDY. 84

D Dall'Alba[1], C Schneider[2], C Nguan[3], A Baghani[2], R Rohling[2], SE Salcudean[2].*

[1]University of Verona, Verona, ITALY; [2]University of British Columbia, Vancouver, BC, CANADA; [3]Vancouver General Hospital, Vancouver, BC, CANADA.

3:15P – 3:30P

013 SHEAR WAVE VELOCITY DISCRIMINATION OF INFLAMED FROM FIBROTIC BOWEL SEGMENTS IN A CROHN'S DISEASE ANIMAL MODEL. 85

JR Dillman[1], RW Stidham.[1], PDR Higgins[1], DS Moons[1], LA Johnson[1], JM Rubin[1].*

[1]University of Michigan, Ann Arbor, MI, USA.

3:30P – 3:45P

032 ANALYSIS OF THE INFLUENCE OF INFLAMMATION, IRON AND WATER DIFFUSIVITY ON LIVER VISCOELASTIC PARAMETERS IN FIBROSIS. 86

H Leitao[1,2,3], S Doblas[1,2], P Garteiser[1,2], G D'Assignies[1,2], F Mouri[1,2], V Vilgrain[1,2], R Sinkus[1,2], BE Van Beers[1,2].*

[1]INSERM, U773, Paris, FRANCE; [2]University Paris Diderot, Sorbonne Paris Cité, Paris, FRANCE; [3]University of Coimbra, Coimbra, PORTUGAL.

3:45P – 4:00P

003 SHEAR WAVE ELASTOGRAPHY AND PARAMETRIC IMAGING ARE COMPLEMENTARY IN ULTRASOUND DIFFERENTIATION OF NON–MALIGNANT ADRENAL MASSES: INITIAL RESULTS. 87

RZ Slapa[1], AA Kasperlik–Zaluska[2], B Migda[1], KT Szopiński[1], A Piwowonski[3], E Roslonowska[2], RK Mlosek[1], WS Jakubowski[1].*

[1]Medical University of Warsaw, Warsaw, POLAND; [2]Center for Postgraduate Medical Education, Warsaw, POLAND; [3]NZOZ Almed, Jaroslaw, POLAND.

4:00P – 4:15P

002 ANALYSIS OF THYROID NODULES VISCOELASTICITY WITH TIME STRAIN CURVES MAY SURPASS CLASSICAL QUALITATIVE AND SEMI–QUANTITATIVE EVALUATION. 88

RZ Slapa[1], B Migda[1], WS Jakubowski[1], J Bierca[2], J Slowinska–Srzednicka[3].*

[1]Medical University of Warsaw, Warsaw, POLAND; [2]Solec Hospital, Warsaw; POLAND; [3]Center for Postgraduate Medical Education, Warsaw, POLAND.

4:15P – 4:45P
COFFEE BREAK — Bar de l'Amphithéâtre

Thursday 4:45P – 5:45P
Session MPT–2: Mechanical Properties of Tissues – II
Chair: S Catheline, France *Co-Chair: C Schmitt, Canada* — Marco Polo

Page No.

4:45P – 5:00P
014 CEREBRAL TISSUE MOTION AND LEUKO–ARAIOSIS IN THE ELDERLY: A CORRELATION STUDY USING ULTRASOUND AND MAGNETIC RESONANCE IMAGING. 89
R Ternifi[1], X Cazals[1], A Lorette[1], T Desmidt[1], V Camus[1], JP Cottier[1], F Patat[2], JP Remenieras[1].*
[1]Université François Rabelais, Tours, FRANCE; [2] CIC–IT 806, CHRU de Tours, Tours, FRANCE.

5:00P – 5:15P
043 ROLE AND OPTIMISATION OF THE INDENTER SIZE FOR QUANTITATIVE POROELASTOGRAPHY. 90
J Fromageau[1], N Bush[1], JC Bamber[1].*
[1]The Institute of Cancer Research and Royal Marsden Hospital, Sutton, Surrey, England, UK.

5:15P – 5:30P
060 VISCOELASTICITY PARAMETERS OF HIFU ABLATED CANINE LIVER TISSUES *EX VIVO*. 91
D Shahmirzadi[1], GY Hou[1], EE Konofagou[1].*
[1]Columbia University, New York, NY, USA.

5:30P – 5:45P
077 EVALUATION OF 2D AORTA ELASTOGRAPHY TECHNIQUES IN PORCINE AORTAS. 92
RGP Lopata[1], MCM Rutten[1], FN van de Vosse[1].*
[1]Eindhoven University of Technology, Eindhoven, The NETHERLANDS.

Thursday 5:45P – 6:45P
Group Photo — TBA

6:45P – 7:15P
WINE BAR – Wine and Light Snacks — Bar de l'Amphithéâtre

After 7:15P *No Conference Activities*

Friday, October 5 8:00A – 10:00P

8:00A – 4:15P
Registration Desk Open — Bar de l'Amphithéâtre
8:00A – 4:15P **Session POS: Posters** — Bar de l'Amphithéâtre
Session EEX: Equipment Exhibit — Bar de l'Amphithéâtre

Friday 8:00A – 10:00A
Session SIP: Signal and Image Processing
Chair: JL Gennisson, France *Co-Chair: AK Thittai, USA* — Marco Polo

Page No.

8:00A – 8:15A
004 SHEAR WAVE IMAGING USING HARMONIC DISTORTION OF SINUSOIDAL EXCITATION. 93
Y Yamakoshi[1], PR Kumar[1], R Tei[1], D Nakai[1], Y Tsuihiji[1].*
[1]Gunma University, Kiryu–shi , Gunma, JAPAN.

(Session SIP continues on next page)

(Session SIP continued from previous page)

8:15A – 8:30A

028 PLANE WAVE IMAGING FOR FAST VASCULAR STRAIN ESTIMATION. 94
HHG Hansen[1], B Wijnhoven[1], CL de Korte[1].*
[1]Radboud University Nijmegen Medical Center, Nijmegen, The NETHERLANDS.

8:30A – 8:45A

041 COMPARING THE PERFORMANCE OF SPARSE ARRAY AND PLANE WAVE IMAGING SYSTEMS IN NON–INVASIVE VASCULAR ELASTOGRAPHY. 95
S Korukonda[1], R Nayak[1], MM Doyley[1].*
[1]University of Rochester, Rochester, NY, USA.

8:45A – 9:00A

042 REPRODUCIBILITY STUDIES IN SHEAR WAVE ELASTOGRAPHY. 96
M Labit[1], H Monpeyssen[2], O Lucidarme[1,3], L Leenhardt[1,2], F Frouin[1], C Pellot–Barakat[1].*
[1]UPMC/INSERM UMR_S 678, Paris, FRANCE; [2]Pitié Salpêtrière Hospital, Paris, FRANCE; [3]Pitié–Salpêtrière Hospital, Paris, FRANCE.

9:00A – 9:15A

045 STRAIN ESTIMATION FOR QUASI–STATIC ELASTOGRAPHY THROUGH ANALYTICAL PHASE TRACKING. 97
L Yuan[1], PC Pedersen[1].*
[1]Worcester Polytechnic Institute, Worcester, MA, USA.

9:15A – 9:30A

054 EXPERIMENTAL EVALUATION OF SIMULTANEOUS MULTISPECTRAL CODED EXCITATION FOR PHOTOACOUSTIC IMAGING. 98
H Zhang[1], K Kondo[1], M Yamakawa[1], T Shiina[1].*
[1]Kyoto University, Kawahara–cho, Shogoin, Kyoto, JAPAN.

9:30A – 9:45A

071 ASSESSING ARTERY WALL DYNAMICS WITH HIGH FRAME RATE ULTRASOUND IMAGING AND THREE DIMENSIONAL PHASE ANALYSIS. 99
P Kruizinga[1], F Mastik[1], N de Jong[1,2,3], AFW van der Steen[1,2], G van Soest[1].*
[1]Erasmus MC–Thorax Center, Rotterdam, The NETHERLANDS; [2]Interuniversity Cardiology Institute, Utrecht, The NETHERLANDS; [3]Delft University of Technology, Delft, The NETHERLANDS.

9:45A – 10:00A

089 DIRECT ELASTIC MODULUS RECONSTRUCTIONS FROM UNIAXIAL STRAIN AND DISPLACEMENT DATA. 100
OA Babaniyi[1], PE Barbone[1], AA Oberai[2].*
[1]Boston University, Boston, MA, USA; [2]Rensselaer Polytechnic Institute, Troy, NY, USA.

10:00A – 10:30A

COFFEE BREAK Bar de l'Amphithéâtre

Friday 10:30A – 12:00P
Session MIP–3: Methods for Imaging Elastic Tissue Properties – III

Chair: R Zahiri Azar, Canada *Co-Chair: P Garteiser, France* Marco Polo

10:30A – 10:45A

062 IMAGING TRANSVERSE ISOTROPIC ELASTIC PROPERTIES OF MUSCLE WITH ULTRASONICALLY TRACKED RADIATION FORCE INDUCED SHEAR WAVES IN 3D. 101
MH Wang[1], BC Byram[1], ML Palmeri[1], NC Rouze[1], KR Nightingale[1].*
[1]Duke University, Durham, NC, USA.

10:45A – 11:00A

081 MR ELASTOGRAPHY OF *IN–VIVO* AND *EX–VIVO* PROSTATE CANCER AND CORRELATION WITH HISTOLOGY: INITIAL RESULTS. 102

RS Sahebjavaher[1,2], G Nir[1], O Mohareri[1], LO Gagnon[3], EC Jones[3], L Goldenberg[3], P Garteiser[2], R Sinkus[2], P Kozlowski[3], SE Salcudean[1].*
[1]University of British Columbia, Vancouver, CANADA; [2]Centre de Recherche Biomedicale Bichat–Beaujon, Paris, FRANCE; [3]University of British Columbia Faculty of Medicine, Vancouver, CANADA.

11:00A – 11:15A

085 SUB–WAVELENGTH RESOLUTION IN SHEAR WAVE IMAGING: THE TIME REVERSAL APPROACH. 103

S Catheline[1], R Souchon[1], JY Chapelon[1].*
[1]INSERM U1032, University of Lyon, Lyon, FRANCE.

11:15A – 11:30A

090 IDENTIFICATION OF NONLINEAR TISSUE ELASTICITY VIA ACOUSTIC RADIATION FORCE. 104

BB Guzina[1], EV Dontsov[1], RR Kinnick[2], MW Urban[2], M Fatemi[2].*
[1]University of Minnesota, Minneapolis, MN, USA; [2]Mayo Clinic College of Medicine, Rochester, MN, USA.

11:30A – 11:45A

092 REALTIME ELASTOGRAPHY IN THE ASSESSEMENT OF UTERINE DISORDERS: DIAGNOSTIC ACCURACY IN A FEASIBILITY STUDY. 105

B Stoelinga[1], WJK Hehenkamp[1], HAM Brölmann[1], JAF Huirne[1].*
[1]VU Medical Center, Amsterdam, The NETHERLANDS.

11:45A – 12:00P

075 SHEAR WAVE GENERATION FOR ELASTICITY IMAGING VIA MODE CONVERSION FROM LONGITUDINAL WAVES AT ELASTICITY BOUNDARY. 106

K Nii[1], K Okubo[1], N Tagawa[1], S Yagi[2].*
[1]Tokyo Metropolitan University, Hino, Tokyo, JAPAN; [2]Meisei University, Hino, Tokyo, JAPAN.

12:00P – 1:30P

GROUP LUNCH — The Pyramid

Friday 1:30P – 3:00P
Session CVE–2: Cardiovascular Elasticity – II

Chair: MM Doyley, USA *Co-Chair: RGP Lopata, The Netherlands* — Marco Polo

1:30P – 1:45P

017 ACQUISITION OF HIGH FRAME RATE MOVIES OF SIMULTANEOUS ACOUSTIC RADIATION FORCE IMPULSE (ARFI) AND SHEAR WAVE VELOCITY IMAGES FOR INTRACARDIAC ECHOCARDIOGRAPHY (ICE) APPLICATIONS IN *IN VIVO* MYOCARDIUM. 107

PJ Hollender[1], SJ Rosenzweig[1], DP Bradway[1], R Goswami[2], PD Wolf[1], GE Trahey[1].*
[1]Duke University, Durham, North Carolina, USA; [2]Duke University Medical Center, Durham, NC, USA.

1:45P – 2:00P

061 SINGLE–HEARTBEAT 2–D MYOCARDIAL ELASTOGRAPHY USING AN UNFOCUSED TRANSMIT SEQUENCE: AN *IN VIVO* FEASIBILITY STUDY. 108

SJ Okrasinski[1], J Provost[1], D Legrand[1], EE Konofagou[1].*
[1]Columbia University, New York, NY, USA.

2:00P – 2:15P

066 COMBINED ULTRASOUND ELASTICITY AND THERMAL STRAIN IMAGING FOR COMPREHENSIVE ASSESSMENT OF ATHEROSCLEROTIC PLAQUE IN A RABBIT MODEL. 109

A Mahmoud[1,2], D Dutta[1], L Lavery[1], K Kim[1,3] – Presented by JM Rubin.*
[1]University of Pittsburgh Medical Center, Pittsburgh, PA, USA; [2]Cairo University, Giza, EGYPT; [3]University of Pittsburgh, Pittsburgh, PA, USA.

(Session CVE–2 continues on next page)

(Session CVE–2 continued from previous page)

2:15P – 2:30P

069 SHEAR WAVE VELOCITY ACQUIRED BY SHEAR WAVE ELASTICITY IMAGING INCREASES WITH TIME IN NORMAL AND HYPO–PERFUSED LANGENDORFF RABBIT HEARTS. 110
M Vejdani–Jahromi[1], DM Dumont[1], A Kiplagat[1], GE Trahey[1], PD Wolf[1] – Presented by Y–J Kim.*
[1]Duke University, Durham, NC, USA.

2:30P – 2:45P

073 ELECTROMECHANICAL WAVE IMAGING OF CANINE AND HUMAN PATHOLOGICAL HEARTS *IN VIVO*. 111
J Provost[1], A Gambhir[1], A Costet[1], J Grondin[1], SJ Okrasinski[1], H Garan[1], EE Konofagou[1].*
[1]Columbia University, New York, NY, USA.

2:45P – 3:00P

074 PERFORMANCE ASSESSMENT AND OPTIMIZATION OF PULSE WAVE IMAGING FOR PULSE WAVE ANALYSIS IN *EX VIVO* CANINE AORTAS AND *IN VIVO* NORMAL HUMAN AORTAS. 112
RX Li[1], D Shahmirzadi[1], WW Qaqish[1], EE Konofagou[1].*
[1]Columbia University, New York, NY, USA.

Friday 3:00P – 3:45P
Session CAA–3: Clinical and Animal Applications – III

Chair: RZ Slapa, Poland *Co-Chair: G Kruger, USA* Marco Polo

3:00P – 3:15P

022 SHEAR WAVE ELASTOGRAPHY OF PEDIATRIC EPILEPTOGENIC TUMORS: PRELIMINARY RESULTS. 113
HW Chan[1,3], A Chakraborty[2], NL Dorward[1], JC Bamber[3], W Harkness[2].*
[1]Royal Free Hospital, London, England, UK; [2]Great Ormond Street Hospital, London, England, UK; [3]Institute of Cancer Research and Royal Marsden Hospital, Sutton, Surrey, England, UK.

3:15P – 3:30P

030 SENSITIVITY OF MAGNETIC RESONANCE ELASTOGRAPHY TO DETECT BRAIN DEVELOPMENT AND MATURATION. 114
K Schregel[1,2], J Le Faouder[2,3], E Würfel[4], S Chatelin[2], P Bedossa[2,5], J Würfel[1], R Sinkus[2].*
[1]University Luebeck, Luebeck, GERMANY; [2] Université Paris Diderot, Sorbonne Paris Cité, Paris, FRANCE; [3]Institut Fédératif de Recherche Claude Bernard, Université Paris–Diderot, Paris, FRANCE; [4]University Goettingen, Goettingen, GERMANY; [5]Beaujon Hospital, Assistance Publique–Hôpitaux de Paris and Université Paris–Diderot, FRANCE.

3:30P – 3:45P

037 ACQUISITION OF FREEHAND ELASTOGRAPHY VOLUMES IN BRAIN TUMOR SURGERY: PRELIMINARY RESULTS. 115
T Selbekk[1,2], F Lindseth[1,2], G Unsgård[2,3].*
[1]SINTEF, Trondheim, NORWAY; [2]The Norwegian University of Science and Technology, Trondheim, NORWAY; [3]St. Olav Hospital, Trondheim University Hospital, Trondheim, NORWAY.

3:45P – 4:15P

COFFEE BREAK Bar de l'Amphithéâtre

Friday 4:15P – 5:30P

Session MMT: Mechanical Measurement Techniques for Tissues

Chair: KJ Parker, USA *Co-Chair: S Chatelin, France* Marco Polo

Page No.

4:15P – 4:30P

012 SUB–VOXEL MICRO-ARCHITECTURE ASSESSMENT BY SCATTERING OF MECHANICAL SHEAR WAVES. 116

SA Lambert[1], S Chatelin[1], SP Nashölm[2], L Juge[1], P Garteiser[1], L ter Beek[3], V Vilgrain[1], BE Van Beers[1], LE Bilston[4], B Guzina[5], S Holm[2], R Sinkus[1].*

[1]Paris Diderot University, Paris, FRANCE; [2]University of Oslo, Oslo, NORWAY; [3]Philips Healthcare, Best, The NETHERLANDS; [4]Neuroscience Research Australia and University of New South Wales, Sydney, NSW, AUSTRALIA; [5]University of Minnesota, Minneapolis, MN, USA.

4:30P – 4:45P

016 HYPER–FREQUENCY VISCOELASTIC SPECTROSCOPY OF A VASCULAR–MIMICKING PHANTOM AND A PORCINE AORTA WITH THE RHEOSPECTRIS INSTRUMENT. 117

C Schmitt[1], A Hadj Henni[1], S LeFloc'h[2], J Ohayon[2], J Vappou[3], G Cloutier[4].*

[1]Rheolution Inc., Montréal, Québec, CANADA; [2]Université Joseph Fourier, Grenoble, FRANCE; [3]University of Strasbourg, Strasbourg, FRANCE; [4]University of Montréal Hospital Research Center (CRCHUM), Montréal, Québec, CANADA.

4:45P – 5:00P

029 *IN VIVO* TIME HARMONIC MULTIPLE FREQUENCY ELASTOGRAPHY OF HUMAN LIVER. 118

H Tzschätzsch[1], J Braun[1], T Fischer[1], R Klaua[2], M Schultz[2], I Sack[1].*

[1]Charité–Univeritätsmedizin Berlin, Berlin, GERMANY; [2]GAMPT mbH, Merseburg, Sachsen–Anhalt, GERMANY.

5:00P – 5:15P

049 SHEAR WAVE SPEED AND DISPERSION MEASUREMENT USING INTERFERENCE PATTERNS FROM A SPECIFICALLY DESIGNED CHIRP SIGNAL. 119

Z Hah[1], A Partin[1], KJ Parker[1].*

[1]University of Rochester, Rochester, NY, USA.

5:15P – 5:30P

053 COMBINED ULTRASOUND AND BIOIMPEDANCE TO ASSESS TISSUE VISCO–ELASTICITY. 120

R Dodde[1], G Kruger[2], L Koziol[1], J Ophir[3], WF Weitzel[1].*

[1]University of Michigan, Ann Arbor, MI, USA; [3]University of Texas Medical School, Houston, TX, USA.

5:30P – 6:00P

WINE BAR – Wine and Light Snacks Bar de l'Amphithéâtre

Friday 7:30P – 10:00P

Crêpe Dinner Closing Reception *Proceedings Book Signing* The Pyramid

Verasonics, Inc.
Redmond, WA, USA.

Verasonics®

On the Cover:
"Terrasse à Sainte–Adresse"
by Claude Monet, 1867
A seaside resort on the Normandy coast in the 19th century.

2012 SPONSORS

The Conference Organizers wish to express appreciation
to the following companies
for providing support of this year's Conference:

Gold Level
($10,000 or more)

UTHealth
The University of Texas
Health Science Center at Houston
THE UNIVERSITY OF TEXAS MEDICAL SCHOOL AT HOUSTON
Diagnostic & Interventional Imaging

****

Bronze Level
($2,000 – $4,999)

Inserm

Université Paris Diderot, Sorbonne Paris Cité,
CRB3, UMR 773, INSERM

****

General Level
(up to $1,999)

CRC Press
Taylor & Francis Group

CRC Press Taylor & Francis Group

RCBU

Rochester Center for Biomedical Ultrasound
The University of Rochester

AUTHOR INDEX

AUTHOR INDEX

Session TUT: Tutorials: New Perspectives and Challenges to the Elasticity Imaging Community

Tuesday, October 2 12:00P – 2:00P

095 **HOW AN INGENIOUS BIOPHYSICAL MEASUREMENT BECOMES A DECISION–MAKING BIOMARKER: THE ARDUOUS JOURNEY FROM IDEA TO IMPACT.**

John C. Waterton[1,2].*

[1]Personalised Healthcare and Biomarkers, AstraZeneca, Alderley Park, Macclesfield, Cheshire, England, UK; [2]Manchester Academic Health Sciences Centre, University of Manchester, Manchester, England, UK.

Background: The ultimate goal of most biomedical research is improve preventive, diagnostic and therapeutic interventions in human disease. This is not just an ethical imperative [1] but is the outcome implied and expected when taxpayers and others fund our research. Unfortunately, many novel and ingenious biophysical (and other) measurement technologies, while initially showing great promise, fail ultimately to benefit patients; these failures of translation and impact [2] are now causing governments increasing concern.

Aims: To describe how a biophysical measurement can be characterized as a biomarker, and to propose a roadmap to impact specifically suitable for biophysical biomarkers, in contradistinction to molecular biomarkers.

Methods: Recent statements on biomarker definition, validation and qualification were considered [3–5] in combination with established approaches to causality in medical research [6,7]. A distinction was drawn between molecular biomarkers, in which a biospecimen is removed from the patient and analysed remotely using an *In Vitro* Diagnostic Device, and biophysical biomarkers, in which the validity and integrity of the method depends critically on the detection of a biosignal in the presence of, and interfaced to, the patient using an *In Vitro* Diagnostic Device. The 50–year history of qualifying imaging biomarkers provides precedent for other biophysical biomarkers.

Results: Three essential (and orthogonal) activities are: (a) technical validation; (b) qualification or biological validation; (c) health technology assessment. A technically valid biomarker can be measured robustly in different clinical settings around the world and gives consistent measurements. A qualified biomarker, when added to a patient's management, improves prediction of subsequent clinical outcome. Health technology assessment shows that expenditure on measuring the biomarker is an effective use of healthcare resources. For biophysical biomarkers, technical validation requires regulatory approval, standardization, objective quantification, phantom design and reproducibility studies in single– and multi–centre/multi–vendor settings with different clinical presentations. Qualification requires correlation with underlying pathology with and without intervention (in animal models where human studies would be impractical or unethical), together with cross–sectional and longitudinal trials correlated with clinical outcome (often, the most difficult challenge in biomarker qualification is distinguishing true–negatives from false–negatives). Health Technology Assessment may include a Health Economic assessment of the incremental cost of saving a Quality–Adjusted Life Year. The time to complete these three activities is typically measured in decades rather than years.

Conclusions: A plausible roadmap from the initial biophysical innovation through to ultimate patient benefit should give funders increased confidence in supporting innovation and help define the critical next steps in a biomarker's qualification journey.

References:

[1] WMA Declaration of Helsinki. www.wma.net/en/30publications/10policies/b3/index.html (accessed 2012–07–17), 2008.

[2] Cooksey, D: A Review of UK Health Research Funding. www.hm–treasury.gov.uk/d/pbr06_cooksey_final_report_636.pdf (accessed 2012–07–17), 2006.

[3] Biomarkers Definitions Working Group: Biomarkers and Surrogate Endpoints: Preferred Definitions and Conceptual Framework. Clin. Pharm. Ther., 69, pp. 89–95, 2001.

[4] Wagner JA, Williams SA, Webster CJ: Biomarkers and Surrogate End Points for Fit–for–Purpose Development and Regulatory Evaluation of New Drugs. Clin. Pharm. Ther., 81, pp. 104–7, 2007.

[5] Waterton JC, Pylkkanen L: Qualification of Imaging Biomarkers for Oncology Drug Development. Eur. J. Cancer, 48, pp. 409–15, 2012.

[6] Bradford–Hill A: The Environment and Disease: Association or Causation? Proc. Roy. Soc. Med., 58, pp. 295–300, 1965.

[7] Cox D, Wermuth N: Causality: A Statistical View. Int. Stat. Rev., 72, pp. 285–305, 2004.

096 **MIND SHAKING – A NEUROLOGIST´S PERSPECTIVE ON CEREBRAL MAGNETIC RESONANCE ELASTOGRAPHY.**

Jens Würfel[1]*.

[1]Institute of Neuroradiology, University Medicine Goettingen, Robert–Koch–Str. 40, D–37075 Goettingen, GERMANY.

The detection of pathological tissue alterations by manual palpation is a simple but essential diagnostic tool, which has been applied by physicians since the beginnings of medicine. The palpation of the brain, however, was a long time hands–on experience exclusive to neurosurgeons and pathologists. Only very recently it has become a domain for physicists and neuroradiologists: Applying Magnetic Resonance Elastography (MRE), we may today non–invasively quantify the biomechanical tissue properties by analyzing the propagation of externally elicited shear waves through the brain parenchyma (Figure 1).

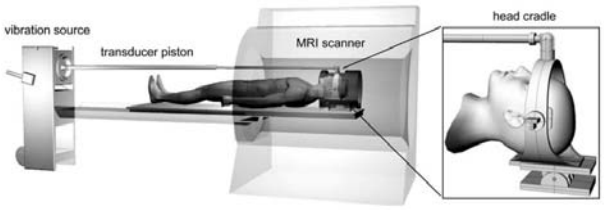

Figure 1: Various methods have been designed to elicit shear waves inside the skull {1}.

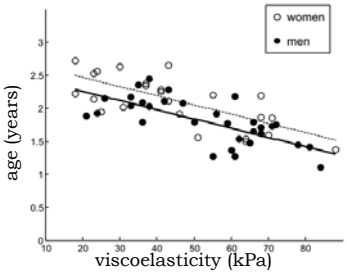

Figure 2: Age and gender dependency.

Initial cerebral MRE studies on healthy volunteers described an ample difference in viscoelasticity between women and men, and they also found a "natural" significant softening of the intracranial tissue during aging [1] (Figure 2). Furthermore, cMRE proved sensitive to occult and diffuse pathological changes, e.g., in neuroinflammatory diseases like multiple sclerosis [2,3] (Figure 3), or normal pressure hydrocephalus [4].

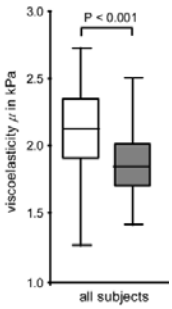

Figure 3: Dramatic viscoelasticity loss in young MS patients {1}.

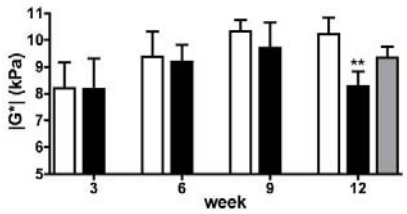

Figure 4: Increase in G* during adolescence, but drop during toxic demyelination (Cuprizone mouse model). Partial recovery during remyelination (grey bar).

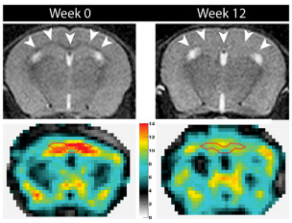

Figure 5: T2 and G* maps in healthy mice (week 0) and after 12 weeks of cuprizone supplemented nutrition.

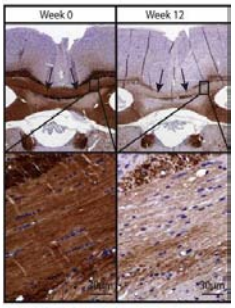

Figure 6: Demyelination of the corpus callosum.

However, only after the transfer to animal models [5] (Figures 4–6) and biopsies, e.g., of intracranial tumors, light was shed on the cellular and molecular background of the viscoelasticity alterations detected *in vivo*. Future work is needed to increase spatial resolution of cMRE as well as patient comfort during the procedure, in order to develop a tool applicable for clinical routine use. Even more important, we need to broaden our knowledge on the relevant structural changes of the underlying physiopathology in order to understand and define relevant disease specific MRE parameters.

Acknowledgements: {1} Courtesy of I. Sack.

References:

[1] Sack et al.: Neuroimage, 46, pp. 652–657, 2009.
[2] Wuerfel et al.: Neuroimage, 49, pp. 2520–2525 2010.
[3] Streitberger et al.: Brain Viscoelasticity Alteration in Chronic–Progressive Multiple Sclerosis. PLoS ONE, 7(1): e29888. doi:10.1371/journal.pone.0029888, 2012.
[4] Freimann et al.: Neuroradiology, 2012.
[5] Schregel et al.: PNAS, 2012.

011 **ELECTROMECHANICAL WAVE IMAGING OF BIOLOGICAL AND ELECTRONIC PACEMAKERS IN CONSCIOUS DOGS *IN VIVO*.**

Alexandre Costet[1], Jean Provost[1], Alok Gambhir[2], Yevgeniy Bobkov[3], Gerard J.J. Boink[3], Peter Danilo Jr[3], Michael R. Rosen[3], Elisa E. Konofagou[1,4].*
[1]Biomedical Engineering Department, [2]Medicine–Cardiology Department, [3]Pharmacology Department, [4]Radiology Department, Columbia University, New York, NY, USA.

Background: Safe and real–time non–invasive imaging of cardiac electrical activation has been a long term goal of clinicians and laboratory investigators. Standard methods currently available in the clinic are all catheter–based and limited to epicardial or endocardial mapping. They are also time consuming and costly. Electromechanical Wave (EW) Imaging (EWI) is a direct ultrasound–based imaging technique that can map the transmural electromechanical activation in all four chambers *in vivo* [1].

Aims: In this study, we assessed the reproducibility of EWI in closed–chest, conscious dogs to determine EWI's potential for longitudinal animal studies. In order to show reproducibility in a variety of cases, we mapped electromechanical activation in conscious animal during normal sinus rhythm (NSR) and during idioventricular rhythm occurring in dogs in heart block, implanted with electronic and biological pacemakers (EPM and BPM respectively).

Methods: Six different dogs (n=6) were used in this study. Four dogs underwent AV node ablation to create heart block and were subsequently implanted with an EPM in the right ventricular (RV) endocardial apex while two additionally received a BPM at the left ventricular (LV) epicardial base. A Verasonics system (Verasonics, Redmond, WA) with a 2.5MHz phased array was used to perform EWI transthoracically in conscious dogs using a flash beam sequence at 2000 frames/s in the apical 2 and 4–chamber views before and 7 days after implantation. In post–implantation animals, EWI was performed during BPM pacing only and during EPM pacing only. Axial incremental displacements and strains were estimated using radiofrequency (RF) cross–correlation with a window size of 9.2mm and a window shift of 0.385mm and a least–squares kernel size of 5.0mm, respectively. Isochrones of the electromechanical activation were then generated in order to assess EWI reproducibility.

Results: During NSR, the EW originated at the right atrium (RA), propagated to the left atrium (LA) and emerged from multiple sources in both ventricles. During BPM, the EW originated from the LV basal lateral wall and subsequently propagated throughout the ventricles. During EPM, the EW originated at the RV apex and propagated throughout both ventricles.

Conclusions: EWI was capable of adequately differentiating BPM from EPM and NSR and identified the distinct pacing origins transthoracically and in conscious dogs These findings indicate the potential of EWI to serve as a simple, direct and noninvasive imaging tool for monitoring of pacing therapies.

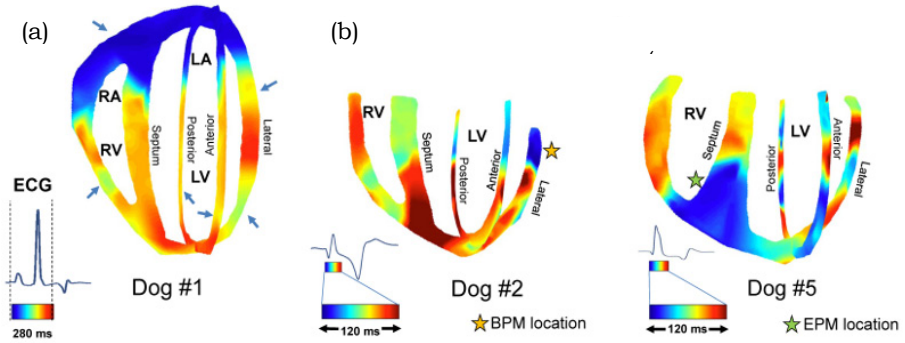

Figure 1: EWI isochrones during NSR, biological and electronic pacing. The orgins of the isochrones correspond to the onset of the P–wave (a) or the QRS (b, c). (a) EWI isochrone of normal sinus rhythm in one dog pre–surgery. Activation at the atria originates from the RA and propagates to the LA. In the ventricles, arrows indicati the sites of early activation. (b) EWI isochrone during biological pacing. Early activation is seen in the basal region of the lateral wall in the LV. (c) EWI isochrone during electronic pacing. Early activation is seen near the apex of the RV.

Acknowledgements: Supported in part by NIH funding (R01EB006042, R01HL094410 and R01HL67101).

References:

[1] Provost J., Lee W–N., et al.: Imaging the Electromechanical Activity of the Heart *In–Vivo*. Proc. Natl. Acad. Sci. U.S.A., Vol. 108, No. 21, pp. 8565–8570, 2011.

* *indicates Presenter*

021 **A NOVEL TECHNIQUE OF DETECTING MAGNETIC RESONANCE IMAGING (MRI)–NEGATIVE EPILEPTOGENIC LESIONS IN FOCAL SYMPTOMATIC EPILEPSY: A CASE REPORT USING INTRAOPERATIVE SHEAR WAVE ELASTOGRAPHY.**

HW Chan[1,3], A Chakraborty[2], CE Uff[1], NL Dorward[1], JC Bamber[3], W Harkness[2].*
[1]Neurosurgery Department, Royal Free Hospital, Pond St, London, NW3 2QG, England, UK; [2]Neurosurgery Department, Great Ormond Street Hospital, Great Ormond St, London, WC1N 3JH, England, UK; [3]Joint Department of Physics, Institute of Cancer Research and Royal Marsden Hospital, Downs Road, Sutton, Surrey, SM2 5PT, England, UK.

Background: Focal symptomatic epilepsy is epilepsy with onset in a cerebral hemisphere, caused by an abnormality in the brain, known as an epileptogenic lesion, and is usually resistant to medical therapy. A small proportion of these patients do not have identifiable lesions on magnetic resonance imaging (MRI). As the success rate of resective surgery in these patients depends on the extent of resection, it is important to detect these lesions on images that guide resection and electrode implantation for seizure monitoring.

Aims: To determine if intraoperative shear wave elastography (SWE) can detect MRI–negative epileptogenic lesions and guide the invasive implantation of deep electrodes in these patients.

Methods: A seven year old patient with medically intractable MRI–negative focal symptomatic epilepsy underwent a two–stage planned operation. The preoperative electroencephalography (EEG) and positron emission tomography (PET) scan had demonstrated possible seizure onset from the right frontal region. During the first stage operation where subdural grid and invasive electrodes were going to be implanted, both intraoperative ultrasound (US) and SWE were performed simultaneously with an Aixplorer® scanner (Supersonic Imagine, France) equipped with a sector transducer (SE12–3) having a bandwidth of 3–12MHz. Young's modulus (YM) was measured within any areas of abnormal stiffness in the region of interest (ROI) using the scanner's built–in Q–Box™ function.

Results: Intraoperative SWE demonstrated an abnormally stiff area about one centimeter deep from the brain surface whilst the simultaneous US B–mode failed to demonstrate an abnormality (Figure 1). The lesion had a mean YM of 74.7kPa whereas the surrounding grey and white matter had mean YM of 36.2kPa and 20.8kPa, respectively. Seven–day post–implantation invasive EEG recording confirmed that the seizure onset was coming from the region where the invasive electrode had been implanted under SWE guidance, i.e., in the region at one centimeter depth from the brain surface. The patient then underwent resection of the right frontal operculum in the second stage (Figure 2). The histological examination demonstrated Type IIb focal cortical dysplasia (FCD) (Figure 3). The region of stiffness at three–centimeter depth (Figure 1) was not resected as the invasive recording did not detect seizure activity from this region. Post–operatively, the patient remained seizure–free with no focal deficit at a six–week outpatient–clinic follow–up.

Conclusions: Intraoperative SWE successfully identified an epileptogenic lesion in a patient with MRI–negative focal symptomatic epilepsy. In the future, this novel technique may be used as an intraoperative adjunct for patients with focal symptomatic epilepsy undergoing resective surgery, especially those with normal MRI appearance.

Acknowledgements: This work was supported by Engineering and Physical Sciences Research Council, UK. Ethical approval was obtained from the National Research Ethics Service (NRES) Committee London – Queen Square Research Ethics Committee (Ref: 08/H0716/92).

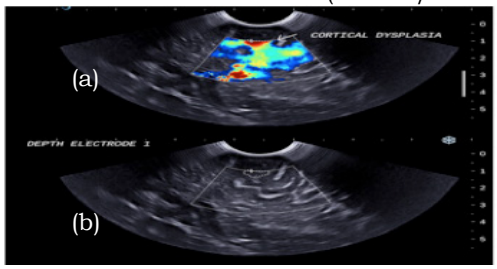

Figure 1: The intraoperative SWE (a) demonstrated an abnormally stiff area 1cm from the brain surface while neither the ultrasound B–mode (b) nor MRI (not illustrated) showed the abnormality.

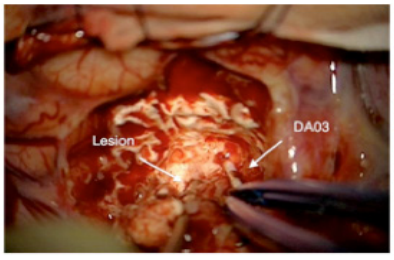

Figure 2: Intraoperative photograph showing the lesion at 1cm from brain surface with the invasive depth electrode *in situ*.

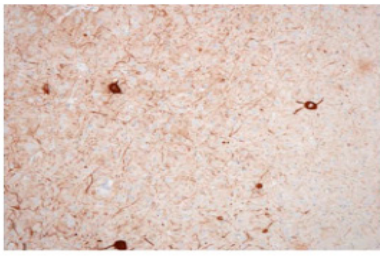

Figure 3: Histology slide showing the presence of balloon cells and dysmorphic neurons, confirming the diagnosis of Type IIb focal cortical dysplasia.

036 **3D RECONSTRUCTION OF *IN VIVO* ARFI AND SWEI IMAGES OF THE PROSTATE.**

Stephen Rosenzweig[1], Mark L Palmeri[1], Thomas Polascik[2], Kathryn R Nightingale[1].*
[1]Duke University Biomedical Engineering, USA; [2]Duke University Medical Center, Durham, NC, USA.

Background: Acoustic radiation force impulse (ARFI) imaging and shear wave elasticity imaging (SWEI) of the prostate have been reported to portray cancer and other pathologies as stiffer than the surrounding tissue [1,2]. While these methods employ similar push excitations, they differ in resolution, contrast and artifacts; SWEI images provide quantitative information, but generally afford poorer resolution and can suffer from reflected wave artifacts [3], whereas ARFI images are typically higher resolution, but do not reflect the true mechanical contrast of the tissue [4].

Aims: The aim of this work is to reconstruct matched ARFI and SWEI images, which are overlaid and compared in order to overcome the challenges of each modality and provide additional information.

Methods: ARFI and SWEI data were collected concurrently, *in vivo*, under an IRB–approved protocol, using a side–fire Acuson ER7B transducer, a Siemens Acuson SC2000 (Mountain View, CA) and a custom transducer rotation stage. The data were then reconstructed in 3D taking advantage of spatial continuity axially, laterally and in elevation as well as left and right propagating shear waves from each push. The custom pulse sequence consisted of rapidly pushing at multiple foci and tracking the resulting displacement on– and off–axis of the push using 16 parallel receive beams for each push location.

Results: To date, data from 7 patients with known prostate cancer have been obtained prior to radical prostatectomy surgery in this ongoing study. Example matched ARFI and SWEI images are shown below where a stiff region has been identified in the basal region of the patient's right side (white circle) as compared to the contralateral region (black circle). The ARFI image contrast is 0.64 and the SWEI image contrast is 0.75; however, the edge resolution is much clearer in the ARFI image as seen at the location of the arrows in the images, indicating the margin of the central gland. Structural information in these modalities is significantly improved over B–mode ultrasound.

Conclusions: We have demonstrated the ability to concurrently acquire ARFI and SWEI data and reconstruct the images utilizing the inherent three dimensional nature of the organ. The high contrast SWEI images allow the user to more readily identify suspicious regions which can then be localized using the ARFI image.

Acknowledgements: This work has been supported by NIH grants EB001040 and CA142824. We thank the Ultrasound Division at Siemens Medical Solutions, USA, Inc. for their technical and in–kind support.

References:

[1] Zhai, L., et al.: Acoustic Radiation Force Impulse Imaging of Human Prostates: Initial *In Vivo* Demonstration. Ultrasound Med Biol, 38(1), pp. 50–61, 2012.
[2] Barr, R.G., et al.: Shear Wave Ultrasound Elastography of the Prostate: Initial Results. Ultrasound Quarterly, 28(1), pp. 13–20, 10.1097, 2012.
[3] Deffieux, T., et al.: On the Effects of Reflected Waves in Transient Shear Wave Elastography. IEEE UFFC, 58(10), pp. 2032–35, 2011.
[4] Nightingale, K., et al.: Analysis of Contrast in Images Generated with Transient Acoustic Radiation Force. Ultrasound Med Biol, 32(1), pp. 61–72, 2006.

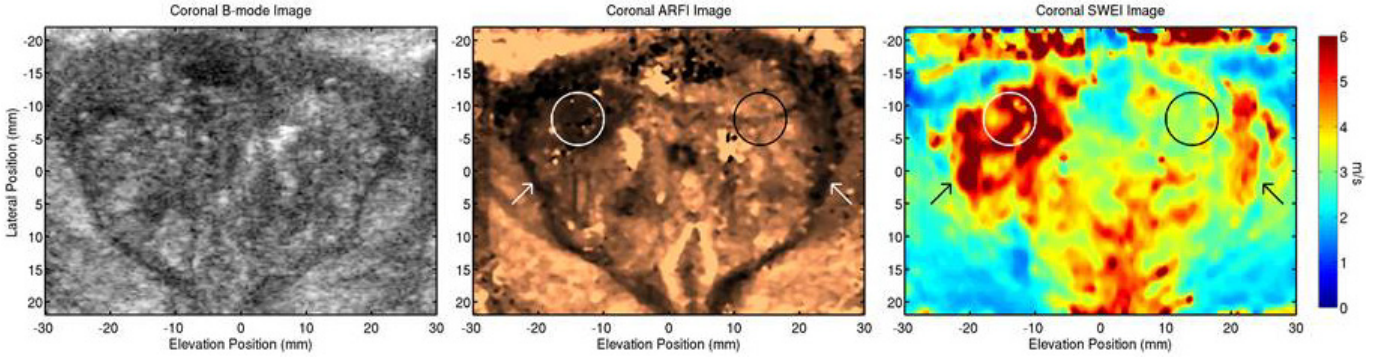

Figure 1: Matched coronal B–mode, ARFI, and SWEI images with the regions for contrast and resolution computations indicated by the circles and arrows, respectively, on the ARFI and SWEI images.

* *indicates Presenter*

046 **ASSESSMENT OF THERAPY-INDUCED TUMOUR NECROSIS WITH MAGNETIC RESONANCE ELASTOGRAPHY.**

Jin Li[1], Yann Jamin[1], Craig Cummings[1], John C. Waterton[2], Jose Ulloa[2], Ralph Sinkus[3], Jeffrey C. Bamber[1], Simon P. Robinson[1].*

[1]CR–UK and EPSRC Cancer Imaging Centre, Division of Radiotherapy and Imaging, The Institute of Cancer Research and Royal Marsden NHS Trust, Sutton, England, UK; [2]Personalised Healthcare and Biomarkers, AstraZeneca, Alderley Park, Macclesfield, Cheshire, England, UK; [3]Centre de Recherche Biomedicale Bichat Beaujon, Clichy, FRANCE.

Background: Magnetic resonance elastography (MRE) provides a quantitative non–invasive approach to image the viscoelastic properties of tissue *in vivo*. Changes in the complex shear modulus G of tumours may provide an emerging imaging biomarker of treatment efficacy. An acute decrease in viscoelasticity has been observed in association with the induction of tumour necrosis following treatment with the vascular disrupting agent CA4P [1]. Improved understanding of the relationship between tumour viscoelasticity and necrosis is of interest to validate the utility of |G| (kPa) as a biomarker of response.

Aims: To investigate and validate the potential of MRE in the detection of drug–induced tumour necrosis.

Methods: SW620 colorectal cancer cells were implanted subcutaneously in the flanks of female CD1 nude mice, in accordance with the UK Animals (Scientific Procedures) Act 1986. MRE data were acquired in anaesthetised mice bearing size–matched SW620 xenografts prior to and 24 hours after treatment with either 200mg/kg of the vascular disrupting agent ZD6126 (n=4), a dose regime known to induce massive central haemorrhagic necrosis [2], or vehicle alone (n=3). 3D MRE data were acquired with a 7 Tesla microimaging horizontal MRI system (Bruker Instruments, Ettlingen, Germany), using a continuous 1kHz sinusoidal wave generated by an electromagnetic shaker (Brüel and Kjaer, Nærum, Denmark), applied directly through a carbon fibre rod to a square piston positioned onto the tumour. Maps of the absolute value of G (i.e., |G|) were reconstructed with an isotropic pixel size of 300μm, and the mean |G| determined from a region of interest covering the whole tumour.

Results: Treatment with ZD6126 resulted in a reduction in |G| in all four tumours (Figure 1), and this reduction was homogeneous across the whole tumour (Figure 2). Mean |G| was significantly reduced from 7.3±0.6kPa to 5.3±0.1kPa ($p<0.05$, Student's t–test) in the ZD6126 treated cohort. The variation of |G| within the treated group was smaller after treatment, most likely a consequence of the massive central necrosis induced by ZD6126.

Conclusions: Tissue viscoelastic properties, as measured by MRE, may provide a robust imaging biomarker for the detection of therapy-induced tumour necrosis.

Acknowledgements: This work was supported by a Dorothy Hodgkin Postgraduate Award from the EPSRC, and by AstraZeneca, The Wellcome Trust and the CR-UK and EPSRC Cancer Imaging Centre.

References:

[1] Jugé, L. et al.: Radiology, 264, pp. 436–444, 2012.
[2] Robinson, S.P. et al.: Br J Cancer, 88(10), pp. 1592–7, 2003.

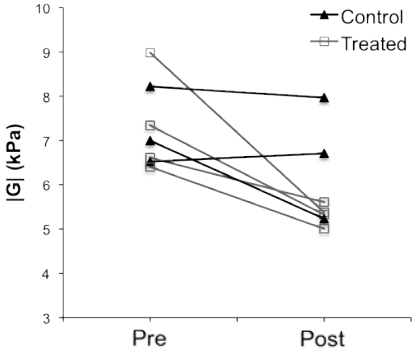

Figure 1: Summary of the effect of ZD6126 or vehicle on tumour |G|.

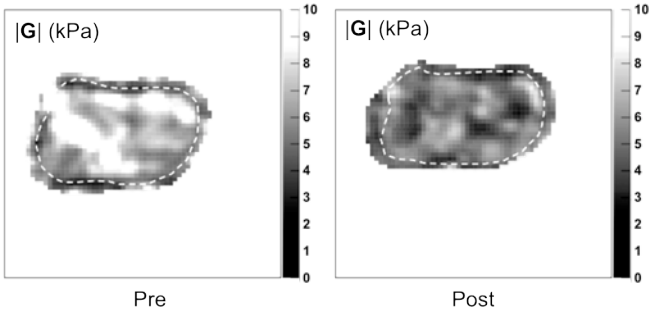

Figure 2: Maps of |G| from one mouse bearing an SW620 xenograft prior to and 24 hours after treatment with ZD6126.

057 **THE ACCUMULATION OF DISPLACEMENT ESTIMATION ERROR OVER LARGE DEFORMATIONS.**

Matthew A. Bayer[1], Timothy J. Hall[1].*
[1]University of Wisconsin–Madison, Madison, WI, USA.

Background: Elastography usually aims to measure the stiffness of tissue, but the elastic nonlinearity may also be a useful diagnostic parameter. Reconstructions of the nonlinearity require displacement estimation over large deformations which must be broken up into steps and accumulated into a final displacement map. Each step contributes an estimation error in the final result. Such a multi–step approach has been used and investigated previously, but previous studies have usually used it as a heuristic in experiment [1], assumed consecutive estimates are independent [2] or were not able to characterize the error properties in detail [3].

Aims: To characterize the error variance of large–deformation accumulated displacement estimates and the covariance between their steps using simulated signals and tracking.

Methods: One–dimensional radiofrequency echo signals were simulated by convolving dense, randomly placed point scatterers with a windowed cosine pulse function. Uncorrelated noise with the same power spectrum as the signal was added to simulate the electronic noise of the system. A total of 20% compressive strain was applied to the scatterers in 180 steps, with a new convolution and noise realization applied at each step. Displacements were estimated by finding the peak of the normalized cross–correlation between signal kernels over a displacement range of one wavelength. Error variances were then measured as a function of stain step size for both single–step and multi–step estimates. The covariance between steps of the accumulated sequences was also measured. All computations were performed in Matlab (The MathWorks Inc., Natick, MA, USA).

Results: Analysis of the covariance between estimation steps shows that errors due to electronic noise are partially anti–correlated and, therefore, tend to cancel out and accumulate slowly. Furthermore, errors due to tissue strain are highly correlated, which together with the single–step dependence on strain, has the effect that accumulated strain–induced error is relatively insensitive to step size, at least for smaller kernels. Tracking kernel length still has a strong effect on the accumulated error. Figure 1a shows the surprisingly weak effects of signal–to–noise ratio (SNR) and step size for a single kernel length, while Figure 1b shows the effects of kernel length for a single SNR.

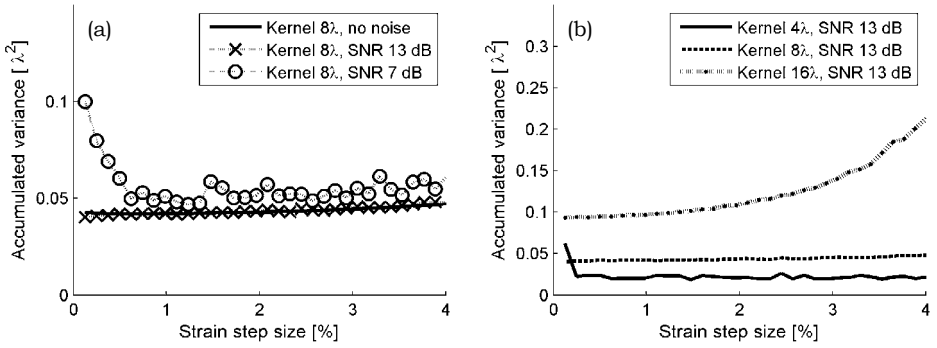

Figure 1: Accumulated variance as a function of strain step size, for varying SNR (a), and kernel sizes (b). Note the different y–axis scales.

Conclusions: These results show that covariance between estimation steps must be considered for a proper analysis of accumulated displacement estimation error. They should also provide guidance for producing more accurate accumulated displacement maps for elastic nonlinearity reconstruction. The simplifying assumptions of our simulations (one–dimensional, uniaxial and uniform strain) may limit their validity when applied to tissue, but they provide a useful and suggestive starting point for more complex experiments.

Acknowledgements: NIH grants R01CA140271 and T32CA009206.

References:

[1] O'Donnell M, Skovoroda AR, et al.: Internal Displacement and Strain Imaging using Ultrasonic Speckle Tracking. IEEE Trans Ultrason Ferroelectr Freq Control, 41(3), pp. 314–325, 1994.
[2] Varghese T, Ophir J: Performance Optimization in Elastography: Multicompression with Temporal Stretching. Ultrasonic Imaging, 18(3), pp. 193–214, 1996.
[3] Du H, Liu J, Pellot–Barakat C: Noise Minimization by Multi–Compression Approach in Elasticity Imaging. Proc IEEE Ultrasonics Symp, pp. 32–35, 2004.

* *indicates Presenter*

067 **MULTI–PARAMETRIC MONITORING OF VISCOELASTIC PROPERTY CHANGES DURING HIFU TREATMENT USING HMIFU *EX VIVO*.**

Gary Y. Hou[1], Danial Shahmirzadi[1], Fabrice Marquet[1], Elisa E. Konofagou[1,2].*
[1]Biomedical Engineering Department, [2]Radiology, Columbia University, New York, NY, USA.

Background: Harmonic Motion Imaging for Focused Ultrasound (HMIFU) is a recently developed radiation–force–based, high–intensity focused ultrasound (HIFU) treatment monitoring method. HMIFU has demonstrated feasibilities both *in vitro* and *in vivo* [1,2].

Aims: The focal oscillatory displacement has been monitored and linked to the relative stiffness changes of the tissues. Here, a multi–parametric evaluation study that includes the displacement and displacement–force phase shift during the entire ablation treatment is performed to investigate viscoelasticity changes *ex vivo*, which were further validated using mechanical testing.

Methods: Liver samples (n=53) were prepared and ablated using four increasing HIFU energies of 36W×10s=360J (n=9; Group 1), 25W×30s=750J (n=15; Group 2), 30W×30s=900J (n=18; Group 3) and 36W×30s=1080J (n=11; Group 4). A therapeutic transducer (f_{center}=4.755MHz, f_{AM}=25Hz, Riverside Research Institute, USA) was used with a confocal pulse–echo transducer (f_{center}=7.5MHz, Panametrics, USA) for simultaneous acquisition of radiofrequency (RF) signals during the excitation with a PRF of 4kHz. A 1–D normalized cross–correlation method (window size: 1mm, 85% overlap) was used on band–pass filtered RF signals to estimate the HMI displacement and phase shift between force and displacement profile during and after ablation. Rheometry (TA Instrument) at 1% shear strain and 10Hz was used to measure the complex shear modulus and stress–strain phase shift.

Results: It was found that the change in HMIFU displacement depended on the ablation energy used. While increasing the ablation energy from Groups 1 to 4, there was an increasing number of cases exhibiting lower displacements (or higher stiffness) post–ablation by 0%, 15% and 60% as the ablation energy increased from Group 1 to 3, respectively. In Group 4, however, all displacements increased indicating lower stiffness at the highest ablation energy. Mechanical testing confirmed this trend with initial ablated–to–normal modulus increase in Groups 1 and 2 (16.8±6.90, 19.5±13.9) and subsequent decrease in Groups 3 and 4 (11.4±9.54 and 12.28±7.42). The phase shift was shown to decrease with ablation between Groups 2 and 4, and mechanical testing confirmed this finding for Groups 2 and 3 (HMIFU: 23.5±18.8°; 8.67±5.58°; 11.9±11.1°; 19.5±8.1°; mechanical testing: 3.92±2.01°; 3.95±1.92°; 11.4±9.54°; 3.71±1.96°). Ablated tissues exhibited increased viscosity and decreased elasticity under the ablation parameters used.

Conclusions: The decrease in elasticity at the highest ablation energies may be attributed to the pulverization of the treated region during boiling (*in situ* peak temperature reached above 107.0°C using barewire T type thermocouple). Both HMIFU and mechanical testing depicted good correlation in the decrease of the phase shift, a parameter independent of acoustic properties. The findings indicate that HMIFU was capable of monitoring viscoelasticy changes of both low and high ablation energy and differentiating between lower ablation energies that led to stiffening through coagulation and ablation energies that lead to softening of the tissue through pulverization.

Acknowledgements: Supported by the National Institutes of Health (NIH Grant R21EB008521, NIH R01EB014496). The authors thank Riverside Research Institute (RRI) for providing the HIFU transducer.

References:

[1] Maleke C. and Konofagou E.E.: Phys. Med. Biol., Vol. 53, pp. 1773–1793, 2008.
[2] Maleke C and Konofagou EE: IEEE Trans. Biomed. Eng., Vol. 57, pp. 7–11, 2010.

080 **SHEAR MODULUS RECONSTRUCTION WITHOUT HOMOGENEITY ASSUMPTIONS: A NEW CURL–BASED FINITE ELEMENT FORMULATION.**

M Honarvar[1], R S Sahebjavaher[1], R Rohling[1], S E Salcudean[1], R Sinkus[2].*
[1]University of British Columbia, Vancouver, CANADA; [2]INSERM UMR 773, CRB3, Paris, FRANCE.

Background: Dynamic elastography involves solving an inverse problem in which the equation of motion or the wave equation is solved for the shear modulus given the displacement measurement data. Due to the nearly incompressible nature of the soft tissue, the dilatational term is very small and cannot be calculated from the measured displacement data. However, the pressure term, which is the product of the Lamé parameter, λ, and the dilatational term, is not negligible [1]. The curl operator can be used to remove this term from the wave equation [2], with the assumption that tissue is locally homogeneous. In regions where there is a high elasticity gradient, this assumption is not satisfied and errors are introduced. In previous work that considers the spatial variation of the shear modulus, Sinkus and co–workers [3] took the first order spatial derivatives of the real–part of the shear modulus into account by estimating the real part of shear modulus with a linear function. We propose a new approach using finite elements.

Aims: To solve for the shear modulus by solving a finite element model based on the curl of the wave equation, without making the assumption of local homogeneity.

Methods: First the curl operator is applied on the wave equation without assuming local homogeneity. After writing the equation in integral form and taking integration by parts we obtain:

$$\int_{\Omega} \varepsilon_{lmi}\mu\left(u_{i,j}+u_{j,i}\right)w_{,mj}\,\mathrm{d}\Omega = \rho\omega^2 \int_{\Omega} \varepsilon_{lmi}u_i\,w_{,m}\,\mathrm{d}\Omega \qquad \text{Equation 1}$$

where ε denotes the Levi–Civita symbol. We use a test function w that is zero and has zero first–order derivatives on the boundary,Ω, so that the boundary integrations become zero. Then Equation 1 is discretized using finite element shape functions and written in matrix form as a linear system of equations with nodal values of shear modulus as unknowns. In order to improve the conditioning of the inverse problem, sparsity regularization [4] and multi–frequency data have been used.

Results: First 2D simulation data (two–component displacements measured over a plane) were used to demonstrate the algorithm. Figure 1 shows the reconstructed shear modulus using the previous curl–based method with the homogeneity assumption (Figure 1a) and the new curl–based method (Figure 1b). Figure 3 shows a comparison of these two methods in the presence of measurement noise. The method was also tested on our previously collected experimental MR elastography data [5] from a CIRS elastography phantom with an excitation frequency of 200Hz. Figure 2 shows the reconstructed elasticity map.

Conclusions: The simulation analysis shows that, in the 2D case, the new method with multi–frequency data is more accurate and stable compared to the previous curl–based method. It was also shown that the new curl–based method can also be applied to MRE data, and all inclusions were visible with similar shapes, sizes and elasticity as the manufacturer's estimated values.

Acknowledgements: This research was supported by Natural Sciences and Engineering Research Council (NSERC).

References:

[1] E. Park and A. M. Maniatty: Phys. Med. Biol., Vol. 51, p. 3697, 2006.
[2] R. Sinkus et al.: Magn. Reson. Med., Vol. 53, pp. 372–387, 2005.
[3] R. Sinkus et al.: Comptes Rendus Mécanique, Vol. 338, pp. 474–479, 2010.
[4] M. Honarvar et al.: Proc.of 10th ITEC, p. 54, 2011.
[5] A. Baghani et al., TMI, Vol. 30 (8), pp. 1555–1565, 2011

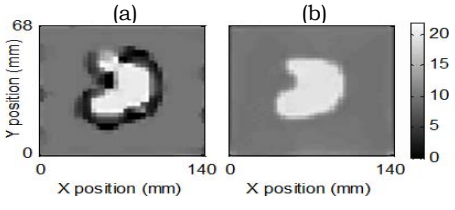

Figure 1: (a) The elasticity map using curl–based method with local homogeneity; (b) using the new curl–based method with multi–frequency data.

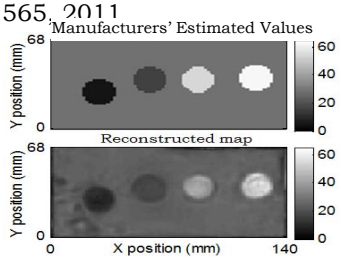

Figure 2: The phantom reconstructed elasticity maps

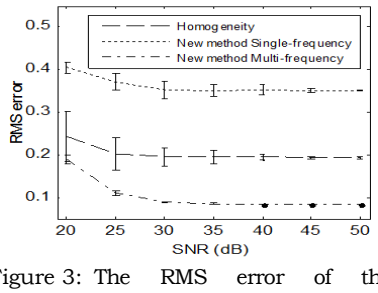

Figure 3: The RMS error of the reconstructed elasticity versus different values of the SNR.

* *indicates Presenter*

083 **IMAGING THE MECHANICAL PROPERTIES OF CELLS.**

D. Thomas Seidl[1], Elizabeth Canović[2], Assad A. Oberai[3], Paul E. Barbone[1], Dimitrije Stamenović[2], Michael L. Smith[2].*

[1]Mechanical Engineering Department, [2]Biomedical Engineering Department, Boston University, MA 02215, USA; [3]Mechanical Aerospace and Nuclear Engineering Department, Rensselaer Polytechnic Institute, Troy, NY 12180, USA.

Background: Traditionally efforts to image the elastic properties of living materials have been applied at the anatomical organizational level of tissues. Cells are complex biochemical machines that are both structural units of a larger system and individual dynamic entities. Engineering models of mechanical cell phenomena (migration, adhesion, spreading, division, etc.) require knowledge of the mechanical properties of cells. Advanced experimental techniques from cellular biomechanics can provide local (sparse) measurements of force and displacement during a controlled deformation of a single cell. These measurements can be used to drive an inverse problem for the spatial distribution of the linear elastic shear modulus over the entire cell. Most of the existing microrheological techniques that measure the mechanical properties of cells yield local (i.e., points in the cell) estimates of material moduli.

Aims: We aim to quantitatively determine the spatial distribution of elastic properties and cytoskeletal prestress within living cells at subcellular spatial and subsecond temporal resolution.

Methods: We investigated the elastic properties of NIH3T3 fibroblasts in this study. The cells were cultured on soft polyacrylamide (PAA) gel substrate (~4–10kPa stiffness) imprinted with a micropattern of 2μm Alexa–633 labeled fibronectin dots on a regularly spaced 6μm grid. The dots were functionalized (and PAA surface left unfouled) so that the cell could only adhere to the dots. Fluorescent 500nm microspheres were phagocytized by the cell before the substrate was deformed uniaxially to 4–10% strain. Cellular traction forces can be calculated by tracking the motion of the micropatterned dots (and knowing the elastic properties of the substrate), and displacements of the nanospheres can be observed in the same manner. Only two images need to be taken during the experiment: one prior to application of uniaxial deformation and another following the motion. The total time of the experiment was less than the time required for substantial remodeling of the cytoskeleton. The cell body was modeled as a linear elastic, isotropic material in plane–stress. We solved the inverse problem for the modulus iteratively by minimizing a displacement data–matching functional constrained to satisfy the elasticity equations.

Results: We were able to match displacements to approximately 0.1μm, which is roughly the expected level of experimental noise. The resulting distributions of cellular stiffness and pre–stress are within the range of expected physiological values.

Conclusions: The results of this study demonstrate the ability to use advanced methods of elastography to quantitatively map the shear modulus and pre–stress distribution within a cell. The temporal resolution depends upon the rate at which the cell can be deformed and imaged (a few seconds), and the spatial resolution depends upon the spacing of the nanospheres (microns).

Acknowledgements: We gratefully acknowledge NIH HL–096005.

References:

[1] S. R. Polio, K. E. Rothenberg, D. Stamenović and M. L. Smith: Acta Biomaterialia, 8, pp. 82–88, 2012.
[2] P. E. Barbone and A. A. Oberai: Phys Med Biol, 52, pp. 1577–1593, 2007.
[3] A. A. Oberai, N. H. Gokhale and G. R. Feijoo: Inverse Probl, 19, pp. 297–313, 2003.

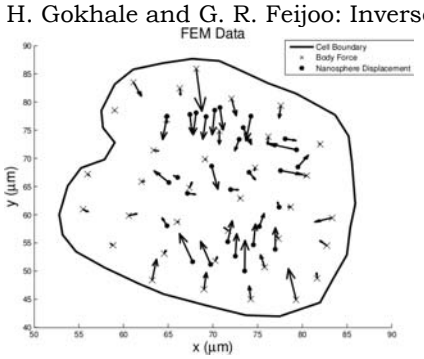

Figure 1: Experimental Data

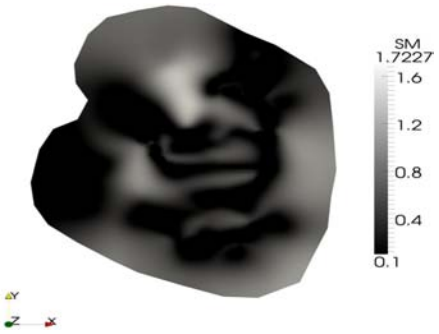

Figure 2: Reconstructed Shear Modulus

001 **MEASURING STRAIN USING THE INVERSE SQUARE RELATION OF RADIATION INTENSITY AND DISTANCE.**

Tareq Alrefae[1].*
[1]Kuwait University, Khaldia, KUWAIT.

Background: Strain is an important quantity in determining elasticity of materials. Knowledge of the amount of elongation or shortening of materials provides key markers that help in assessing its intactness and viability. In addition to being widely available, techniques for strain measurements are diverse in the detection methods of materials' elongation or shortening. For example, elastography, which is applied in biomedical applications, utilizes sonogram techniques in determining strain measurements [1]. Another example is that of strain gages which rely on the sensitivity of electrical properties to change in length. Strain gages are commonly used in mechanical applications [2]. More examples are found in the literature [2]. To further enrich the library of strain measurement techniques, this work presents a simple method that relies on basic radiation measurements. Specifically, the presented method utilizes the inverse square relation of radiation intensity (I) and distance. When this relation is paired with the normal strain (ε) equation, it becomes easy to theoretically relate strain and radiation intensity, resulting in Equation 1.

$$\epsilon = \sqrt{\frac{I_1}{I_2}} - 1 \qquad \text{Equation 1}$$

Aims: The goal of this work is to develop a simple method to measure strain using the inverse square relation of radiation intensity and distance [3].

Methods: The set–up in Figure 1 is arranged with an NaI(Tl) detector (Canberra, USA) and an elastic band as the sample. One end of the elastic band is hooked to a stationary rod, while the other is hooked to a moveable rod. A ^{137}Cs point source is attached to the moveable rod. Both rods are assembled on a bench equipped with a scale that shows the distance between the rods. To measure the angles θ_1 and θ_2 in Figure 1, a long–arm protractor is used. To accommodate for the geometry of the set–up, Equation 1 is modified to the following relation:

$$\epsilon = \sqrt{\frac{I_1}{I_2}\frac{\theta_2}{\theta_1}} - 1 \qquad \text{Equation 2}$$

Results: Figure 2 shows a plot of the strain values obtained from the proposed technique (ε_r) versus strain values taken from the bench scale (ε_a). Ideally, the plot should present a straight line with a slope of unity and a zero y–intercept. The plot, however, deviates from the ideal values. The main reason for such deviation is the stochastic nature of radioactive decay. Overcoming this source of error is achievable by prolonging the dwell time of radiation measurement.

Conclusions: A simple technique is presented to measure strain. This technique, which involves basic radioactivity measurements, is based on the fundamental inverse square relation of radiation intensity and distance. The stochastic nature of radioactive decay poses the main source of error. Overcoming this discrepancy is achieved by prolonging the dwell time of radiation measurement.

References:

[1] Ophir J, Cespedes I, Ponnekanti H, Yazdi Y, Li X: Elastography: A Quantitative Method for Imaging the Elasticity of Biological Tissues. Ultrason Imaging, 13, pp. 111–34, 1991.
[2] Bower AF: Applied Mechanics of Solids. CRS Press, Boca Raton, FL, USA, 2010.
[3] Knoll GF: Radiation Detection and Measurement. Wiley, New York, NY, USA, 2000.

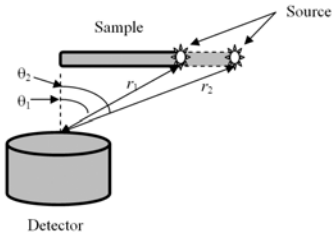

Figure 1: Experimental set–up.

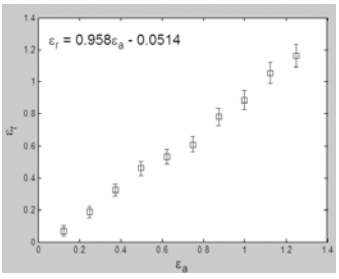

Figure 2: Strain values obtained from the proposed technique (ε_r), versus strain values taken from the bench scale (ε_a).

* *indicates Presenter*

026 **LOW–AMPLITUDE SHEAR WAVES GENERATION IN A BRAIN TISSUE–MIMICKING PHANTOM USING AN ELECTROMECHANICAL ACTUATOR: A PRELIMINARY STUDY.**

Jean–Pierre Remenieras[1], Redouane Ternifi[1], Emmanuel Nicolas[1] and Samuel Callé[1].*
[1]François Rabelais University, UMRS INSERM U930 team 5, 10 bd Tonnelle, 37032 Tours, FRANCE.

Background and Aims: Quantitative measurements of the elastic modulus of cerebral tissue are of interest in biomechanical studies of brain trauma, characterization of brain lesions and such Alzheimer's disease where normal brain tissue is slowly replaced by senile plaques and neurofibrillary tangles. In this preliminary study, we propose to test the feasibility of measuring shear wave propagation in tissue–mimicking phantom material inserted into a human skull.

Methods: Our dynamic elastography method consists of the use of a low–frequency electromechanical actuator (type 4826, Brüel & Kjaer, Denmark) coupled to an ultrafast ultrasound (US) scanner (Aixplorer, SSI, France). A linear US probe, specially designed for brain applications (128 elements, 1.8–4.5MHz bandwidth with a central frequency, f_0, of 2.8MHz), is placed perpendicularly to the tissue in order to follow the shear component (z component) of the wave particle velocity in the x–direction. This probe is controlled using the imaging system whose external trigger synchronizes the low–frequency shaker. With the ultrafast mode of this system, the recorded data are demodulated In–phase and Quadrature (IQ) complex data. These data are taken after the step of beamforming and sampled at f_0 of the US emission. This sample frequency is sufficient because the Doppler signal has a bandwidth centered on zero frequency with a 100% (of f_0) maximum bandwidth. Special attention was paid to the tissue velocity estimator based on "subsample Doppler mean frequency estimation" in the time domain [1]. An axial resolution of 1.5λ, i.e. 0.9mm, is obtained. For each subsample volume at a given depth, the mean Doppler signal is estimated with an observation window of 16 samples, given a temporal resolution of 1.6ms with 50% overlap. The experimental setup is presented in Figure 1a, including the ultrafast US imaging system, function generators, the low frequency amplifier and actuator. This experimental setup has first been validated on a cubic tissue–mimicking phantom with a calibrated elasticity, made of a mixture of SEBS copolymer and mineral oil. The shear source is a 5cm square Plexiglas plate placed on the top of the phantom and the shear wave is considered as a plane wave [2].

Results: Figure 1b shows the particle velocity of the soft medium for different lateral distances, x, at the axial distance, z=2cm, of the array. The x–axis corresponds to the direction of the wave propagation, and the spatial sampling corresponds to the distance between 2 array elements, 300µm. The first element of the linear array is located at the top of the 2D space/time representation shown in Figure 1b. The temporal evolution of the particle velocity recorded at z=2cm / x=X_1 (classically X_1 is 1cm due to the geometry of the experimental setup) and at z=2cm / x= X_{128}=X_1+3.8cm are plotted in blue and red in Figure 1c, respectively. The time delay is due to the propagation of the shear wave for a distance of 3.8cm, and the diminution of the amplitude is due to the viscosity of the phantom (viscous oil was added to increase viscosity). The amplitude of the particle velocity at 100Hz is around 25cm/s. Shear wave phase velocity is estimated in the time domain at 4.7m/s, which gives a Young modulus of 60kPa, in agreement with the calibrated elasticity of the phantom.

Conclusions: This work presents preliminary results of shear wave propagation in tissue–mimicking phantom inserted or not into a human skull. Adaptation of the system for *in vivo* experiments is also in progress in our laboratory.

References:

[1] A. Hoeks et al.: Subsample Volume Processing of Doppler Ultrasound Signals. Ultrasound Med Biol, 20(9), pp. 953–965, 1994.
[2] S. Catheline et al.: Measuring of Viscoelastic Properties of Homogeneous Soft Solid using Transient Elastography: An Inverse Problem Approach. J.Acoust. Soc. Am., 116 (6), pp. 3734–3741, 2004.

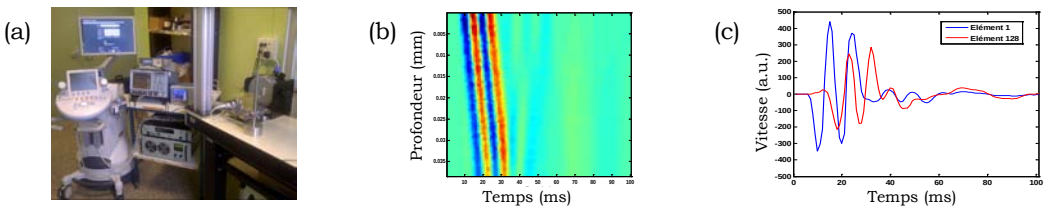

Figure 1: (a) Experimental setup for *in vitro* experiments.
(b) Transient shear wave as a function of the axial distance, x, in the SEBS phantom.
(c) Classical temporal evolution of the particle velocity recorded at z=2cm, x=X1 (blue) and X1+3.8cm (red).

033 **TOWARDS QUANTITATIVE ELASTICITY ESTIMATION BY CROSS-CORRELATION OF SHEAR WAVES.**

Nicolás Benech[1], Javier Brum[1], Stefan Catheline[2], Carlos A. Negreira[1].*
[1]Laboratorio de Acústica Ultrasonora, Facultad de Ciencias, Montevideo, URUGUAY; [2]LabTAU INSERM U–1032, University of Lyon, Lyon, FRANCE.

Background: Green's function retrieval by cross–correlation of diffuse fields has been widely investigated in many areas of physics including elastography [1,2]. In an ideal equipartitioned field, the cross–correlation (CC) computation is equivalent to a perfect time–reversal (TR) experiment [3]. Under this condition, two inversion methods were developed to estimate the shear elastic modulus, μ, in soft tissues: the focal size and the phase method [4]. The focal size method is based on the fact that the focal size of the TR focusing is limited by the shear wavelength. Thus, computing the focal spot size locally would bring a direct estimation of the shear wavelength, λ, if the relationship between them is known. The phase method is based in estimating the time–of–flight of the TR field around the focus. Both methods attempt to estimate the shear wave speed, C, which is related to μ as $\mu = \rho C^2$, where ρ is the material density of the tissue. In previous work, they were applied to image the shear elastic modulus in liver *in vivo* [5].

Aims: The aim of this work is to deepen the investigation of both inversion methods to bring quantitative estimation of the local shear elasticity in soft tissues. In particular, the goal is to establish an analytical relationship between the focal size and λ. On the other hand, a relationship between the time–of–flight and the shear wave speed should also be investigated since it is known that near field effects give diffraction corrections in this case [6].

Methods: In this work a complex low frequency wave field is created in the volume of a tissue–mimicking phantom by randomly tapping its surface with fingers [5]. This wave field is imaged during a 6 second window using an ultrafast electronic (Multichannel device 1000 fps, Lecoeur Electronique, France) with a linear, 64–element array at a frequency of 6MHz. The low frequency field is imaged by a standard speckle tracking technique in a 64x50 points grid within the volume of the sample. The CC field is computed between an arbitrary position, r0, and all other positions of the observation points grid. According to theoretical derivations, the CC field is equivalent to a TR field which converges at r_0 and then diverges. In order to estimate μ from this data, an analytical expression for the TR process in elastic solids is needed. In this work, the spatial focusing profile is derived from the elasto–dynamic Green's function adapted to the soft–solid case.

Results: The analytical expression for the TR field allows for developing inversion algorithms to estimate the shear elastic modulus. Diffraction corrections, coming from near field effects, are easily implemented in both methods to estimate the shear wave speed. When tested in homogeneous phantoms, the results obtained are in good agreement with independent estimations from transient elastography experiments. When tested in heterogeneous phantoms, the quality of the results depends on the contrast between the inclusion and the background. In some cases, artifacts on the final image are observed.

Conclusions: The work presented here represents a step forward in elasticity estimation from the CC field interpreted in the frame of TR. The diffraction corrections included in the inversion algorithm improve the final elasticity image in soft tissues. The results obtained here can be used in imaging modalities like passive elastography from physiological noise [5]. The experimental data suggest that the eventual presence of image artifacts around inclusions are due to scattered waves not taken into account in the inversion algorithm. This topic will be addressed in future works.

References:

[1] J. Brum, S.Catheline, N. Benech, C. Negreira: Shear Elasticity Estimation from Surface Waves: The Time–Reversal Approach. J. Acoust. Soc. Am., 124 (6), pp. 3377–3380, 2008.
[2] S. Catheline, N. Benech, J. Brum, C. Negreira: Time-Reversal of Elastic Waves in Soft–Solids. Phys. Rev. Lett, 100, p. 064301, 2008.
[3] F. Sánchez–Sesma, J. Pérez–Ruiz, F. Luzón, M. Campillo, A. Rodríguez–Castellanos: Diffusive Fields in Dynamic Elasticity. Wave Motion, 45, pp. 641–654, 2008.
[4] N. Benech, S. Catheline, J. Brum, T. Gallot, C. Negreira: 1D Elasticity Assessment in Soft–Solids from Shear Wave Correlation: The Time–Reversal Approach. IEEE Trans. Ultras. Ferroelec. Freq. Control, 56 (11), pp. 2400–2411, 2009.
[5] T. Gallot, S. Catheline, P. Roux, J. Brum, N. Benech, C. Negreira: Passive Elastography: Shear Wave Tomography From Physiological Noise Correlation In Soft Tissues. IEEE Trans. Ultras. Ferroelc. Freq. Control, 58 (6), pp. 1122–1125, 2011.
[6] L. Sandrin, D. Cassereau, M. Fink: The Role of the Coupling Term in Transient Elastography. J. Acoust. Soc. Am., 115 (1), pp. 73–83, 2004.

* *indicates Presenter*

035 **POTENTIAL FOR QUANTITATIVE MICRO–ELASTOGRAPHY USING A MULTI–CHANNEL OPTICAL COHERENCE TOMOGRAPHY.**

E. Elyas[1,2], J.T. Erler[3], S.P. Robinson[2], T.R. Cox[3], D. Woods[4], P.Clowes[1], J.C. Bamber[1,2].*

[1]Joint Department of Physics ,[2]CR–UK and EPSRC Cancer Imaging Centre, The Institute of Cancer Research and The Royal Marsden NHS Foundation Trust, Sutton, Surrey, England, UK; [3]Biotech Research and Innovation Centre (BRIC), University of Copenhagen, Copenhagen, DENMARK; [4]Michelson Diagnostics Ltd, Orpington, Kent, England, UK.

Background: Ultrasound and magnetic resonance elastography provide quantitative images of mechanical properties of tissue such as Young's modulus and have proven invaluable for clinical diagnosis and characterisation of a wide range of tumours. Extension of these methodologies to image mechanical properties on a microscopic scale is expected to provide additional essential information on soft tissue mechanobiology, by facilitating hitherto impossible *in vitro* and *in vivo* experiments to study the relationship between local variations in extracellular matrix stiffness and cellular behaviour, as obtained using established microscopy. Optical coherence tomography (OCT) is an optical backscatter imaging modality with a resolution on the micron–scale. Through its ability to measure sub–micron displacements, such as those associated with shear deformation, OCT is a good candidate imaging modality on which to base a future micro–elastography system.

Aims: This work aims to demonstrate the potential of a novel method for quantitative OCT–based micro–elastography, which takes advantage of unique capabilities of a particular OCT system to simultaneously acquire four parallel spatially-separated optical backscatter A–lines.

Methods: A vibrating needle was used to generate bursts of 4–10 cycles of 500Hz shear waves within gelatine phantoms of varying stiffness. Shear displacements were measured as a function of time and distance from the needle, using four M–mode images acquired simultaneously using a four–channel swept–source OCT system (Michelson Diagnostics, UK). Displacement was arranged to be in the OCT–axial direction and the vibrating needle was positioned within the OCT scan plane so that shear waves propagated along the line from one optical channel to another. Shear–wave speed was then calculated from inter–channel differences of shear–wave arrival time, obtained by cross–correlating the time–displacement signals between channels. A preliminary automated technique was developed for creating 2D elastograms by scanning the four channels together, using the internal mirrors and galvanometers of the OCT system, so as to repeat the measurements at different distances from the needle. Shear wave decay was observed by the same method.

Results: The results confirm that the measured shear–wave speed increases, as expected, in proportion with the gelatine concentration (Figure 1), and the amplitude decreases as gel stiffness rises. The main source of variation in repeat experiments was that associated with gel batch–to–batch differences in shear–wave speed.

Conclusions: This novel technical approach shows promise for the eventual provision of micro–elastography as a research tool in cancer cell biology. Further work is required to optimise the system and to create 3D elastograms.

Acknowledgements: We are grateful to the Institute of Cancer Research, the EPSRC, the CR–UK and the NIHR for funding various aspects of this work and to Michelson Diagnostics for system support.

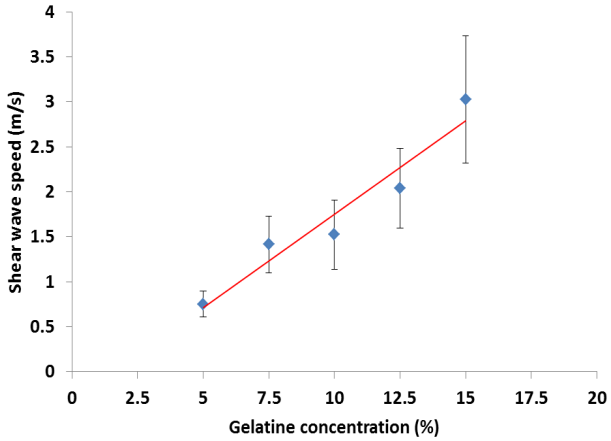

Figure 1: Measured shear wave speed as a function of gelatine concentration. Each data point corresponds to the average of all the measurements obtained using the 4–channel method. The error bars correspond to plus and minus one standard deviation over multiple gels, measurement positions and channel combinations.

* *indicates Presenter*

044 **IMAGE GUIDED PROSTATE RADIOTHERAPY USING CYBERKNIFE: A PRELIMINARY COMPARISON WITH 4D ULTRASOUND.**

Leo Garcia[1], Tuathan O'Shea[1], Emma J. Harris[1], Karen Rosser[2], Rollo Moore[2], Philip M. Evans[3], Jeffrey C. Bamber[1].*

[1]Institute of Cancer Research and Royal Marsden NHS Foundation Trust, Joint Department of Physics, Downs Road, Sutton, Surrey SM2 5PT, England, UK; [2]The Royal Marsden NHS Foundation Trust, Fulham Road, London SW3 6JJ, England, UK; [3]University of Surrey, Faculty of Engineering and Physical Sciences, Guildford, Surrey GU2 7HX, England, UK.

Background: The effectiveness of radiotherapy (RT) is degraded by patient motion from sources such as respiration, the cardiac cycle, bowel movement and intra–fraction variation in patient position. Proposed solutions have included increasing the planning target volume, which increases dose to healthy tissue, and breath–holding techniques, which have limited applicability and do not guarantee a stationary tumor. Instead, a promising research field is image guided radiotherapy (IGRT), in which the patient would be imaged during treatment, measuring tissue motion and accounting for it by gating or adjusting the treatment beam. The CyberKnife (Accuray Inc., Sunnyvale, CA) RT system compensates for tissue motion by tracking fiducial implants within tissue using stereoscopic x–ray imaging combined with infra–red surface markers. This has two disadvantages: surgical implantation of markers and additional ionizing radiation dose to the patient. These problems may be overcome using ultrasound (US) imaging. US delivers no ionizing dose to the patient and has superior soft tissue imaging capability. We have previously demonstrated the feasibility of diagnostic US IGRT for liver tracking [1–3].

Aims: The accuracy and precision of 3D displacement estimates from a CyberKnife x–ray motion tracking system are directly compared to the same motion monitored using a 4D diagnostic US scanner. We hypothesize that US will be at least as accurate as the x–ray system, and so, eventually, be used for imaging during RT of organs such as the liver or prostate that may be visualized by an US probe positioned not to interfere with, or be affected by, the radiation beam.

Methods: Radiofrequency (RF) echo data were acquired using a Gage Compuscope 14200 in a PC running Stradwin 4.6 software (University of Cambridge, UK) and a 4D probe (GE RSP 6–12) interfaced to a DIASUS US scanner (Dynamic Imaging, Livingstone, UK). Gold fiducial implants were injected into an echogenic tissue–mimicking PVA cryogel phantom. The phantom, in a water bath, was translated in 3D using a motorized platform (Galil Motion Control, Rocklin, CA, USA) according to prostate motion schemes derived from *in–vivo* intra–fraction prostate motion data acquired using the Calypso localization system (Calypso Medical, Seattle, WA, USA). The x–ray and US data sets were synchronized using coded motion. A 3D RF cross–correlation block–matching algorithm was used to track US speckle motion, and the results were compared with x–ray tracking of the fiducial markers.

Results: For motion schemes where the prostate position varied slowly, good agreement was found between the defined motion and both the CyberKnife and 4D US tracking systems, with tracking accuracies in the region of ±0.5mm. Rapid prostate movements could not always be followed by the CyberKnife system, whereas US tracking was able to follow all of the motions generated. For the US probe used, tracking performance deteriorated rapidly beyond 3.5cm depth, due to poor echo signal–to–noise ratio. This would not prevent imaging the prostate by transperineal scanning.

Conclusions: This first comparison of 4D US speckle tracking with x–ray fiducial marker tracking suggests the potential to provide US–based tracking of intra–fraction tissue displacements for motion compensation on the CyberKnife RT system, without loss of tracking accuracy and with the potential benefits of high volume rate imaging, no additional ionizing radiation dose and elimination of the need to surgically implant markers.

Acknowledgements: Funding from the Engineering and Physical Sciences Research Council is gratefully acknowledged, as is the help and support from the radiotherapists at the Royal Marsden Hospital.

References:

[1] Hsu A, Miller N, Evans P, Bamber J and Webb S: Feasibility of using Ultrasound for Real–Time Tracking During Radiotherapy. Medical Physics, 32, p. 1500, 2005.

[2] Harris E, Miller N, Bamber J, Symonds–Tayler J and Evans P: Speckle Tracking in Phantom and Feature–Based Tracking in Liver in the Presence of Respiratory Motion using 4D Ultrasound. Physics in Medicine and Biology, 55, p. 3363, 2010.

[3] Bell Lediju M A, Byram B, Harris E, Evans P, Bamber J: *In Vivo* Liver Tracking with a High Volume Rate 4D Ultrasound Scanner and a 2D Matrix Array Probe. Physics in Medicine and Biology, 57, p. 1359, 2012.

** indicates Presenter*

052 **A FAST ACOUSTIC FIELD MAPPING APPROACH BASED ON FABRY–PEROT SENSOR WITH HIGH–SPEED CMOS CAMERA.**

Bing Cong[1], Kengo Kondo[1], Makoto Yamakawa[2], Tsuyoshi Shiina[1], Takao Nakajima[3], Yasufumi Asao[2,3].*
[1]Graduate School of Medicine, Kyoto University, Kyoto 606–8507, JAPAN; [2]Advanced Biomedical Engineering Research Unit, Kyoto University, Kyoto 606–8501, JAPAN; [3]Canon, Inc., Tokyo 146–8501, JAPAN.

Background: A Fabry–Perot (FP) polymer–film–based ultrasound sensor provides an inherently broadband response and excellent detection sensitivity compared to piezoelectric or PVDF transducers. It is thus expected to be used for medical ultrasound imaging, and its application to photoacoustic imaging has been investigated [1]. However, at present, mapping acoustic fields takes much time for scanning, which hinders real–time measurement.

Aims: Mapping acoustic fields in water for imaging purposes, traditional methods need to mechanically scan sensors within a focused laser beam and a stationary photodiode. A method to map acoustic fields with Charge Coupled Device (CCD) array has been proposed [2]. It samples signals of acoustic field by switching the laser irradiation, which is not easy to realize high frequency sampling such as megahertz. Then, we proposed a new approach, which utilizes a high–speed Complementary Metal Oxide Semiconductor (CMOS) camera to map acoustic field without mechanically scanning and to sample signals with the shutter of the camera.

Methods: The system employs a large diameter Tunable Laser Source (TLS) laser beam (TL780–B Thorlabs, Inc.) to illuminate the sensor. The beam reflected from the sensor is imaged by a CMOS camera (Phantom–V710 Vision Research, Inc.) with 128x128 elements (2.56x2.56mm^2). The laser wavelength is swept with an interval of 30 picometre, and one CMOS image is recorded for each step. The images then provide the wavelength dependent reflectivity curve. For each sensor point, the sensor is optimally biased. The CMOS images are recorded at discrete time intervals after the excitation of an ultrasound transducer, and the acoustic fields can be acquired by reconstructing images when the sensor is optimally biased. A megahertz sampling rate can be achieved by recording the CMOS images within the camera's frame rate at different time delays after excitation of an ultrasound transducer since the frame rate of the present CMOS camera is on the order of hundreds of kilohertz.

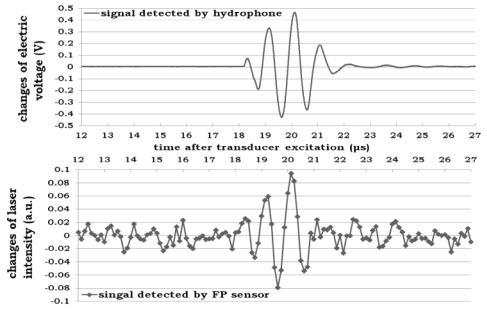

Figure 1: Signal waves detected by hydrophone and FP sensor

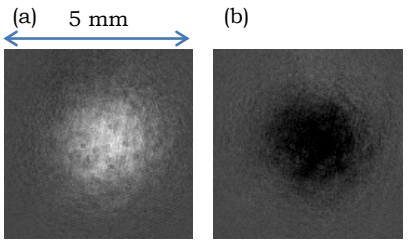

Figure 2: Measured acoustic fields by FP sensor

Results: The system successfully mapped the acoustic field induced by a focused 1MHz PZT transducer (v314–su OLYMPUS, Inc.). The exposure time of CMOS camera was 0.294μs and achieved sampling frequency was 8MHz. The signal waves detected by a hydrophone and FP sensor are plotted in Figure 1a and 1b, respectively. The corresponding acoustic fields induced by the transducer at a positive peak (t = 20.125μs) (negative peak (t = 19.625μs)) are depicted in Figure 2a and 2b, respectively.

Conclusions: The experiment results indicate that an acoustic field can be detected and mapped by using an FP sensor with a high–speed CMOS camera. If the uniformity of the FP sensor and the frame rate of the CMOS camera can be further developed, this approach should be able to provide fast acoustic field mapping with wide–band and high sensitivity, which is useful for high resolution and wide–area image reconstruction of ultrasound images including photoacoustic imaging and tissue elasticity imaging. We believe the development of this approach will expand the usefulness of tissue elasticity imaging.

References:

[1] E. Zhang, J. Laufer, and P.C. Beard: Backward–Mode Multiwavelength Photoacoustic Scanner using a Planar Fabry–Perot Polymer Film Ultrasound Sensor for High–Resolution Three–Dimensional Imaging of Biological Tissues. Applied Optics, 47(4), pp. 561–577, 2008.
[2] M. Lamont and P.C. Beard: 2D Imaging of Ultrasound Fields using CCD Array to Map Output of Fabry–Perot Polymer Film Sensor. Electronics Letters, 42(2), pp. 187–189, 2006.

* *indicates Presenter*

068 **APPLICATIONS OF COHERENCE OF ULTRASOUND AND LOW FREQUENCY WAVES.**

Chikayoshi Sumi[1], Yousuke Ishii[1], Naoto Yamazaki[1], Yuto Hirabayashi[1].*
[1]Sophia University, 7–1, Kioi–cho, Chiyoda–ku, Tokyo 102–8554 JAPAN.

Background: The developments of useful ultrasound (US)–echo–based tissue displacement measurement methods and beamforming methods increase the applications of displacement/strain measurements (e.g. various blood flow, motions of the heart, liver, etc.). For instance, our previously developed combination of the multidimensional autocorrelation method (MAM) and lateral modulation (LM) methods (e.g. [1,2]) or a single beam method (e.g. [3]) resulted in accurate two– or three–dimensional displacement vector/strain tensor measurements. We have also been developing combined digital US diagnosis/treatment systems (e.g. [4]), in which (i) diagnostic US echography can be performed, (ii) a high intensity focused US treatment can also be performed for echo–based and/or radiation–force–based diagnostic measurement/imaging, as well as the combination with diagnostic ultrasound, (iii) radiation force can also be used for echo–based measurement/imaging. For high speed scanning, simultaneous transmissions of plural focused beams or plane waves are also performed. Synthetic aperture processing can also be performed.

Aims: Useful applications of coherence of ultrasound and low frequency waves are performed using such systems. Specifically, spectral frequency divisions and/or coherent superpositions of spectra or echo signals are performed with weighting for yielding (1) high spatial resolution imaging/treatment, (2) accurate displacement vector/strain tensor measurements, (3) desired mechanical and/or thermal sources, (4) desired low frequency deformations or low frequency wave propagations and (5) accurate temperature measurements, etc. Interference of US or low frequency beams/waves are properly used for synthesizing new beamforming/wave parameters such as a wavefront, a propagation direction, a steering angle, frequencies, bandwidths, focuses, etc. Quasi–beams/quasi-waves can also be generated by signal processing (i.e., not physically generated ones). Using several sources also allows the generation of various propagation directions of low frequency waves/various deformation fields. For instance, an anisotropic measurement is allowed. External compressions/vibrations can also be used. Temporal and/or spatial filtering can also be performed in the frequency domain to change beam/wave properties or separate signals or waves (e.g. plural crossed beams/waves, and mechanical and thermal strains, etc.).

Methods: Simulations and agar phantom experiments were performed. The first experiment was the evaluation of generated point spread functions (PSFs), mechanical sources and thermal sources together with the evaluations of generated beams and waves. The generated beams and waves were evaluated in the frequency domain as mentioned above. Alternatively, the generated mechanical and thermal sources were evaluated by estimating autocorrelation functions on received echo signals or by performing the reconstructions of the mechanical and thermal sources using our previously reported solutions for inverse problems. The second experiment was the evaluation of signal–to–noise ratios of generated spectra. This was performed in a frequency domain by the evaluation of the positions of signal spectra moments and a distribution of signal spectra together with the stochastic evaluation of noise spectra.

Results: The PSFs and sources were evaluated for the spectra frequency division and coherent superposition. The geometries of PSFs and sources depended on focus methods and apodization functions such as rectangular, power and Gaussian functions etc. The spectra frequency division and coherent superposition respectively decreased and increased bandwidths (i.e., spatial resolutions). The geometries were also controlled using filtering in a frequency domain (e.g., an imaging beam was generated using concave treatment applicators with variable powers). Signal separations were also possible. The corresponding specific results will be presented in the full paper version of this abstract.

Conclusions: The mixing and division of spectra was effective. The PSF estimated using an autocorrelation function will be used for mechanical and thermal reconstructions. For the use of nonlinearity and harmonic components for imaging and treatment, the US beamforming and generation of the low frequency wave should be performed with simultaneous or successive plural transmissions or vibrations, although the signal processing methods can also be used approximately in any cases. Incoherent superposition with plural spectra divisions was also effective for speckle reduction. All these can also be performed microscopically and will be reported in detail elsewhere.

References:

[1] C. Sumi et al: IEEE Trans. on UFFC, Vol. 55, pp. 2607–2625, 2008.
[2] C. Sumi et al: Reports in Medical Imaging, Vol. 5, pp. 23–50, 2012.
[3] C. Sumi et al: Reports in Medical Imaging (in press).
[4] C. Sumi: Proc of 1st Int Tissue Elas Conf, p. 23, 2002.

* *indicates Presenter*

082 **QUANTITATIVE MODULUS RECONSTRUCTIONS IN NON–RECTILINEAR 3D SCAN GEOMETRIES.**

D. Thomas Seidl[1], Jean–Francois Dord[2], Assad A. Oberai[2], Paul E. Barbone[1], Christopher Uff[3], Leo Garcia[3], Jeffrey C. Bamber[3].*

[1]Mechanical Engineering Department, Boston University, Boston, MA 02215, USA; [2]Mechanical Aerospace and Nuclear Engineering Department, Rensselaer Polytechnic Institute, Troy, NY 12180, USA; [3]Institute of Cancer Research, Joint Department of Physics, 15 Cotswold Rd, Sutton, Surrey SM2 5NG, England, UK.

Background: A number of common ultrasound probe types produce sector–type geometries in the lateral and/or elevation direction. These include phased and curvilinear arrays in 2D imaging and many mechanically swept or electronically steered arrays used for 3D imaging. Such sector geometries present several technical challenges to modulus reconstruction. One is that the direction of sound propagation, and hence the direction in which displacements can be most reliably measured, varies in space. Hence, it is not coincident with the dominant physical motion, which tends to be uniaxial. Modulus reconstructions are performed by matching measured and predicted displacements. Thus, a second challenge is that the displacement matching norm must account for spatial variations the measurement precision. A third challenge is that boundary conditions along the inclined faces of the sector scan can be more difficult to estimate accurately than in a rectangular image.

Aims: To develop, implement and evaluate various measures to address the challenges of modulus reconstruction in a sector scan format, in three dimensions.

Methods: A tissue phantom with stiff a spherical inclusion buried in a less stiff background was made. The background material was 6% gelatin (by weight), while the inclusion was composed of 14% gelatin. In the experiment, the phantom was compressed to 5% strain in increments of 1%. At each loading step, a radiofrequency image was acquired at 66.6MHz sampling rate using a Gage Compuscope 14200 in a PC running Stradwin 4.6 software (University of Cambridge, Cambridge, UK) interfaced to a Diasus ultrasound scanner (Dynamic Imaging, UK) and a GE RSP 6–12MHz 4D probe. The force exerted on the ultrasound probe handle was independently measured and recorded. Two methods to accommodate spatial variation of the measurements were evaluated. In one case, displacements from a parallelopiped region of interest were projected onto regular Cartesian grid for inversion. A second approach involved modifying the objective functional to take arbitrary axial variation into account. To accommodate imprecisely known boundary conditions, new finite elements were developed and implemented that allow displacement conditions to be imposed with a penalty term, and thus allow the user to specify weightings to enforce those conditions.

Results: The projection method gave acceptable results near the inclusion but suffered from boundary artifacts. The functional modification by itself produced relatively poor results throughout due to errors in the boundary conditions. These were improved by the use of new elements to relax boundary conditions.

Conclusions: The combination of the functional modification and boundary condition treatment can significantly improve elastic modulus reconstruction and quantification from sector scan geometries. Further work is necessary, however, to identify a systematic approach to the treatment of boundary conditions in these geometries.

Acknowledgements: We gratefully acknowledge support from NIH–R01CA140271 in the US, and from the EPSRC in the UK.

References:

[1] TG Fisher, TJ Hall, Si Panda, MS Richards, PE Barbone, J Jiang, J Resnick, S Barnes: Volumetric Elasticity Imaging with a 2–D CMUT Array. Ultras in Med and Biol, 36(6), pp. 978–990, 2010.

[2] MS Richards, PE Barbone and AA Oberai: Quantitative Three Dimensional Elasticity Imaging from Quasi–Static Deformation: A Phantom Study. Phys. Med. Biol., 54, pp. 757–779, 2009.

Figure 1: 3D Scan Geometry

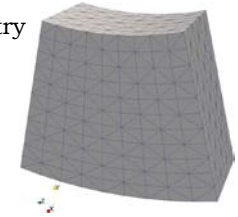

Figure 2: Projection Method Result

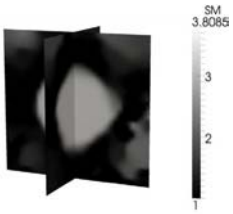

* *indicates Presenter*

Invited Presentation:

091 **EMERGING APPROACHES TO QUANTITATIVE EVALUATION OF THE CERVIX FOR PRETERM BIRTH PREDICTION.**

Helen Feltovich[1,2].*
[1]Ob/Gyn Department, Maternal–Fetal Medicine, Intermountain Healthcare, Provo, UT USA; [2]Medical Physics, University of Wisconsin–Madison, Madison, WI, USA.

Background: A multitude of pathophysiologic pathways culminate in the final common denominator of cervical softening, shortening and dilation that leads to preterm birth (PTB). A precise description of specific microstructural changes to the cervix is imperative if we are to identify the causative upstream molecular processes and resultant biomechanical events associated with each unique pathway. Currently, we have no reliable clinical tools for quantitative and objective evaluation, which likely contributes to the reason the singleton spontaneous preterm birth rate has not appreciably changed in more than 100 years. Fortunately, promising techniques to evaluate tissue hydration, collagen structure and/or tissue elasticity are emerging. These will add to the body of knowledge about the cervix and facilitate coordination of molecular studies, ultimately leading to novel approaches to preterm birth prediction and, finally, prevention.

Aims: The purpose of this work was to review existing and emerging qualitative, semi-–quantitative and quantitative methods of cervical evaluation for preterm birth prediction.

Methods: Tissue hydration, collagen structure and tissue elasticity all change progressively with cervical remodeling: hydration increases, collagen disorganizes and elasticity (softness) increases. Current approaches to microstructural assessment attempt to assess hydration, describe various aspects of collagen structure and/or directly measure some aspect of tissue elasticity. We compiled information about these various approaches by reviewing the literature and talking with the investigators.

Results: Methods focusing on tissue hydration include cervical surface area, electrical impedance, acoustic attenuation and stromal differentiation. Those addressing collagen structure include cervical gland area, light induced fluorescence, second harmonic generation (SHG), Raman spectroscopy and backscattered power loss. Finally, methods addressing tissue elasticity include cervical consistency index, mean gray level, elastography, aspiration and shear wave speed. The promise of these methods for preterm birth prediction/prevention depends on their ability to extract specific information from the cervix and their ease of use.

Conclusions: Ultimately, a combination of these methods (and likely some not yet conceived) seems necessary for comprehensive study of the cervix. An orchestrated approach of complimentary techniques should facilitate novel approaches to the prediction, prevention and treatment of spontaneous PTB.

Acknowledgements: NIH R21HD061896 and R21HD063031

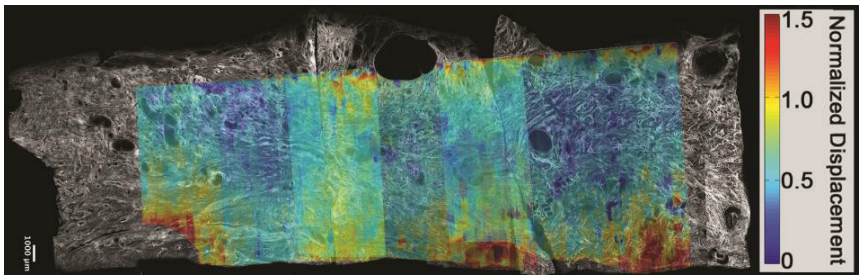

Figure 1: Backscattered Power Loss: A composite SHG image of a 43mm x 13mm longitudinal slice of human cervix showing the B–mode and quantitative ultrasound (QUS) data registered with the SHG image data. The excess backscattered power loss is highest (red) in the region of the central layer, indicating collagen is mostly highly aligned in this area (confirmed by the underlying SHG microscope image).

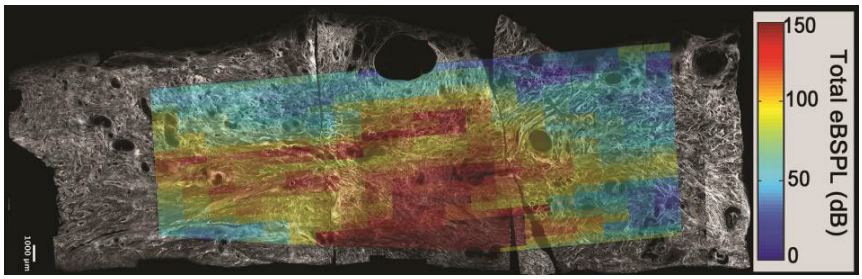

Figure 2: Shear wave speed: SHG and normalized displacement image registered and superimposed, showing that the displacements are uniform in the central layer of the cervix. This suggests that similar shear wave excitation could be induced in the central layer anywhere along the endocervical canal to fully assess that specific area.

* *indicates Presenter*

025 **SHEARWAVE™ ELASTOGRAPHY BE1 MULTINATIONAL BREAST STUDY: ADDITIONAL SWE™ FEATURES SUPPORT POTENTIAL TO DOWNGRADE BI–RADS® 3 LESIONS.**

Fritz KW Schäfer[1], Joël Gay[2], Claude Cohen–Bacrie[2] and David O Cosgrove[3].*
[1]University Hospital, Kiel, GERMANY; [2]Supersonic Imagine, Aix–en–Provence, FRANCE; [3]Imperial College, London, England, UK.

Background: Shear wave elastography has been shown to be useful in aiding classification of breast masses.

Aims: To determine the benefit of ShearWave™ Elastography (SWE™) in the ultrasound characterization of BI–RADS® 3 breast lesions in a diagnostic population.

Methods: 303 BI–RADS 3 lesions (median size: 11mm, range: 46.5) from the multicenter BE1 prospective study population [1,2] were analyzed, of which 201 (66%) had cytology or core biopsy, and the remaining 102 had a minimum follow–up of one year; 8 (2.6%) were malignant. Seven SWE features were evaluated with regards to their ability to downgrade benign BI–RADS 3 masses. The performances of each SWE feature was assessed by evaluating the number of lesions correctly reclassified and the impact on cancer rates within the new BI–RADS 3' lesion group.

Results: No malignancy was found with an E Color "Black to Dark blue", which allowed to downgrade 110/303 benign masses ($p<0.0001$), with a non–significant increase in BI–RADS 3' malignancy rate from 2.6% to 4.1%. E Max≤20kPa could downgrade 48/303 ($p<0.0001$) lesions with a lower increase in BI–RADS 3' malignancy rate (3.1%). No other SWE features were useful to reclassify benign BI–RADS 3 lesions.

Conclusion: Applying simple reclassification rules, SWE assessment of the maximum stiffness of the lesions enabled to downgrade a sub–group of benign BI–RADS 3. This was accompanied by a non–significant increase in the malignancy rate in the new BI–RADS 3 class.

Acknowledgements: We thank Jean–Michel Maixent, PhD, and Pierre–Yves Louis, PhD, University of Poitiers for their support and guidance in the statistical analysis.

References:

[1] Cosgrove DO, Berg WA, Doré CJ, Skyba DM, Henry JP, Gay J, Cohen–Bacrie C, the BE1 Study Group: Shear Wave Elastography for Breast Masses is Highly Reproducible. Eur Radiol, 22, pp. 1023–1032, 2012.

[2] Berg W, Cosgrove D, Doré JC, Schäfer F, Svensson W, Hooley R, Ohlinger R, Mendelson EB, Balu–Maestro C, Locatelli M, Tourasse C, Cavanaugh B, Juhan V, Stavros TA, Tardivon A, Gay J, Henry JP, Cohen–Bacrie C, for the BE1 Investigators: Shearwave Elastography Improves the Specificity of Breast Ultrasound: The BE1 Multinational Study of 939 Masses. Radiology, 262, pp. 435–449, 2012.

064 **ELASTOGRAPHIC FINDINGS COMPARISON OF CANCEROUS BREAST LESIONS OBSERVED *IN VIVO*.**

Elisabeth Brusseau[1], Valérie Detti[1], Agnès Coulon[2], Emmanuèle Maissiat[2], Mojgan Devouassoux–Shisheboran[3], Nawèle Boublay[4], Loïc Boussel[1,2], Jérémie Fromageau[5], Nigel Bush[5], Jeffrey C. Bamber[5].*

[1]CREATIS; CNRS UMR5220, Inserm U1044, INSA–Lyon, Université Lyon 1, 7 av. Jean Capelle, 69621 Villeurbanne, FRANCE; [2]Service de Radiologie, [3]Anatomie et Cytologie Pathologiques, Hospices Civils de Lyon, Hôpital de la Croix–Rousse, 69004 Lyon, FRANCE; [4]Hospices Civils de Lyon, Pôle Information Médicale Evaluation Recherche, Université Lyon 1, EA 4129, Memory Research Centre (CMRR), Lyon, FRANCE; [5]Joint Department of Physics, Institute of Cancer Research and Royal Marsden Hospital, Downs Rd, Sutton, Surrey SM2 5PT, England, UK.

Background and Aims: In previous studies, we reported on the clinical application of our 2D locally regularized strain estimation method and on the use of the mean Normalized Correlation Coefficient (NCC) map to locally provide an indication of reliability for strain image interpretation. Different types of breast lesions were examined, showing great variability in tissue response to compression [1]. In this study, the analysis is refocused on cancers, comparing lesion characteristics between B–mode and strain images and considering the available histological details to better appreciate the contribution of elastography.

Methods: Ten clinical cases of malignant lesions were examined, consisting of five invasive ductal carcinomas Grade I (IDC I), four with Grade II and one with Grade III. In this two–center study, data were acquired at the Hôpital de la Croix–Rousse, Lyon, France, with an Ultrasonix (Sonix RP or MDP) ultrasound scanner equipped with an L14–5W/60 linear probe and at the Royal Marsden Hospital, London, England, with an Acuson 128XP ultrasound system, working with an L7EF probe. Radiofrequency echo data were sampled at 40MHz and processed off–line.

Results: The mean correlation coefficient maps associated with the malignant lesions presented a high mean value that varied between 0.78 and 0.97, with a mean 0.91 over the ten cases considered. In this study, all the malignant masses examined appeared stiffer than the surrounding tissues. In addition, when compared to the corresponding lesions in the ultrasound B–mode images, the stiffer regions in the elastograms frequently appeared significantly larger and with a different overall shape. In Figure 1, elastography results for two IDC II are presented, supplemented with their histological section. For these two cases, we can observe that the agreement between the shapes of the lesions in the *in vivo* images and those in the histological sections tends to be better for elastography than for B–mode imaging.

Conclusions: The differences observed between B–mode and strain images are consistent with previously published findings [2,3]. Determination of the biological significance of the complementary information provided by elastography requires studying the relationship between elastographic and histological details. For future analysis, particular attention will be paid to considering, as far as is possible, the histological section of the whole tumor in a plane corresponding to the imaging plane.

References:

[1] Brusseau et al.: Response to Compression of Different Breast Lesions Observed *In Vivo* with 2D Locally Regularized Strain Estimation Method. Tenth International Tissue Elasticity Conference, pp. 63, 2011.

[2] Garra et al.: Elastography of Breast Lesions: Initial Clinical Results. Radiology, 202, pp. 79–86, 1997.

[3] Itoh et al.: Breast Disease: Clinical Application of US Elastography for Diagnosis. Radiology, 239, pp. 341–350, 2006.

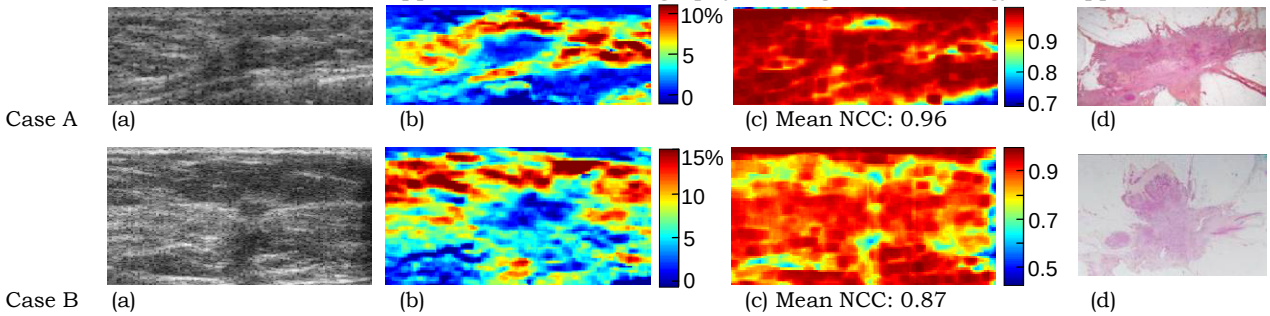

Figure 1: Examples of breast lesion deformation under compression for two IDC II. For each case (a) ultrasound image, (b) strain image, (c) mean NCC map and (d) histological section are shown.

* *indicates Presenter*

086 **COMPARISON OF STRAIN ELASTOGRAPHY, SHEARWAVE ELASTOGRAPHY AND SHEARWAVE ELASTOGRAPHY WITH A QUALITY MEASURE IN EVALUATION OF BREAST MASSES.**

RG Barr[1,2] – Presented by A Milkowski**.*

[1]Northeastern Ohio Medical College, Rootstown, Ohio, USA; [2]Radiology Consultants Inc., Youngstown, Ohio, USA.

Background: Shear wave imaging (SVI) in the breast often codes some cancers as soft. These may have a surrounding ring of high shear wave velocity (V_s) suggesting they are malignant [1]. If the lesion codes soft without a high V_s ring the lesion may be interpreted as benign. The coding of the malignancy as soft can be due to poor shear wave propagation. The addition of a quality measure (QM) can determine if an adequate shear wave formed for accurate measurements.

Aims: The aim of this presentation is to compare the predictive value of strain (EI), SVI without and with QM.

Methods: Patients scheduled for an ultrasound (US) breast biopsy were recruited. In addition to conventional US, EI, and SVI were performed using a modified Siemens S2000 (Siemens Ultrasound, Mountain View, CA, USA) modified to perform SVI with a QM. A 14MHz linear probe was used for conventional US and EI and a 9MHz linear probe was used for SVI. Lesions were evaluated for V_s and the QM. The highest V_s in the lesion or surrounding ring (if present) was used. V_s was classified as benign (less than 4.5m/s) or malignant (greater than 4.5m/s). For strain an EI/B–mode ratio of <1 was considered benign while EI/B–mode=>1 was considered malignant [2]. Results were correlated with pathology. Lesions with no signal or low quality factor are considered not evaluable. ROC curves were obtained.

Results: 144 patients with 166 lesions were enrolled. Patient age averaged 48.5 (18–81yrs). Lesion size averaged 10.6 (5mm to 43mm). Pathology was benign in 110 (66.3%) and malignant in 56 (33.7%). Benign lesions 16 (14.6%) had no SWE signal, 89 (80.9%) were benign on SVI and 5 (4.5%) were malignant. In the malignant lesions SVI had no V_s in 10 (18.1%), 25 (44.6%) were benign, and 21 (37.5%) were malignant. The QM was low in all cases where no SVI signal was obtained. In 19/25 (76.0%) soft malignant lesions, 2/5 (40%) hard benign lesions and 6/89 (6.7%) soft benign lesions. The QM was high in 3/25 (12.0%) soft malignant lesions which were lymphoma. In EI there were 3 false negative lesions all of which were lymphoma. On EI there were 94 true negative lesions, 13 false positive lesions, and 53 true positive lesions. In cases where there was low QM, if the lesion was solid, it was most likely a cancer, and if it was cystic, it was most likely benign.

Technique	# Evaluable	Sensitivity (%)	Specificity (%)	AUCOC
Strain (EI)	163	95	88	0.9595
SVI - QM	166	41	95	0.6756
SVI + QM	138	78	94	0.7988
SVI lowQM solid m	166	93	87	0.9006

Conclusions: Strain (EI) imaging had the highest sensitivity while SVI had the highest specificity (without or with QM). There was a significant improvement in the sensitivity of SVI with the addition of the quality measure; however, an additional 16.9% of cases could not be evaluated. This study is limited being a single center unblinded study.

Acknowledgements: Dr. Barr acknowledges Siemens Ultrasound for a research grant and being a lecturer, Philips Ultrasound for a research grant, being a lecturer, being on an advisory board, and Supersonic Imagine for an equipment grant.

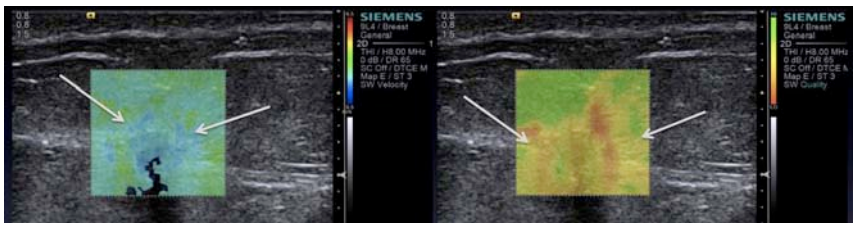

Figure 1: (a) SVI of an Invasive Ductal Carcinoma with a Vs suggestive of a benign lesion. (b) The associated Quality Measure image demonstrates poor shearwave propagation and therefore the lesion is not evaluable.

References:

[1] Berg WA et. al: Radiology, 262(2), pp. 435–449, 2012.
[2] Barr RG et. al: JUM, 81, pp. 281–287, 2012.

088 **TISSUE ELASTICITY AS A MARKER OF PELVIC FLOOR CONDITIONS: CLINICAL RESULTS.**

Heather van Raalte[1], Vladimir Egorov[2], Vincent Lucente[3].*

[1]Princeton Urogynecology, 601 Ewing Street, Suite B–19, Princeton, NJ 08540, USA; [2]Artann Laboratories, 1459 Lower Ferry Rd., Trenton, NJ 08618, USA; [3]The Institute for Female Pelvic Medicine and Reconstructive Surgery, 3050 Hamilton Blvd, Suite 200, Allentown, PA 18104, USA.

Background: Changes in the elasticity of vaginal walls, connective support tissues and muscles are thought to be significant factors in the development of pelvic organ disorders. Previously, we clinically tested the Vaginal Tactile Imager (VTI) which has allowed imaging of the vagina at specified locations and an assessment of the associated tissue elasticity [1,2]. The 3–D vaginal tactile image is a spatial scalar map of stress data (pressures) acquired at a surface of vaginal wall under deformation resulting from applied transvaginal probe with pressure sensors.

Aims: The objective of this study is to estimate ranges of normality for tissue elasticity of vagina and its support structures by means of 3–D tactile imaging.

Methods: This is sub–analysis of the dataset of 57 women recruited for clinical studies. The dataset included 32 women with normal pelvic support and 25 women with pelvic organ prolapse (Stage I–III), average age 59±18 from 21 to 90 years old. Transvaginal probe included pressure sensor array and six degree–of–freedom motion tracking sensor. A standard physical examination was performed by an urogynecologist to characterize pelvic floor conditions. The tissue elasticity (Young's modulus) was calculated from spatial gradients in resulting 3–D tactile image. The vaginal wall deformations were in the range from 5 to 40mm depending on the tissue elasticity under the probe with the applied force not exceeding 10N.

Results: Figure 1 presents a typical example of tactile imaging for normal pelvic floor conditions. The four rectangles in the sagittal plane (Figure 1) at apical and mid–vagina anterior and posterior compartments show areas used for tissue elasticity calculations. Two axial tactile planes in Figure 1 also contain areas for tissue elasticity calculation. We found for normal pelvic support the ranges for tissue elasticity (Young's modulus, kPa) for apical anterior [4.2; 16], apical posterior [3.8; 18], mid anterior [6.0; 25], mid posterior [8.0; 34], and mid lateral vaginal walls [7; 27]. The elasticity values calculated at the mid lateral vaginal walls might be related to the conditions of underlying puborectalis, levator ani and obturator internus muscles, calculated at mid posterior to the rectovaginal fascia and perineal body, apical posterior elasticity to the uterosacral ligaments, anterior elasticity to vesical and pubocervical fascia. We estimated an average value of tissue elasticity for anterior and posterior under prolapse conditions as 2.5±1.1kPa.

Conclusions: Our findings suggest that the normality ranges for tissue elasticity of vagina and its support structures evaluated by VTI might be used as the markers in diagnosis of pelvic floor conditions.

Conclusions: Our findings suggest that the normality ranges for tissue elasticity of vagina and its support structures evaluated by VTI might be used as the markers in diagnosis of pelvic floor conditions.

Acknowledgements: NIH/NIA Grant AG034714.

References:

[1] IEEE Trans. Biomed. Eng., 57(7), pp. 1736–44; 2010
[2] Int. Urogynecology J., 23(4), pp. 459–66, 2012.

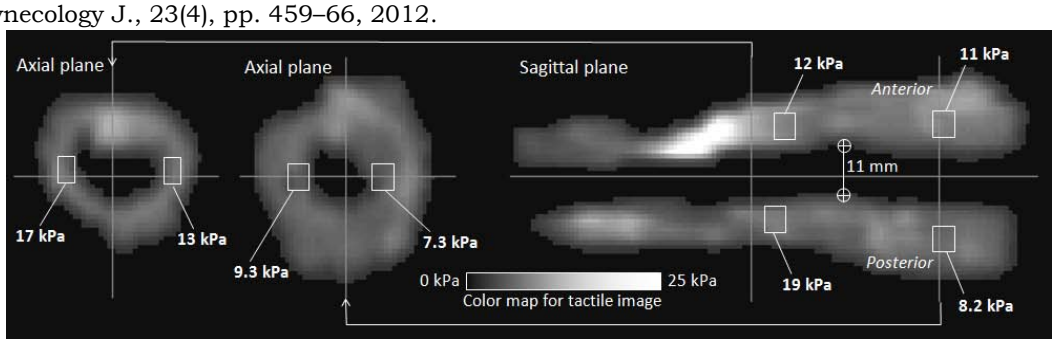

Figure 1: Two axial (mid and apical from left to right), and saggital cross–sections of 3–D vaginal tactile image received with VTI for a patient (53 y.o.) with normal pelvic floor condition as was found by physical examination. Young's modulus was calculated for areas specified by a rectangle.

* *indicates Presenter*

008 **QUANTITATIVE SHEAR WAVE ELASTOGRAPHY OF THE PROSTATE: CORRELATION TO SEXTANT AND TARGETED BIOPSIES.**

Jean–Michel Correas[1], Ahmed Khairoune[1], Anne–Marie Tissier[1], Aline Criton[2], Vassilis Vassiliu[1], Arnaud Méjean[3], Olivier Hélénon[1].*

[1]Radiology Department, Necker Hospital, 149 rue de Sèvres, Paris, FRANCE; [2]SuperSonic Imagine, 510 rue René Descartes, Aix–en–Provence, FRANCE; [3]Urology Department, HEGP Hospital, 12 rue Leblanc, Paris, FRANCE.

Background: For over 30 years, the screening standard for prostate cancer has been the combination of digital rectal examination (DRE) and prostate specific antigen (PSA) test. An abnormal or rising serum PSA level or an abnormal digital rectal examination, triggers further evaluation, typically with transrectal ultrasound (TRUS)–guided sextant biopsies. However, none of these tools for prostate cancer are giving satisfaction. PSA screening leads to a substantial number of unnecessary biopsies in patients with no cancer or with indolent cancer that do not need immediate treatment, with an estimated over–detection rate ranging from 27% to 56% [1]. The false negative rate of prostate biopsy varies from 17 to 21% in patients with a first series of biopsies negative [2, 3].

Aims: Prostate TRUS elastography has been developed in order to identify stiff tissues, as it is well known from DRE that prostate cancer is stiffer than normal prostate tissue. The purpose of this study was to evaluate the performance of real time quantitative Shear Wave Elastography (SWE) for prostate lesion detection and characterization to pathology provided by systematic sextant and targeted biopsies.

Methods: 84 patients presenting increased PSA values (4–15ng/mL, 9.3±7.7) were prospectively enrolled after signing an informed consent form. The prostate was studied using TRUS with spatial compounded B–mode, color Doppler ultrasound (CDUS) and SWE with an Aixplorer ultrasound system (Supersonic Imagine, Aix–en–Provence, France). The prostate was entirely scanned from base to apex in SWE mode for the detection of stiff areas. Twelve elasticity measurements were taken at the level of systematic biopsy sites (in kPa). Additional elasticity measurements were performed for each nodule detected at US by either B–mode or SWE. Ratios between nodules and adjacent parenchyma were systematically calculated. SWE measurements were correlated to systematic posterior sextant biopsies (n=12) and targeted biopsies (n=2–7).

Results: A significant prostate cancer was detected in 40 patients (core size ≥2 mm, Gleason score ≥6). A total of 912 sextant biopsies (with 153 positive cores) and 252–targeted biopsies (with 101 positive cores) on 90 nodules were performed. Among these 90 nodules, 41 corresponded to adenocarcinomas while 49 were adenomyomatous hyperplasia or focal prostatitis. Prostate cancer nodules exhibited higher stiffness (mean 51±45kPa) than the adjacent peripheral gland (mean 22±11kPa; p=0.01). The stiffness ratio between nodule and adjacent parenchyma was significantly higher for cancer (4.0±1.9) compared to benign nodules (1.5±0.9; p<0.002). The cut–off values for highest NPV were for stiffness values 35kPa and for elasticity ratio 1.5 SWE performance (Sensitivity (Se), Specificity (Spe), Positive Predictive Value (PPV), Negative Predictive Value (NPV) and Accuracy (Acc)) was: for SWE values Se=76%; Spe=89%; PPV=89%; NPV=89%; Acc=87%; for SWE ratio: Se=98%; Spe=80%; PPV=80%; NPV=98%; Acc=88%. AUC ROC curve was 0.83 for SWE values and 0.91 for SWE ratio. In 6 patients, no lesion was detected with conventional TRUS, but 3 exhibited a cancer. SWE detected 2 of these 3 cancers, while the third one had a single 3mm positive core. For the 912 systematic biopsies, SWE was positive for 117 of the 153 positive cores (76%). No correlation was found between grade and stiffness as all but 2 lesions were either Gleason 6 or 7.

Conclusions: SWE of prostate is an additional diagnostic imaging method that can be added to routine prostate TRUS for cancer detection and targeted biopsies. Multi–centric clinical trials remain necessary to confirm these preliminary data.

References:

[1] Kelloff GJ, Choyke P, Coffey DS: Challenges in Clinical Prostate Cancer: Role of Imaging. AJR Am J Roentgenol, 192, pp. 1455–1470, 2009.

[2] Singh H, Canto EI, Shariat SF et al.: Predictors of Prostate Cancer after Initial Negative Systematic 12-Core Biopsy. J Urol, 171, pp. 1850–1854, 2004.

[3] Mian BM, Naya Y, Okihara K et al.: Predictors of Cancer in Repeat Extended Multisite Prostate Biopsy in Men with Previous Negative Extended Multisite Biopsy. Urology, 60, pp. 836–840, 2002.

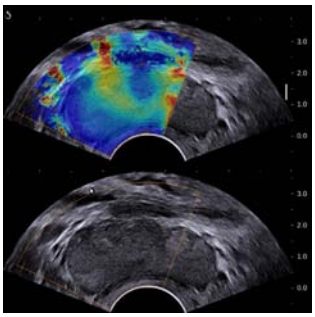

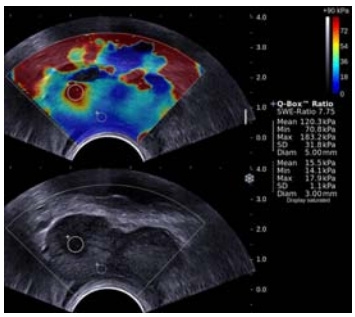

Normal Prostate on SWE Typical Stiff Prostate Cancer on SWE

079 **REAL–TIME STRAIN IMAGING OF THE PROSTATE USING THE ABLATHERM® HIFU DEVICE.**

Lucie Brasset[1], Remi Souchon[1], Stefan Catheline[1], Jean–Yves Chapelon[1], Albert Gelet[2], Olivier Rouviere[2].*

[1]INSERM, Laboratory of Therapeutic Applications of Ultrasound (LabTAU), Lyon, FRANCE; [2]Hospices Civils de Lyon, Edouard Herriot Hospital, Department of Urology, Lyon, FRANCE.

Background: Transrectal high–intensity focused ultrasound (HIFU) has become a reasonable option for the treatment of prostate cancer, with 5–year disease–free survival similar to that of radiotherapy. However, future improvements are desirable in patient selection, localization of the tumor foci, assessment of the volume treated and early detection of recurrence [1]. Previous studies demonstrated that strain imaging has the potential to detect cancer foci [2] and HIFU lesions [3]. However, image quality *in vivo* was suboptimal because acquisition frame rates were low and real time capabilities were missing.

Aims: Develop a fast, real time and stable strain imaging system that can be used during HIFU therapy of the prostate. We hypothesized that high quality strain imaging of the prostate was feasible through the combination of high acquisition frame rate and stable probe positioning (to minimize undesired motion), directional compression (to ensure that the principal direction of displacements coincides with the direction of propagation of the ultrasound beam) and real time feedback (allowing the visual assessment of consistency between consecutive images and corrective action whenever image quality was deemed unsatisfactory).

Methods: Axial images of the prostate were acquired before and after HIFU treatment in five patients. Strain imaging was performed using the transrectal imaging probe integrated in the Ablatherm® HIFU device (Edap–TMS, Vaulx–en–Velin, France) and a Hawk 2102EXL scanner (B&K Medical, Herlev, Denmark) equipped with a research interface. The transrectal probe was attached to a motorized table, thus ensuring stability of the system, and covered with a balloon. The balloon was filled with a coupling liquid to provide acoustic coupling. Prostate compression was performed by filling the balloon. Strain images were calculated and displayed in real time using a time–domain cross–correlation algorithm [4] running on an 8–core computer. The algorithm uses pre–calculated sums to speed–up the calculation [5].

Results: The strain imaging system was capable of imaging the prostate in real time, with a frame rate up to 60 frames per second. Excellent correlation (>0.95) was obtained in most parts of the gland, except in highly hypoechoic areas. The zonal anatomy of the prostate was clearly visible in the strain images in all patients, with a soft peripheral zone and a stiff transition zone. These features were consistent with those previously observed *in vitro* [2].

Conclusions: The system provided high–quality strain images of the prostate in all patients. Future work is now needed to assess the performance of the system for cancer foci detection and for the assessment of the treated volume.

Acknowledgements: The authors gratefully acknowledge EDAP–TMS for technical support.

References:

[1] Rouviere O et al.: Transrectal High–Intensity Focused Ultrasound Ablation of Prostate Cancer: Effective Treatment Requiring Accurate Imaging. Eur J Radiology, 63, pp. 317–327 2007.
[2] Souchon R et al.: Human Prostate Elastography: *In Vitro* Study. Proc IEEE Ultrasonics Symp, pp. 1251–1253; 2003.
[3] Souchon R et al.: Visualisation of HIFU Lesions using Elastography of the Human Prostate *In Vivo*: Preliminary Results. Ultrasound Med Bio, 29(7), pp. 1007–1015, 2003.
[4] Zahiri–Azar R and Salcudean SE: Motion Estimation in Ultrasound Images using Time Domain Cross Correlation with Prior Estimates. IEEE Transactions on Biomedical Engineering, 53(10), pp. 1990–2000 2006.
[5] Luo J and Konofagou EE: A Fast Normalized Cross–Correlation Calculation Method for Motion Estimation. IEEE Transactions on Ultrasonics, Ferroelectrics and Frequency Control, 57(6), pp. 1347–1357, 2010.

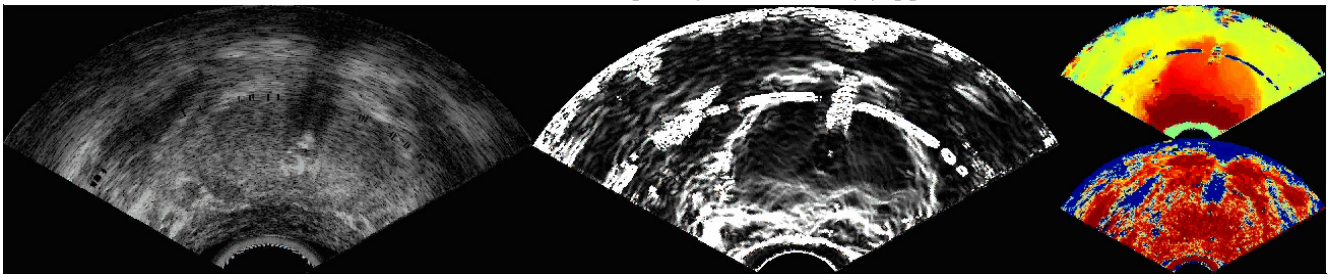

Figure 1: The system provided high–quality strain images, as illustrated by these typical sonogram and strain images. Displacement (upper right) and cross–correlation (lower right) images were displayed in real time and were used for quality control, demonstrating consistent displacements and high (>0.95) correlation.

* *indicates Presenter*

006 **RHEOLOGICAL STUDY OF A POLYMER SPHERE USING A 3–D SHEAR WAVE SCATTERING MODEL IN DYNAMIC ELASTOGRAPHY.**

Emmanuel Montagnon[1,2], Anis Hadj–Henni[3], Cédric Schmitt[3], and Guy Cloutier[1,2,4].*
[1]Laboratory of Biorheology and Medical Ultrasonics, Université de Montréal Hospital Research Center (CRCHUM), Montréal, Québec H2L 2W5, CANADA; [2]Institute of Biomedical Engineering, Université de Montréal, Montréal, Québec H3C 3J7, CANADA; [3]Rheolution Inc., 5795 De Gaspé, #208–B, Montréal, Québec H2S 2X3, CANADA; [4]Radiology, Radio–Oncology and Nuclear Medicine Department, Université de Montréal, Montréal, Québec H3T 1J4, CANADA.

Background: Numerous methods have been proposed to assess biological tissue elasticity in the context of dynamic ultrasound elastography [1]. Viscosity and dispersive effects are generally either neglected or oversimplified by assuming *a priori* rheological models of homogeneous media. To consider heterogeneous media containing mechanical heterogeneities such as tumors, we propose applying a three–dimensional shear wave scattering model [2] in an original inverse problem approach to thoroughly assess the complex shear modulus of a viscoelastic sphere.

Aim: To determine the governing rheological model of a viscoelastic sphere by coupling the ultrasound dynamic elastography technique with a shear wave scattering model.

Methods: A polymer gel (polyvinyl chloride) was prepared by mixing a plastic basis solution and a plastic softener (M–F Manufacturing Co., Fort Worth, TX, USA, #2228LP and #4228S) at different volume ratios. Reference measurements of the polymer mechanical properties between 200–450Hz were performed using RheoSpectris, a viscoelastic spectroscope (Rheolution Inc., Montreal, QC, Canada). Several spheres prepared with this polymer gel were then embedded in a one liter agar–gelatin (4:3 mass ratios) phantom, softer or harder than the polymer sphere. Ultrasound radiofrequency (RF) data were acquired using the V–1 Verasonics scanner (Redmond, WA, USA). Shear waves were induced using either external vibration or acoustic radiation force. Stationary displacement data were extracted from transient shear wave cross–correlations using the fast Fourier transform. The inverse problem considered the diffraction pattern produced by the sphere and consisted in minimizing the difference between experimental and theoretical displacement profiles to assess its storage (G') and loss (G") viscoelasticity moduli.

Results: The polymer viscoelastic parameters estimated by using the external vibrator were very similar to the RheoSpectris–derived results within the 200–450Hz frequency range (Figure 1a). When a local radiation force was used, good agreement between theoretical and experimental displacements was also obtained (see the example of Figure 1c at 230 Hz). In this example, the theoretical model considered the viscoelastic parameters estimated by the inverse problem applied on experimental data (Figure 1b).

Conclusions: In this study, a three–dimensional model–based approach allowed assessing the rheological behavior of a spherical dispersive material. The model remains valid in the case of the acoustic radiation force vibrating source, under the plane wavefront assumption. Applications of these methods aim to characterize mechanical properties of breast tumors.

Acknowledgements: This research was jointly supported by the Natural Sciences and Engineering Research Council of Canada (grant #CHRP–365656–09) and the Canadian Institutes of Health Research (Grant #CPG–95288), and by an infrastructure grant of the Canadian Foundation for Innovation.

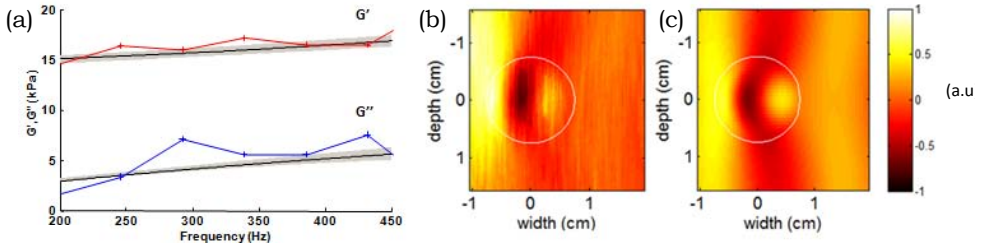

Figure 1: (a) Estimated shear (G') and loss (G") moduli from 200–450Hz. Colored areas indicate means and standard deviations of the reference Rheospectris method. Experimental displacement map at 230Hz (b) obtained by using an acoustic radiation force and estimated theoretical map (c) in the case of a sphere softer than the surrounding medium. Both maps are normalized accordingly to respective maximum displacements amplitude (arbitrary unit).

References:

[1] M. M.Doyley: Physics in Medicine and Biology, Vol. 57, No. 3, pp. R35–R73, 2012.
[2] N. G. Einspruch, E. J. Witterholt, and R. Truell: Journal of Applied Physics, Vol. 31, pp. 806–818, 1960.

015 **ON THE ADVANTAGES OF IMAGING THE AXIAL–SHEAR STRAIN COMPONENT OF THE TOTAL SHEAR STRAIN IN BREAST TUMORS.**

Arun K. Thittai[1], Belfor Galaz[1,2] and Jonathan Ophir[1].*

[1]Ultrasonics Laboratory, Diagnostic and Interventional Imaging Department, The University of Texas Medical School, Houston, TX, USA; [2]Physics Department, Universidad de Santiago de Chile (USACH), Santiago, CHILE.

Background: Axial–shear strain elastography was described recently as a method to visualize the state of bonding at an inclusion boundary. In a previous publication, we have shown further that strain fill–in in asymmetric breast lesions can discriminate between benign and malignant lesions *in vivo* [2]. Although total shear strain elastography was initially proposed for this purpose, it did not evolve beyond the reported Finite Element Model (FEM) and Simulation studies. One of the major reasons for this was the practical limitation in estimating the tissue motion perpendicular (lateral) to the ultrasound (US) beam as accurately as the motion along the US beam (axial). Nevertheless, there has been a sustained effort in developing methods to improve the lateral motion tracking accuracy and thereby obtain better quality total shear strain elastogram (TSSE). We hypothesize that in some cases, even if good quality TSSE becomes possible, it may be advantageous to utilize just the axial–shear strain (one of the components of the total shear strain) elastogram (ASSE).

Aim: To demonstrate that it may be advantageous to utilize only the ASSE to distinguish between firmly–bonded and loosely–bonded asymmetric inclusions instead of the TSSE.

Methods: FEM and corroborating phantom experiments were performed. A 2D plane strain model was built by using the FEM software ANSYS® (Ansys Inc, PA) (details in Ref [1]). The stiff elliptical–shaped inclusion was oriented at 45º with respect to the axis of axial compression and was modeled as being either firmly–bonded or loosely–bonded. For phantom experiments, we utilized previously acquired experimental data obtained from an elastographic experiment performed on "Phantom 4" reported in [2].

Results: Figure 1 compares the images of the axial and lateral components of the total shear strain as predicted by the FEM. The total shear strain, obtained as half the sum of these two components is also shown. Unlike the cancellation of the axial and lateral shear components resulting in a null total shear strain image of the inclusion, the axial– and lateral–shear strains reinforce each other to yield finite non–zero values inside the rotation image. It is easily observed that the rotation image resembles the axial–shear strain image with only very slight differences in the strain pattern outside the inclusion. Figure 2 compares the ASSE, LSSE and TSSE obtained from the phantom experiment. As expected, observe that the LSSE is of appreciably inferior image quality compared to the ASSE. However, despite this limitation, "fill–in" in the inclusion [2] can be visualized only in the ASSE and the LSSE and is essentially absent in the TSSE, as predicted by the FEM results. Also, note that the rotation elastogram has finite values inside the inclusion and resembles the ASSE although it is visibly much noisier.

Conclusions: In this work, we have shown using an FEM and tissue–mimicking gelatin phantom experiments that the dramatic occurrence of fill–in is observable only in the ASSE and not in the TSSE. The results confirm that not only it is advantageous to use ASSE, which is one of the components of total shear strain, but it may be the *only* quality image that can exploit the 'presence' or 'absence' of fill–in to assess the bonding conditions of asymmetric inclusions.

Acknowledgements: Supported in part by NIH grant R21–CA135580–01 and the John S. Dunn Foundation.

References:

[1] Thitai Kumar A, Krouskop TA, Garra BS and Ophir J: Visualization of Bonding at an Inclusion Boundary using Axial–Shear Strain Elastography: A Feasibility Study. Phys Med Biol, 52, pp. 2615–33, 2007.

[2] Thittai AK, Galaz B, and Ophir J.: Axial–Shear Strain Distributions in an Elliptical Inclusion Model: Experimental Validation and *In Vivo* Examples with Implications to Breast Tumor Classification. Ultras. Med. Biol., 36(5), pp. 1–7, 2010.

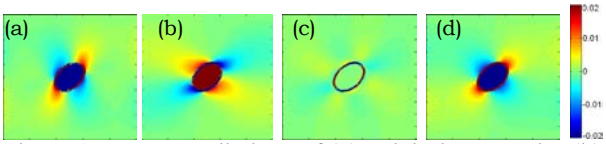

Figure 1: FEM predictions of (a) Axial–shear strain; (b) Lateral–shear strain; (c) total shear strain image and (d) Rotation image.

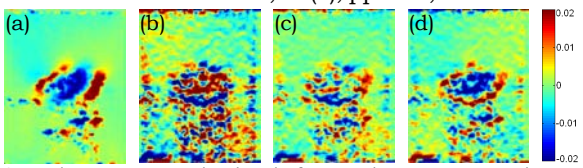

Figure 2: Elastograms obtained from Phantom experiment of (a) ASSE (b) LSSE (c) TSSE and (d) Rotation elastogram. Observe the presence of "fill–in" in ASSE and not in TSSE. Observe also that the image quality of ASSE is appreciably better compared to LSSE, TSSE or Rotation elastogram.

* *indicates Presenter*

018 **INVESTIGATING DIFFERENCES IN SHEAR WAVE SPEEDS IN MOUSE TUMORS WITH DIFFERENT COLLAGEN CONTENT.**

Veronica Rotemberg[1], Taylor Jordan[1], Xuan Cao[1], Mark L. Palmeri[1,2], Fan Yuan[1], Kathryn R. Nightingale[1]*

[1]Biomedical Engineering Department, Duke University, Durham, NC, USA

[2]Anesthesiology Department, Duke Medical Center, Durham, NC, USA

Background: Noninvasive determination of malignancy and response to treatment of tumors is an important clinical goal. Acoustic Radiation Force Impulse (ARFI) and Shear Wave Elasticity Imaging (SWEI) imaging provide an excellent toolset for investigating this problem because they use standard diagnostic ultrasound scanners to interrogate the underlying mechanical properties of tissues noninvasively. Displacement measurements are inversely proportional to tissue stiffness, and high–resolution, qualitative images that reflect the mechanical properties of underlying tissue can be reconstructed from ARFI data. Radiation force can also be used to perform SWEI, where the speeds of the shear waves generated by ARF are monitored to generate quantitative stiffness estimates. Radiation force based methods have been described for characterizing the mechanical properties of tissues and lesions in human prostates [1], livers [2,3], kidneys [4], and breasts [5].

Aims: Radiation force based methods were used to test the hypothesis that stiffness of cancerous tumors could be consistently measured and that tumors with higher collagen content would be significantly stiffer than tumors with lower collagen content [6].

Methods: The study investigated two tumor types using thirteen mice with a 4T1 mouse mammary tumor [7] or B16.F10 melanoma tumor implanted in the right hind limb [6]. Tumors were interrogated using a SIEMENS S–2000TM ultrasound scanner with a 14L–5 linear array. The radiation force excitation and displacement tracking parameters used were a 7.27MHz frequency and lateral focusing (F/1) at 0.35, 0.55 and 0.75cm in depth. The radiation force excitation contained 500 cycles for a 69μs push duration. For each tumor, 3 tumor planes were interrogated with qualitative ARFI images as well as quantitative shear wave speed (SWS) datasets. The SWS datasets acquired 7 radiation force excitation locations spaced 0.8mm apart with 6.35mm of tracking lateral to the push location. A RANSAC–based time–of–flight algorithm estimated shear wave speeds [8].

Results: Mammary tumors had significantly higher SWS than the melanoma tumors (3.57+/-0.62m/s vs. 1.56+/-0.32m/s, respectively, $p<0.01$). The variance seen across melanoma tumors (10.5%) was much smaller than that seen across mammary tumors (38.3%). This could be due to increased heterogeneity in mammary tumors as well as decreased precision of the SWS estimate at higher speeds. The SWS data correlated with the collagen contents in these tumors measured in a previous study [6].

Conclusions: Mammary and melanoma tumors show significantly different shear wave speeds. This successful quantification and differentiation of tumor shear wave speeds in different types of tumors might have future potential for diagnosis and/or treatment monitoring.

Acknowledgements: This work was supported by NIH grants R01 EB002132, R01 CA142824 and T32 GM007171, and F30 DK095544. Special thanks to Siemens Healthcare, Ultrasound Business Unit, Mountain View, for their technical assistance.

References:

[1] Zhai, L., et al.: Characterizing Stiffness of Human Prostates using Acoustic Radiation Force. Ultrasonic Imaging, 32(4), p. 13, 2010.

[2] Palmeri, M.L., et al.: Noninvasive Evaluation of Hepatic Fibrosis using Acoustic Radiation Force–Based Shear Stiffness in Patients with Nonalcoholic Fatty Liver Disease. Journal of Hepatology, 55(3), pp. 666–72, 2011.

[3] Bavu, E., et al.: Noninvasive *In Vivo* Liver Fibrosis Evaluation using Supersonic Shear Imaging: A Clinical Study on 113 Hepatitis C Virus Patients. Ultrasound in Medicine and Biology, 37(9), pp. 1361–73, 2011.

[4] Clevert, D.A., et al.: Evaluation of Acoustic Radiation Force Impulse (ARFI) Imaging and Contrast-Enhanced Ultrasound in Renal Tumors of Unknown Etiology in Comparison to Histological Findings. Clin Hemorheol Microcirc, 43(1–2), pp. 95–107, 2009.

[5] Bai, M., et al.: Virtual Touch Tissue Quantification using Acoustic Radiation Force Impulse Technology: Initial Clinical Experience with Solid Breast Masses. J Ultrasound Med, 31(2), pp. 289–94, 2012.

[6] Henshaw, J., B. Mossop, and F. Yuan: Relaxing Treatment of Solid Tumors: Effects on Electric Field-Mediated Gene Delivery. Molecular Cancer Therapeutics, 7, pp. 2566–-2573, 2008.

[7] Das Roy, L., et al.: Breast–Cancer-Associated Metastasis Is Significantly Increased in a Model of Autoimmune Arthritis. Breast Cancer Res, 11(4), 2009.

[8] Wang, M.H., et al.: Improving the Robustness of Time–of–Flight Based Shear Wave Speed Reconstruction Methods using RANSAC in Human Liver *In Vivo*. Ultrasound in Medicine and Biology, 36(5), pp. 802–813, 2010.

019 **FULLY AUTOMATED BREAST ULTRASOUND ELASTOGRAPHY SYSTEM.**

Reza Zahiri Azar[1,2], Corina Leung[1], Thomas Chen[1], Kris Dickie[1], John Dixon[1], Kwun–Keat Chan[1], Laurent Pelissier[1].*

[1]Ultrasonix Medical Corporation, Richmond, BC, CANADA. [2]University of British Columbia, Vancouver, BC, CANADA.

Background: The automated breast ultrasound system (ABUS) has recently been introduced as a new imaging device for breast screening and monitoring of cancer treatment (Ultrasonix Medical Corp, Richmond, BC, Canada). ABUS enables clinicians to acquire full volumes of the breast tissue in less than a minute. During the exam, the patient lies face down on the ABUS bed while the breast rests inside the imaging dome without undergoing any compression. Once the patient is comfortable, the ABUS automatically rotates a custom concave ultrasound transducer (-12cm radius and 11cm foot print) 360º around the breast tissue to capture full 3D ultrasound volumes. The volume data are then transferred to the viewer for reviewing purposes.

Aim: To add strain imaging capability to the ABUS system for automated 3D strain imaging of the breast.

Methods: The ABUS system is equipped with a motion stage to allow for adjusting the position of the dome with respect to the bed. This position adjustment is used mainly to ensure full tissue contact with the ultrasound transducer as well as making the scanning comfortable for the patient. In this work, this motion stage was used to apply slight compression to the breast tissue. Thus, allowing us to automatically acquire pre– and post–compression radiofrequency (RF) volumes for elastography. To validate the system, an experiment was performed on a breast elastography phantom (Model 059, CIRS, Norfolk, Virginia, USA). The phantom was placed upside down inside the dome and fixed to the bed. First, pre–compression RF volume and the corresponding B–mode volume (400 frames per 360º) were acquired (7cm imaging depth, 384 scan lines, 10MHz transmit frequency and 40MHz sampling frequency). Using the motion stage, the phantom was then compressed approximately one percent. The post–compression RF volume was then acquired using the same settings. Axial displacements and strain images were estimated from these two RF volumes using the cross–correlation algorithm (2mm window size with 75% window overlap) and the least squares strain estimator (3mm kernel size). Finally, both strain volume and B–mode volume were transferred to the viewer for review.

Results: An example of the corresponding coronal, sagittal and transverse views of both B–mode and strain images are shown in Figure 1. This Figure shows that the inclusions which can not be seen in the B–mode views can easily be detected in the strain views.

Conclusions: Compared to the free hand elastography, the proposed automated system is expected to be less prone to strain imaging variations which are introduced by different scanning and compression techniques. Also, the fact that the entire breast tissue is resting in the dome minimizes the unwanted tissue motions and enables the system to reproduce the strain images. Currently the usability of the system in clinical setup is being studied. Further investigations are required to study the effect of the internal tissue motions, due to breathing and heartbeat, in the estimated strain images.

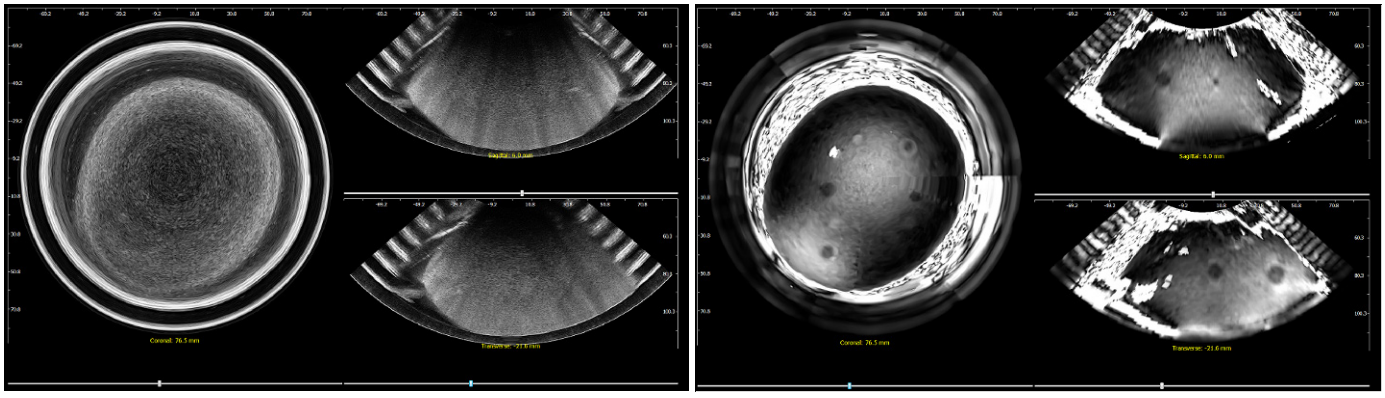

(a) B–mode (b) Strain

Figure 1: An example of corresponding coronal (left), sagittal (top right), and transverse (bottom right) cross sections of B–mode volume (a) and strain volume (b). In the strain views, dark represents low strain value and bright represents high strain value. Also, regions with low correlation coefficients are shown in white.

* *indicates Presenter*

047 ***IN VIVO* MEASUREMENT OF VOLUMETRIC STRAIN FOR THE ASSESSMENT OF INTRAHEPATIC PRESSURE ALTERATIONS.**

Sebastian Hirsch[1], Thomas J. Kroencke[1], Jing Guo[1], Rolf Reiter[1], Sebastian Papazoglou[1], Ingolf Sack[1], Jürgen Braun[2].*

[1]Radiology Department, [2]Institute of Medical Informatics, Charité–University Medicine Berlin, Berlin, GERMANY.

Background: Liver cirrhosis often causes portal hypertension which frequently leads to intestinal bleeding or the buildup of fluid within the abdomen. The distortion of hepatic blood flow due to increased portal pressure can be treated by Transjugular Intrahepatic Portosystemic Stent Shunting (TIPSS). This intervention creates an artificial channel within the liver that establishes communication between the inflow portal vein and the outflow hepatic vein. Successful TIPSS can significantly reduce flow obstructions in the portal area of the liver and therewith reduce portosystemic pressure gradients. In contrast to the classical assumption that soft tissue is incompressible, recent studies report on poroelastic characteristics of brain tissue [1,2], thus motivating us to apply compression–sensitive elastography to the human liver.

Aims: TIPSS is not expected to affect the shear modulus of the liver. Instead, the alteration of intrahepatic pressure conditions may influence mechanical constants related to compression and pressure. As shown by 3D vector–field MRE of lung [3], volumetric strain is sensitive to different pressure states of tissue. In this work, we aimed to test the sensitivity of volumetric strain to TIPSS.

Methods: MRE of the liver was performed in 10 patients with liver cirrhosis before and after TIPSS implantation using a 1.5T MRI scanner with a piezo–electrical vibration generator. The vibration generator was operated with time–harmonic signals of 25 and 50Hz frequency. 3D vector fields were acquired by means of a single–shot EPI sequence in 10 transversal slices of 5mm thickness and 2.73x2.73mm² in–plane resolution. Shear strain and volumetric strain were derived from complex wave fields obtained by Fourier transformation using the curl and divergence operators based on multi–dimensional gradients [4]. The magnitudes of the complex oscillatory divergence and the corresponding curl components were averaged within the entire liver considering the 5 most central slices.

Results: On average, TIPSS reduced the portal pressure by 11.0±2.8mmHg. This pressure change was not translated to the shear modulus (5.5±2.4kPa prior to the intervention and 4.9±2.2kPa post treatment, P=0.46). Shear strain given by the rms of curl components was not significantly altered either (0.13±0.05% vs. 0.12±0.05%, P=0.28). In contrast, volumetric strain showed a significant correlation with TIPSS treatment. The divergence of the harmonic field increased in all 10 patients from mean values of 0.028±0.011% to 0.033±0.014% (P=0.00064), prior and post intervention, respectively. Figure 1 demonstrates the display of shear strain and volumetric strain in a patient and displays the alteration of volumetric strain in both groups.

Conclusions: Volumetric strain is sensitive to the change in hepatic pressure due to TIPSS treatment. The observed reciprocal correlation of volumetric strain with pressure is opposed to the reported increase of volumetric strain in the lungs upon inhalation [3]. This inverse behavior may indicate the intrinsically different nature of pressure development in lung and liver. While lung pressure can be modeled by an air–cavity phantom under external load [3], intrahepatic pressure is communicated by the vascular tree which obeys complex autoregulatory mechanisms [5].

References:

[1] Klatt et al.: Proc. 10th ITEC, Arlington, Texas, p. 115, 2011.
[2] Mcgarry et al.: Proc. of the 20th Conference of the ISMRM, Melbourne, p. 2519, 2012.
[3] Hirsch et al.: Magn Reson Med, doi:10.1002/mrm.24294, 2012.
[4] Anderssen & Hegland: Math Comput, 68, pp. 1121–1141, 1999.
[5] Roadbard: Am Heart J, 65, pp. 648–655, 1963.

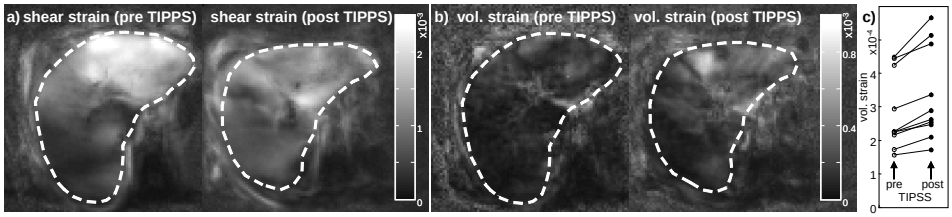

Figure 1: Shear strain and volumetric strain at 50Hz harmonic excitation in human liver. Two stages were examined, once with hepatic hypertension due to flow obstruction in the portal vein and a second time after TIPSS implantation leading to a reduction of hepatic pressure. While shear strain is not altered due to TIPSS (a), volumetric strain is significantly higher in post–TIPPS patients indicating a higher compressibility of liver tissue (b). TIPSS–induced increase in volumetric strain was observed in all patients (c).

* *indicates Presenter*

048 **COMPRESSION SENSITIVE MAGNETIC RESONANCE ELASTOGRAPHY.**

Sebastian Hirsch[1], Frauke Beyer[1], Jing Guo[1], Sebastian Papazoglou[1], Heiko Tzschätzsch[1], Andreas Fehlner[1], Ingolf Sack[1], Jürgen Braun[2].*

[1]Radiology Department, [2]Institute of Medical Informatics, Charité – University Medicine Berlin, Berlin, GERMANY.

Background: Tissue pressure is an important parameter for the diagnosis of various diseases from hepatic hypertension, lung fibrosis to hydrocephalus. The intrinsic pressure of a material is related to its effective compression modulus that scales volumetric strain to pressure [1]. According to the theory of poroelasticity, volumetric strain in biological tissue may arise from the in– and outflow of compartmental fluids like blood or CSF [2,3]. In order to measure compressibility, one needs to analyze local volumetric strain given by the divergence of motion fields.

Aims: The purpose of this study is to test the sensitivity of the divergence of harmonic motion fields measured by 3D MRE to tissue pressure. Tissue pressure is imposed by air pressure applied to agarose phantoms made compressible through inclusion of air bubbles. Three experiments are demonstrated: 1) Rheometer experiments to measure compressibility by static compression; 2) MRE to measure the divergence of the harmonic wave field at different values of excess air pressure and 3) MRE under normal air pressure with increasing motion amplitude for imposing an increasing oscillating pressure.

Methods: Phantoms were built from 1.5% and 0.5% agarose solved in hot water. Gas bubbles were created by adding different amounts of $NaHCO_3$ and citric acid into the hot agarose–water solution, yielding phantoms of variable density and reduced compression modulus as tested by a torsional rheometry device (MCR 301, Anton Paar, Austria) equipped with a circular contact plate (Ø 5cm) and operated in axial motion mode. For MRE, the phantoms were encased in a pressure chamber which was placed in a head cradle [1] inside a 1.5T MR scanner (Siemens Sonata, Erlangen, Germany). 3D vector field MRE was performed as described elsewhere [4]. The divergence of complex wave fields at vibration frequency (50Hz) was calculated based on multi–dimensional derivative operators [5].

Results: Rheometer experiments illustrate that the compression modulus of agarose phantoms decreases with the bulk density, indicating that gas bubbles contribute to the compressibility of the effective medium (Figure 1A). The normalized displacement field divergence increases with external air pressure (Figure 1B), the slope of that relation being correlated with the density of the effective medium (Figure 1C). The expectation value of the magnitude of the oscillating displacement field divergence is linearly dependent on the measured mean displacement field, as can be expected from theory (Figure 1D). The slope of this relation is proportional to the inverse of the compression modulus, 1/K. The comparison of the lines for a phantom with gas bubbles and a solid one yields a ratio of compression moduli of 3 (solid/bubble).

Conclusions: By measuring volumetric strain MRE is sensitive to the inherent pressure and the compressibility of tissue. The introduced phantoms represent a valid model for compressible materials such as lung tissue [1]. However, further work is necessary for modeling the permeation of biological tissue by fluid–filled vessels which may result in a more complex pressure–strain relationship than the model introduced herein.

References:

[1] Hirsch et al.: Magn Reson Med, doi:10.1002/mrm.24294, 2012.
[2] Leiderman et al.: Phys Med Biol, 51, pp. 6291–313, 2006.
[3] Perrinez et al.: IEEE Trans Biomed Eng, 56, pp. 598–608, 2009.
[4] Romano et al.: Magn Reson Med, doi: 10.1002/mrm.24141, 2012.
[5] Anderssen and Hegland Math Comput, 68, pp. 1121–1141, 1999.

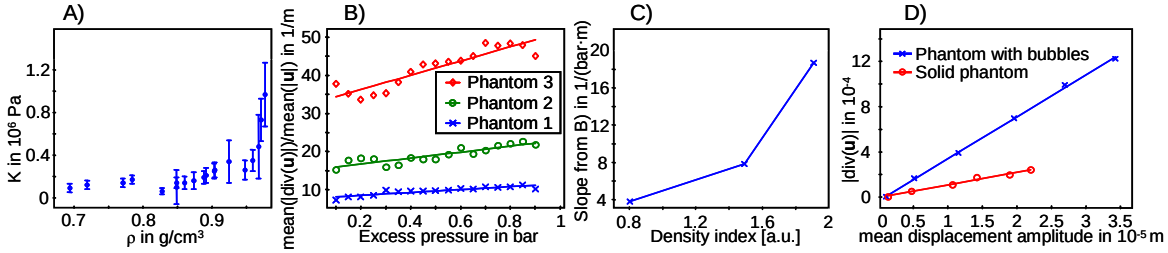

Figure 1: A) Compression moduli of agarose phantom with different gas bubble concentrations obtained from rheometer experiments. B) Dependence of the normalized displacement field divergence on external air pressure for 3 phantoms with different gas bubble concentrations (1: lowest concentration, 3: highest concentration). C) Slopes of the fits from B) as a function of bulk density. The density index is a relative measure of the bubble concentration derived from MRE magnitude images. D) Relation between measured values of |div(u)| and the stimulated displacement amplitude.

* *indicates Presenter*

007 **ELASTICITY IMAGE CALCULATION FROM X–RAY TOMOSYNTHESIS IMAGES UNDER COMPRESSION.**

JG Kim[1], JH Shin[1], SY Lee[1].*
[1]Kyung Hee University, 1732 Deogyeong–daero, Yongin–si, Gyeonggi–do, KOREA.

Background: Ultrasound and MRI have been exclusively used for tissue elasticity imaging owing to their high sensitivity to tissue displacements. But, ultrasound and MRI elastography have not been widely adopted for routine clinical practice of breast cancer detection due to their low image quality.

Aims: We have tried to obtain elasticity images from x–ray tomography images with the motivation that x–ray elastography would be a good complementary solution to the x–ray mammography that suffers from low sensitivity and specificity in detecting early stage breast cancers.

Methods: We made a cylindrical–shaped elasticity phantom, shown in Figure 1a, which has a hard cylindrical inclusion enclosed in a soft background. We took tomosynthesis images of the phantom using a micro–CT by limiting the scan angle to less than 60° degrees. The tomosynthesis images have the in–plane resolution of 74.3μm with the image matrix size of 560x560. Since x–ray imaging signal lacks phase information, we applied amplitude–based image correlation to the two image sets, one obtained with less compression and the other with more compression, to calculate displacements of the feature pattern around a given pixel. The image correlation matrix size was 40x40x40, which limited the spatial resolution of resulting displacement images. We calculated the displacements for all the pixels, and we derived the strain map by applying differentiation to the displacement maps.

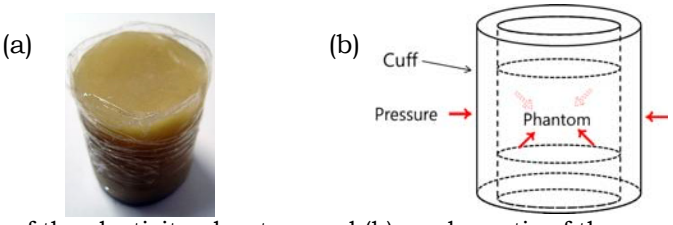

Figure 1: (a) A photograph of the elasticity phantom and (b) a schematic of the compressing device.

Results: We have shown the displacement map on the lateral plane in the middle of the phantom in Figure 2. The displacement maps have been obtained with varying the compressing force and compared with the FEM analysis results. The displacement maps show high correlation with the maps calculated by FEM simulation on the 3D phantom model. Figure 2c shows the corresponding strain maps derived from the displacement image.

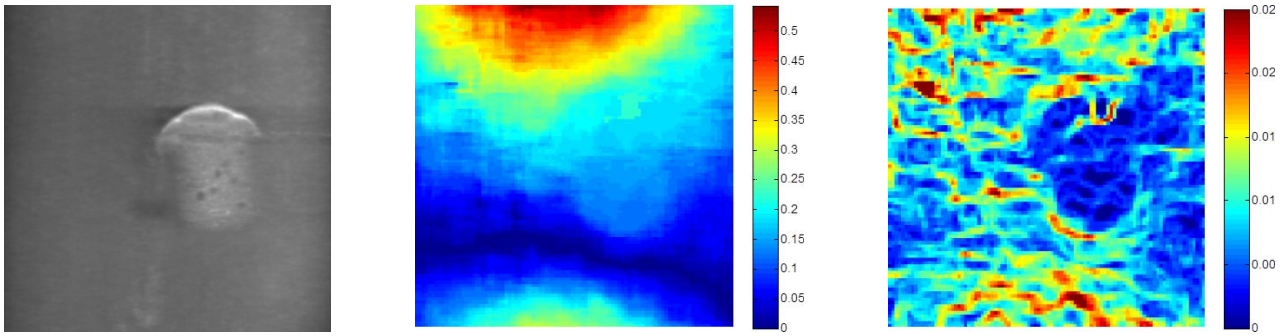

Figure 2:(a) Tomosynthesis Image; (b) Displacement Map; (c) Strain Map.

Conclusions: The strain images have high level of noise and artifacts as compared to static ultrasound elastography images. However, we believe the experimental results suggest a possibility of x–ray elastography.

Acknowledgements: This work was supported by the National Research Foundation of Korea (NRF) grant funded by the Korea government (No: 2009–0078310).

References:

[1] J. Ophir et al.: Proceedings of the Institution of Mechanical Engineers, Part H: J Eng. Med, 213(3), pp. 203–233, 1999.
[2] J. Bishop et al.: Phys. Med. Biol, 45, pp. 2081–2091, 2000.

027 **ELASTIC MODULUS RECONSTRUCTION FOR TRANSVERSE VASCULAR CROSS–SECTIONS WITH AND WITHOUT COMPOUND STRAIN IMAGING.**

HHG Hansen[1], Michael S Richards[2], Marvin M. Doyley[2], Chris L. de Korte[1].*
[1]Radboud University Nijmegen Medical Center, Geert Grooteplein 10, Nijmegen, THE NETHERLANDS;
[2]University of Rochester, Hopeman Engineering Building, Rochester, NY, 14627, USA.

Background: Atherosclerotic plaques with a large soft lipid pool and a thin fibrous cap are more prone to rupture than fibrotic plaques [1]. The elastic Young's modulus for both types of plaques differs. Young's modulus images can be derived from displacement maps of the arterial wall obtained after deformation [2].

Aims: This study investigated if the reconstruction of relative Young modulus images for transverse vessel cross–section could be improved by using beam steered acquisitions and subsequent compounding of the angular axial displacement estimates [3,4].

Methods: Three vessel phantoms were created from gelatin–agar solutions: homogeneous phantoms with a concentric and an eccentric lumen and a two–layered phantom with a soft layer inside and an eccentric lumen. Radiofrequency (RF) data were obtained of the phantoms before and after 4mmHg intraluminal pressure increase at beam steering angles of -30º, 0º and 30º using a linear array transducer (L11–3, Philips, f_c = 7.5MHz). In analogy to these experiments, RF data were simulated for a similar transducer using Field II© [5]. 2D displacements for each angle were estimated using a coarse–to–fine 2D cross–correlation based algorithm. Relative Young's modulus images of the phantoms were constructed using the 0º axial displacement field combined with either the 0º lateral displacement field or the lateral displacement field obtained by compounding the axial displacement fields of +30º and -30º beam steering. To compare the accuracy of the modulus reconstruction the median absolute differences between the axial and lateral displacements input to and output by the reconstruction method were calculated. Furthermore, for both approaches the median and inter–quartile range (IQR) of the relative modulus estimates for each separate phantom layer were calculated and compared to the real values.

Results: The median difference between lateral displacements used as input for the reconstruction and those corresponding to the reconstructed modulus image was reduced by a factor two to three when using the lateral displacements derived from compounding instead of 0º lateral estimates. The relative Young's modulus images also became more accurate when using compounding: the IQR reduced approximately a factor 2 compared to the images derived from 0º estimates only.

Conclusions: Compounding enables a more accurate reconstruction of the relative Young's modulus for vascular structures in a transverse imaging plane than 0º imaging can. However, future studies will have to be performed to show the suitability of this technology for vulnerable plaque detection.

Acknowledgements: This research is supported by the Dutch Technology Foundation STW (NKG 07589), Applied Science Division of NWO and the Technology Program of the Ministry of Economic Affairs. The authors also acknowledge Philips Medical Systems for their support.

References:

[1] Finn et al.: Arteriosclerosis Thrombosis and Vascular Biology, 30, pp. 1282–92, 2010.
[2] Richards et al.: Physics in Medicine and Biology, 56(22), pp. 7223–46, 2011.
[3] Hansen et al.: Physics in Medicine and Biology, 55(11), pp. 3201–18, 2010.
[4] Techavipoo et al.: IEEE Transactions on Medical Imaging, 23(12), pp. 1479–89, 2004.
[5] Jensen et al.: Medical and Biological Engineering and Computing, 34(Suppl. 1, Pt 1), pp. 351–53, 1996.

* *indicates Presenter*

055 **MULTI–SCALE COMPRESSION–BASED QUANTITATIVE ELASTOGRAPHY AND ITS APPLICATION TO BLOOD PRESSURE ESTIMATION.**

AM Zakrzewski[1], SY Sun[1], MW Gilbertson[1], B Vannah[1], L Chai[1], J Ramos[1], BW Anthony[1].*
[1]Massachusetts Institute of Technology, Cambridge, MA, USA.

Background: Quantitative compression–based elastography provides a method for doctors to identify pathological tumors using elastic modulus estimations. Current quantitative implementations of elastography use few assumptions but must be faster for use in a clinical setting.

Aims: This study aims to improve the speed of current elastography methods and to apply these methods to estimate blood pressure and arterial wall stiffness.

Methods: In order to generate the necessary input into the quantitative elastography model, pre–compression and post–compression radio frequency data are simulated with Field II while a cross–correlation displacement tracking technique estimates the tissue displacement field [1]. The inverse problem is uniquely solved in Matlab using the Levenberg–Marquardt non–linear optimization scheme [2], and the associated geometrically non–linear, materially linear elastic forward problem is solved in the commercially available finite element package Abaqus. A coarse–to–fine multi–scale approach is used such that each finite element's elastic modulus is iteratively interpolated onto an increasingly finer mesh. In order to confirm the validity and utility of the multi–scale algorithm, elastography was performed on experimental copolymer and mineral oil phantoms [3] using a Terason 3000t system and a high–fidelity force–controlled ultrasound probe [4]. The multi–scale technique is also used to estimate simultaneously the elasticity of soft tissue, blood pressure, and arterial wall stiffness from radio frequency data simulated with Field II. In order to solve this inverse problem and minimize the objective function, the blood pressure and arterial wall stiffness are included as additional variables to optimize, along with the material stiffness of each finite element.

Results: Using the multi–scale approach described above, the elastic modulus of soft tissue containing a stiff inclusion is reconstructed in 20–25 iterations to within 5% of the true value in simulations and to within 5% of the measured value in phantoms. Simulation models that include blood pressure and an arterial wall (Figure 1) reconstruct the pressure, artery stiffness and bulk stiffness to within 5% of the known values. The accuracy of the blood pressure and artery model suggests that this method can be applied clinically for non–invasive continuous blood pressure measurement.

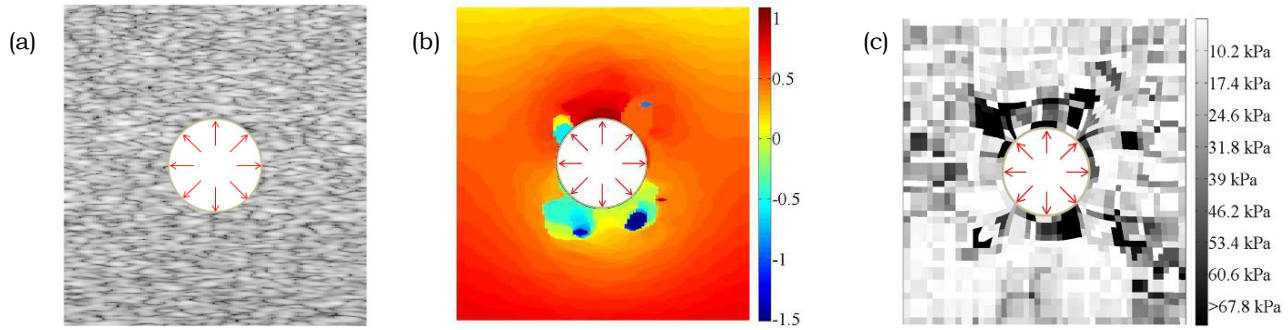

Figure 1: Elastography performed on simulated data to reconstruct arterial wall stiffness, blood pressure and soft tissue stiffness. (a) The B–Mode image is shown with an artery and blood pressure; (b) the axial displacement has been calculated; (c) the elasticity distribution is shown. In this Figure, the true soft tissue stiffness, arterial stiffness and blood pressure are 15kPa, 400kPa and 80mmHg, respectively.

Acknowledgements: This work was supported by General Electric Global Research based in Niskayuna, NY. Kai Thomenius is acknowledged for his insight and suggestions to improve this work.

References:

[1] Sun SY, Anthony BW, Gilbertson MW: Trajectory–Based Deformation Correction in Ultrasound Images. SPIE Conf. Medical Imaging, 2010.
[2] Han L, Noble JA, and Burcher M: The Elastic Reconstruction of Soft Tissue. IEEE Int. Symp. Biomedical Imaging, pp. 1035–1038, 2002.
[3] Oudry J, Bastard C, Miette V, Willinger R, Sandrin L: Copolymer–in–Oil Phantom Materials for Elastography. Ultrasound Med. Biol., Vol. 35, pp.1185–1197, 2009.
[4] Gilbertson MW, Anthony BW: Impedance–Controlled Ultrasound Probe. SPIE Conf. Medical Imaging, 2011.

056 **RECONSTRUCTING THE MECHANICAL PROPERTIES OF CORONARY ARTERIES FROM DISPLACEMENTS MEASURED WITH A SYNTHETIC APERTURE ULTRASOUND IMAGING SYSTEM.**

Steven J. Huntzicker[1], Sanghamithra Korukonda[1], Marvin M. Doyley[1].*
[1]University of Rochester, Rochester, NY, 14627, USA.

Background: A stroke may occur when an atherosclerotic plaque ruptures in the carotid artery. Non–Invasive Vascular Elastography (NIVE) visualizes the strain distribution within the carotid artery, which is related to its mechanical properties. However, NIVE elastograms are difficult to interpret because strain is displayed in Cartesian rather than Polar Coordinates. Transforming axial and lateral displacements measured with a synthetic aperture (SA) ultrasound imaging system to the vessel coordinate system can resolve this problem [1]. However, strain provides only approximate estimate of tissue mechanical properties [2].

Aims: In this work, we explore the feasibility of computing shear modulus and Poisson's ratio from displacements measured with a synthetic aperture ultrasound imaging system [1,3].

Methods: The finite element method (FEM) and the Field II acoustic model were used to synthesize pre– and post–deformed radiofrequency (RF) echo frames of the carotid artery under different physiological conditions. A SONIX RP ultrasonic imaging system (Ultrasonix, Richmond, BC, Canada) equipped with a 128–element linear transducer array (L38/14–5 probe) and a multichannel data–acquisition system (Sonix DAQ®, Ultrasonix, Richmond, BC, Canada) was used to acquire sparse–array data from a heterogeneous vessel phantom. This scanner was programmed to acquire sparse–array data with seven active transmission elements and 128 reception elements. In both the simulated and phantom studies, we estimated axial and lateral displacements by applying a two–dimensional echo tracking method to the beam–formed RF echo frames. We estimated shear modulus and Poisson's ratio elastograms by applying a constrained two–parameter iterative inversion method to the axial and lateral displacements.

Results: Figure 1 shows a representative example of elastograms (shear modulus, Poisson's ratio, axial, and lateral displacements) obtained from the heterogeneous vessel phantom. The modulus contrast recovered from the vessel phantom agreed well with those estimated by independent mechanical testing. More specifically, using a Landmark Servo–Hydraulic Test System (MTS, Minnesota, USA) and a 5–lb load cell, the modulus contrast between the plaque and the vessel wall was 1.7±0.04. A modulus contrast of 1.65±0.02 was estimated from the recovered modulus elastograms. The simulation study also revealed similar observations. The Poisson's ratio elastograms revealed a small modulus contrast which was not observed in the simulation study.

Conclusions: Axial and lateral displacements estimated from beam–formed SA data were good enough to produce useful shear modulus and Poisson's ratio elastograms of the carotid artery. We plan to conduct more detailed studies to further evaluate the potential of model–based elastography in NIVE.

Acknowledgements: A National Heart and Lungs Research Grant (R01 HL088523) funded this work.

References:

[1] Korukonda, S. Doyley, M.M.: Estimating Axial and Lateral Strain using a Synthetic Aperture Elastographic Imaging System. Ultrasound Med. Biol., 37, pp. 1893–1908, 2011.
[2] Doyley, M.M.: Model–Based Elastography: A Survey of Approaches to the Inverse Elasticity Problem. Phys. Med. Biol., 57(3), pp. R35–R73, 2012.
[3] Korukonda, S. Doyley, M.M.: Visualizing the Radial and Circumferential Strain Distribution within Vessel Phantoms using Synthetic Aperture Elastography. IEEE Trans on Ultras and Ferr and Freq Cntrl, (in press).

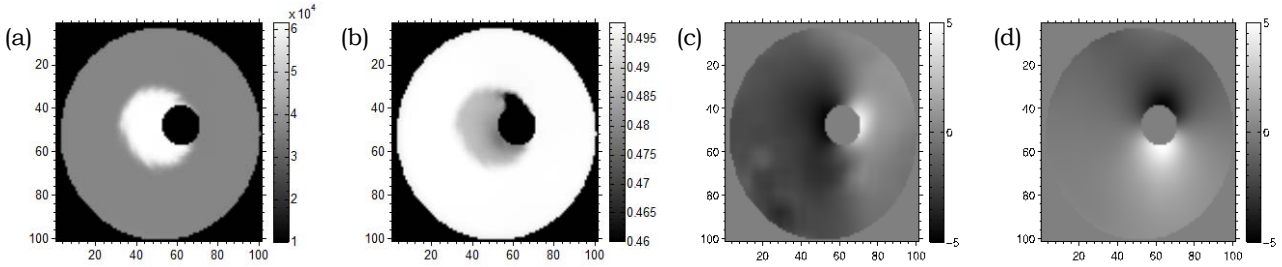

Figure 1: (a) Young's modulus (units kPa); (b) Poisson's ratio; (c) x–coordinate displacement (x1E5/m); (d) y–coordinate displacement (x1E5/m).

* *indicates Presenter*

063 **THE ADJOINT WEIGHTED EQUATION (AWE) METHOD FOR THE SOLUTION OF INVERSE PROBLEMS OF INCOMPRESSIBLE ISOTROPIC ELASTICITY**.

Uri Albocher[1], Isaac Harari[1], Paul E. Barbone[2], Assad A. Oberai[3].*
[1]Tel Aviv University, Tel Aviv, ISRAEL; [2]Boston University, Boston, MA, USA; [3]Rensselaer Polytechnic Institute, Troy, NY, USA.

Background: In quantitative elastography, inverse problems of elasticity are solved for material property distributions (e.g., shear modulus). Typically, the problems are solved using iterative optimization approaches where the difference between a measured displacement field and a predicted displacement field (calculated from the momentum equation) is minimized. These methods are considered robust and handle partial displacement measurements well, but are computationally expensive. In cases where full field measurements of all displacement components are available, direct (non–iterative) approaches can be considered. Here, the measured displacement data are inserted into the momentum equation, and the equation is solved for the sought material properties directly. This procedure does not involve any iterations, and the solution is obtained from a single solving of the equation, providing a significant step towards real time imaging.

Aims: In anticipation of improved methods to measure all displacement vector components, our purpose is to create an efficient and robust tool for directly solving the inverse problem of two– and three–dimensional incompressible isotropic linear elasticity.

Methods: We analyze the uniqueness of the inverse problem of three–dimensional incompressible isotropic elasticity. We find that when two independent displacement fields are available the shear modulus distribution can be completely determined if it is known at five distinct points. To solve the inverse problem directly, we use the adjoint weighted equation (AWE) method, a novel formulation for direct (non–iterative) solutions of inverse problems [1]. We use several simple model problems with simulated data to test the ability of the AWE method to reconstruct the shear modulus distribution. These include inclusion problems where a circular inclusion is embedded in a homogeneous background. We also investigate the performance of the method in the presence of noise and consider options to improve the reconstruction.

Results: We successfully solve the inverse problem of incompressible isotropic elasticity using the AWE formulation and reconstruct the shear modulus. The reconstructions are most accurate when the distribution of the shear modulus in the inclusion is continuous. When the shear modulus is discontinuous some accuracy is lost, but the overall shape of the inclusion and the inclusion/background interface are captured well. We also find that at low levels of noise in the displacements, the AWE can still provide fair results. At higher levels of noise, closer to those obtained using ultrasound equipment, we find that smoothing the displacement data and adding regularization to the AWE can significantly improve the results.

Conclusions: The AWE method, as a direct solution approach, can provide fast reconstruction of material properties compared to conventional optimization approaches. We find that with some adaptations, the method can also handle noise making it a potential tool for real time imaging. The availability of this and related direct inversion approaches motivates the development of techniques to measure all components of the displacement field.

Acknowledgements: This research was supported by Grant No. 2004400 from the United States–Israel Binational Science Foundation (BSF), Jerusalem, Israel.

References:

[1] P. E. Barbone, C. E. Rivas, I. Harari, U. Albocher, A. A. Oberai, Y. Zhang: Adjoint–Weighted Variational Formulation for the Direct Solution of Inverse Problems of General Linear Elasticity with Full Interior Data. Int. J. Numer. Meth. Eng., 9, pp. 1–23, 2009.

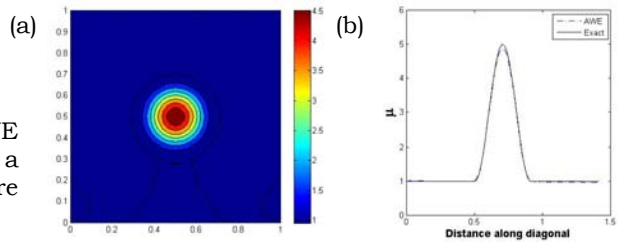

Figure 1: Shear modulus reconstruction using the AWE method of a circular inclusion inside a homogeneous background. Solution in the entire domain (a) and along the diagonal (b).

020 **MULTI–BAND CONFIDENCE PROCESSING FOR TWO–PASS SPECKLE TRACKING IN ECHOCARDIOGRAPHY.**

Emily Y. Wong[1], Colin B. Compas[2], Ben A. Lin[2], Albert J. Sinusas[2], James S. Duncan[2], Matthew O'Donnell[1].*
[1]University of Washington, Seattle, WA, USA; [2]Yale University, New Haven, CT, USA.

Background: In myocardial strain imaging using ultrasound speckle tracking, large interframe strains can cause significant peak–hopping artifacts. An iterative, or multi–pass, process for speckle tracking, using displacement estimates from the previous pass as an initial guess for a subsequent pass, can improve displacement accuracy if initial guesses are close to the true correlation coefficient peak [1,2]. Different peak–hopping patterns are observed when speckle tracking is performed on different frequency components of the radiofrequency (RF) data.

Aims: The goal is to reduce peak–hopping artifacts using a two–pass approach in combination with a multi–band confidence algorithm to assess the quality of the displacement guess at each pixel by comparing correlation results from multiple sub–bands.

Methods: In this study, RF data were acquired from the anterior wall of the left ventricle in an open–chest dog using a commercial 2–D phased array (iE33, Philips, Andover, MA). RF images were filtered into five frequency bands (centered about 2.0–4.0MHz). In the first pass, 2–D phase–sensitive correlation–based tracking (search region 33x9 pixels (axial x lateral)) was applied to adjacent frames of the broadband image and each sub–band image to produce six sets of 2–D displacement estimates. Following the first pass, a confidence index was found for each pixel based on the number of sub–bands with matching displacement estimates, the magnitude of the correlation coefficient and estimated strain values. Cubic interpolation was performed between pixels in the broadband image for which the confidence weight exceeded a threshold. Second pass tracking using the resultant displacements was performed with a small search region (5x3 pixels (axial x lateral)) to reduce peak–hopping (resolution of 0.2mm and 2.5° (axial and azimuthal)). Displacements were compared to results from a single pass approach using identical tracking resolution.

Results: The two–pass approach with multi–band selection criteria reduced peak–hopping compared to the single pass method without sacrificing spatial resolution. With the two–pass method, the variance of the interframe displacement was reduced by 42% axially and 60% laterally. The variance of axial and lateral displacements accumulated from end diastole to peak systole (Figure 1) was reduced by 57% and 87%, respectively.

Conclusions: Two–pass multi–band confidence processing can improve the quantification of myocardial deformation using speckle tracking and may be valuable in the assessment of cardiac function using echocardiography.

Acknowledgements: This work was supported by NIH Grant 5R01HL082640–04.

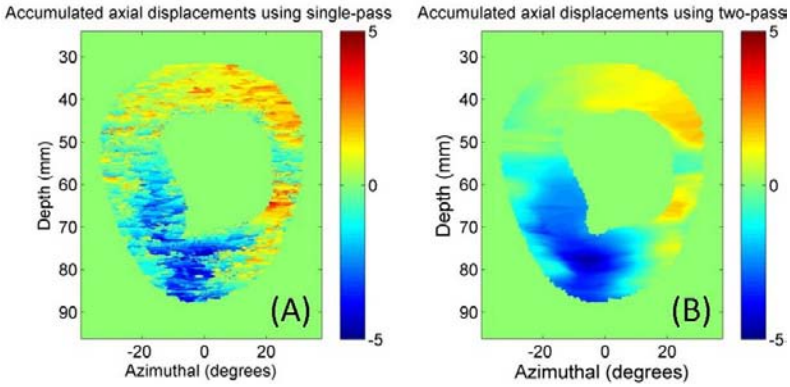

Figure 1: Accumulated axial displacements for an open–chest canine experiment using (A) single pass and (B) multi–band two–pass methods.

References:

[1] Yeung, et al.: Multilevel and Motion Model–Based Ultrasonic Speckle Tracking Algorithms. Ultrasound Med Biol, 24, pp. 427–441, 1998.
[2] Chen, et al.: Improvement of Elastographic Displacement Estimation Using A Two–Step Cross–Correlation Method. Ultrasound Med Biol, 33, pp. 48–56, 2007.

* *indicates Presenter*

034 **A FEASIBILITY STUDY OF ULTRASOUND STRAIN IMAGING FOR RISK ASSESSMENT OF CAROTID ATHEROSCLEROTIC PLAQUES VALIDATED BY MAGNETIC RESONANCE IMAGING.**

Shengzhen Tao[1], Lingyun Huang[2], Xiaochang Pan[1], Manwei Huang[3], Xihai Zhao[1], Le He[1], Jianwen Luo[1], Jing Bai[1], Chun Yuan[1,4].*

[1]Biomedical Engineering Department, Tsinghua University, Beijing, CHINA; [2]Philips Research Asia, Shanghai, CHINA; [3]Ultrasonography Department, China Meitan General Hospital, Beijing, CHINA; [4]Radiology Department, University of Washington, Seattle, WA, USA.

Background: Conventional B–mode ultrasound images and Doppler blood flow measurement are mostly used to evaluate degree of carotid atherosclerotic plaques, but it is lack of histological validation in clinical ultrasound. On the other hand, the correspondence between multi–contrast MR sequence and histology has been constructed [1]. Therefore, the feasibility of a multi–modality plaque imaging should be investigated.

Aims: In this work, we propose an MRI and ultrasound comprehensive feasibility study to quantitatively measure morphologic and mechanic property of the carotid atherosclerotic plaques and develop the risk indicator of plaques.

Methods: Sequences of 2D ultrasound radio–frequency (RF) frames were acquired from a 65 year old male human subject with carotid plaques using L9–3 transducer on a Philips (Bothell, WA, USA) iU22 ultrasound system. The displacement of plaques between adjacent RF frames was estimated using a coarse–to–fine 2D speckle tracking algorithm based on cross–correlation and correlation filtering. Then the strain values along the ultrasound beam were calculated for a 2D Savitzky–Golay digital differentiator to indicate relative stiffness of different plaque compositions. The strain value was not normalized by pressure in the current processing so that only regions of interest with similar hemodynamic condition were compared. The same patient took double blinded MRI scanning for carotid arteries on a Philips Achieva 3T TX MR scanner (Philips, Best, the Netherlands) using a multi–contrast imaging protocol including 3D time–of–flight (TOF), magnetization prepared rapid gradient–echo (MP–RAGE), and black–blood T1– and T2–weighted sequences. 3D MR images of this patient were reconstructed, and slices at the same position of the ultrasound incidence angle were selected in the Philips MR workstation (Philips WorkSpace) using an algorithm of multi–planar reconstruction (MPR). Carotid plaque tissue compositions on MRI images were characterized according to the published criteria [1–3], while echogenecity and strain values in the ultrasound images were investigated and compared with MRI results.

Results: The plaques with intra–plaque hemorrhage (IPH) on MP–RAGE MR images and lipid–rich necrotic core (LRNC) on T2–weighted MR images were defined as high risk. In ultrasound results, the calcified area (Ca) of the plaque showed high echogenecity and low deformation, the IPH showed mid–high echogenecity and intermediate deformation, and the LRNC showed the lowest echogenecity and large deformation. The locations of the calcification, IPH and LRNC are in good agreement with findings on MR images.

Conclusions: Based on the MR images validated by histological results, we perform a quantitative measurement of the morphology and mechanic property of high–risk plaques. It shows that the combination of echogenecity and strain values obtained from ultrasound RF signals is feasible to quantitatively evaluate the vulnerability of atherosclerotic plaques.

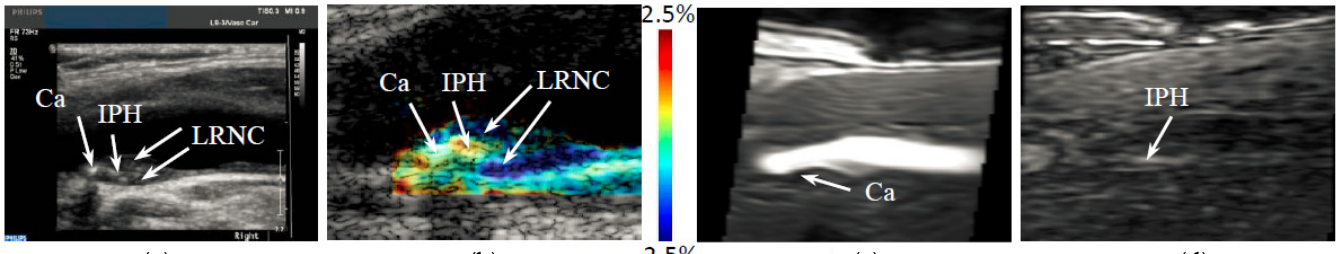

Figure 1: (a) B–mode image, (b) strain image overlaid onto the B–mode image, (c) TOF MR image, (d) MP–RAGE MR image

References:

[1] Cai JM, Hatsukami TS, Ferguson MS, Small R, Polissar NL, Yuan C: Circulation. 106(11), pp. 1368–73, 2002.
[2] Saam T, Ferguson MS, Yarnykh VL, Takaya N, Xu D, Polissar NL, Hatsukami TS, Yuan C: Arterioscler. Thromb. Vasc. Biol. 25(1), pp. 234–9, 2005.
[3] Ota H, Yarnykh VL, Ferguson MS, Underhill HR, Demarco JK, Zhu DC, Oikawa M, Dong L, Zhao X, Collar A, Hatsukami TS, Yuan C: Radiology. 254(2), pp. 551–63, 2010.

039 **IMAGING VULNERABLE PLAQUES WITH ACOUSTIC RADIATION FORCE IMPULSE (ARFI) IMAGING: FEM SIMULATION RESULTS.**

JR Doherty[1], GE Trahey[1] and ML Palmeri[1].*
[1]Duke University, Durham, NC, USA.

Background: Plaque rupture is the most common cause of cardiovascular related events including sudden cardiac death and stroke. Histopathological evidence has shown that a vulnerable plaque is typically characterized by a large lipid core and a thin fibrous cap. However, current evaluation methods are unable to visualize these features *in vivo* and cannot reliably identify patients most at risk. With the ability to characterize the mechanical properties (i.e., stiffness) of structures deep within the body, Acoustic Radiation Force Impulse (ARFI) Imaging [1] is a non–invasive ultrasound–based elasticity imaging method that has shown promise for identifying soft, lipid pools from stiffer, more stable regions.

Aims: The purpose of this work is to simulate ARFI imaging of carotid plaques using Finite Element Method (FEM) models. The ability of ARFI imaging to identify the lipid pool is evaluated across a wide range of material properties. Where rupture of plaque could lead to serious consequences, the maximum Von Mises stress associated with the induced deformation is also investigated for each simulation.

Methods: FEM meshes of five carotid plaques were constructed based on *in vivo* high resolution magnetic resonance imaging (MRI) and histology images published by Li et al. [2]. In a parametric analysis, the specified Young's Modulus assigned to the media, lipid and fibrous cap components was modified across a wide range of values. Following the work performed by Palmeri et al. [3], an ARFI excitation was modeled by scaling simulated pressure fields with empirically determined intensity values. The material was modeled as a linear, isotropic and elastic solid. LS–DYNA (Livermore Software Technology Corp, Livermore, CA) was used to perform the FEM simulation to obtain datasets of the axial displacements and Von Mises stresses that occur through time from the impulsive acoustic radiation force excitation.

Results: As shown in Figure 1, the ability to detect the lipid pool is largely dependent upon the stiffness of the lipid component. An increased contrast was observed with an increase in the ratio of the lipid pool stiffness to that of the media and fibrous cap. Stress concentrations from the induced deformation were largely concentrated within the fibrous cap and media components. Increased fibrous cap stiffness resulted in an increased Von Mises stress as shown in Figure 2. Maximum stresses were located at the edges of the acoustic radiation force excitation and were <1.2kPa for all cases.

Conclusions: The FEM simulations demonstrate the feasibility of using ARFI to differentiate the lipid pool from the surrounding media and fibrous cap. While the specific mechanisms of rupture are unknown, the Von Mises stresses modeled herein due to ARFI are orders of magnitude lower than published results on the simulated stresses due to blood pressure in models of the same geometry [2].

Acknowledgements: This work is supported by NIH Grant R01–HL075485.

References:

[1] Nightingale, K. R, et al.: On the Feasibility of Remote Palpation using Acoustic Radiation Force. J. Acoust. Soc. Am., Vol. 10, pp. 625–634, 2001.
[2] Li, Z., et al.: Stress Analysis of Carotid Plaque Rupture Based on *In Vivo* High Resolution MRI. Journal of Biomechanics, Vol. 39, pp. 2611–2622, May 2006.
[3] Palmeri, M. L, et al.: A Finite-Element Method Model of Soft Tissue Response to Impulsive Acoustic Radiation Force. IEEE Trans. Ultrason. Ferroelect. Freq. Cont., Vol. 52, pp. 1699–1712, 2005.

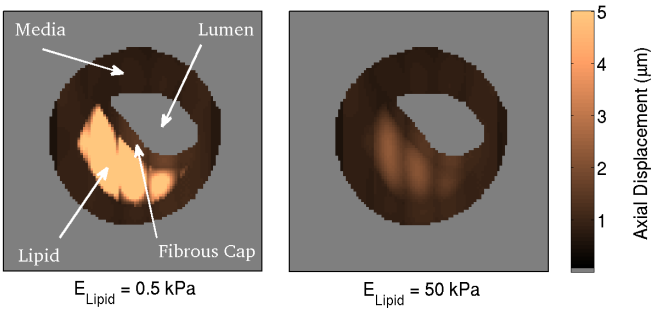

Figure 1: Simulated ARFI images comparing the axial displacements in models with a lipid Young's Modulus (E_{lipid}) of 0.5 and 50kPa.

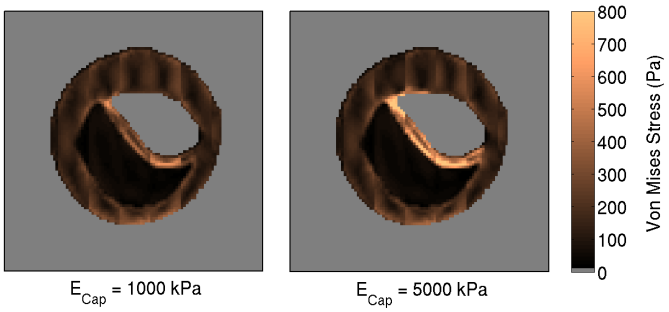

Figure 2: Simulated Von Mises stress contours comparing the stresses in models with a fibrous cap Young's Modulus (E_{cap}) of 1000 and 5000kPa.

* *indicates Presenter*

058 **TOWARDS THE QUANTIFICATION AND IMAGING OF STRESS USING MODEL–BASED INTRAVASCULAR ULTRASOUND ELASTOGRAPHY.**

Michael S. Richards[1], Renato Perucchio[2], Marvin M. Doyley[1].*
[1]Electrical and Computer Engineering Department, [2]Mechanical Engineering Department, University of Rochester, Rochester, NY, USA.

Background: The study of arterial plaque mechanics is essential to the detection and monitoring of vulnerability. Intravascular ultrasound elastography (IVUSe) has been used for identification of plaque components often associated with "vulnerability", either through strain imaging or reconstruction based elastography. However, it is the peak stresses within plaques, rather than the plaque material itself, that is directly responsible for predicting plaque rupture [1].

Aims: This work expands upon a previously developed IVUSe reconstruction technique [2], using intra–luminal pressure measurements and measured two component displacement vector fields to reconstruct quantitative modulus images. The mechanical model is used to calculate the principal stress images, which are then compared to known stresses, for simulation studies, and other vulnerable plaque features.

Methods: We conducted simulations and phantom studies with known pressures and material parameters to determine the accuracy of the calculated stress images and to determine the variability of the calculation to assumed model parameters (i.e., boundary conditions, Poisson's ratio). Simulated vessels and vessel phantoms were designed with a soft lipid–like plaque bordering the inner lumen, separated by a plaque cap of varying thickness. The two–component displacement vector field was measured from the IVUS images using an image registration displacement estimator. The measured displacements and pressures were then used to reconstruct the elastic modulus and calculate the resulting principal stress images.

Results: Maximum principal stresses were calculated at the centroid of each finite element. Simulation results showed good correlation for principal stresses (~25% RMS error). Phantom stress images were normalized to an applied pressure of 1kPa for comparison. Resulting stress images show a clear stress peak for the phantom created with a smaller cap width, which was qualitatively consistent with the simulated results. Stress peaks are localized near the sides of the plaques in both phantoms, also consistent with simulated results. The mean principal stress on the inner lumen for the small–capped phantom was ~0.40kPa, and the large–capped phantom was ~0.32kPa.

Conclusions: Peak stresses were higher in simulations with smaller cap thicknesses. Phantom studies further supported the simulation results, showing a higher peak stresses in phantoms having a thinner cap region separating the plaque from the inner lumen under comparable loading conditions.

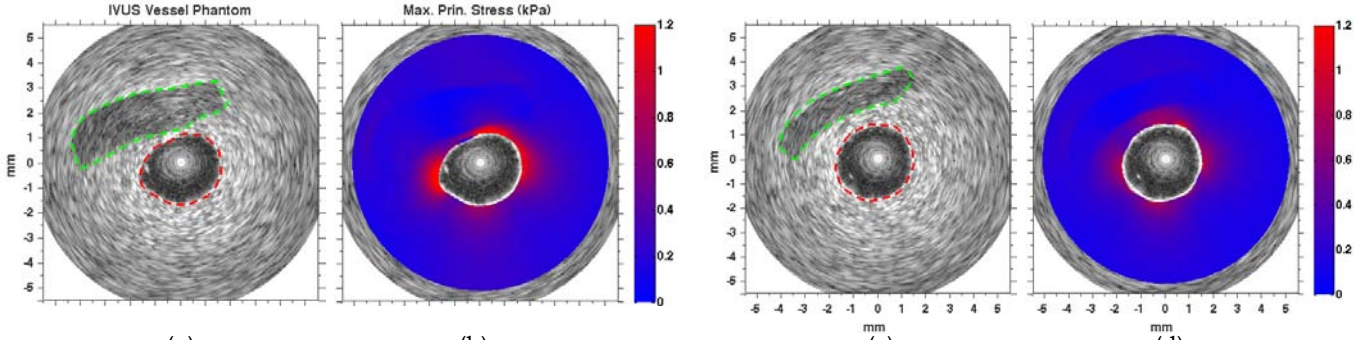

Figure 1: PVA vessel phantom with soft "plaque" region. (a) shows a larger plaque with a smaller cap region and (c) a smaller plaque with a thicker cap region. (b) and (d) Corresponding calculated maximum principal stress in kilopascals (normalized to 1 kPa applied luminal pressure).

Acknowledgements: This work is funded by the National Heart and Lungs Research grant R01 HL088523.

References:

[1] P.D. Richardson, M.J. Davies and G.V.R. Born: Influence of Plaque Configuration and Stress Distribution on the Fissuring of Coronary Atherosclerotic Plaques. Lancet, Vol. 334, 1989.
[2] M. S. Richards, M.M. Doyley: Investigating the Impact of Spatial Priors on the Performance of Model–Based IVUS Elastography. Phys Med Biol, Vol. 56, No. 22, 2011.

* *indicates Presenter*

059 **EFFECTS OF THE WALL INCLUSION SIZE AND MODULUS CONTRAST ON THE REGIONAL PULSE WAVE PROPAGATION ALONG THE ARTERIAL WALL *IN SILICO*.**

Danial Shahmirzadi[1] and Elisa E. Konofagou[1] – Presented by RX Li[1].*
[1]Columbia University, VC 12–232, 622 West 168th Street, New York, NY, 10032, USA.

Background: Arterial stiffness has previously been reported as an independent indicator of cardiovascular diseases such as aortic aneurysm. Existing stiffness measurements methods *in vivo* are either invasive (e.g., catheterization) or provide only an average global estimate (e.g., tonometry). Previous studies of pulse wave propagation along inhomogeneous arterial walls have shown that a global PWV estimate might not effectively detect the presence of local stiffness changes [1]. Pulse wave imaging (PWI) is a noninvasive and local estimation method [2–4] for regional pulse wave velocity (PWV) measurement and visualization.

Aims: Examining the effects of inclusion size and modulus contrast on the regional pulse wave propagation and velocity along the simulated arterial wall.

Methods: A 3D fluid structure interaction (FSI) simulation of pulse wave propagation was performed in Coupled Eulerian–Lagrangian (CEL) explicit solver of Abaqus 6.10–1 (Simulia, RI, USA). The Lagrangian domain, mimicking the canine aorta, composed of a straight geometry tube (L=250mm; r_i=12 mm, t=2.2mm) with a linearly elastic wall (E_{wall}=5.12MPa, ρ_{wall}=1050kg/m^3 and Poisson's ratio ν=0.48). The Eulerian domain encompassed the Lagrangian tube, simulating the presence of a Newtonian fluid medium (ρ_{fluid}=1000kg/m^3, speed of sound C_0=1483m/s and viscosity η=0.0001Pa.s). The FSI was defined as a frictionless two–way coupling between the tube and the fluid medium. The tube inlet and outlet were fully constrained in x–y–z directions, and a rectangular initial velocity (V_0=5m/s) was applied on the inlet as the driving force for the dynamic wall motion. The first simulation was performed on the homogenous wall (no inclusion) as the reference model. The effects of the inclusion size were examined based on a set of simulations of the wall containing a 2 and 10mm long inclusion with a Young's modulus of 1.50 times the E_{wall}=5.12MPa. To examine the effects of the inclusion modulus contrast, a set of simulations were performed on the wall containing a 2mm long inclusion with a Young's modulus of 1.50 and 2.00 times the E_{wall}=5.12MPa. The wall radial displacement along the entire tube length (longitudinal spatial resolution of 5mm) was measured at multiple time–points (temporal resolution of 0.375ms), and the information was mapped onto a 2D spatio–temporal plane which allowed the visualization of the entire wave propagation.

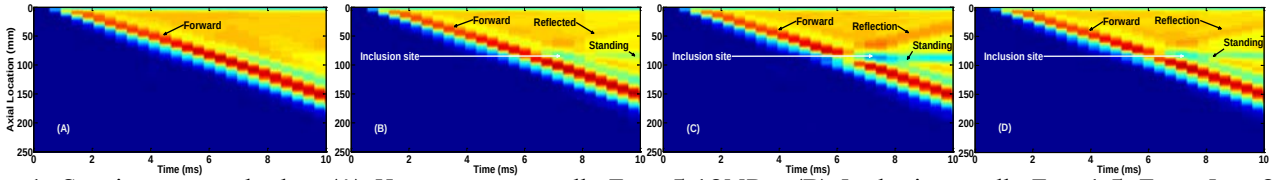

Figure 1: Spatio–temporal plot: (A) Homogenous wall: E_{wall}=5.12MPa; (B) Inclusion wall: E_{inc}=1.5×E_{wall}, L_{inc}=2mm; (C) Inclusion wall: E_{inc}=1.5×E_{wall}, L_{inc}=10mm; (D) Inclusion wall: E_{inc}=2.0×E_{wall}, L_{inc}=2mm.

Results: Figure 1 provides the spatio–temporal plots of the wall displacement for the homogenous wall (Figure 1A), and the inhomogeneous walls (Figures 1B–1D). It is seen that a small portion of the main forward wave gets reflected at the site of the inclusion while the rest continues to travel forward beyond the inclusion site under a PWV which remains almost unaffected (not shown)[1]. Quantitative and qualitative reflection patterns depend on the inclusion properties, e.g. increase in both the inclusion size (Figures 1B–1C) and modulus contrast (Figures 1B–1D) was found to increase the reflection wave magnitude. Also, the low wall displacement at the inclusion site forms a standing wave whose width is correlated to the inclusion size (Figures 1B–1C).

Conclusions: This study of pulse wave propagation along the inhomogeneous arterial walls *in silico* highlighted the need for regional PWV measurements, such as those obtained by PWI, in order to detect the changes in regional wall stiffness. In particular, it was found that spatio–temporal plots of the wall displacement contain qualitative and quantitative information that can collectively be used to obtain the size and modulus contrast of the zone entailing the regional changes. Future studies will focus on examining the pathological conditions, such as the inhomogeneity in modulus and geometry seen in aortic aneurysm, in order to determine the implications in PWI *in vivo*.

References:

[1] Shahmirzadi et al.: Artery Res, in press, 2012.
[2] Fujikura et al.: Ult Imag, 29(3), pp. 137–54, 2007.
[3] Luo et al.: IEEE Ultras Symp, pp. 859–62, 2008.
[4] Vappou et al.: Am J Hyp, 23(4), pp. 393–398, 2010.

* *indicates Presenter*

005 **ACUTE EFFECTS OF CANNABINOÏD RECEPTORS ACTIVATION ON BRAIN MECHANICAL PROPERTIES AND CEREBRAL BLOOD FLOW IN THE JUVENILE RAT HIPPOCAMPUS.**

Simon Chatelin[1], Marie Humbert–Claude[2], Philippe Garteiser[1], Valérie Vilgrain[1], Bernard E. Van Beers[1], Zsolt Lenkei[2], Ralph Sinkus[1].*
[1]Paris Diderot University, Sorbonne Paris Cité, INSERM, CRB3, UMR773, Paris, FRANCE; [2]Laboratoire de Neurobiologie, ESPCI–CNRS, UMR7637, Paris, FRANCE.

Background: Recent studies suggest a significant influence of type-1 cannabinoïd receptors (CB_1R) on the puberty maturation processes [1] including neuronal remodeling and modifications of cortical mechanical properties in the postnatal brain. A preliminary study showed a decrease of the hippocampus elasticity within 15 minutes after CB_1R agonist injection [2].

Aims: To assess the significance and causes of this effect, MR–Elastography (MRE) and Arterial Spin Labeling (ASL) perfusion imaging were performed, as illustrated in Figures 1 and 2 respectively.

Methods: The experimental protocol (carried out in a 7T MRI scanner) consisted of an anatomical T2–weighted MR scan, a baseline MRE acquisition, intra–peritoneal drug injection, a delay of 15 minutes and a second MRE acquisition. The tests were conducted on 10 day old rats (n=11) injected with the cannabinoïd receptor (CB1R) agonist CP55940 (0.7mg/kg). MRE was acquired using a spin–echo sequence with EPI (Echo Planar Imaging) readout and synchronous motion–encoding gradients to encode 3 orthogonal displacement maps in phase images (10 axial slices of 300µm isotropic resolution). Mechanical waves were generated using a uni–axial modal exciter (1000Hz).

Results: Elasticity values were expressed as percent of baseline G_d values (4.35±0.23 and 2.62±0.25kPa for h. and th. respectively). CP55940 injection induced a significant decrease of the elastic modulus in the hippocampus (-16.5±4.9%, p=0.0013) (Figure 3). No significant modification was observed in the thalamus (p>0.1). This effect was significantly reversible (p<0.01) to within 3.4% of the baseline value. These results are in agreement with the expression pattern of CB_1R in the hippocampus and thalamus in the rat brain [4], as confirmed in this study by histology. Moreover, pre–injection of the specific CB_1R antagonist AM251 (3mg/kg) 15 minutes prior to the CP55940 completely suppressed the decrease of G' [2]. No variation was observed regarding brain viscosity. ASL results show a significant CBF decrease of 17.7% and 16.2% 15 minutes after injection for hippocampus and thalamus respectively (Figure 3). However, the lack of significant CBF difference between these two regions as well as the non–return of CBF measurements to their baseline values within one hour after injection shows that, by themselves, CBF modifications cannot explain the observed changes in mechanical properties after CB_1R agonist injection.

Conclusions: This study shows for the first time a significant temporal alteration of young rat brain mechanical properties after cannabinoïd injection, which cannot be explained solely by a decreased CBF. CB_1R receptors may play an important role in the neuronal remodeling with significant effects on brain stiffness, especially in the hippocampus, which plays a major role in memory and learning functions.

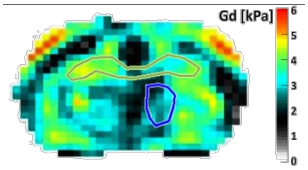

Figure 1: Example of Elasticity map obtained by MRE.

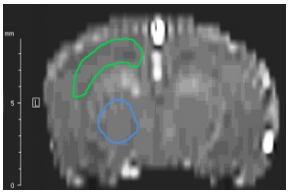

Figure 2: Example of CBF map obtained by ASL perfusion imaging.

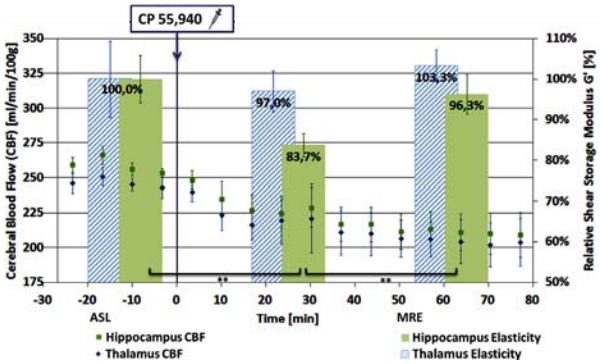

Figure 3: Time evolution of elasticity and CBF after CB_1R agonist injection.

References:

[1] Schneider M, Koch M: Neuropsychopharmacology, 30(5), pp. 944–57, 2005.
[2] Chatelin S, Humbert–Claude M, et al.: Proc. ISMRM, (915), 2012.
[3] Sinkus R, Tanter M, et al.: Magn Reson Imaging, 23, p. 159, 2005.
[4] Romero J, Garcia–Palomero E, et al.: Synapse, 26, pp. 317–323, 1997.

* *indicates Presenter*

023 ***IN VIVO* HEEL PAD ELASTICITY INVESTIGATION: COMPARING MALES TO FEMALES.**

S Matteoli[1,2], MM Madsen[1], A Virga[2], JE Wilhjelm[1], A Corvi[2], ST Torp–Pedersen[3].*

[1]Biomedical Engineering Group, Electrical Engineering Department, Technical University of Denmark, Ørsteds Plads Bldg. 348, DK–2800 Kgs. Lyngby, DENMARK; [2]Mechanics and Industrial Technologies Department, University of Florence, via di S. Marta 3, 50139 Florence, ITALY; [3]The Parker Institute, Frederiksberg Hospital, Nordre Fasanvej 57, DK–2000 Frederiksberg, DENMARK.

Background: The interest in quantifying the mechanical properties of human soft tissues is an important aspect of diagnosing diseased tissues. Knowledge of the mechanical properties of heel pad tissue may be used in tools for screening patients for the purpose of preventing further complications in the foot (e.g. ulcerations may be prevented in diabetics [1]) as well as of obtaining validated examination methods for medico–legal purposes. In order to investigate whether there are any differences between healthy and diseased heel pads when dealing with their biomechanics, it is first necessary to establish a "normal" range of biomechanical parameters. Even though the heel pad biomechanics has been investigated for more than 25 years in healthy individuals as well as in subjects with pathological conditions, studies differ both in terms of method applied and population studied, and it is not feasible to compare the numerical results.

Aims: The present study concentrates on collecting a bank of "normal" data characterizing the heel pad biomechanics. Specifically, the heel pad elasticity of a group of healthy volunteers was measured with a compression device (Figure 1) and the difference between males and females was statistically investigated.

Methods: One hundred and twenty seven healthy subjects were enrolled (Figure 2) for compression tests. Only the dominant foot was tested, i.e. the foot normally used to kick the ball when playing football. All subjects declared to have never had injuries/trauma to any of the feet. Subjects engaged in professional sport were not included in this study. A detailed description of both compression device (Figure 1) and procedure used for experimental tests can be found in [2]. All subjects also underwent ultrasound measurements, so that the unloaded heel pad thickness (UHPT) could be measured. The elastic modulus (E) was calculated from the stress–strain characteristics by averaging the modulus found in the first and last 30% parts (considered almost linear) of the loading curve. Student t–test was used for statistical analysis and a P–value less than 0.05 was chosen to indicate a statistical significance.

Results: The heel pad showed the typical non–linear visco–elastic behavior (Figure 3). The UHPT was found to be 14.6±1.98mm and 15.8±1.92mm for females and males, respectively. E was found to be 0.076±0.012MPa for females and 0.085±0.015MPa for males. Statistical analysis showed that there was a statistically significant difference for UHPT and E (P–value<0.001).

Conclusions: This study showed a statistically significant difference between males and females in UHPT and E. Specifically, males had thicker and stiffer heel pads than females as also reported by [3], but in contrast with [4]. Thicker heel pads in men might be due to the greater growth hormone concentration, while in women the high level of estrogen might result in a lower stiffness [3,5,6].

References:

[1] Sopher R et al.: The Influence of Foot Posture, Support Stiffness, Heel Pad Loading and Tissue Mechanical Properties on Biomechanical Factors Associated with a Risk of Heel Ulceration. J Mech Behav Biomed, 4(4), pp. 572–582, 2011.
[2] Fontanella CG et al.: Investigation on the Load–Displacement Curves of a Human Healthy Heel Pad: *In Vivo* Compression Data Compared to Numerical Results. Med Eng Physics, in press, 2012.
[3] Alcantara E et al.: Influence of Age, Gender, and Obesity on the Mechanical Properties of the Heel Pad under Walking Impact Conditions. J App Biomech, 18(4), pp. 345–356, 2002.
[4] Boros RL and Challis JH: Heel Pad Properties of Males and Females. Med Sci Sports Exerc, 35(5), p. 360, 2003.
[5] Prichasuk S: The Heel Pad in Plantar Heel Pain. J Bone Joint Surg Br, 76B(1), pp. 140–142, 1994.
[6] Prichasuk et al.: The Heel–Pad Compressibility. Clin Orth Rel Res, 300, pp. 197–200, 1994.

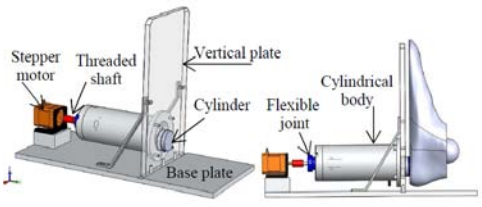

Figure 1: Compression device

	All	Females	Males
Subjects	127	63	64
Age (years)	36.6±14.6	36.7±14.4	36.6±14.7
Weight (kg)	71.7±13.5	64.2±9.2	79.2±12.8
Height (cm)	173.6±9.8	166.8±5.7	180.4±8.3
BMI (kg/m^2)	23.7±3.1	23.0±2.7	24.3±3.3
Physical activity (hours/week)	4.0±3.9	4.7±4.1	3.3±3.6

Figure 2: Anthropometric characteristics

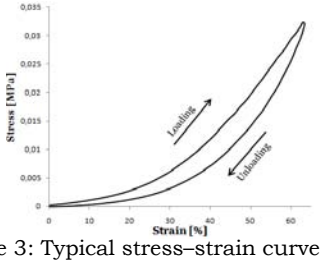

Figure 3: Typical stress–strain curve

* *indicates Presenter*

031 **MULTIFREQUENCY VS MONOFREQUENCY MR ELASTOGRAPHY FOR THE CHARACTERIZATION OF LIVER FIBROSIS AND INFLAMMATION.**

P Garteiser[1,2], G D'Assignies[1,2], H Leitao[1,2,3], RS Sahebjavaher[1,2,4], SA Lambert[1,2], F Mouri[1,2], V Vilgrain[1,2], BE Van Beers[1,2], R Sinkus[1,2].*

[1]INSERM, U773, F–75205, Paris, FRANCE; [2]University Paris Diderot, Sorbonne Paris Cité, UMRS773, F–75205, Paris, FRANCE; [3]University of Coimbra, Coimbra, PORTUGAL; [4]University of British Columbia, Vancouver, BC, CANADA.

Background: Magnetic Resonance Elastography (MRE) is a non–invasive modality that quantifies the mechanical properties of tissues [1,2]. Theoretical and physical considerations indicate that the presence of microscopic obstacles may influence not only the absolute value of viscoelastic parameters, but also their relationship with frequency [3,4]. In particular, the frequency behavior of mechanical parameters may be modeled as a power law, in which case the exponent parameter represents a mechanical property inherent to a given material. Yet, most studies use a single excitation frequency thus knowledge about frequency related mechanical properties is very limited.

Aims: Our aim is to determine which of the monofrequency parameters G' (kPa), the storage modulus, G" (kPa), the loss modulus, G_{abs} (kPa), the absolute value of the shear modulus, β (mm^{-1}, 2π over the wavelength) and α (mm^{-1} the attenuation coefficient) or their corresponding multifrequency parameters (the exponent coefficients $\gamma_{G'}$, $\gamma_{G"}$ γ_{Gabs}, γ_{β}, γ_{α} of their response to frequency as modeled with a power law; i.e. $G' = \omega^{\gamma_{G'}}$; $G" = \omega^{\gamma_{G"}}$, $G_{abs} = \omega^{\gamma_{G_{abs}}}$, $\beta = \omega^{\gamma_{\beta}}$, $\alpha = \omega^{\gamma_{\alpha}}$ with ω the frequency) correlates best with the METAVIR score.

Methods: All patient studies were performed under informed consent and within the agreement of local ethical guidelines. Twenty patients with viral hepatitis B (n=5), C (n=14) and nonalcoholic fatty liver disease (n=1) underwent MRE. Liver inflammation/fibrosis was assessed with METAVIR scoring of percutaneous biopsies. For MRE, a gradient–echo sequence was used (TR/TE=112ms/9.6ms, 4mm resolution). Three–directional motion encoding (eight phase offsets) was performed on simultaneous 28, 56 and 84Hz mechanical waves transduced by an electromechanical actuator. Complex viscoelastic parameters were calculated by demodulation and local inversion of the linear viscoelastic 3D wave equation. Monofrequency and multifrequency parameters were compared among inflammatory grades and fibrosis stages, using the Kruskal–Wallis test and Dunn's post–test.

Results: At 28Hz G_{abs} and β discriminated between F1 vs F3 (P<0.05) but not among the other stages. G', G" and α at 28Hz did not significantly differ between any of the fibrosis stages, and the same was seen with G', G", G_{abs}, α and β at 56Hz and 84Hz. None of the monofrequency parameters was able to discriminate inflammation grades. Using a multifrequency approach, γ_{β} and $\gamma_{G'}$ could discriminate between F0 vs F3 and F1 vs F3 (P<0.05), and γ_{Gabs} between F0 vs F3 (P<0.05). γ_{β}, γGabs and γG" varied significantly between inflammation grades A0 vs A1 (P<0.05). No significant variation of γ_{α} was found among the different inflammation grades. A significant correlation was found between inflammation and γ_{β} and γ_{Gabs}.

Conclusions: The exponent parameters of β and G" derived from the multifrequency data provided better discrimination between inflammation grades and fibrosis stages than monofrequency parameters. Hence, modeling the frequency response of liver tissue in various degrees of fibrosis and inflammation as a power law seems to be a viable approach to exploit multifrequency MRE data as quantitative indicators of diffuse liver disease. Moreover, using multifrequency–derived viscoelastic parameters (exponents) will allow standardization among MR elastography research groups.

References:

[1] Huwart L. 2008, Gastroenterology 135:32-40
[2] Lambert S. 2012, ESGAR procs
[3] Holm S. 2010, JASA 127:542-8
[4] Asbach P. 2010, Radiology 257:80-86

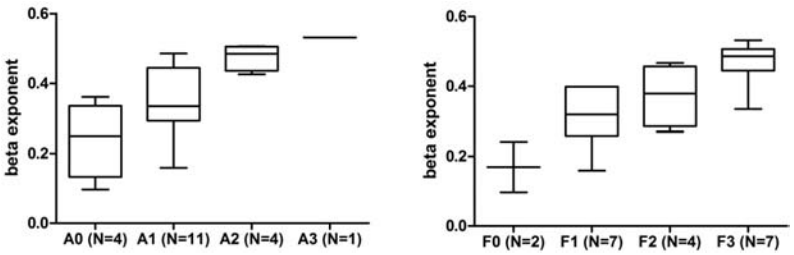

Figure 1: Box plot of the exponent parameter of the frequency dependence of 2π/λ as a function of inflammation grade (left) or fibrosis stage (right). The parameter varied significantly between F0 vs F3 and F1 vs F3 for fibrosis and between A0 vs A2 for inflammation.

038 **DYNAMIC SHEAR ELASTICITY PROPERTIES OF BLOOD COAGULATION ASSESSED BY SHEAR WAVE IMAGING AND CLASSIC RHEOLOGY.**

Miguel Bernal[1], Jean–Luc Gennisson[1], Mathias Fink[1], Patrice Flaud[2], Mickael Tanter[1].*
[1]Institut Langevin – Ondes et Images, ESPCI ParisTech, CNRS UMR7587, INSERM U979, 1 rue Jussieu, 75005 Paris, FRANCE; [2]Matière et Systèmes Complexes, CNRS UMR7057, Université Paris VII Denis Diderot, 10 rue Alice Domon et Léonie Duquet, 75205 Paris Cedex 13, FRANCE.

Background: Millions of people worldwide are affected by deep venous thrombosis (DVT) every year. Pulmonary embolism, a dangerous complication, affects about 30 to 50% of these patients [1]. This happens when the thrombus breaks off from veins and blocks the pulmonary arteries. The diagnosis and treatment of DVT usually depends on the risk of breakage and stability of the clots. The stability has been related to the age and elasticity of the blood clots [2,3].

Aims: This work describes the use of the Supersonic shear wave imaging (SSI) technique in the study of dynamic shear elasticity properties of blood coagulation. We compared the results from this technique with classical rheology studies.

Methods: Blood was collected from pigs and anticoagulated using ethylenediaminetetraacetic acid (EDTA). Coagulation was initiated using calcium ions. Ultrasound radiation force was used to generate shear waves with 100µs tone bursts of 8MHz at 3 different locations in the lateral direction. The shear wave displacements were measured by ultrafast imaging at a repetition rate of 2kHz. Using a time–of–flight algorithm, shear wave speed (Vs) was recovered giving access to the shear elasticity (µ) according to $\mu=\rho Vs2$. Using a Haake Mars II classical rheology (between 0.2 and 25Hz) was done simultaneously on the same blood sample. Three different types of experiments were done: dual systems (70 minutes), ultrasound alone (2 hours) and a multi–day experiment (ultrasound alone).

Results: SSI allowed the visualization of two dimensional (2D) maps of elasticity at every time point. The spatial shear elasticity of aregion of interest (ROI) in the sample varied with time, from a minimum of 67.4±8.7Pa at coagulation (about 5 minutes) to a maximum of 2168.4±326.8 at 91 minutes. It decreased to 753.5±138.8Pa after 18 hours, 763.1±107.1 after 24 hours and to 708.3±117.41 after 96 hours. In the dual experiments, using G' (conservation modulus) and G" (loss modulus) values from the rheology experiments, we calculated the phase velocities at 25Hz. The values at coagulation and minute 70 were 0.54±0.02m/s and 0.63±0.01m/s, respectively. While the values from the SSI experiments for the mean phase velocities (50–350Hz) increased from 0.46±0.12m/s at coagulation to 0.76±0.01m/s at the same time points. Syneresis phenomenon (expulsion of free water from the clot) was visible in the 2 hour B–mode experiment at the bottom of the sample. This affected the shear elasticity and created two regions in the blood clot. The mean phase velocity values were similar for the two regions at coagulation, 0.56±0.01 and 0.54±0.1m/s, respectively, but differed with time. At minute 15 (beginning of syneresis viewed by B–mode), the velocities were 0.85±0.04 for the syneresis region and 0.90±0.01m/s for no syneresis. At minute 120, they were 0.83±0.09 and 1.06±0.06m/s, respectively. The spatial median shear values for two ROI's in the two regions of the 2D maps at minute 120 were 748.5±145.1 and 1477.9±465.7Pa.

Conclusions: The phase velocity values obtained with the SSI technique showed good agreement with those calculated from the classical rheology experiments. SSI proved to be useful mapping the elasticity of clots in 2D at multiple time points. It allowed the quantification of the mechanical properties of the thrombi and their heterogeneities, illustrated by the dynamic mapping of syneresis region appearance showing that this technique has potential use in predicting thrombi breakage. Future studies include *in vivo* experiments in small animals and quantifying the viscosity in order to try to estimate thrombus age.

References:

[1] J. Hirsh and J. Hoak: Management of Deep Vein Thrombosis and Pulmonary Embolism. A Statement for Healthcare Professionals. Council on Thrombosis (in consultation with the Council on Cardiovascular Radiology), American Heart Association. Circulation, Vol. 93, No. 12, pp. 2212–45, Jun 1996.
[2] S. Y. Emelianov et al.: Triplex Ultrasound: Elasticity Imaging to Age Deep Venous Thrombosis. Ultrasound in Medicine and Biology, Vol. 28, No. 6, pp. 757–767, 2002.
[3] H. Xie et al.: Correspondence of Ultrasound Elasticity Imaging to Direct Mechanical Measurement in Aging DVT in Rats. Ultrasound in Medicine and Biology, Vol. 31, No. 10, pp. 1351–9, Oct 2005.

* *indicates Presenter*

050 **SHEAR WAVE DISPERSION MEASURES FAT CONCENTRATION IN A MOUSE LIVER MODEL.**

Zaegyoo Hah[1], Alexander Partin[1], Gil Zimmerman[1], Christopher T. Barry[2], Robert A. Mooney[2], Deborah J. Rubens[2], Kevin J. Parker[1].*

[1]Electrical and Computer Engineering Department, University of Rochester, Rochester, NY, USA; [2]University of Rochester Medical Center, Rochester, NY, USA.

Background: Nonalcoholic fatty liver disease (NAFLD) is characterized by accumulation of fat within the liver. In the most severe cases, NAFLD can progress to nonalcoholic steatohepatitis (NASH) and subsequently to liver cirrhosis. Since in many cases NAFLD can be asymptomatic, a non–invasive and painless method for the measurement of fat concentration within the liver would very beneficial.

Aims: We aim to assess our hypothesis, as illustrated in Figure 1a, that higher fat concentration within a liver will introduce higher shear speed dispersion, while slightly reducing the shear wave speed. This is a consequence of adding a viscous component to the liver [1]. Our objective in this study is to compare experimentally measured shear speed dispersion within liver specimens grouped by measured fat concentrations.

Methods: A total of 70 mouse liver specimens were scanned *ex vivo* over a four month period. 35 mice fed with a regular diet (Lean) and 35 fed with high fat diet (Obese). After hepatectomy, each liver specimen was embedded in a gelatin phantom and scanned with multiple frequencies between 200 and 350Hz using the CrW (crawling wave) imaging technique [2]. Using an estimation algorithm, a shear speed dispersion per 100Hz and shear speed at a reference frequency of 250Hz were obtained for each liver sample. For the hypothesis assessment, the estimated results are presented on a two parameter plot of dispersion slope (vertical axis) and shear speed at reference frequency (horizontal axis). The livers were categorized into two groups, Group 1 containing less than 50% fat and Group 2 with 50% fat or greater. The data were analyzed using two approaches. In the sample–by–sample approach, each liver specimen's estimate is placed in the plot, Figure 1b, where box plot size indicates the standard deviation within each group. In the group approach, Figure 1c, a linear regression with 95% confidence intervals was used to obtain the values for dispersion and shear speed of each of two groups. These values, together with the upper and lower bounds obtained with linear regression, are presented as box plots.

Results: In the sample–by–sample analysis, the dispersion per 100Hz in m/s/Hz and the shear speed in m/s for the two groups are: (0.13, 2.5) for Group 1 and (0.55, 1.9) for Group 2. The group analysis shows the following results: (0.12, 2.51) for Group 1 and (0.64, 1.93) for Group 2. Paired t–tests provided the following p–values: $p<0.001$ for shear wave speed dispersion per 100Hz and $p<0.01$ for shear speed at a reference frequency of 250 Hz.

Conclusions: Both approaches show statistically significant differences in the dispersion slope and shear speed of liver samples with different fat concentrations. Analysis plots (Figures 1b, 1c) demonstrate a good support of the hypothesis (Figure 1a).

References:

[1] Carstensen EL et al.: Elastography in the Management of Liver Disease. Ultrasound Med. Biol., 34, pp, 1535–1546, 2008.

[2] Zhe Wu et al.: Elastographic Imaging of Interference Patterns for Estimation of Shear Velocity Distribution in Biomaterials. J. Acoust. Soc. Am., 120(1), pp. 535–545, 2006.

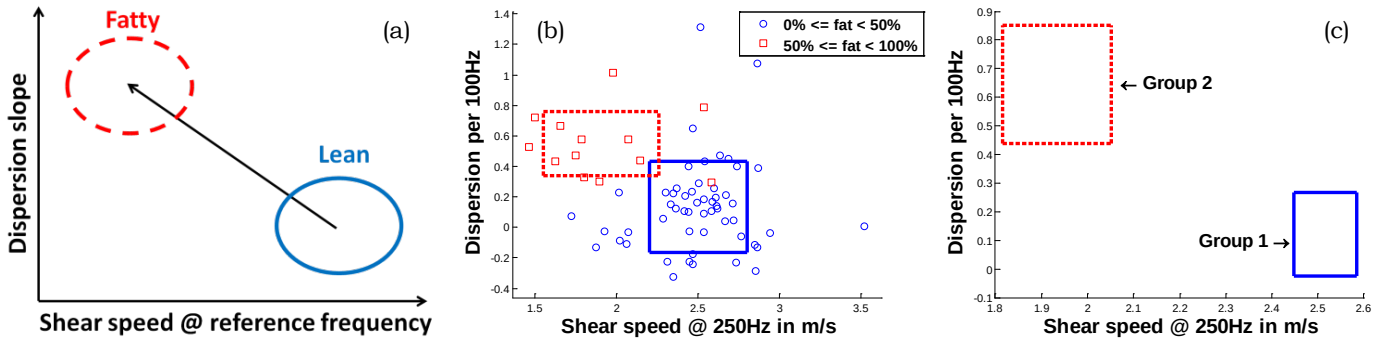

Figure 1: (a) Our hypothesis. The arrow represents the general progression from normal liver to fatty liver. (b) Sample–by–sample analysis plot. (c) Group analysis plot.

Invited Presentation:

097 **LIVER STIFFNESS MEASUREMENT USING VIBRATION-CONTROLLED TRANSIENT ELASTOGRAPHY: ROLE IN THE MANAGEMENT OF PATIENTS WITH CHRONIC LIVER DISEASES.**

Laurent Sandrin[1]*.
[1]Echosens, 30 Place d'Italie, 75013 Paris, France

Liver Stiffness Measurement (LSM) using Vibration–Controlled Transient Elastography (Fibroscan®, Echosens, Paris, France) is used more and more in routine clinical practice and research worldwide. Initially perceived as an alternative to liver biopsy for the diagnosis of liver fibrosis in patients with chronic liver diseases, the role of LSM has largely evolved. In this presentation, the role of LSM in the management of patients with chronic liver diseases will be discussed. We will introduce recent developments and ongoing studies with Fibroscan®.

Figure 1: In 2012, about 1500 Fibroscan® (Echosens, Paris, France) are used in routine clinical practice and research worldwide. Photograph of Fibroscan® 502 Touch.

Invited Presentation:

098 **HAS THE QUANTITATIVE STRAIN METHOD OF SHEAR WAVE SPEED REACHED CLINICAL MATURITY? AN ANALYSIS USING HYPE AND TECHNOLOGY ADOPTION MODELS.**

Andy Milkowski[1]*.

[1]Siemens Medical Solutions USA, Inc., Issaquah, WA, 98029 USA.

This presentation will demonstrate that Shear Wave Speed has reached a "slope of enlightenment" in Gartner's Hype [1] maturity model and "crossed the chasm" in Moore's technology adoption lifecycle [2] and therefore result in rapid clinical implementation over the next number of years.

The consultancy company Gartner developed a Hype Model that graphically shows the relative maturity of technologies. The model provides a model to help enterprises decide when to adopt a new technology. Geoffrey Moore used the technology adoption lifecycle model to describe adoption of disruptive innovations.

This presentation will historically review the strain technologies in the breast and liver as they progressed from a period of hype to understanding their relevance and role in medicine. Liver fibrosis assessment will be discussed through the clinical consensus in literature as well as recent progress in standards committees. Lastly, the latest technological breakthroughs – quality assessments of shear wave speeds – and how that may be maturing the classification of breast masses.

The audience will understand the state of maturity of Shear Wave Speed technology and the resultant rapid adoption in a clinical setting to enable appropriate guidance in organizations.

References:

[1] Linden, F., Fenn, J.: Understanding Gartner's Hype Cycle. Gartner Group, 05–30–2003.

[2] Moore, G.: Crossing the Chasm: Marketing and Selling High–Tech Products to Mainstream Customers. New York: Harper Business, 1999.

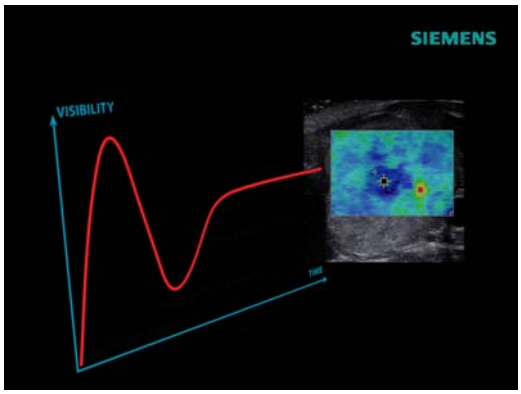

Recent innovations in Shear Wave Speed illustrate the maturity of elasticity technology on Gartner's Hype Model.

Invited Presentation:

099 **THE MODERN ULTRASOUND RESEARCH INTERFACE.**

Reza Zahiri Azar[1], Corina Leung[1], Kris Dickie[1], Laurent Pelissier[1].*
[1]Ultrasonix Medical Corporation, Richmond, BC, CANADA.

Ultrasound is one of the most inexpensive and safest methods to capture real–time medical images. These advantages have made it popular in many medical applications as well as numerous research studies. As a result, having access to its data for research purposes has gained a lot of interest in the past few decades and has been shown to enable new imaging techniques such as elastography and photo–acoustic imaging. Furthermore, having control over all its internal parameters has also proven to be critical in several advanced imaging modes such as ultrafast imaging and angular compounding.

Previous to system designs like the Ultrasonix, research was carried out mainly by using frame grabbers to obtain the analog video signal from the ultrasound, or very large scale systems that could be digitally programmed, but remained immobile. With the miniaturization of technology, and the ability to use more programmable components, the ultrasound market has seen more functional and portable devices become available to researchers. Further, a proper *research interface* is required that makes use of modern software development techniques to efficiently provide data for researchers.

Since the introduction of the research package in 2001, Ultrasonix has always tried to improve the experience of the researchers by allowing them to tailor the system to their custom working environment while still maintaining clinical integrity of using a robust medical device. Its PC–based architecture has drastically simplified the acquisition of ultrasound data, allowing the researcher to have access to these data at every step of the signal processing, starting from pre–beamformed ultrasound data up to the final ultrasound image, in both off–line and real–time modes, on the system itself as well as over the internet. Its programmable hardware and open architecture have also allowed the user to reconfigure all the imaging parameters including all the transmit and receive parameters as well as adjusting all the internal parameters according to their custom applications. Its open architecture has allowed the researcher to integrate his work directly into the system as additional plug ins, thus eliminating the need for additional hardware. Its clinically driven interface has also allowed the researcher to collect data in the clinical environment directly. In addition, custom ultrasound transducers can be easily integrated onto the device allowing researchers to use the system for many different applications.

In this presentation, we will review some of the latest technologies and systems that are developed using Ultrasonix research devices from more than 200 research sites around the world. We will also reveal some works–in–progress technologies that may be implemented into research devices in the near future to help further improve the experience of the researchers.

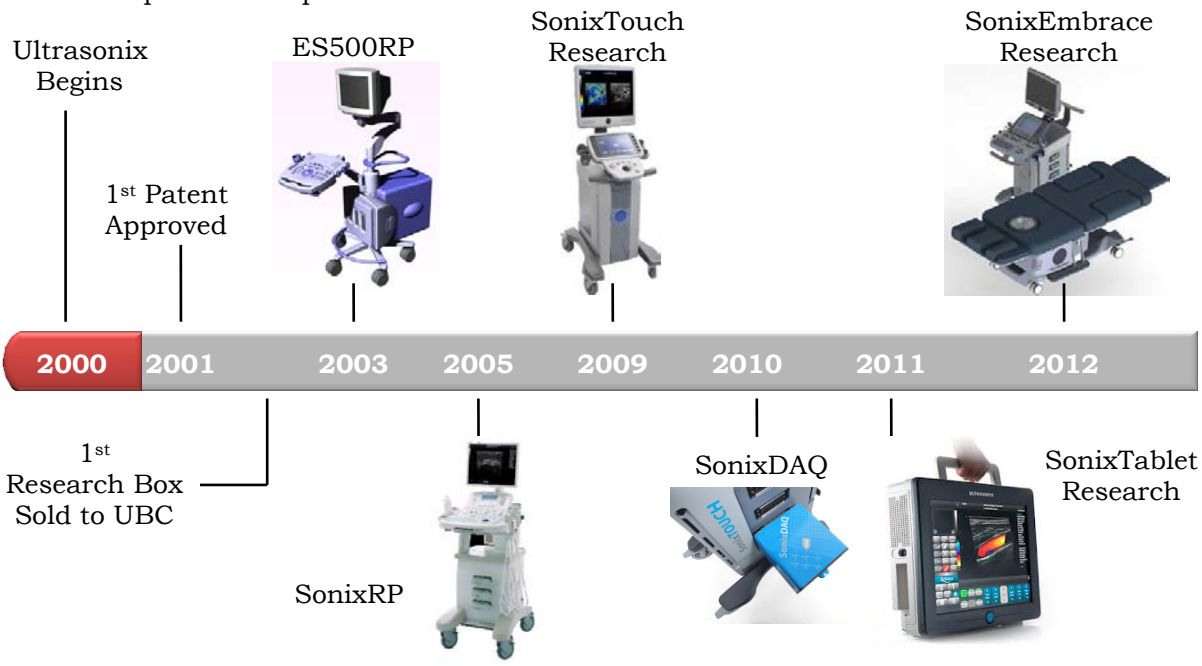

Research Device Time–Line, Ultrasonix Medical Corporation.

* *indicates Presenter*

Invited Presentation:

100 **A NEW PARADIGM IN ULTRASOUND IMAGING.**

J Souquet[1], J Bercoff[1].*
[1]Supersonic Imagine, Aix–en–Provence, FRANCE.

Background: Today there is an intrinsic limitation regarding frame rate acquisition of ultrasound information coming from the body. This limitation is due in part to the speed at which the ultrasound wave propagates in the tissue but also to the architecture of every system on the market whereby the somewhat sequential nature for data acquisition limits the speed at which images can be displayed.

The new paradigm consists of the creation of a new ultrasound system architecture with heavily parallelized acquisition where the receive beamformer is achieved in software. With such a unique architecture, we have demonstrated acquisition frame rate of more than 5000 frames/sec. Such architecture is an enabler of new approaches to ultrasound: speed of sound optimization, transmit synthetic flat focus, etc.

Advantages: Some of those advantages will be demonstrated; however one of the most interesting approaches is to leverage such frame rate for transient elastography. Transient elastography is a unique patented approach to elastography (assessment of tissue elasticity) totally user skill independent. The new approach consists of sending a shear wave into tissue and assess the speed at which the shear wave propagates in real time. Shear wave velocity is directly proportional to the square root of the Young's modulus, therefore, by inverse problem knowing the shear wave velocity, we can derive the elastic properties of tissues and provide a full 2D map of tissue stiffness.

Presentation: We will demonstrate how one can generate shear wave propagation in tissues, why ultra fast frame rate acquisition is a must and share clinical results obtained on different organs like breast, thyroid, liver, prostate and MSK.

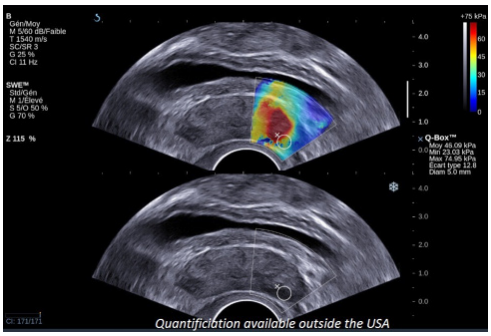

Prostate Lesion

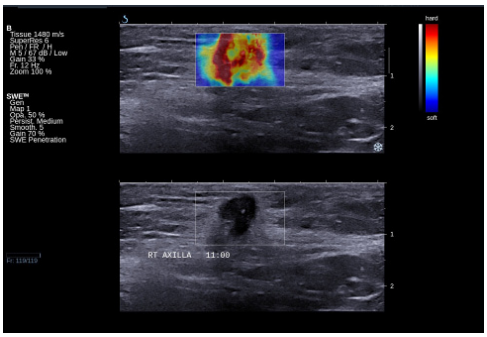

Breast Lesion

051 **SHEAR WAVE IMAGING WITH A CONVENTIONAL SCANNER: THE PASSIVE ELASTOGRAPHY APPROACH.**

Stefan Catheline[1], Rémi Souchon[1] and Jean–Yves Chapelon[1].*
[1]INSERM u1032, University of Lyon, Lyon, FRANCE.

Background: In order to be quantitative, static elastography uses strong assumptions on the stress field homogeneity. In practical *in vivo* situations, the stress field cannot be controlled, thus static elastography results in a strain imaging technique not systematically related to the medium elasticity. However, one of its crucial advantages resides in its simple implementation on commercial ultrasonic scanners with a typical 50Hz maximum frame rate. In this presentation, we propose a solution to control the stress fields while keeping a standard frame rate imaging (50Hz).

Methods: The idea is to replace the homogeneous stress assumption by an equipartitioned field assumption. Indeed, a homogeneously distributed shear wave diffuse field is used with a time reversal approach to create a point force and, from the resulting strain field, compute a shear elasticity mapping. It is thus a mix between shear wave imaging and strain imaging; the stress is piloted by the shear wave equation and, more precisely, by the equipartition principle of energy density on one hand, the elasticity emerges from the Hooke's law on the other hand. Experiments on a CIRS® phantom containing three inclusions, 5mm diameter with elastic moduli ranging from 14 to 80kPa, were performed. The experiment is as follows: in the first step, a diffuse wave field is created inside the sample by random finger impacts on the surface for 20 seconds. The 2D displacement field is then measured inside the soft solid using speckle tracking algorithms developed in elastography. It involves a 192–channel array working at 12MHz with a repetition frequency of 50Hz. In the second step, the displacement at one point chosen as a virtual source is correlated to the other points of the image in order to compute a time reversal field in the computer. The under–sampling of displacements in time does not alter the spatial coherence. Quantitative elasticity images are retrieved from the computed time reversal field using slightly different approaches: wavelength, displacement and strain estimations. These approaches are compared and their validation tested through finite difference simulations and experiments. A first *in vivo* test on the thyroid of a healthy volunteer will be discussed.

Results: Normalised shear elasticity maps are retreived from a diffuse shear wave field from a CIRS® phantom, Figure 1. The characteristics given by the constructor are 80kPa, 45kPa and 14kPa for the inclusions from left to right. The background, 25kPa is used for the normalised shear elasticity $\bar{\mu}$. Our results, 3.6, 2.2 and 0.54 are in good general agreement with those of the constructor, 3.2, 1.8 and 0.56, respectively.

Conclusions: The diffuse field approach offers new possibilities of imaging in elastography. It includes the use of low frame rate imaging devices to track shear waves.

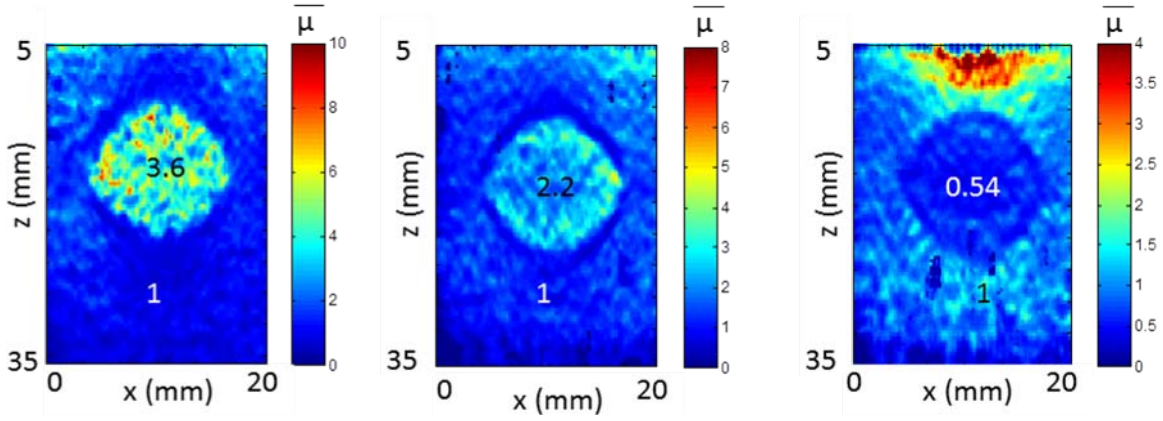

Figure 1: Normalised shear elasticity maps retreived from a diffuse shear wave field of three spherical inclusions of a CIRS® phantom using a 50Hz B&K scanner. The characteristics given by the constructor are 80kPa, 45kPa and 14kPa for the inclusions from left to right. The background, 25kPa is used for the normalised shear elasticity $\bar{\mu}$.

093 **VISCOELASTIC STRESS RELAXATION (VISR) INDEPENDENCE FROM MUSCLE FIBER ORIENTATION WITH LARGE FOCAL CONFIGURATION.**

Mallory R. Scola[1], Caterina M. Gallippi[1].*
[1]Joint Department of Biomedical Engineering, The University of North Carolina at Chapel Hill, Chapel Hill, NC, USA.

Background: Viscoelastic Stress Relaxation (ViSR) ultrasound is a new method for quantitatively assessing the viscoelastic properties of tissue [1]. Using two successive acoustic radiation force (ARF) impulses and monitoring induced displacements in the region of excitation, ViSR measures the stress relaxation time constant in viscoelastic materials, τσ, which equals viscosity coefficient over relaxed elastic modulus in the Voigt model. The key advantages of ViSR ultrasound are that τσ measurements are quantitative and independent from the applied ARF magnitude, and measurements are made only in the ARF region of excitation making it less dependent on tissue homogeneity than methods that rely on shear wave propagation. Moreover, we hypothesize that ViSR measurements of τσ are independent of muscle fiber orientation by using a large focal configuration.

Aims: The purpose of this work is to evaluate the impact of ARF impulse beamwidth on the variance of τσ measurements due to fiber orientation.

Methods: Four different focal configurations were implemented and included F/1.5, F/3, F/4 and F/5. The lateral and elevational point spread functions (PSF) of each focal configuration were characterized in a water bath with a hydrophone. ViSR ultrasound was performed in excised porcine muscle using each focal configuration. The angle of rotation between the transducer and the muscle fibers was varied from 0° (transducer parallel to fibers) to 90° (transducer perpendicular to fibers), with 15° steps. Imaging was performed using a Siemens ACUSON AntaresTM imaging system specially equipped for research purposes and a VF7–3 linear array transducer. ViSR was implemented using two 300–cycle ARF excitations administered to the same region of excitation and separated by 0.35ms in time.

Results: As expected, increasing the F/# of the beam broadened the beam laterally and reduced the difference between the lateral and elevational beamwidths. The measured full width at half maximum values of the 2D PSFs at the focal depth are given in Table 1 and show that for F/5, the lateral and elevational beamwidths are nearly equivalent. Mean ViSR measurements of τσ for the four focal configurations across fiber angle are depicted in Figure 1. For F/1.5, τσ was smallest (0.39 ± 0.03 ms) when the transducer was at 0° (lateral axis parallel to muscle fibers, elevational axis perpendicular to muscle fibers) and largest (0.73 ± 0.08 ms) when the transducer was at 90° (lateral axis perpendicular to muscle fibers, elevational axis parallel to muscle fibers), the mean τσ across all angles of rotation had a variance of 0.012. For F/3, τσ varied from 0.44±0.05ms (0°) to 0.64±0.06ms (90°), with a variance of mean τσ across all angles of 0.005. For F/4, τσ varied from 0.50±0.03ms (0°) to 0.60±0.04ms (90°), with a variance of mean τσ across all angles of 0.002. For F/5, τσ varied from 0.57±0.01ms (0°) to 0.59±0.02ms (15°), with a variance of mean τσ across all angles of 7×10-5.

Conclusions: Results showed a decrease in variance of mean τσ values across fiber orientation as the lateral beamwidth approached the elevational beamwidth suggesting that ViSR is independent of fiber orientation when using a large focal configuration.

Acknowledgements: This work was supported by National Institutes of Health Grant R01NS074057.

References:

[1] MR Scola and CM Gallippi: Multipush (MP) ARF Assessment of Viscoelastic Properties in Tissue–Mimicking Phantoms. Proc. of the 37th Intl. Symp. on Ultra. Imag and Tiss. Charac., Arlington, VA, June 11–13, 2012.

F/#	Elevational Beamwidth	Lateral Beamwidth	Elevational/ Lateral
F/1.5	2.87 mm	1.33 mm	2.16
F/3	2.91 mm	1.80 mm	1.62
F/4	2.84 mm	2.00 mm	1.42
F/5	2.79 mm	2.93 mm	0.95

Table 1: Elevational and Lateral Beamwidths of Focal Configurations.

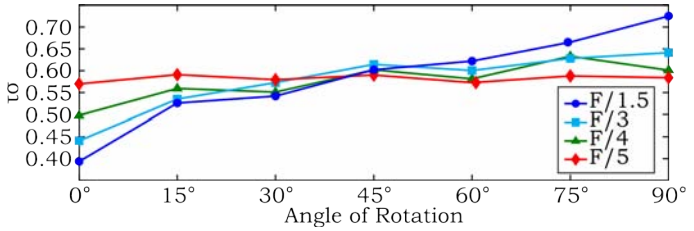

Figure 1: Stress relaxation (τσ) as a function of angle of rotation between the transducer and muscle fibers.

065 **NON–INVASIVE MECHANICAL STRENGTH MONITORING OF VASCULAR GRAFT DURING BABOON CELL CO–CULTURE USING ULTRASOUND ELASTICITY IMAGING.**

D Dutta[1], KW Lee[2], RA Allen[2], Y Wang[2,4], J Brigham[3], K Kim[1,2,4] – Presented by JM Rubin.*
[1]Heart and Vascular Institute, University of Pittsburgh Medical Center, Pittsburgh, PA, USA; [2]Bioengineering Department, [3]Civil and Environmental Engineering Department, [4]McGowan Institute for Regenerative Medicine, University of Pittsburgh, Pittsburgh, PA, USA.

Background: Mechanical strength is a key design factor in engineered vascular grafts for maintaining high burst pressure while preserving compliance of the native vessels. To date, most assessments are made invasively at the end of cell culture; hence, such measurements cannot be correlated with cell growth.

Aims: The aim of this study is to monitor the compliance of a polymer–based vascular graft as fibroblast and smooth muscle cells (SMC) grow on it using non–invasive ultrasound (US) elasticity imaging (UEI).

Methods: Fibroblasts and SMCs isolated from baboon artery were co–cultured on a porous tubular graft inside a bioreactor. The graft was fabricated from a biodegradable elastomer [1]. Flow of cells was maintained using a pulsatile pump, and the pressure was recorded. At the end of days 0, 6 and 13, US radiofrequency frames were captured over one complete pump cycle, and 2D phase–sensitive speckle tracking was applied to estimate the displacement field, from which the average compliance of the graft was determined. Using this average compliance, and the geometry obtained via B–scan, a finite element (FE) model of the scaffold was created and solved for the experimentally observed pressure conditions. Direct mechanical pressure–diameter test using laser micrometer was also performed, and the results were compared to US speckle tracking results.

Results: Axial displacement maps indicating overall distensions of the graft wall are shown superimposed on B–scan images in Figure (a). Average compliance of the graft at the end of days 0, 6 and 13 are plotted in Figure (b). The FE displacement field in Figure (c) qualitatively matches with the displacement field obtained via US speckle tracking thereby confirming that the average compliance value is representative of the overall mechanical strength of the graft. The average compliance of the graft (in %/100mmHg) after days 6 and 13 was found to be 52 and 22.5, respectively, through direct mechanical pressure–diameter tests, which matched closely with the speckle tracking results (50 and 20.2, respectively, as presented in Figure (b)).

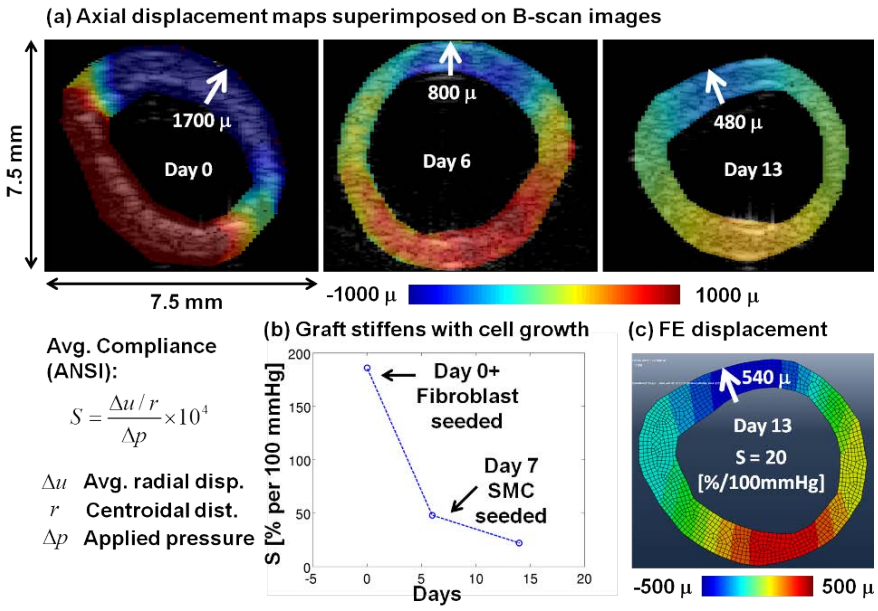

Conclusions: The feasibility of non–invasively monitoring the compliance of a vascular graft with cell growth via UEI is demonstrated. The stiffness increase with multiplication of flibroblasts and SMC agrees well with the mechanical measurements and previous scientific observations. An inverse problem formulation to obtain the compliance distribution in the graft is underway that will help correlate any non–uniformity in graft compliance with non–uniform cell growth.

Acknowledgements: This study was supported in part by NIH 1R21EB013353–01 (PI: Kim). Small animal imaging system (Vevo2100) was supported through NIH 1S10RR027383–01 (PI: Kim).

References:

[1] Lee KW, Stolz DB, Wang Y: Substantial Expression of Mature Elastin in Arterial Constructs. Proc Natl Acad Sci USA, 108, pp. 2705–10, 2011.

* *indicates Presenter*

070 **MEASURING BLADDER VISCOELASTICITY USING ULTRASOUND.**

IZ Nenadic[1], B Qiang[1], MW Urban[1], A Nabavizadeh[1], JF Greenleaf[1], M Fatemi[1].*
[1]Mayo Clinic College of Medicine, Rochester, MN, USA.

Background: Changes in bladder mechanical properties are associated with various diseases. A technique capable of quantifying bladder elasticity and viscosity could be useful in diagnosis and progression of pathology and has the potential to improve the quality of patient care.

Aims: In this study, we propose an ultrasound technique for quantifying elasticity and viscosity of the bladder wall. The approach uses radiation force to excite Lamb waves in the bladder wall and track the motion using pulse–echo ultrasound for the purpose of measuring bladder elasticity and viscosity. The method is applied to measure elasticity and viscosity of an excised and *in vivo* pig bladder wall.

Methods: Focused ultrasound radiation force excites impulsive Lamb waves in the bladder wall and pulse–echo methods measure the motion at several points along the line of wave propagation. Cross–spectral analysis of the echoes is used to calculate wall motion as a function of time. A two–dimensional fast Fourier transform (2D–FFT) of the bladder wall motion as a function of time yields the k–space whose coordinates are frequency (f) and wave number (k). Since the wave velocity c=f/k, the phase velocity at each frequency can by calculated by searching for peaks at the given frequency and dividing the frequency (f) coordinate by the wave number (k) coordinate for the given peak. The Lamb wave dispersion equation is fit to the dispersion data to estimate bladder viscoelasticity. The use of the Lamb wave dispersion equation for flat plate–like organs has been extensively validated in our previous work [1].

Due to curvature of the bladder wall, finite element analysis (FEA) of viscoelastic plates surrounded by a liquid was used to study the effect of bladder curvature on the velocity dispersion. FEA studies were performed using ABAQUS 6.8–3 (SIMULIA, Providence, RI). A flat and a curved plate with the radius of curvature of 4cm, both 2mm thick and assumed to obey the Voigt model where the Young's modulus was 25kPa and viscosity 2Pa·s, were excited with an impulse using a line source. The k–space analysis was used to obtain the Lamb wave velocity dispersion.

In *ex vivo* studies, an excised pig bladder was filled with water until the surface was taut and placed inside a water tank. The inside of the urethra was covered with industrial glue and attached to rubber tubing. A digital pressure gauge (Omegadyne, Inc., Sunbury, OH, USA) was used to measure the pressure inside the bladder. A programmable ultrasound imaging platform (Verasonics, Inc. Redmond, WA, USA) operating a linear array L7–4 transducer (Phillips Healthcare, Andover, MA, USA) was used to excite 200–400μs impulse in the bladder wall and track the motion. Detection pulses were transmitted at a pulse repetition frequency of 4kHz and center frequency of 5MHz. The k–space method was used to calculate the velocity dispersion and the Lamb wave dispersion equation was fit to estimate tissue elasticity and viscosity. The same approach was used for *in vivo* animal studies.

Results: The FEA simulations show that the velocity dispersion is affected by the curvature. Compensating for the angle of curvature in the displacement vector in the curved plate simulations produces the same dispersion as in the flat plate. The *ex vivo* bladder elasticity and viscosity were 48.7kPa and 3.5Pa·s. The *in vivo* bladder elasticity and viscosity were 26.1kPa and 0.9Pa·s.

Conclusions: The FEA results demonstrate that, if accounted for the curvature, the Lamb wave dispersion equation for the flat plate can be used to estimate elasticity and viscosity of the bladder. The *ex vivo* and *in vivo* porcine bladder studies demonstrate the feasibility of the proposed technique to quantify elasticity and viscosity of the bladder tissue.

Acknowledgements: The authors would like to thank to Thomas Kinter and Randall Kinnick for their technical expertise and Jennifer Milliken for administrative support. This project is supported by grant number R01EB002167 and R01EB002640 from the National Institute of Biomedical Imaging and Bioengineering. The content is solely the responsibility of the authors and does not necessarily represent the official views of the National Institute of Biomedical Imaging and Bioengineering or the National Institutes of Health.

References:

[1] I. Z. Nenadic, M. W. Urban, S. A. Mitchell, J.F. Greenleaf: Lamb Wave Dispersion Ultrasound Vibrometry (LDUV) Method for Quantifying Mechanical Properties of Viscoelastic Solids. Phys Med Biol, 56(7), pp. 2245–2264, 2011.

072 **INFERRING TISSUE MICROSTUCTURE USING ELASICITY IMAGING.**

Assad A. Oberai[1], Elizabete Rodrigues–Ferreira[1,2], Paul E. Barbone[3], Timothy J. Hall[4]*

[1]Rensselaer Polytechnic Institute, 110 8th Street, Troy, NY, 12180, USA; [2] Université Libre de Bruxelles, Campus Plaine C.P. 218/1, 1050 Bruxelles, BELGIUM; [3]Boston University, 110 Cummington Street, Boston, MA 12180, USA; [4]University of Wisconsin–Madison, 1005 WIMR, 1111 Highland Avenue, Madison, WI 53706, USA.

Background: The progression of cancer is accompanied by changes in the micro–structural organization of tissue [1]. In particular, it has been observed that an increasingly invasive phenotype is accompanied by an increase in the concentration of collagen fiber bundles and their reorganization from a highly coiled state to a straight, almost rod–like state. These changes in the microstructural organization lead to changes in macroscopic properties. For example, a higher concentration of collagen implies a larger linear elastic modulus and a decrease in tortuosity would mean a smaller "toe" region in the stress–strain curve.

Aims: The main aim of our study is to demonstrate that elasticity imaging techniques that are used to determine linear and nonlinear elastic properties can be extended in order to create images of average micro–structural properties of tissue. Further, that these images may be useful in diagnosing malignant tumors.

Methods: This aim is achieved through 1) Developing a nonlinear, elastic constitutive model derived from tissue micro–structure that contains fiber bundle concentration and tortuosity as parameters. 2) Implementing this model in an inverse problem framework in order to determine the spatial distribution of these parameters from measured displacements. 3) Using displacement measured in benign and malignant tumors in order to test the hypothesis that the spatial distribution of micro–structural parameters can be used to diagnose cancerous tumors.

Results: The response from the nonlinear constitutive law derived from the tissue–microstructure was analyzed in a uniaxial stress–stretch test. It was found that the fiber bundle concentration determined the initial elastic modulus and fiber bundle tortuosity determined the strain at which the departure from a linear stress–strain behavior takes place. Tissue displacement data from a small set of patients was used in order to create images of fiber bundle concentration and tortuosity. These images were analyzed in order to establish correlation between these properties and malignancy. It was found that fiber bundle tortuosity held the potential of being able to diagnose cancerous tumors.

Conclusions: An elasticity imaging based approach for determining the average micro–structural properties of tissue was developed and implemented. Its potential in diagnosing malignant tumors in a small set of patients was also examined.

Acknowledgements: Support from the NIH and the NSF is acknowledged.

References:

[1] P. Schedin, and P.J. Keely: Mammary Gland ECM Remodeling, Stiffness, and Mechanosignaling in Normal Development and Tumor Progression. Cold Spring Harbor perspectives in Biology, 3(1), a003228. doi:10.1101/, 2011.

* *indicates Presenter*

076 **HIGH FREQUENCY RHEOLOGY USING ULTRASOUND TRANSIENT ELASTOGRAPHY ON HYDROGEL.**

Jean–Luc Gennisson[1], Alba Marcellan[2], Alexandre Dizeux[1], Mickaël Tanter[1].*

[1]Institut Langevin – Ondes et Images, ESPCI ParisTech, CNRS UMR 7587, INSERM U979, 1 Rue Jussieu 75005 Paris FRANCE; [2]Physico–Chimie des Polymères et des Milieux Dispersés, ESPCI ParisTech, CNRS UMR 7615, Université Pierre et Marie Curie, 10 rue Vauquelin, 75231, Paris Cedex 05, FRANCE.

Background: Dynamic ultrasound (US) elastography was developed the last decades to assess elastic properties of living tissues, which significantly helps physicians to characterize pathologies. Compared to classical rheology, this technique allows quantifying the mechanical properties of tissues in a frequency range of hundreds of Hertz. Work was performed on hydrogel due to their high building reproducibility and their interesting mechanical properties (highly deformable and self–healing).

Aims: In this presentation, two objectives were pursued: (1) to validate US elastographic measurement by comparing those with classical rheology and (2) to characterize hydrogels at high frequency (>50 Hz).

Methods: Hydrogels were synthetized by radical polymerization of a hydrophilic monomer in presence of water, chemical cross–linker and varied amount of nano–filler. A well–controlled synthesis protocol was optimized in order to get reproducible materials. A fine tuning of viscoelastic properties was obtained by adjusting the gels' formulation. Classical rheology experiments were carried out in plane–shear geometry in order to get the elastic moduli G' and loss moduli G" from 0.1–10Hz. Transient elastography (TE) [1] and Supersonic Imaging (SSI) [2] techniques were used to characterize at high frequency polymers (from 50–1200Hz). TE uses a frequency controlled vibrator fixed at a rigid plate embedded in gels in order to generate plane shear waves. SSI generated shear waves by using ultrasonic radiation force. In both techniques, an ultrafast US device (up to 10,000 frames/s) was used to acquire shear displacements. By using a time of flight detection algorithm, the shear wave speeds were recovered as a function of frequency. In TE, as plane shear waves are generated, shear attenuation is also assessed. Then by using the expression of G' and G" as a function of speed V and attenuation, α, V and α at high frequency were extrapolated from rheological measurement (by assuming a power law) and correlated with experimental US data.

Results: Two hydrogels were tested with different concentrations of scatterers (SP2 and SP5). In these gels, the scatterers are silicon particles which increase the gel resistivity. Hydrogels were weakly dispersive, with an assessed mean speed V_{TE_SP2} = 3.1±0.8 m/s (from 50–800Hz) and V_{TE_SP5} = 5.8±0.4 m/s (from 50–525Hz) and an assessed attenuation following a quadratic law as a function of frequency ($\alpha_{SP2} < \alpha_{SP5}$) in TE. With the SSI technique only, the speed was recovered V_{SSI_SP2} = 3.1±0.1 m/s and V_{SSI_SP5} = 6.4±0.2 m/s (from 400–1200Hz). With classical rheology, a mean value of G' and G" was recovered (SP2 $G' = 3630\omega^{0.093}$, $G'' = 486\omega^{0.122}$; SP5 $G' = 984\omega^{0.142}$, $G'' = 2384\omega^{0.157}$) allowing calculation of theoretical speeds and attenuation at high frequency. A significant correlation was obtained between measured speeds (r_{SP2}=0.93, r_{SP5}=0.88 in TE; r_{SP2}=0.85, r_{SP5}=0.95 in SSI) and attenuations (r_{SP2}=0.88, r_{SP5}=0.79 in TE) when comparing results from rheology and elastography.

Conclusions: The results demonstrate the capability of dynamic US elastography to quantify rheological properties at high frequencies in order to better characterize materials. Future works will be focused on attenuation quantification using the SSI technique.

References:

[1] S. Catheline, J.L. Gennisson, M. Tanter et M. Fink: Observation of Shock Transverse Waves in Elastic Media. Phys. Rev. Lett., 91(16), pp. 43011–43014, 2003.

[2] Bercoff J, Tanter M, Fink M: Supersonic Shear Imaging: A New Technique for Soft Tissue Elasticity Mapping. IEEE–UFFC, 51(4), pp. 396–409, 2004.

Special Topic

024 **EFSUMB GUIDELINES ON THE CLINICAL USE OF ELASTOGRAPHY.**

David O. Cosgrove[1], Fabio Piscaglia[2], Christoph Dietrich[3] for the Guidelines Team.*
[1]Imperial College, London, England, UK; [2]Hospital S. Orsola–Malpighi, Bologna, ITALY; [3]Caritas Krankenhaus, Bad Mergentheim, GERMANY.

Background: Elastography has emerged as a clinically useful addition to conventional ultrasound in many diagnostic applications. However, there is a need to improve standards of practice and interpretation.

Aims: The European Federation of Ultrasound in Medicine and Biology (EFSUMB) recognized the need for a set of Guidelines to inform users of the technique in helping to standardize aspects of the implementation of elastography, especially the display modes and to improve clinical practice and interpretation. The EFSUMB Guidelines that are currently nearing completion aim to further this process.

Methods: A steering committee commissioned experienced European users to submit sections of guidelines along the lines of those previously published for contrast enhanced ultrasound [1,2]. An introductory section on the basic principles is followed by sections covering parts of the body in which elastography is widely used, including the breast, the liver, endoscopic uses, the bowel, the prostate, the thyroid and the musculoskeletal system.

Results: The edited document is to be submitted to the European Journal of Ultrasound (Ultraschall in der Medizin) with a target date of January 2013.

Conclusions: It is hoped that the EFSUMB Guidelines on Elastography will be as useful as the CEUS Guidelines in improving clinical practice.

Acknowledgements: The contribution of the EFSUMB Elastography Guidelines team and of Lynne Rudd, General Secretary of EFSUMB, are gratefully acknowledged.

References:

[1] Claudon M, Cosgrove D, Albrecht T, et al.: Guidelines and Good Clinical Practice Recommendations for Contrast Enhanced Ultrasound (CEUS) – Update 2008. Ultraschall in der Medizin, 29, pp. 28–44, 2008.
[2] Piscaglia F, Nolsoe C, Dietrich CF, et al.: The EFSUMB Guidelines and Recommendations on the Clinical Practice of Contrast Enhanced Ultrasound (CEUS): Update 2011 on Non-Hepatic Applications. Ultraschall in der Medizin, 33, pp. 33–59, 2012.

Special Topic

101 **THE RADIOLOGICAL SOCIETY OF NORTH AMERICA'S QUANTITATIVE IMAGING BIOMARKER ALLIANCE EFFORT TO DEVELOP AND VALIDATE CROSS-SYSTEM SHEAR WAVE SPEED MEASUREMENTS FOR STAGING LIVER FIBROSIS.**

Timothy J Hall[1], Brian S Garra[2,3], Andy Milkwoski[4], Paul L Carson[5], Dan Sullivan[6], David Cosgrove[7], Anthony Samir[8], Claude Cohen–Bacrie[9], Keith A Wear[3], Mark L Palmeri[6].*

[1]University of Wisconsin–Madison, Madison, WI, USA; [2]VA Medical Center, Washington, DC, USA; [3]Center for Devices and Radiological Health, US Food and Drug Administration, Silver Spring, MD, USA; [4]Ultrasound, Siemens Healthcare, Mountain View, CA, USA; [5]University of Michigan, Ann Arbor, MI, USA; [6]Duke University, Durham, NC, USA; [7]Imperial College, London, England, UK; [8]Massachusetts General Hospital, Boston, MA, USA; [9]Supersonic Imagine, Aix–en–Provence, FRANCE.

Background: We are undertaking development of a protocol and data analysis methods to allow direct cross–platform comparison of shear wave speed (SWS) measurements in liver for staging fibrosis. Several systems that measure SWS in the liver are commercially available, and several peer–reviewed manuscripts report the ability to differentiate among fibrosis stages. However, there are many confounding variables that produce substantial variability in quantitative SWS estimates including shear wave spectrum, diffraction, tracking method, operator–related effects, patient motion and motion filters, reflected waves and reflection filters, hemodynamics, measurement acceptance criteria and anatomy. Providing a common SWS estimate result among systems would speed clinical adoption of the technology.

Aims: Our efforts are designed to determine the underlying system–related causes for differences in SWS estimates and develop methods to allow direct cross–platform comparison of measurement results. In addition, we intend to determine the major clinical and biological factors that significantly influence SWS measurement and interpretation. We will develop a protocol for measurements that minimizes the influence of system-related, clinical, and biological confounding factors.

Methods: The Radiological Society of North America (RSNA) has formed the Quantitative Imaging Biomarker Alliance (QIBA) which is a consortium of researchers, healthcare professionals and industry representatives who are collaborating to identify the barriers and solutions that would allow reliable, valid, cross–platform quantitative measurements of clinically useful information from imaging methods. The Alliance is organized by modality committees and within each modality committee is one or more Technical Committee whose efforts involve developing a specific class of biomarker. Each Technical Committee is supported by one or more Subcommittees that investigates and documents specific areas of interest. The Ultrasound Modality Committee was formed in March 2012 and has a single Technical Committee for Shear Wave Speed Measurement. Our first main goal is to reduce variability in SWS as a noninvasive measure of liver fibrosis. We have a subcommittee to determine which phantom materials are suitable for testing cross–platform SWS measurement performance and validating methods to independently assess phantom material properties. A second subcommittee is determining why various SWS measurement systems provide different results in the same media, how those measurements might be directly compared and determining the range of valid measurement conditions. A third subcommittee is tasked with determining the clinical and biological factors that influence SWS measurements and how those factors might be mitigated. Together we will create a QIBA/UPICT (Uniform Protocol for Imaging in Clinical Trials) protocol that specifies methods for data acquisition, analysis and interpretation as well as a QIBA Profile that will provide specific claims of what can be accomplished by following the QIBA Protocol. This QIBA Profile will also tell vendors how their system can be compliant with the profile. We will then validate this profile across imaging systems with phantoms and volunteers and work with other organizations such as drug and instrument companies and clinical trials organizations. We will forward our profile to the FDA so that they can consider our recommendations for use in evaluating clinical trials and approvals/clearances of quantitative measures.

Results: Practical phantom materials have been identified. Many system–dependent, clinical and biological factors that can influence SWS estimates have been identified. Although we are just getting started, we are well along the path to Protocol development.

Conclusions: A great deal of progress has been made in a few short months. We benefit significantly from the involvement of some of the developers of these imaging system technologies.

Acknowledgements: The QIBA effort is funded in part by the RSNA and a contract with NIBIB (HHSN268201000050C). The mention of commercial products, their sources, or their use in connection with material reported herein is not to be construed as either an actual or implied endorsement of such products by the FDA.

009 ***IN VITRO* COMPARISON OF ULTRASOUND BASED ELASTOGRAPHY TECHNIQUES**

Stéphanie Franchi–Abella[1], Caroline Ellie[2], Jean–Michel Correas[2].*
[1]Radiopediatrie, Kremlin–Bicêtre Hospital, 78, rue du Général Leclerc 94270 Le Kremlin–Bicêtre, FRANCE; [2]Radiologie Adulte, Necker Hospital, 149 rue de Sèvres, Paris, FRANCE.

Background: Imaging viscoelastic properties of tissues *in vivo* has been an important challenge and research field for the last few decades. Today elastography imaging is available with various techniques from several ultrasound diagnostic imaging manufacturers. These elastography techniques are based on two different physical principles: strain and Shear Wave Velocity (SWV).

Aims: The purpose of this study was to assess the performance of these two techniques *in vitro* on a calibrated elasticity phantom.

Methods: A skilled ultrasound operator performed all acquisitions on a tissue–mimicking phantom developed for elastography calibration. This phantom contains spherical inclusions of known elasticity embedded in a homogeneous background material (BG) (CIRS 049A Elasticity Phantom Elastography Phantom, USA). With strain elastography, alternative compression and decompression cycles were applied with adequate pressure (using quality index when available). With SWV, no pressure was applied by the transducer on the phantom. Two inclusions had a lower elasticity than the BG: Inclusion 1=12±3kPa, Inclusion 2=18±4kPa. Two inclusions had a higher elasticity than the BG; Inclusion 3=44±6kPa, Inclusion 4=74±10kPa. The BG's elasticity was 30±5kPa. The imaging protocol was performed using high frequency linear transducers on four different inclusions. Quantitative and semi–quantitative measurements were acquired using the ratio between the BG and each inclusion. Based on the elasticity of each inclusion and BG provided by the phantom manufacturer, the theoretical ratios were calculated. These theoretical ratios were compared to the ratios obtained with measurements obtained using the different elastography techniques. For the SWV technique, the absolute values of inclusions and BG were also compared with the phantom values. Five manufacturers were enrolled in this study (named A, B, C, D and E). A, B and C used the strain principle to estimate tissue elasticity while D used both principles and E only SWV.

Results: Table 1 provides the relative difference (in percent) between measured elasticity ratios for all manufacturers/probes and the theoretical ratio for the different inclusions for both strain and SWV. Table 2 provides the relative difference (in percent) between measured elasticity values for manufacturers D and E and the theoretical elasticity values for the different inclusions and BG.

Manufacturer–Probe–Technique	Inclusion 1 (%)	Inclusion 2 (%)	Inclusion 3 (%)	Inclusion 4 (%)
A–Probe1–Strain	22.50	4.10	–19.00	–17.0
B–Probe1–Strain	60.00	21.00	–12.70	–7.7
B–Probe2–Strain	26.25	14.17	–12.40	–13.7
B–Probe3–Strain	17.50	8.33	–16.50	–23.0
C–Probe1–Strain	25.00	11.70	–18.50	–19.8
D–Probe1–Strain	1779.00	493.00	–47.00	–82.0
D–Probe1–SWV	53.00	31.00	–20.00	–13.0
E–Probe1–SWV	–37.00	–8.30	8.2.	1.2

Table 1: Relative difference (in percent) between measured elasticity ratios for all manufacturers/probes and the theoretical ratio for the different inclusions for both strain and SWV.

Manufacturer–Probe–Technique	Inclusion 1 (%)	Inclusion 2 (%)	Inclusion 3 (%)	Inclusion 4 (%)	BG (%)
D–Probe1–SWV	–35.2	–30.3	–39.0	10.0	–33
E–Probe1–SWV	–31.7	–23.3	–1.4	1.3	–8

Table 2: Relative difference (in percent) between measured elasticity values for manufacturers D and E and the theoretical elasticity values for the different inclusions and BG.

Conclusions: Our study shows both techniques are adequate when assessing whether or not an inclusion is harder/softer than its surrounding tissue. However, strain stiffness estimation presents high variability depending on the probe/system, while SWV based elastography is more accurate to assess both absolute and contrast stiffness especially for system E.

* *indicates Presenter*

010 **MONITORING SURGICAL RESECTION OF TUMORS WITH ULTRASOUND STRAIN IMAGING.**

TS Pheiffer[1], BC Byram[3], MI Miga[1,2].*
[1]Vanderbilt University, Nashville, TN, USA; [2]Vanderbilt University Medical Center, Nashville, TN, USA; [3]Duke University, Durham, NC, USA.

Background: Resection of tumors is often performed by the surgeon using tactile sensory information to distinguish between normal and abnormal tissue. Ultrasound strain imaging has potential to supplement conventional guidance methods with quantitative information about tissue stiffness at depth. It has been suggested that strain imaging may be capable of distinguishing tumor from normal tissue during surgery [1–3]. With respect to diagnostic lesion inspection, localization with strain imaging of a potential surgical target is well understood. In this work, we assess the efficacy of this modality to monitor resection.

Aims: The aim of this work is to demonstrate the feasibility of using ultrasound strain imaging to monitor a tumor remnant during surgical resection.

Methods: A phantom was constructed of tissue–mimicking polyvinyl alcohol gel with graphite scatterers and a fabric sphere to serve as the target lesion. The tumor was incrementally resected in three stages, with larger amounts excised at each stage until complete removal was accomplished. Strain imaging was performed of the tumor remnant at each stage of resection, and the tumor cavity was irrigated with water to eliminate air pockets introduced by the resection process. An Acuson Antares ultrasound machine (Siemens, Munich, Germany) was used with a VFX13–5 probe at a frequency of 11.4MHz. Strain images were generated using the eSie Touch Elasticity Imaging software on the ultrasound machine. All imaging was conducted freehand with the probe in approximately the same location lateral to the resection site.

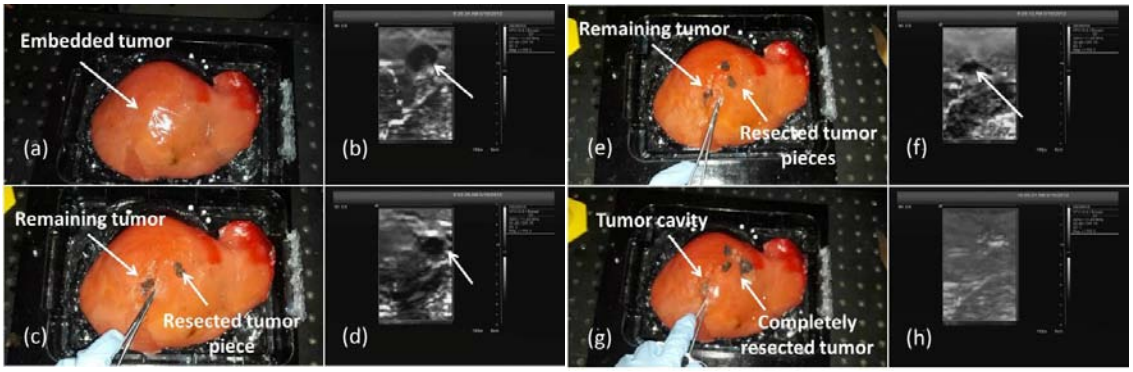

Figure 1: Effects of tumor resection on strain imaging in a cryogel phantom. (a), (c), (e) and (g) show increasing amounts of tumor resection, from no resection to total resection. (b), (d), (f) and (h) show the corresponding strain images of the tumor remnant.

Results: The strain images show the tumor mass with clear contrast against the bulk phantom material prior to resection. After resection of approximately one third of the tumor volume, the lesion still appears in the strain images with a corresponding reduction in image slice cross– sectional area. After resection of another third of the tumor, the tumor mass still clearly appears in the strain images but with a more noticeable decrease in cross–sectional area. Following the complete resection of the entire tumor mass, strain imaging no longer showed a region of low strain in the resection cavity.

Conclusions: The phantom study performed shows the feasibility of using ultrasound strain imaging as a tool for monitoring surgical resection of lesions. It was shown that the excision of tumor mass and the creation of a resection cavity did not obstruct the creation of strain images. In addition, the lesion area in the images decreased in correlation with decreasing remnant tumor volume. Ultrasound strain imaging shows promise as a surgical localization method and awaits further studies within the clinical environment.

Acknowledgements: This work is funded by the National Institutes of Health: grant R01 NS049251 of the National Institute for Neurological Disorders and Stroke.

References:

[1] Chakraborty, A., J.C. Bamber, and N.L. Dorward: Preliminary Investigation into the Use of Ultrasound Elastography during Brain Tumour Resection. Ultrasound, 20(1), pp. 33–40, 2012.
[2] Scholz, M., et al.: Current Status of Intraoperative Real–Time Vibrography in Neurosurgery. Ultraschall Med, 28(5), pp. 493–7, 2007.
[3] Selbekk, T., et al.: Tissue Motion and Strain in the Human Brain Assessed by Intraoperative Ultrasound in Glioma Patients. Ultrasound in Medicine and Biology, 36(1), pp. 2–10, 2010.

040 **MONITORING CRYOABLATION LESIONS WITH QUANTITATIVE ULTRASOUND ELASTOGRAPHY: A FEASIBILITY STUDY.**

Diego Dall'Alba[1], Caitlin Schneider[2], Christoper Nguan[3], Ali Baghani[2], Robert Rohling[2], Septimiu E. Salcudean[2].*

[1]University of Verona, Verona, ITALY; [2]University of British Columbia, Vancouver, BC, CANADA; [3]Vancouver General Hospital, Vancouver, BC, CANADA.

Background: The use of ultrasound (US) elastography (UE) has been widely investigated as a method for monitoring the ablation zone in HIFU or radiofrequency (RF) ablation. UE cannot be used to monitor cryoablation (CA) since the ice–ball zone causes strong reflections and wide shadows. However, the mechanical stresses caused by ice crystal formation do change the tissue's microscopic structures which should also affect its macroscopic elastic properties.

Aims: In this study, we propose to monitor whether tissue has been properly frozen during CA by using UE to monitor tissue elasticity before and after thawing, when the ablated tissue can be imaged again by US. We present an *ex–vivo* animal study that confirms the feasibility of this approach.

Methods: 4 samples obtained from 2 pig kidneys after excision were frozen twice with a protocol that follows the clinical guidelines. Freezing is obtained by immersion in a bath of dry–ice and acetone with a low conductivity coupling container protecting the sample against cryo–shock. The freezing speed was 6°C/minute and thawing speed was 3°C/minute. Each cycle took approximately 35 minutes plus 25 minutes to ensure that the temperature before and after the experiment are the same. The temperature profile is reported in Figure 1. The samples were measured before and after the freezing cycles with absolute UE, using motion tracking as described in [1] and modulus reconstruction based on local frequency estimation [2]. Excitation is provided by an external device (LDS Mod. V203, B&K, Denmark), controlled between 50 and 100Hz. The data were acquired with a US device (Sonix Touch, Ultrasonix, Canada) with a 3D mechanical probe (4DL14–5/38, at 5MHz). A region of interest in the UE data is manually selected within the volume (10 planes for each excitation frequency), and the mean value and the standard deviation is reported in Figure 2.

Results: Preliminary results show a significant difference between tissue elasticity before and after freezing as showed in Figure 1. The significance of the change is also confirmed by a Tukey's Honestly Significant Difference test ($\alpha<0.05$).

Conclusions: The results confirm the feasibility of CA monitoring after complete tissue thawing, extending for the first time the use of UE imaging to CA.

References:

[1] A. Bahgani, S.E. Salcudean and R. Rohling: A High Frame Rate US System for the Study of Tissue Motions. IEEE Trans. UFFC, 57, pp. 1535–47, 2010.

[2] A. Manduca et al.: Local Wave–Length Estimation for MRE. IEEE Int. Conf. on Image Proc., pp. 527–530, 1996.

Figure 1: Measured tissue elasticity before and after the experiment.

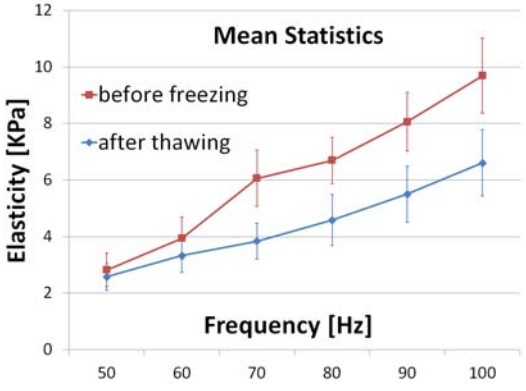

Figure 2: Temperature profile during freezing/thawing cycles.

* *indicates Presenter*

013 **SHEAR WAVE VELOCITY DISCRIMINATION OF INFLAMED FROM FIBROTIC BOWEL SEGMENTS IN A CROHN'S DISEASE ANIMAL MODEL.**

Jonathan R Dillman[1], Ryan W Stidham.[1], Peter DR Higgins[1], David S Moons[1], Laura A Johnson[1], Jonathan M Rubin[1].*

[1]University of Michigan, Ann Arbor, MI, USA

Background: Crohn's Disease is a relapsing and remitting form of transmural inflammatory bowel disease that affects the gastrointestinal tract of both children and adults. Deposition of fibrosis within the bowel wall as response to inflammation occurs unpredictably in some Crohn's disease patients with resultant stricture formation and bowel obstruction. Presently, no diagnostic test can confirm the degree of fibrosis relative to inflammation in a reliable, non–invasive manner.

Aims: To determine if acoustic radiation force impulse (ARFI) elastography–derived bowel wall shear wave velocity (SWV) can distinguish inflamed from fibrotic intestine in a Crohn's disease animal model.

Methods: Appropriate University Committee on the Use and Care of Animals approval was obtained. An acute inflammation Crohn's disease model was produced by treating Lewis rats with a single trinitrobenzenesulfonic acid (TNBS) enema, with imaging performed two days later (n=8). Colonic fibrosis in Lewis rats was achieved by administering repeated TNBS enemas over four weeks, with imaging performed seven days later to allow resolution of acute inflammation (n=8). Nine transcutaneous bowel wall SWV measurements (Virtual Touch IQ/Acuson S3000 ultrasound system; Siemens Medical Solutions, USA) were obtained from the rectosigmoid colon region in all rats without and with applied strain. Mean bowel wall SWVs without and with applied strain were compared between animal cohorts. Receiver operating characteristic curves were created to assess diagnostic performance. Three rats were excluded from analysis due to demise.

Results: Mean bowel wall SWVs were significantly higher for fibrotic versus acute inflammation cohort rats at 0% (3.42±1.12 vs. 2.30±0.51m/s; p=0.047) and 30% (6.27±2.20 vs. 3.61±0.87m/s; p=0.021) applied strain. Both acute inflammation and fibrotic cohort rats demonstrated linear increases in mean SWVs with increasing applied strain with no overlap in the 95% confidence intervals. The mean slopes (0.054±0.029 vs. 0.114±0.044; p=0.016) and y–intercepts (2.07±0.32 vs. 3.33±1.14; p=0.023) were significantly different. The c–statistic of SWV for differentiating fibrotic from inflamed bowel was 0.764.

Conclusion: Bowel wall SWV distinguishes fibrotic from inflamed intestine in a Crohn's disease animal model. This finding could have a major impact in the diagnosis and treatment of strictures in Crohn's disease where fibrotic strictures can only be treated surgically, while inflammatory strictures are treated medically. In addition, the linearity of the slopes in the shear wave vs. applied strain model would remove pre–loading effects up to at least 30% applied strains, which could significantly impact measurement variations that may exist due to different operator pre–loads.

Acknowledgement: This study was funded in part and equipment was provided by Siemens Medical Solutions.

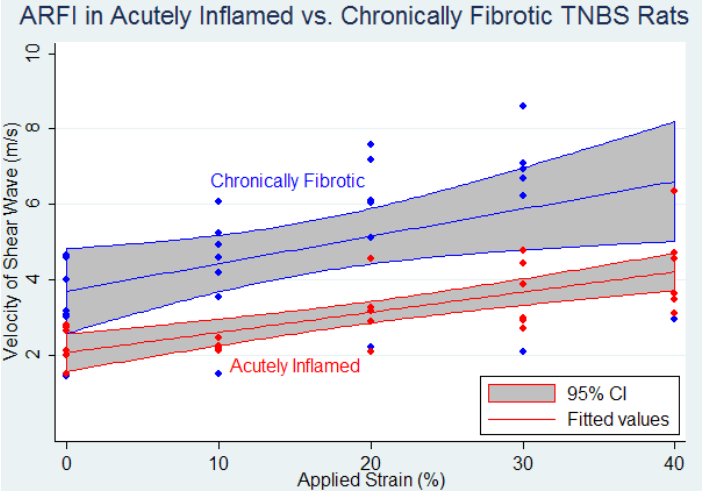

032 **ANALYSIS OF THE INFLUENCE OF INFLAMMATION, IRON AND WATER DIFFUSIVITY ON LIVER VISCOELASTIC PARAMETERS IN FIBROSIS.**

H Leitao[1,2,3], S Doblas[1,2], P Garteiser[1,2], G D'Assignies[1,2], F Mouri[1,2], V Vilgrain[1,2], R Sinkus[1,2], BE Van Beers[1,2].*

[1]INSERM, U773, F–75205, Paris, FRANCE; [2]University Paris Diderot, Sorbonne Paris Cité, UMRS773, F–75205, Paris, FRANCE; [3]University of Coimbra, Coimbra, PORTUGAL.

Background: Increased liver steatosis, inflammation and iron are often observed in patients with liver fibrosis [1,2]. Moreover, the apparent diffusion coefficient (ADC) is associated with water content and the collagen matrix, and restricted diffusion is found with higher stages of fibrosis [3]. Yet, the influence of these factors on liver viscoelastic parameters determined by MR elastography is not fully understood.

Aims: The purpose of our study was to assess the relationship between hepatic viscoelasticity and steatosis, inflammation, iron and ADC.

Methods: All patient studies were performed under informed consent and within the agreement of local ethical guidelines. Thirty–seven patients with chronic viral hepatitis B (n=11) and C (n=26) underwent MR elastography (MRE), diffusion–weighted imaging (DWI) and multiecho imaging (ME) at 1.5T. Liver inflammation, fibrosis, inflammation and steatosis were assessed on percutaneous liver biopsies taken within a maximum delay of two months (mean 29 days). For MRE, we used a spin–echo EPI sequence (TR/TE=320ms/40ms, 4mm in–plane resolution, 3–directional encoding). Mechanical waves (50Hz) were coupled into the liver by an electromechanical actuator. DWI was performed with a spin echo EPI sequence (TR/TE=300/56, 4mm in–plane resolution, 11 b–values from 10 to 500s/mm^2). ME with an EPI readout (TR/TE=120/n×2.3ms; n=1;10) was used to quantify iron and fat. The following viscoelastic parameters were calculated by local inversion of the complex linear viscoelastic 3D wave equation: storage modulus, G' (kPa), loss modulus G" (kPa), absolute value of the shear modulus, G_{abs} (G_{abs}^2=G'^{2}+G"^{2}), propagation coefficient β (2π over the wavelength, mm^{-1}) and attenuation, α (mm^{-1}). The ADC was obtained by fitting a monoexponential function to the pixel intensities obtained at increasing diffusion sensitizing gradient strengths. Fat content was assessed by fitting separate monoexponential functions to the pixel intensities as a function of echo time on in–phase (water + fat) and out of phase (water – fat) echo images, subtracting the respective values predicted by the fit at zero echo time and dividing by two. The iron content was determined by mapping of the T2* MR relaxation coefficient according to the method exposed by Wood et al. [4]. Spearman rank correlation (r) and multiple regressions coefficients (RC) were calculated.

Results: A positive correlation was found between liver fibrosis and all the viscoelastic parameters, with the exception of α (G': r=0.59, *P*<0.001; G": r=0.36, *P*<0.05; G_{abs}: r=0.60, *P*<0.001; β: r=-0.51, *P*<0.01).Correlations were also found between inflammation and G' and G_{abs} (r=0.38, *P*<0.05), whereas ADC inversely correlated with G_{abs} (r=-0.34, *P*<0.05). No correlation was found between steatosis or iron and viscoelasticity. With multiple regression (see Table 1; "n.i.m.": not in model), the influence of fibrosis was significant on G': RC=0.19, *P*=0.003; G": RC=0.14, *P*=0.036; G_{abs}: RC=0.19, *P*=0.002 and β: RC=-0.18, *P*=0.007, but not α. ADC influenced G_{abs} (RC=-429, *P*=0.049). No independent effect was found for steatosis, inflammation and iron.

	A	F	%FF	Fe	ADC
G'	n.i.m.	RC = 0.19 *P* = 0.003	n.i.m.	n.i.m.	n.i.m.
G''	n.i.m.	RC = 0.14 *P* = 0.036	n.i.m.	n.i.m.	n.i.m.
G_{abs}	n.i.m.	RC = 0.19 *P* = 0.002	n.i.m.	n.i.m.	RC = -429 *P* = 0.049
β	n.i.m.	RC = -0.18 *P* = 0.007	n.i.m.	n.i.m.	n.i.m.
α	n.i.m.	n.i.m.	n.i.m.	n.i.m.	n.i.m.

Conclusions: In the multiple regression model, steatosis, inflammation and iron did not correlate with the hepatic viscoelastic parameters. However, a significant individual correlation was found between inflammation and shear and storage moduli. In contrast, decreased water diffusion in liver fibrosis correlated with increased shear modulus in the multiple regression model. These results suggest that a common cause may explain water diffusivity and altered wave propagation in hepatic fibrosis as suggested in phantom and simulation studies [5].

References:

[1] Huwart: Gastroenterology, 135, pp. 32–40, 2008.
[2] Miller: AJR, 196, pp. 553–560, 2011.
[3] Bonekamp: J Clin Gastroenterol, 45(10), pp. 885–92, 2011.
[4] Wood et al.: Blood, 106(4), pp. 1460–5, 2005.
[5] Chatelin et al.: ISMRM Procs, 20, p. 2528, 2012.

* *indicates Presenter*

003 **SHEAR WAVE ELASTOGRAPHY AND PARAMETRIC IMAGING ARE COMPLEMENTARY IN ULTRASOUND DIFFERENTIATION OF NON–MALIGNANT ADRENAL MASSES: INITIAL RESULTS.**

Rafal Z Slapa[1], Anna A Kasperlik–Zaluska[2], Bartosz Migda[1], Kazimierz T Szopiński[3], Antoni Piwowonski [4], Elzbieta Roslonowska[2], Robert K Mlosek[1], Wiesław S Jakubowski[1].*

[1]Diagnostic Imaging Department, Medical University of Warsaw, Second Faculty of Medicine with English and Physiotherapy Divisions, Warsaw, POLAND; [2]Endocrinology Department, Center for Postgraduate Medical Education, Warsaw, POLAND; [3]Dental and Maxillofacial Radiology Department, First Faculty of Medicine, Medical University of Warsaw, Warsaw, POLAND; [4]NZOZ Almed, Jaroslaw, POLAND.

Background: Only some non–malignant adrenal masses present pathognomonic features on reference examination with computed tomography. Proper diagnosis in this cohort of lesions is important for further management.

Aims: To evaluate possibilities of differentiation of non–malignant masses of adrenals with application of a new method for evaluation of stiffness of the tissues, supersonic shear wave elastography, and a new technique for evaluation of enhancement after administration of an ultrasound contrast agent, parametric imaging.

Methods: In the first phase of the study, 16 non–malignant adrenal masses in 13 patients were evaluated with supersonic shear wave elastography with Aixplorer (Supersonic Imagine, France) convex 1–6MHz probe. In the second phase of the study, 15 non–malignant adrenal masses in 12 patients were evaluated in dynamic examination after administration of 2.4ml of ultrasound contrast agent Sonovue (Bracco) with Aplio XG (Toshiba, Japan) convex 1–6MHz and parametric imaging (Toshiba, Japan). The final diagnosis was based on CT, MRI, biochemical studies, follow up and/or surgery.

Results: In the first group, there were 6 hyperplastic nodules, 6 adenomas, 3 cysts and 1 myelolipoma. Mean stiffness of hyperplastic nodules, adenomas, myelolipoma and cysts was: 6.3, 6.8, 29.4, and 0kPa, respectively. In the second group, there were 5 myelolipoma, 5 hyperplastic nodules, 3 adenomas, 1 haemangioma and 1 cyst. Patterns of parametric imaging of arrival time, time and time–to–peak of hyperplastic nodules presented characteristic differential features of peripheral laminar inflow of Sonovue. Patterns for adenomas varied, possibly due to the presence or lack of hormonal hyperfunction. Patterns for adenomas may overlap with those for cysts. Patterns for myelolipoma and haemangioma were different from those for other non–malignant adrenal masses.

Conclusions: (1) Shear wave elastography and parametric imaging may be complementary in ultrasound differentiation of non–malignant adrenal masses. (2) Shear wave elastography may differentiate rare adrenal cysts from solid masses. Parametric imaging may differentiate adrenal adenomas from hyperplastic nodules. (3) Further multicenter large scale studies evaluating ultrasound differentiation of adrenal masses are warranted.

Acknowledgements: Supported by the Ministry of Science and Higher Education of Poland grant Nr N N402 481239 in years 2010–2013. We thank Miro, Inc. Poland, a representative of Supersonic Imagine, Inc., France for lending the Aixplorer for trial.

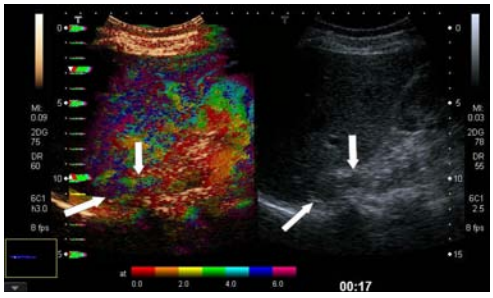

Figure 1: Two nodules (arrows) of right adrenal nodular hyperplasia. On the parametric image of the arrival time (color) the characteristic peripheral laminar inflow of Sonovue is visible.

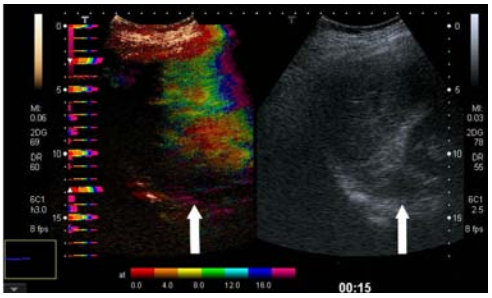

Figure 2: Right adrenal adenoma (arrow). On the parametric image of the arrival time (color) peripheral & central inflow of Sonovue is visible.

002 **ANALYSIS OF THYROID NODULES VISCOELASTICITY WITH TIME STRAIN CURVES MAY SURPASS CLASSICAL QUALITATIVE AND SEMI–QUANTITATIVE EVALUATION.**

Rafal Z Slapa[1], Bartosz Migda[1], Wiesław S Jakubowski[1], Jacek Bierca[2], Jadwiga Slowinska–Srzednicka[3].*

[1]Diagnostic Imaging Department, Medical University of Warsaw, Faculty of Medicine II with English and Physiotherapy Divisions, Warsaw, POLAND; [2]Surgery Department, Solec Hospital, Warsaw; POLAND; [3]Endocrinology Department, Center for Postgraduate Medical Education, Warsaw, POLAND.

Background: It is assumed that elasticity is linear with deformation in the range of 1%. However, observation of time–strain curves of thyroid nodules subjected to free–hand strain elastography indicates both linear and non–linear portions of relaxation.

Aims: The purpose of the study was to evaluate a new linear/non–linear approach for strain elastography of thyroid nodules based on the analysis of time strain curves and compare it with classical elasticity score and thyroid strain ratio methods.

Methods: During 2009–2011, 67 patients scheduled for thyroidectomy (62 with multinodular goiter and 5 with a single thyroid nodule) were evaluated with B–mode and power Doppler ultrasound of the whole thyroid and neck lymph nodes. During the ultrasound examination, 96 dominant nodules were examined with strain elastosonography with Aplio XG (Toshiba, Japan) with a linear 5–17MHz transducer. The stiffness of each thyroid nodule was evaluated on the pair of images with classical features of strain elastosonography qualitatively (with elasticity scores) and semi–quantitatively with thyroid tissue strain/nodule strain ratios with application of elasto Q (Toshiba, Japan). Moreover, a novel, original approach to elasticity data based on evaluation of time strain curves (elasto Q) was applied.

Results: The incidence of thyroid cancer that was not known before our ultrasound examination (5 nodules) in our study shows that cancer is present in 9% of the 54 patients. Final diagnosis established 7 papillary carcinomas (6 in multinodular goiter), 4 follicular adenomas and 85 benign nodular goiter nodules. Classical elastographic analysis with elasticity score and elasticity ratio on statistical analysis did not show a significant difference between cancer and benign nodules (p–value=0,431 and 0,156, respectively). On linear/non–linear analysis of time strain curves, excellent differentiation (p=5.6x10–9) was possible with new parameter: the Relative Length of Non–Linear Relaxation (with threshold 0.5, sensitivity 100% and specificity 85.4%, area under ROC=0.975).

Conclusions: (1) The incidence of thyroid cancer that was not known before our ultrasound examination in our study is comparable to the incidence of cancer in the general population of multinodular goiter patients even though the number of cancers in the study is small. (2) The analysis of linear and non–linear elastography data may greatly improve differential diagnosis of thyroid nodules. (3) Different timing for conversion from linear to non–linear relaxation between papillary thyroid cancer and benign thyroid nodules may indicate that viscosity may be the differential factor. (4) Further multicenter large scale studies evaluating the usefulness of linear/non–linear elastography phenomena in differential diagnostics of thyroid cancer are warranted. Studies involving evaluation of vioscoelasticity (e. g., shear wave spectroscopy) could be applied to investigate the model of thyroid nodules differentiation.

Acknowledgements: I would like to thank Dr. Jeffrey Bamber and other lecturers at 10th ITEC 2011 in Arlington for inspiration. Supported by the Ministry of Science and Higher Education of Poland grant Nr N N402 476437, 2009–12.

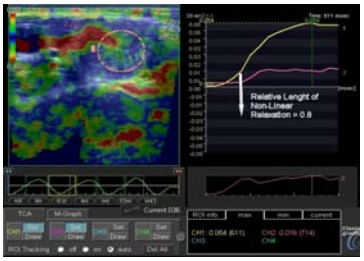

Figure 1: Papillary carcinoma of the thyroid in patient with nodular goiter. Elasticity score=1 and thyroid tissue/nodule strain ratio=0.3 both indicate benign lesion. Relative Length of Non–Linear Relaxation=0.8 truly indicates malignant lesion.

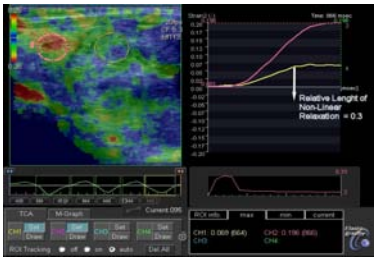

Figure 2: Benign thyroid nodule in patient with nodular goiter. Elasticity score=3 and thyroid tissue/nodule strain ratio=2.8 both indicate malignant lesion. Relative Length of Non–Linear Relaxation=0.3 truly indicates benign lesion.

* *indicates Presenter*

014 **CEREBRAL TISSUE MOTION AND LEUKO–ARAIOSIS IN THE ELDERLY: A CORRELATION STUDY USING ULTRASOUND AND MAGNETIC RESONANCE IMAGING.**

R. Ternifi[1], X. Cazals[1], A. Lorette[1], T. Desmidt[1], V. Camus[1], J.P. Cottier[1], F. Patat[2] and J.P. Remenieras[1].*
[1]Université François Rabelais, UMRS INSERM U930, 10 bd Tonnellé, 37032 Tours, FRANCE; [2]CIC–IT 806, CHRU de Tours, Tours, FRANCE.

Background: Leuko–araiosis (LA) is the term describing lesions and rarefaction of the cerebral White Matter (WM) and is frequently seen in aged individuals. Although the mechanism of LA remains unknown, a decrease in cerebral perfusion is suspected to be linked to LA. Many patients can have LA without associated any clinical abnormality, however, new findings suggest that LA may be clinically important [1,2]. Patients with LA have a decreased prognosis in terms of death, stroke and myocardial infarction occurrences.

Aims: The aim of our work was to study the relationship between LA and the natural brain tissue velocity due to pulsed cerebral perfusion. Brain velocities were measured with an analog of the Tissue Pulsatility Imaging (TPI) method described by Kucewicz [3], which already been used by our group for depressed patients [4].

Methods: Nine healthy female volunteers between the ages of 60 and 85 were enrolled in this cross–sectional study. Transcranial acquisitions were performed with a 2MHz phased–array probe through the right temporal bone window, and off–line estimations of velocity were performed by 1D correlation methods on the radiofrequency (RF) lines of the collected 2D data. Velocity signals were then filtered around the cardiac frequency to remove the respiratory component. MRI examinations were performed on a 1.5T GE system using dedicated software (MRIcro) to obtain a volumetric analysis. The primary endpoints of the study were the maximum brain velocity (TPImax), the absolute MRI volume of WM hypersignals (VAbs) and the relative volume of the right hemisphere (VRel). The Pearson correlation coefficient was used for statistics.

Results: Our main finding is that TPImax decreases significantly when the severity of LA increases, see Figure 1. Significant inverse correlation between TPImax and VRel (ρ=-0.81, $p<0.004$) is observed despite the small size of our recruitment.

Conclusions: For LA and other neurodegenerative pathologies being considered to have a strong link with brain vascular defects, the ultrasonic TPI method appears to be valuable and promising.

References:

[1] Wang L et al.: Neuroradiology, 53(5), pp. 373–381, 2011.
[2] Hirono N et al.: Stroke, 31(9), pp. 2182–8, 2000.
[3] Kucewicz JC et al.: Ultras Med Biol, 33, 5, pp. 681–90, 2008.
[4] Desmidt T et al.: Psych Res, 30,193, pp. 63–4, 2011.

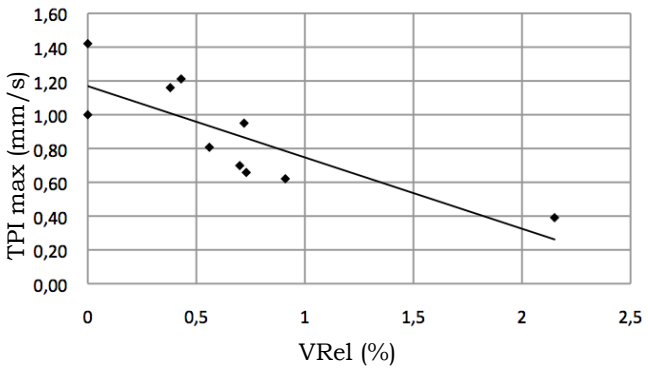

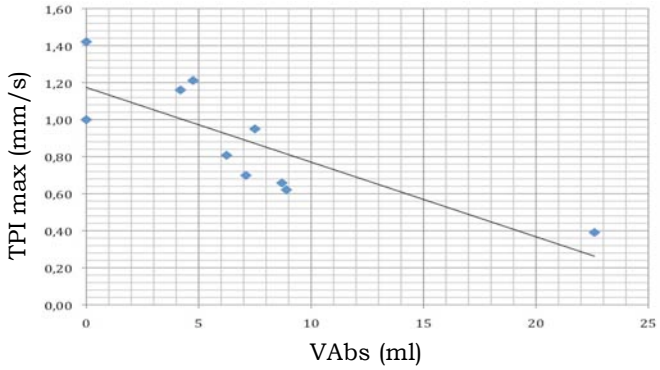

043 **ROLE AND OPTIMISATION OF THE INDENTER SIZE FOR QUANTITATIVE POROELASTOGRAPHY.**

Jérémie Fromageau[1], Nigel Bush[1], Jeffrey C. Bamber[1].*
[1]The Institute of Cancer Research and Royal Marsden Hospital, 15 Cotswold Road, Sutton, Surrey, England, UK.

Background: It is known that subjecting a poroelastic object that has free and permeable boundaries to a sustained unidirectional compression results in a 3D internal volumetric strain that varies with position and time, which can be used to estimate tissue properties such as permeability, related to interstitial pressure and the capacity of fluid to diffuse through the elastic porous matrix. Experimentally, it is desirable to apply a uniform compression, but this has the drawback that the response is dependent on the size of the poroelastic object, and this is unknown *in vivo*.

Aims: In this study we investigated a technique to solve this problem by applying the compression with an indenter on a very limited surface of the tissue (much smaller than the size of the object), which produces a spatially-limited region of fluid motion and to determine the optimum indenter size for which the effect of sample size become negligible.

Methods: Simulations using MARC Mentat™ (MSC Software) were used to study the spatio–temporal dependence of volumetric strain from cylindrical samples compressed with an indenter of size varying from 0mm to the sample diameter. The results were quantified in terms of relaxation time and compared with those from experiments using agarose ultrasound–scattering phantoms with similar geometry and boundary conditions. Experimental observations were made with an ultrasound scanner (DIASUS, Dynamic Imaging), using a 3D 7MHz probe. The probe was connected to a test instrument (Instron 3342), permitting control of its displacement and recording of the applied pressure for the duration of the experiment. For the uniform compression, the probe itself was used as the compressor. The volumetric strain in the phantom was estimated from the radiofrequency (RF) echo signals using a 2×2D cross–correlation elastography method.

Results:

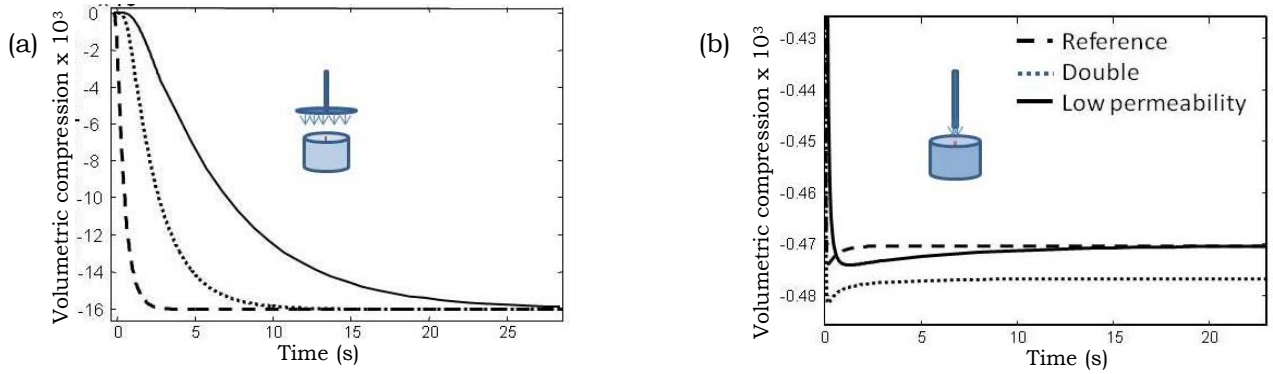

Figure 1: Simulated volumetric strain relaxations at the centre of a reference cylindrical poroelastic sample. (a) For a uniform compression applied on the reference cylinder (dot line), a cylinder of double diameter (dashed line) and a cylinder of same reference size but lower permeability (solid line). Changes of either scale or permeability lead to an increase of the relaxation time, and it can be challenging to discriminate the two effects. (b) For an indentation compression, the relaxation time to depend only on the permeability (same coding).

Conclusions: The results showed that when compressing with a small indenter, the strain relaxation rate depends only on permeability, unlike the uniform compression where it also depends on the size of the object. It should therefore be possible to use the technique for a reliable quantitative characterization. The time constant for strain relaxation is also much shorter than for the uniform compression experiment, making it more suitable for clinical implementation.

Acknowledgements: This work was supported by grants from EPSRC (EP/E030505/1).

** indicates Presenter*

060 **VISCOELASTICITY PARAMETERS OF HIFU ABLATED CANINE LIVER TISSUES *EX VIVO*.**

Danial Shahmirzadi[1], Gary Y. Hou[1] and Elisa E. Konofagou[1].*
[1]Columbia University, VC 12–232, 622 West 168th Street, New York, NY, 10032, USA.

Background: The feasibility of using elasticity imaging techniques for high–intensity–focused–ultrasound (HIFU) ablation monitoring and assessment has been previously demonstrated both *in vitro* and *in vivo* (e.g. [1,2]). Nonetheless, effective use of these techniques requires quantitative assessment of the changes in the mechanical properties of the ablated tissue during the treatment process. The present study focuses on the ablation effects on the liver tissue viscoelasticity *ex vivo*.

Aims: To quantify the viscoelastic shear properties of thermally–ablated canine live tissue *ex vivo*.

Methods: Canine liver specimens (n=6) were freshly excised immediately after sacrifice and kept immersed in de–ionized and degassed phosphate–buffered saline (PBS) at room temperature during the entire in vitro experimentation process. A therapeutic transducer (f_{center} = 4.755MHz, f_{AM}=25Hz, Riverside Research Inst, NY) was used to thermally ablate the liver test samples under 4 increasing HIFU energy levels of 36 W×10s=360J (n=9; Group 1), 25W×30s=750J (n=15; Group 2), 30W×30s=900J (n=18; Group 3), and 36W×30s=1080J (n=11; Group 4). After completion of the thermal ablation, the same test samples were tested regarding their viscoelastic parameters using a rheometer (TA Instrument, DE). The complex shear modulus (G*) and shear phase shift (δ) were obtained under a shear strain of ε=1% at a sweeping frequency range of f=0.1–10Hz. The measurements were also used to compute the tissue dynamic shear viscosity coefficient (η').

Results: Figure 1 shows an example of a very large HIFU lesion in a liver sample. The shear complex modulus and dynamic viscosity for the unablated and ablated samples are shown in Figure 2 as a function of shear strain frequency (logarithmic scale). Most notably, the results indicate that all of the ablated samples (Groups 1–4) possess a shear complex modulus and a dynamic viscosity of about an order of magnitude higher than those of the unablated samples. However, the stiffening of ablated samples in Groups 1 and 2 (i.e. lower thermal energies) is greater than that of samples in Groups 3 and 4 (i.e. higher thermal energies), all compared to the unablated tissue. The complex modulus and the dynamic viscosity were also found to hold direct and reverse relationships, respectively, to the frequency.

Conclusions: The findings in this study indicated that raising the thermal ablation energy does not guarantee a monotonic increase in stiffness or viscosity of the ablated tissue with HIFU exposure. The shift from high stiffening to reduced stiffening that occurs at the higher ablation energies could possibly be explained in terms of the tissue thermo–mechanical effects occurring at very high temperatures. Specifically, *in situ* peak temperature measurements of higher than 107°C in samples under similar experimental parameters [3] indicate that tissue pulverization is likely to occur during boiling of the tissue thereby altering both the structural and mechanical properties of the tissue. Quantification of such phenomena plays a significant role in proper adjustment of the elasticity imaging experimental set up in order to generate the target ablated lesion effectively. Future studies are needed to examine the tissue viscoelastic behavior under a wider range of thermal ablation energies (i.e. including lower levels) in order to better differentiate between high tissue stiffening due to coagulation at lower ablation energies and reduced tissue stiffening due to pulverization at higher ablation energies.

References:

[1] Maleke et al.: Phys Med Biol, 53, pp. 1773–1793, 2008.
[2] Maleke et al.: IEEE Trans Biomed Eng, 57, pp. 7–11, 2010.
[3] Hou et al.: IEEE Int Ultras Symp, in press, 2012.

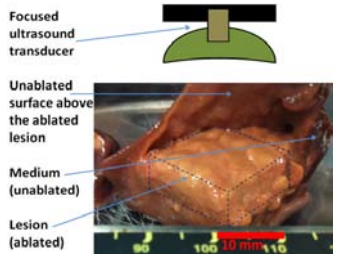

Figure 1: An example image of a very large HIFU lesion in a canine liver sample *ex vivo*.

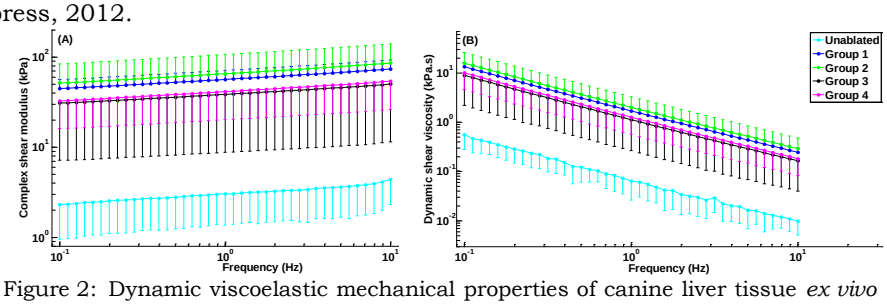

Figure 2: Dynamic viscoelastic mechanical properties of canine liver tissue *ex vivo* as a function of temperature: (A) Complex shear modulus (G*); (B) Shear dynamic viscosity coefficient (η'). The error bars (either upper or lower) indicate the standard deviations in each group.

* *indicates Presenter*

This Page intentionally left blank.

004 **SHEAR WAVE IMAGING USING HARMONIC DISTORTION OF SINUSOIDAL EXCITATION.**

Yoshiki Yamakoshi[1], Parajuli Raj Kumar[1], Reisen Tei[1], Daisuke Nakai[1], Yui Tsuihiji[1].*
[1]Gunma University, 1–5–1 Tenjin–cho, Kiryu–shi , Gunma 376–8515 JAPAN.

Background: Continuous shear wave excitation (CSWE) has potential in tissue characterization, and numerous methods have been proposed in order to reconstruct different kinds of maps [1,2]. For example, a shear wave propagation map gives information about the mechanical structure of a medium, such as adhesion and denaturation of tissue. However, the problem of CSWE is that the spatial resolution is limited by wavelength of shear wave, and it is difficult to introduce high frequency shear wave due to large attenuation in tissue.

Aims: We propose an imaging method which reconstructs phase modulation component of harmonic distortion in continuous shear wave excitation.

Methods: A local velocity map is used in order to recover the phase modulation component of shear wave harmonic distortion. First, the complex displacement map is calculated from an ultrasonic wave Doppler signal by using cross–correlation of up–sampled radio–frequency (RF) signals. Then, the vibration phase map is derived. A local velocity map is reconstructed from spatial differentiation of the vibration phase map along the shear wave propagation direction. When there is no phase modulation in the shear wave, the local velocity map becomes a shear wave velocity map. But if there is small amplitude phase modulation, the phase modulation appears on the shear wave velocity map as wave–front pattern of the harmonic component. The normal direction of the pattern shows the propagation direction, and the interval between the peaks corresponds to the wavelength. Visibility of the pattern shows the modulation index. In order to reconstruct the harmonic component of the shear wave, Fourier analysis method is well known. However, in real–time image reconstruction, spectral resolution of Fourier analysis is not enough for the harmonic component of small amplitude. The proposed method uses spatial differentiation of the vibration phase in order to obtain the harmonic component, image of relative high signal–to–noise (S/N) is obtained when the data acquisition time is limited.

Results: Images which are obtained for an agar gel phantom are shown in Figure 1. The vibration frequency is 700Hz. Figure 1a is the real part of the complex displacement which shows the wave–front of the fundamental component of the shear wave. Figure 1b shows the phase modulation component which is reconstructed by the proposed method. Figure 1c is the real part of complex displacement which is reconstructed for 3rd order harmonic component by Fourier analysis method. From the result, the wave–front of small amplitude harmonic distortion, which is difficult to observe by Fourier analysis method, is reconstructed by the proposed method. In this experiment, harmonic distortion at the vibrator head, which is measured by 3axes accelerometer, is -47dB (3rd order). Existence of the phase modulation is also observed on complex displacement vector space. Figure 2 shows an experimental result *in vivo* (muscle of upper arm). The vibration frequency is 250Hz. Figure 2a is the shear wave amplitude map for the fundamental component. Figures 2b and 2c are the local velocity map and the phase modulation component, respectively.

Conclusions: We proposed a visualization method of the harmonic component with small amplitude. Although the result is preliminary, this map might be useful in observation of mechanical structure of medium.

References:

[1] Y. Yamakoshi, J. Sato, and T. Sato: Ultrasonic Imaging of Internal Vibration of Soft Tissue under Forced Vibration, IEEE Trans. on UFFC, 37, 45–53, 1990.
[2] K. Parker, M. Doyley and D. Rubens: Imaging the Elastic Properties of Tissue: The 20 Year Perspective, Phys. Med. Biol. 56, R1–R29, 2011.

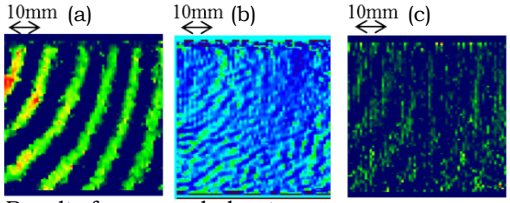

Figure 1: Results for agar gel phantom
(a) Complex displacement spectrum map (real part).
(b) Phase modulation map by the proposed method.
(c) 3rd order harmonic component reconstructed by Fourier analysis method (real part of complex displacement).

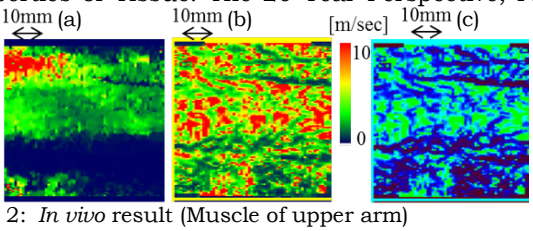

Figure 2: *In vivo* result (Muscle of upper arm)
(a) Shear wave amplitude map for fundamental component.
(b) Local velocity map by the proposed method.
(c) Phase modulation map reconstructed by the proposed method.
Vibration frequency is 250Hz.

028 **PLANE WAVE IMAGING FOR FAST VASCULAR STRAIN ESTIMATION.**

HHG Hansen[1], Bart Wijnhoven[1], Chris L. de Korte[1].*
[1]Radboud University Nijmegen Medical Center, Geert Grooteplein 10, Nijmegen, The NETHERLANDS.

Background: Ultrasound strain imaging can be used to assess local mechanical properties of tissue. From conventional non–steered ultrasound acquisitions, the vertical displacement and strain can be estimated accurately. For the estimation of strains in transverse vascular cross–sections an accurate assessment of the horizontal displacement and strain component is also required. These can be derived by compounding of axial displacements estimated at two additional beam steering angles [1]. However, compounding might be difficult because the artery is in motion during the change of beam steering angle. Therefore, high frame rates are required. Plane wave ultrasound transmission allows higher frame rates [2,3]. However, the question is how plane wave transmission affects strain estimation accuracy.

Aim: To compare the strain estimation accuracy obtained with single or multi–angle plane wave transmission and focused 0° and multi–angle focused imaging.

Methods: A finite element model (FEM) of a vessel with a vulnerable plaque was constructed. Based on the FEM, the 2D displacement and strain fields were calculated for an intraluminal pressure increase of 4mmHg (strains ranged from 0 to ~5%). Radiofrequency (RF) data of the vessel before and after deformation were simulated using Field II software. RF data were simulated for a linear array transducer (3–11MHz, f_c=8.5MHz, pitch=135µm) that either transmitted focused pulses or plane waves at beam steering angles of -30°, 0° and 30°. In receive, dynamic focusing was applied by using delay–and–sum post–processing [4]. Band limited noise was added to obtain a signal–to–noise ratio of 20dB. Displacements were iteratively estimated using 2D cross–correlation. Next, radial, circumferential and principal strains were derived using 1D least squares strain estimators, and the median and inter–quartile ranges (IQR) of the absolute differences between the estimated strains and the FEM principal strains were determined. Strains were compared to focused 0° transmission and reception, multi–angle focused transmission and reception, 0°plane wave transmission and multi–angle reception and multi–angle plane wave transmission and reception.

Results: Table I shows the strain results for the various methods and the corresponding frame rates. Compounding after focused transmission resulted in the most accurate strain results, followed by compounding after multi–angle plane wave transmission, compounding after 0° plane wave transmission and 0° focused imaging. The differences between the various methods were all significantly in favor of the method with lower median value (Wilcoxon, $P<0.05$), except for the comparison marked by "*" in Table I.

	0° Focused Imaging (%)	**Compound Focused Imaging (%)**	**Compound Multi-Angle Plane Wave Imaging (%)**	**Compound 0° Plane Wave Imaging (%)**
Radial Strain	0.65 (0.28–1.21)	0.24 (0.11–0.43)	0.33 (0.15–0.67)	0.51 (0.20–1.32)
Circum Strain	0.68 (0.30–1.27)*	0.29 (0.14–0.54)	0.49 (0.21–1.01)	0.66 (0.31–1.24)*
Principal 1	0.74 (0.32–1.35)	0.28 (0.13–0.53)	0.40 (0.18–0.75)	0.64 (0.30–1.33)
Principal 2	0.69 (0.29–1.34)	0.25 (0.12–0.45)	0.38 (0.16–0.89)	0.49 (0.19–1.21)
Frame Rate	120 Hz	40 Hz	4000 Hz	12000 Hz

Table 1: The median and IQR of the absolute differences between the FEM strain fields and the strains estimated based on RF data obtained by the various transmission methods.

Conclusions: Strain compounding after plane wave transmission outperforms conventional 0° strain estimation and has the additional advantage that frame rates can be increased up to a factor 100. Compared to compound focused imaging, compound plane wave imaging performs slightly worse. However, because frame rates are 100–300 times faster, compound plane wave imaging might turn out to be more accurate in pulsating arteries because it suffers less from motion artifacts. Experimental studies and *in vivo* experiments in pulsating vascular structures will have to be carried out to test this hypothesis.

Acknowledgements: This research is supported by the Dutch Technology Foundation STW (NKG 07589), Applied Science Division of NWO and the Technology Program of the Ministry of Economic Affairs.

References:

[1] H.H.G. Hansen et al.: Physics in Medicine and Biology, Vol. 5, No. 11, pp. 3201–3218, 2010.
[2] H. Hasegawa and H. Kanai: IEEE Trans. Ultrason. Ferroelectr. Freq. Control, Vol. 55, No. 12, pp. 2626–2639, 2008.
[3] M. Tanter et al.: IEEE Trans. Ultrason. Ferroelectr. Freq. Control, Vol. 49, No. 10, pp. 1363–1374, 2002.
[4] T. L. Szabo: Diagnostic Ultrasound Imaging, 2004.

* *indicates Presenter*

041 **COMPARING THE PERFORMANCE OF SPARSE ARRAY AND PLANE WAVE IMAGING SYSTEMS IN NON–INVASIVE VASCULAR ELASTOGRAPHY.**

*Sanghamithra Korukonda[1], Rohit Nayak[1], Marvin. M. Doyley[1]**
[1]Electrical and Computer Engineering Department, University of Rochester, Rochester, NY, 14627 USA.

Background and Aims: Non–Invasive Vascular Elastography (NIVE) of the carotid artery is an emerging diagnostic technique that can improve the detection and characterization of cardiovascular disease. To fully describe arterial motion and produce reliable strain elastograms, it is necessary to acquire high quality axial and lateral displacements. Parallel–receive imaging techniques allow for real time imaging of the artery along with customized beamforming for improved displacement estimation and strain recovery. The aim of this work is to compare the efficacy of two such techniques viz. sparse array [1] and compounded plane wave [2] imaging in the context of NIVE.

Methods: Simulation and experimental studies were performed to compare the two techniques in terms of standard image quality (IQ) metrics such as root mean square error and elastographic contrast to noise ratio. Finite element modeling software, Abaqus™, was used to generate mechanical models of carotid cross–sections subjected to an intra–luminal pressure of 600Pa. Field II was used to simulate a 128 element simulated linear array (center frequency 5MHz and sampling frequency of 40MHz) modeled on the specification of the L14–5/38 probe. Sparse array (SA) scans with 15 transmit elements and 15 plane wave (PW) scans steered over ±14º, in increments of 2º, were acquired of the pre– and post–compressed carotid cross–sections. SA and PW images were beamformed by numerically summing coherent wavefronts at each location within the image. Compounded PW images (CPW) were obtained by spatially adding steered PW images. 2D cross–correlation analysis was performed to obtain axial and lateral displacement estimates that were combined to generate radial and circumferential strain. Experimental studies were performed with a SONIX RP system (Ultrasonix, Inc., Vancouver, Canada), equipped with an L14–5/38 linear array probe to corroborate the simulation study. Tissue–mimicking vessel phantoms subjected to intra–luminal pressures differences ranging from 5–20mmHg were imaged using the SA and PW systems.

Results: Strain elastograms obtained with the SA, PW and CPW systems were inspected visually and evaluated using predefined IQ metrics. While CPW imaging improves the error produced by PW strain elastograms, the SA strain elastograms exhibit 20% less error than the PW systems. Figure 1 shows strain elastograms obtained from a simulated phantom containing a soft plaque (3 o'clock). The plaque, seen as a region of localized high strain, is clearly demarcated in the radial (b) and circumferential (d) strain elastograms obtained with the SA. The plaque is also seen the plane wave elastograms (b, d), though it is not as clearly defined. Compounding improves the strain images (d, h), but the images are not as clear as those obtained with the sparse array. Similar observations were made in the experimental studies.

Conclusions: Both PW and SA systems produce reasonable vascular strain elastograms. While compounding improves the lateral sensitivity of PW imaging, SA imaging produces superior strain elastograms both in simulation and experiment. These results warrant pre–clinical investigations into the utility of sparse array based vascular elastography.

Acknowledgements: This work was supported by startup funds from the University of Rochester.

References:

[1] S. Korukonda and M.M. Doyley: Axial and Lateral Strain Estimation using a Synthetic Aperture Elastographic Imaging System. Ultrasound in Medicine and Biology, Vol. 37, No. 11, pp. 1893–1908, 2011.
[2] G. Montaldo, M. Tanter, J. Berco, N. Benech, and M. Fink: Coherent Plane-Wave Compounding for Very High Frame Rate Ultrasonography and Transient Elastography. IEEE Trans. on UFFC, 56(3), pp. 489–506, 2009.

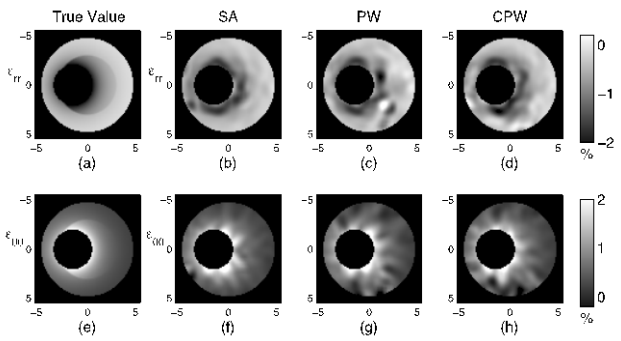

Figure 1: Comparison of radial (a–d) and circumferential (e–h) strain elastograms obtained from sparse array (SA), plane wave (PW) and compounded plane wave (CPW) imaging systems with the theoretical values obtained from the simulation.

042 **REPRODUCIBILITY STUDIES IN SHEAR WAVE ELASTOGRAPHY.**

Mickael Labit[1], Hervé Monpeyssen[2], Olivier Lucidarme[1,3], Laurence Leenhardt[1,2], Frédérique Frouin[1], Claire Pellot–Barakat[1].*

[1]UPMC/INSERM UMR_S 678, 91 Boulevard de l'Hôpital, Paris, FRANCE; [2]Nuclear Medicine Department, [3]Radiology Department, Pitié–Salpêtrière Hospital, 83, boulevard de l'Hôpital, Paris, FRANCE.

Background: Ultrasonic shear wave elastography has a unique capability of providing quantitative maps of the Young's modulus E(kPa) of soft tissue [1]. In most applications, the degree of malignancy of suspicious structures is directly derived from the mean elasticity value computed in manually selected regions of interest (ROIs) about the lesion. The operator dependant steps required to measure this elasticity index can be a source of inaccuracy and bias which need to be identified.

Aims: The purpose of this work was to study the manual steps involved in the making and measuring of shear wave maps and to propose automatic analysis and recommendations in order to improve the accuracy of the elasticity index and avoid biased measurements that could lead to diagnosic errors.

Methods: Ultrasonic shear wave images of a breast elastography phantom as well as of thyroid tumors and patient livers were acquired on the (SSI) Aixplorer machine with the SL15–4 linear and SC6–1 transducers. Manual interventions performed after localizing the lesion plan include: 1) freezing a stable frame, 2) positioning the shear wave window, 3) selecting a ROI in the tumor. For Step 1, 30 video clips of patient livers as well as 5 clips of phantom of 10 seconds each were acquired. The average elasticity of a central area of the shear wave window was computed throughout the clip and an automatic extraction of the frame presenting the smallest difference with its neighbors was performed (Figure 1). To study Step 2, the shear window was placed in 20 different locations of the B–mode frame of homogeneous areas of the phantom. The mean elasticity according to the axial and lateral distances was computed. For Step 3, an algorithm enabling the automatic selection of a representative ROI inside thyroid tumors and phantom inclusions was developed, based on criteria of homogeneity and size.

Results: 1) The automatic frame selection allows the reproducible detection of the most stable elastogram in 80% of the liver clips and 100% of the phantom clips. The 20% failure occurred for left livers where the raw data clip quality is poor. 2) Column–like artifacts were observed when the shear window was placed at the top of the phantom (Figure 2). An inaccuracy of up to 7kPa of the elasticity index (almost 30% of the estimate) was observed (Figure 3). This artifact appears mainly under 6mm of depth (Figure 4) when the shear window is at the top. This is not as strikingly observed when the shear window is deeper. 3) The automatic ROI selection provides reproducible elasticity measures in the thyroid.

Conclusions: Automatic frame and ROI selection methods were proposed to allow intra– and inter–operator reproducibility of elasticity measurements. Important artifacts observed when the elastography map is at the top border of the frame suggest that measurements should be made at least 6mm from the skin surface. An ultrasonic standoff pad could also be used in order to minimize this effect when exploring superficial organs.

References:

[1] M. Tanter et al.: Breast Lesion Viscoelasticity and Supersonic Shear Imaging. Ultrasound in Med. and Biol., Vol. 34, No. 9, pp. 1373–1386, 2008.

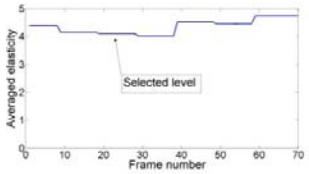

Figure 1: Average elasticity calculated throughout one video clip. Each step corresponds to a renewal of the elastogram.

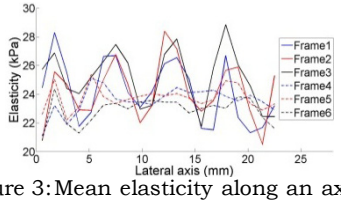

Figure 3: Mean elasticity along an axial depth of 6mm as function of the lateral position.

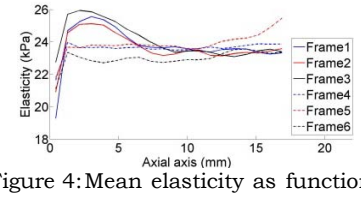

Figure 4: Mean elasticity as function of the axial position.

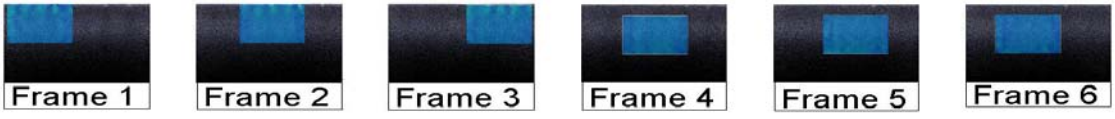

Figure 2: B–mode and superimposed elastograms from a homogeneous phantom area. The shear window was placed at various locations at the top of the frame (Frames 1–3) and at 5mm from the top (Frames 4–6).

* *indicates Presenter*

045 **STRAIN ESTIMATION FOR QUASI–STATIC ELASTOGRAPHY THROUGH ANALYTICAL PHASE TRACKING.**

Lili Yuan[1], Peder C. Pedersen[1].*
[1]Worcester Polytechnic Institute, 100 Institute Road, Worcester, MA, USA.

Background: Quasi–static elastography with an externally applied force often involves strain of several percent. In such cases, cross–correlation (CC) based methods are computationally demanding and prone to ambiguity, while speckle tracking has resolution limitations and may have decorrelation–induced errors.

Aims: To develop a robust and efficient method for extracting axial displacement (DPM) and strain in response to the applied forcing function in freehand quasi–static elastography. The method is based on tracking the analytical phase through a slow time sequence of radio frequency (RF) signals.

Methods: For 1D axial DPM estimation, a sequence of RF signals as a function of slow time (applied external force function) is recorded. Via the Hilbert transform, amplitude and wrapped phase of the analytical signal are obtained along fast time. The (fast time wrapped) phase values for all RF signals are stored in a phase matrix, where rows and columns represent slow and fast time, respectively. Let the analytical signal phase at a specified time, t_0, be φ_0. Our method is an efficient way of tracking φ_0 across the phase matrix, while recording the time shift in the fast time location of φ_0, proportional to DPM of scatterers initially at t_0. This method is distinctly different from other reported phase–based methods with limited resolution due to windowing, such as extracting DPM from the complex CC at zero lag [1], or at zero phase [2] and weighted phase separation [3]. In our current implementation, only phase values near 0 radians are retained, as illustrated by the phase bands in Figure 1a, which can have bifurcation or other anomalies when the corresponding amplitude is low. Therefore, an amplitude threshold is applied to the phase matrix, giving the result in Figure 1b. Finally, discontinuous phase bands are removed, with only connected phase bands retained, as seen in Figure 1c. Connected component labeling is then used to recognize zero phase trajectories, and slow time shifts are computed by subtracting row index at pre–compression. The axial strain is estimated by applying 2D linear least square fitting to DPM maps.The method was first tested with a simulated tissue–mimicking 30mm×15mm phantom with a 5mm diameter circular inclusion at its center whose stiffness was 5 and 10 times that of the surrounding tissue. Using finite element analysis (FEA) method (Comsol), axial compressions of 0.8%, 5% and 10% were applied to the phantom, and the ultrasound RF signals of the compressed medium were simulated with Field II. The DPM and strain were computed with the phase tracking method and compared to the results from FEA and standard CC. The method was then tested experimentally on a tofu phantom, using an Ultrasonix RP 4MHz transducer at a high frame rate. A time sequence of 2D RF lines for several cycles of the manual forcing function was acquired and the corresponding DPM along slow time were determined and compared with CC result.

Figure 1: (a) Phase matrix showing wrapped phase values near 0 radians (limited in +/-0.2π); (b) Phase matrix with normalized amplitude threshold applied; (c) Phase matrix with amplitude threshold applied and discontinuous phase curves removed.

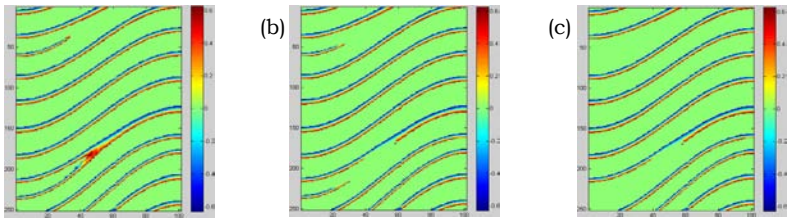

Results: The DPM and strain from Comsol and Field II simulations and experiments confirm the validity of the phase tracking method. For DPM magnitudes on the order of 0.5 to 1 mm, the error at peak compression is typically 5%. In comparison to a standard implementation of the conventional CC method, our analytical–phase method was at least 10 times faster, with a resolution, accuracy, SNRe, and CNRe comparable to or better than what we obtained with the CC method.

Conclusions: The phase tracking method has been implemented with a fast time sampling rate of 30 times the center frequency and the slow time sampling rate chosen so that the maximum DPM of scatterers between consecutive RF lines is $\lambda/10$ or less. The method minimizes performance degradation through region of low RF signal amplitude, generally caused by destructive interference, by tracking only wrapped fast time phase, which is not affected by phase anomalies common to unwrapped phase.

Acknowledgements: Funding by the Telemedicine and Advanced Technology Research Center is greatly appreciated.

References:

[1] O'Donnell M et al.: IEEE UFFC, 41(3), pp. 314–325, 1994.
[2] Pesavento A et al.: IEEE UFFC, 46(5), pp. 1057–1067, 1999.
[3] Lindop JE et al.: IEEE UFFC, 55(1), pp. 94–111, 2008.

054 **EXPERIMENTAL EVALUATION OF SIMULTANEOUS MULTISPECTRAL CODED EXCITATION FOR PHOTOACOUSTIC IMAGING.**

Haichong Zhang[1], Kengo Kondo[1], Makoto Yamakawa[2], Tsuyoshi Shiina[1].*
[1]Graduate School of Medicine, [2]Advanced Biomedical Engineering Research Unit, Kyoto University, Kawahara–cho, Shogoin, Kyoto 606–8507, JAPAN.

Background: Research on tissue elasticity using ultrasound has been done in many centers for many applications. Photoacoustic imaging, which is expected to be combined with ultrasonic imaging, can expand the capacity of ultrasound by showing functional imaging of tissue [1].

Aims: The aim of this study is to acquire multispectral information for functional images with a high signal–to–noise ratio (SNR) and a high frame rate by using coded excitation.

Methods: We propose coded excitation using m–sequences and related sequences that have good autocorrelation and cross–correlation properties. In this study, we demonstrate the feasibility through experimental evaluation. Preferred pairs of m–sequences and related sequences such as Gold codes are binary sequences having good cross–correlation. Thus, we investigated the coded excitation method to separate multispectral components, which are irradiated with coded laser pulses from different laser sources, into separate spectral components. The performance increases as the pulse repetition frequency (PRF) and code length increase. Theoretical consideration in previous research using Gold codes has showed a clear SNR improvement compared with averaging [2]. Here, we conducted an experiment to verify the separation of spectral components through two–wave simultaneous sending. We compared the separated signals with the signals acquired by single–wavelength irradiation using the same codes to examine the reproducibility of separation. Two laser modules (532nm Nd: YVO_4 and 700nm OPO–YAG) were used, and the data were captured by a 9mm hydrophone. Two strings (red and green) and a black rubber wire were used as the absorber to contrast wavelength dependency (Figure 1a).

Results: As a result, the separated signals were almost equivalent to the signals acquired by a single–wavelength irradiation. For instance, the SNR improvement of separated signals of 532nm over non–coded signals was 5.00dB (Figure 1d), and the improvement of single–wavelength signals after 63 averages was 5.57dB (Figure 1b) when the PRF was 10kHz and a 63–bit preferred pair of m–sequence was used. The PRF in this experiment was 10kHz because of the performance limitation of our laser system, but a faster laser module will allow faster PRF. At the same time, it was also confirmed that the proposed method can reduce the sending time cost for multispectral information. The 11.69dB improvement of SNR compared with averaging was achieved by simulation under the conditions that four 1023–bit Gold codes were used.

Conclusions: The experiment successfully validated the feasibility of simultaneous multispectral coded excitation. The advantage over the previous study is that only one sequence is needed to be irradiated compared with orthogonal Golay codes [3] that must be as many sequences as the number of components. The proposed method can provide a huge impact since the demand for multispectral photoacoustic imaging is expected to increase more and more.

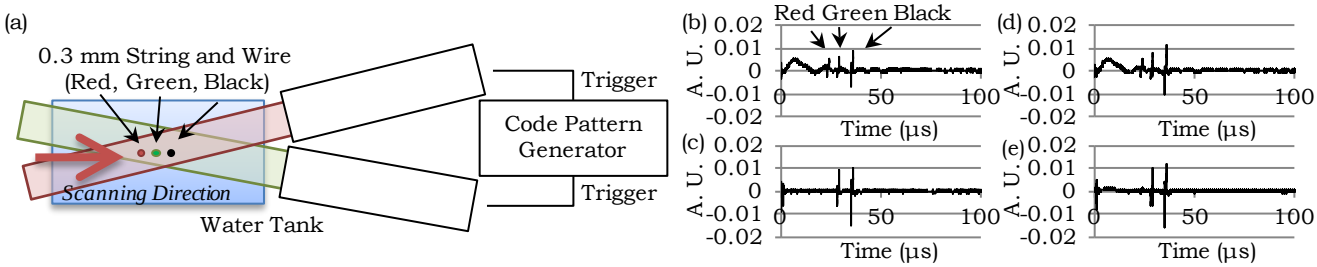

Figure 1: (a) Experimental setup; (b) 532nm laser single irradiation result; (c) 700nm laser single irradiation result; Two wavelengths simultaneous irradiation results separated into (d) 532nm and (e) 700nm.

Acknowledgements: This work was supported by a Grant–in–Aid for Scientific Research A (No. 22240063) from the Japan Society for the Promotion of Science.

References:

[1] L. V. Wang: Medical Physics, Vol. 35, pp. 5758–5767, 2008.
[2] H. Zhang , K. Kondo, M. Yamakawa, T. Tsuyoshi: Jpn Journal of Applied Physics, Vol. 51, No. 7, p. 07GF03, 2012.
[3] M. P. Mienkina, C. S. Friedrich, N. C. Gerhardt, M. F. Beckmann, M. F. Schiffner, M. R. Hofmann, and G. Schmitz: Optics Express, Vol. 18, p. 9076, 2010.

* *indicates Presenter*

071 **ASSESSING ARTERY WALL DYNAMICS WITH HIGH FRAME RATE ULTRASOUND IMAGING AND THREE DIMENSIONAL PHASE ANALYSIS.**

Pieter Kruizinga[1], Frits Mastik[1], Nico de Jong[1,2,3], Antonius FW van der Steen[1,2] and Gijs van Soest[1].*
[1]Erasmus MC–Thorax Center, Rotterdam, THE NETHERLANDS; [2]Interuniversity Cardiology Institute, Utrecht, The NETHERLANDS; [3]Delft University of Technology, Delft, The NETHERLANDS.

Background: Viscoelastic properties of the human carotid artery (CA) wall and of possible lesions within are key parameters in the clinical evaluation of the CA [1]. These viscoelastic properties can be assessed by monitoring the motion of the arterial wall caused by arterial pulse waves [2]. Plane–wave ultrasound (US) imaging is a high frame rate (>1kHz) technique that allows for monitoring arterial wall motion at all relevant physiological speeds [3]. However, fast and robust extraction of accurate motion profiles from multiple ultrasound frames remains challenging.

Aims: This study demonstrates that arterial wall motion can be assessed through three–dimensional (3D) phase analysis of high frame rate ultrasound data.

Methods: To test our phase analysis method, we performed high frame rate plane wave US imaging of the CA of a healthy volunteer. The ultrasonic plane waves were transmitted using a broadband (4–10MHz, -6dB bandwidth) 128 elements linear array (Vermon). All 128 elements were excited simultaneously or subsequently with a 1.5 cycle, 7MHz Gaussian modulated sine pulse. The array was interfaced with a programmable US system using 12 bits digitization, 80 or 40MHz sampling (Lecoeur Electronic). Acquisition depth was set to 2cm. The total acquisition time ranged from 0.8 to 2 seconds. Imaging frame rates from 1 to 35kHz were realized through a tradeoff between the number of imaging frames, acquisition time and sampling frequency. Through Fourier domain beamforming, we obtained the reconstructed analytical signal. The magnitude was used for conventional B–mode imaging and the phase for 3D motion analysis. We imaged displacement, velocity and acceleration based on the phase and its first and second order time derivatives. Only the relevant phase samples were considered through a hard threshold mask obtained from the magnitude data. The algorithm was implemented on graphic processing unit (GPU) allowing for fast processing of the 3D motion analysis.

Results: Figure 1 shows the result of our 3D motion analysis of the lower arterial wall by displaying one sample of all channels and all samples of one channel over time. Two frames were selected to emphasize frame–to–frame dynamics captured with the 3D motion analysis. The velocity maps show a specular pattern that reflects local variability in arterial wall dynamics. For all samples, we measured a total displacement of 0.46mm, a velocity of 4.2mm/sec measured at the 95% percentile and -1.2mm/sec at the 5% percentile. These values and the position, velocity and acceleration profiles we measured correspond well to those found in literature.

Conclusions: Local arterial wall dynamics can be well assessed through 3D motion analysis of high frame rate plane wave ultrasound data.

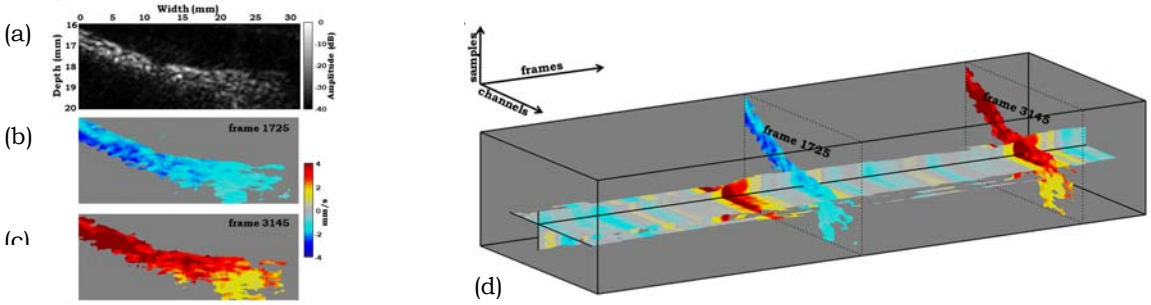

Figure 1: (a) B–mode envelope image of the lower arterial wall; (b, c) Two selected frames from the time–series in (d); (d) Time–series of lower arterial wall (tissue velocity) of all samples of a single channel and all channels of a single sample over time obtained with 2.5kHz frame rate US imaging. The data set shown is 2 seconds long.

References:

[1] Reneman RS, Meinders JM, Hoeks APG: Non-Invasive Ultrasound in Arterial Wall Dynamics in Humans: What Have We Learned and What Remains to be Solved. European Heart Journal, 26, pp. 960–966, 2005.
[2] Meairs S, Hennerici M: Four-Dimensional Ultrasonographic Characterization of Plaque Surface Motion in Patients with Symptomatic and Asymptomatic Carotid Artery Stenosis. Stroke, 30, pp. 1807–1813, 1999.
[3] Tanter M, Bercoff J, Sandrin L, and Fink M: Ultrafast Compound Imaging for 2-D Motion Vector Estimation: Application to Transient Elastography. IEEE Trans. Ultrason. Ferroelect. Freq. Contr., 49, pp. 1363–1374, 2002.

089 **DIRECT ELASTIC MODULUS RECONSTRUCTIONS FROM UNIAXIAL STRAIN AND DISPLACEMENT DATA.**

Olalekan Babaniyi[1], Paul E. Barbone[1], Assad A. Oberai[2].*

[1]Mechanical Engineering Department, Boston University, 110 Cummington St, Boston, MA 12180, USA; [2]Mechanical, Aerospace and Nuclear Engineering Department, Rensselaer Polytechnic Institute, 110 8th Street, Troy, NY, 12180, USA.

Background: A basic step in the process of ultrasound elasticity imaging is the measurement of tissue displacement while it is being deformed. With conventional ultrasound technology, only one component of the displacement field can be measured precisely, that coinciding with the direction of ultrasound propagation. Other displacement components can be estimated, but with much less precision. On the other hand, if all displacement components were available precisely, then direct (i.e. noniterative) modulus reconstructions could be performed, even from freehand quasistatic compression data. Thus the lack of high precision lateral displacement estimates prevents direct modulus reconstructions from data acquired from freehand compression.

Aims: The aim of this work is to develop a new processing method to estimate high precision displacement vector and strain tensor fields from precise measurements of a single displacement component field. The strains can then be used to calculate the material properties directly.

Methods: A processing method was created to calculate full displacement vector fields and 2D strain tensor fields from measurements of a single component of the displacement vector field. The formulation applies conservation of momentum locally, but does not require *a priori* knowledge of the modulus distribution, nor does it involve iterative modulus updates.

Results: The new processing method was tested with simulated displacement data in which one of the displacement components was corrupted by 50% noise, and the full displacement and strain fields were recovered from this test. The recovered displacement and strain fields were within 3% of the target values. The processing method was also tested with measured displacement data from a gelatin phantom under uniaxial compression and from clinically measured *in vivo* ultrasound data. The full displacement and strain fields were recovered from these tests. The recovered strains from both experiments have been used to calculate the material properties directly; c.f. Figure 1a and b. The results of reconstructing the modulus directly from the processed displacement fields are consistent with those obtained by iterative modulus updates.

Conclusions: The new processing method has been successfully used to recover high precision displacement vector and 2D strain tensor estimates from single component displacement field measurements. The recovered strains are sufficiently precise to allow direct modulus reconstructions. The direct reconstruction methods are fast enough to allow 2D reconstructions to be performed in real time.

Acknowledgements: The authors are grateful to T.J. Hall (University of Wisconsin) and J. Jiang (Michigan Technological University) for providing displacement fields measured in the phantom.

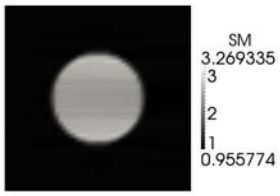

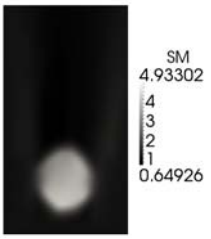

Figure 1: (a) Reconstruction from Simulated Data (b) Reconstruction from Phantom Data

* *indicates Presenter*

062 **IMAGING TRANSVERSE ISOTROPIC ELASTIC PROPERTIES OF MUSCLE WITH ULTRASONICALLY TRACKED RADIATION FORCE INDUCED SHEAR WAVES IN 3D.**

MH Wang[1], BC Byram[1], ML Palmeri[1], NC Rouze[1], KR Nightingale[1].*
[1]Duke University, Durham, NC, USA.

Background: The mechanical properties of skeletal muscle are consistent with a transverse isotropic model of elasticity due to the parallel arrangement of thin muscle fibers. As a result, the shear wave speed (SWS) is fastest along the direction of the fibers and slowest across the fibers. With the recent availability of 2D matrix array ultrasound transducers, shear wave propagation can now be monitored in a 3D volume using ultrasound. This overcomes the inherent limitation in determining the fiber orientation, which is 3D in nature, from 2D cross–sectional images.

Aims: To determine the muscle fiber orientation and SWS along and across the fibers in 3D using ultrasonically tracked shear waves.

Methods: Shear wave imaging was performed on freshly excised canine muscle embedded in agar. An annular focused HIFU piston transducer (H–101, Sonic Concepts, Bothell, WA) was used to induce shear wave propagation with acoustic radiation force. A 2.8MHz 2D matrix array transducer (4Z1C on an SC2000 scanner, Siemens Healthcare, Ultrasound Business Unit, Mountain View, CA, USA) inserted in the central opening of the HIFU piston was used for monitoring the resulting shear wave displacement in 3D. The shear wave propagates along the plane of symmetry of the muscle fibers. To determine the orientation of this plane, the SWS was measured in all possible directions from a single point (the push focus at 60mm). SWS measurements in directions oblique to the plane of propagation are associated with high uncertainty. Therefore, the plane orientation containing SWS measurements with the lowest measurement uncertainty was determined to be the plane of shear wave propagation. The fiber orientation was estimated by fitting an ellipse to the SWS measured within this plane and finding the angle of the major axis. To verify the 3D muscle fiber orientation determined from SWS measurements, high–resolution 3D ultrasound volumes of the samples were obtained using a high frequency 14MHz 1D array (14L5 on the S2000 scanner, Siemens Healthcare) mechanically swept using a translation stage. The 14L5 B–mode volumes were rigidly registered to the 2D matrix array data using fiducial markers which were visible in both. To determine the fiber orientation in the 14L5 B–mode volume, 3D line enhancement filtering was performed followed by a 3D Radon transform (RT). The angle giving the highest variance in the 3D RT was taken as the fiber orientation.

Results: The SWS measured from a single shear wave acquisition in one muscle sample has been analyzed to date with on–going accrual. The SWS within the plane of propagation is shown in Figure 1. The push axis was intentionally made non–perpendicularly to the muscle fibers. The normal of the shear wave plane of propagation, as determined from SWS measurements, was 26° from the push axis. There was a 5.8° difference between the angle of this plane and the 3D RT fiber orientation. The difference between the major axis of the SWS within this plane and the projection of the 3D RT fiber orientation in this plane was 3°. The difference between the fiber orientation measured from SWS and 3D RT (red and green arrows in Figure 1) was 6.5°. The length of the major axis (SWS along the fibers) was 5.2m/s, while the length of the minor axis (SWS across the fibers) was 3.0m/s.

Conclusions: Muscle fiber orientation in 3D and the SWS along and across the fibers can be determined by monitoring shear wave propagation in 3D with ultrasound.

Acknowledgements: NIH grants R01 EB–002132 and R01 CA142824.

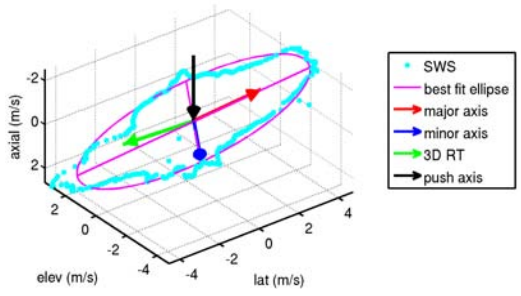

Figure 1: Polar plot of the SWS within the plane of propagation at the push focus and the best–fit ellipse. The major and minor axes of the SWS and the fiber axis from 3D RT are shown by arrows.

081 **MR ELASTOGRAPHY OF *IN–VIVO* AND *EX–VIVO* PROSTATE CANCER AND CORRELATION WITH HISTOLOGY: INITIAL RESULTS.**

Ramin S. Sahebjavaher[1,2], Guy Nir[1], Omid Mohareri[1], Louis O. Gagnon[3], Edward C. Jones[3], Larry Goldenberg[3], Philippe Garteiser[2], Ralph Sinkus[2], Piotr Kozlowski[3], Septimiu E. Salcudean[1].*
[1]University of British Columbia (UBC), Vancouver, BC, CANADA; [2]Centre de Recherche Biomedicale Bichat–Beaujon, Paris, FRANCE; [3]UBC Faculty of Medicine, Vancouver, BC, CANADA.

Background: Mechanical properties of tissue are important indicators of disease potential. Viscoelastic properties of the prostate have been shown to correlate with prostate cancer for *ex–vivo* specimens using MR elastography (MRE) [1], and several *in–vivo* studies using ultrasound elastography techniques [2]. One feasibility study compared results from *in–vivo* prostate cancer MRE with biopsy [3]. In this study, we performed MRE *in–vivo* (on a 3T MRI) and *ex–vivo* (on a 7T MRI) for one patient. To the best of our knowledge, this is the first time, that both *in–vivo* and *ex–vivo* MRE images are compared together and with histopathology.

Aims: To identify the cancerous tumors in the elasticity images in both *in–vivo* and *ex–vivo* cases and correlate them to the whole mount histopathology marked with the Gleason score.

Methods: *In–vivo*: The MRE images were acquired using a novel gradient echo sequence named eXpresso [4]. The wave images were acquired on a 128×128×24 matrix with 2mm isotropic voxel size. Eight vibration phases were encoded the mechanical excitation of 70Hz (trans–perineal). The entire MRE acquisition lasted about 8 min for the 3D wave field. Images were processed offline similarly to the approach described in [5]. *Ex–vivo*: A conventional motion–sensitized spin–echo pulse sequence was used for MRE. The 3D wave field was acquired in 9 slices for a 64x64 matrix with 1mm isotropic voxel of size. The mechanical excitation was applied externally using a passive electromagnetic driver positioned in the fringe field of the scanner at 800Hz. The total imaging time was 22 min. *Histology*: Following the surgery, the whole prostatectomy specimen was immersed in formalin for 72 hours prior to *ex–vivo* MRE. The outline of the tumor along with its Gleason score were delineated manually on the histology slide by an experienced pathologist.

Results: *In–vivo*: The peak amplitude of the mechanical wave was 130µm with a mean of 25µm in the prostate. No patient discomfort was reported when specifically asked. In the axial plane, the prostate gland is outlined in Figure 1(a) T2W and the reconstructed shear modulus (b) G' and (c) loss modulus G". The histology is shown in (d) where the outline of the large (Gleason score of 4+3) and smaller (3+3) tumors are shown. The mean values of G' were {3.0 and 0.8kPa} for Gleason scores of {4+3 and healthy tissue}, respectively. Also, the mean values for G" were {1.7 and 0.4kPa} for the same regions of interest, respectively. *Ex–vivo*: Similar to the *in–vivo* case, the tumor can be clearly identified in Figure 1 (b) and (c). The mean values of G' were {120 and 47.2kPa}, and G" were {146 and 57.8kPa} for Gleason scores of {4+3 and healthy tissue}, respectively.

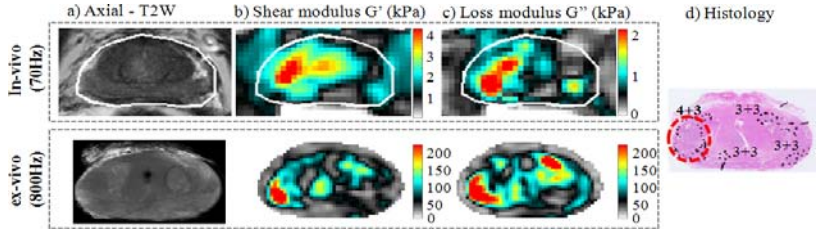

Conclusions: A very promising correspondence between reconstructed shear and loss moduli G' and G", and the matching histology slide can be observed in both i*n–vivo* and *ex–vivo*. The data show differences in shear modulus, and especially in loss modulus, between normal and cancerous tissue in the prostate. The stiffness of the prostate dramatically increases after the fixation as described previously [6]. One of the limitations of this initial study was registration was not performed. Also, stiffer structures within the prostate may be mistaken for tumors. We are presently accruing patients to obtain sufficient images to carry out a meaningful statistical analysis. These results further strengthen the case for MRE techniques which promise to improve staging of prostate cancer.

Acknowledgements: This work was supported by NSERC, CIHR and Philips Healthcare.

References:

[1] Dresner et al.: Proc. 11th ISMRM, p. 578, 2003.
[2] Krouskop et al.: Ultrasonic Imaging, 20(4), p. 260–274, 1998.
[3] Li et al.: Acta Radiologica, 52(3), p. 354–358, 2011.
[4] Sahebjavaher et al.: Proc 23rd ESMRMB, p. 124, 2011.
[5] Sinkus et al.: PMB, 45, p. 1649, 2000.
[6] McGrath et al.: Proc. 19th ISMRM, p. 1478, 2011.

* *indicates Presenter*

085 **SUB–WAVELENGTH RESOLUTION IN SHEAR WAVE IMAGING: THE TIME REVERSAL APPROACH.**

Stefan Catheline[1], Rémi Souchon[1], Jean–Yves Chapelon[1].*
[1]INSERM U1032, University of Lyon, Lyon, France.

Background: When a wave field is measured within the propagative medium, for instance in seismology, magnetic resonance elastography (MRE) or ultrasound (US) based elastography, it is known that, the resolution is ultimately limited by the measuring point density and not the wavelength [1]. Indeed, in contrast with far field conventional imaging systems, *in situ* measurement enables the retrieval of the near field details needed for super resolution. From a time reversal interpretation point of view, because of diffraction, even if the source is point–like, the wave refocuses on a spot size that cannot be smaller than half a wavelength except in the presence of an acoustic sink. The acoustic sink plays the inverse role of a source: it absorbs the energy of an incoming wave. Thus surpassing the diffraction limit for imaging implies that the acoustic sink can be recreated.

Aims: Here we report numerical and experimental results obtained with a passive acoustic sink where a focal spot size only depends on the spatial sampling of the field.

Methods: The experiment is as follows: in the first step, a diffuse wave field is created inside the sample by random finger impacts given from the surface for 10 seconds. The 2D displacement field is then measured inside the soft solid using speckle tracking algorithms developed in elastography. It involves a 64 channel array working at 5MHz with a repetition frequency of 2000Hz. In the second step, the displacement at one point chosen as a virtual source is correlated to the other points of the image in order to compute a time reversal field in the computer. In the third and last step, the decomposition of the time reversal field into the causal and anticausal Green's function is computed from a spatial Fourier transform. Thus, these functions imply the existence of a source and a sink respectively that both overcome the diffraction limit.

Results: The refocusing spots issued from the Green' s function retrieval are compared to time reversal, Figure 1. The effect of the windowing inherent to the imaging technique of elastography on the Fourier transform will be discussed. Although no new information is brought by this approach, it is shown that imaging with an evanescent wave is possible and that it conserves the symmetry properties of the source.

Conclusions: So the conclusion is that, in the absence of noise in the data, the tomography resolution of the *in situ* imaging technique depends only on the spatial sampling of the field inside the medium of propagation; in MRE it depends on the MR image, in US elastography on the sonogram and in seismology on the distance between geophones and not on the shear and Rayleigh wavelength, respectively.

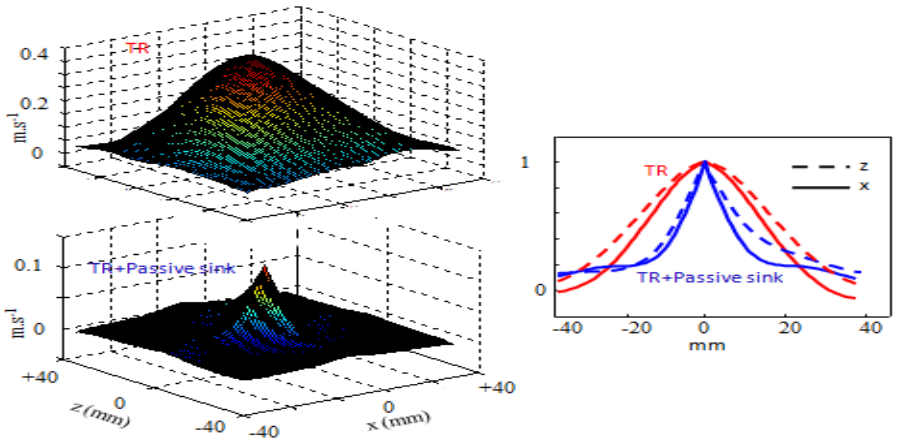

Figure 1: Focus spots along x and z directions are obtained from time reversal. They are compared to the anticausal Green's function (TR+passive sink). The size of the focus spot depends only on the spatial sampling of the field.

Reference:

[1] Tanter et al.: Médecine Nucléaire, 31 , pp. 132–141, 2007.

* *indicates Presenter*

090 **IDENTIFICATION OF NONLINEAR TISSUE ELASTICITY VIA ACOUSTIC RADIATION FORCE.**

BB Guzina[1], EV Dontsov[1], RR Kinnick[2], MW Urban[2], M Fatemi[2].*
[1]University of Minnesota, Minneapolis, MN, USA; [2]Mayo Clinic College of Medicine, Rochester, MN, USA.

Background: The theory of continuum mechanics demonstrates that the strain energy density in an isotropic, nonlinear elastic solid is a function of the invariants of the Green–Lagrangian strain tensor, and can be expanded in Taylor series using two second–order moduli (e.g., the usual bulk modulus and shear modulus) and three independent third–order moduli in terms of the G–L strain tensor invariants [1] as

$$U = \tfrac{1}{2}(K+\tfrac{4}{3}G)I_1^2 - 2GI_2 + \tfrac{1}{6}BI_1^3 + CI_1I_2 + DI_3.$$

In the existing applications of the acoustic radiation force (ARF) [2], the small–strain shear waves generated by the ARF are often deployed to estimate tissue's local shear moduli via measurements of the germane shear wave speed. However, the amplitude of thus created shear waves has remained largely unexplored in part due to lack of understanding of the mechanics of the ARF in soft tissues. In a recent study [3], it was found that the magnitude of the acoustic radiation force in an isotropic tissue–like solid, generated by the action of focused ultrasound field, is related linearly to the particular third–order modulus (denoted above by C) that is responsible for the nonlinear coupling between volumetric and deviatoric modes of deformation. While the remaining third–order moduli B and D, affiliated respectively with volumetric and deviatoric deformations, have received mounting attention in the literature, their coupling companion C has been scarcely explored.

Aims: Prompted by recently developed theory of the ARF in tissue–like solids, this study aims to: i) locally estimate the third–order modulus, C, from the amplitude of the shear waves generated by the ARF; ii) cross–validate thus obtained estimates of C via an independent measurement technique, and iii) examine the level of variability of C in selected tissue–mimicking phantoms.

Methods: One effective way to measure the third–order moduli is the technique known as acoustoelasticity [1,4] that exploits the variation of (small–strain) elastic wave speed with the level of pre–existing (finite) static deformation. In this study, acoustoelasticity experiments were performed on uniaxially–stressed tissue–mimicking phantoms wherein the small–strain shear waves were generated by the ARF. Equipped with the newly established theory of the ARF in soft solids, the value of C is independently assessed by matching the amplitude of the observed and modeled displacement field (see the snapshot of the generated shear-waves in Figure 1, whose amplitude is proportional to C – K; K denotes the shear modulus).

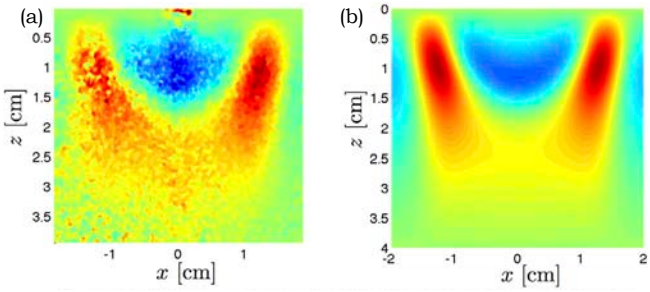

Figure 1: Shear waves generated by ARF in a paraffin–based phantom: (a) Experiment versus (b) Model.

Results: The results demonstrate that the phantoms tested, while clearly exhibiting nonlinear elastic behavior, differ significantly in magnitude of the back–calculated third–order modulus, C. The estimates of the latter coefficient obtained respectively via acoustoelasticity and the theory of the ARF have shown significant degree of consistency.

Conclusions: The lessons from this study are three–fold and suggest that: i) the recent model for the ARF in soft solids provides rational description of the amplitude of shear waves generated by the ARF; ii) the third–order modulus, C, could potentially provide a new diagnostic modality for the interrogation of soft tissues, and iii) that the latter parameter can be computed locally via the use of the ARF with no additional requirements in terms of the ultrasound testing equipment.

Acknowledgements: The support provided by the endowed Shimizu Professorship and Doctoral Dissertation Fellowship from the University of Minnesota during the course of this study is kindly acknowledged.

References:

[1] T.D. Murnaghan: Am. J. Math., 59, p. 235, 1937.
[2] A.P. Sarvazyan, O.V. Rudenko, and W.L. Nyborg: Biomedical Applications of Radiation Force of Ultrasound: Historical Roots and Physical Basis. Ultras. Med. Biol., 36, pp. 1379–1394, 2010.
[3] E.V. Dontsov and B.B. Guzina: Acoustic Radiation Force in Tissue–Like Solids Due to Modulated Sound Field. J. Mech. Phys. Solids, in press (http://dx.doi.org/10.1016/j.jmps.2012.04.006).
[4] M.F. Hamilton and D.T. Blackstock, eds.: Nonlinear Acoustics. Academic Press, 1998.

* *indicates Presenter*

This Page intentionally left blank.

075 **SHEAR WAVE GENERATION FOR ELASTICITY IMAGING VIA MODE CONVERSION FROM LONGITUDINAL WAVES AT ELASTICITY BOUNDARY.**

K. Nii[1], K. Okubo[1], N. Tagawa[1], S. Yagi[2].*
[1]Tokyo Metropolitan University, 6–6 Asahigaoka, Hino, Tokyo, JAPAN; [2]Meisei University, 2–1–1 Hodokubo, Hino, Tokyo, JAPAN.

Background: The latest real–time elastography systems have a tendency to use shear waves propagating tumor [1]. As an influential method using shear waves, acoustic radiation force impulse (ARFI) imaging has been proposed for quantitative measurement of tissue elasticity [2]. However, the potential for effects on the living body of ARFI are a cause for concern, and various examinations of those are strongly demanded, for example as a subject of rise in temperature by pulses with long duration [3].

Aims: We are aiming to establish a method for generating shear waves in the body with low risk for the living body using a mode conversion of the longitudinal pulse transmitted as a source of vibration. As a fundamental research for this concept, in this study, we evaluate the characteristics of the mode conversion mechanism at the elasticity boundary through numerical simulations.

Methods: In this study, we use the PZFlex, a standard FEM simulator for ultrasound propagation, to examine the state of shear wave generation due to mode conversion. We model a layered elasticity boundary using soft tissue with an elastic modulus of 1.0kPa, which is placed on the input side of longitudinal waves with the width of 20mm, and hard tissue with various values of elastic modulus. The density of all the tissues is fixed as 1000g/cm^3. The attenuation coefficient of longitudinal waves is 0.5dB/cm/MHz for soft tissue and 0.7dB/cm/MHz for hard tissue. To make it easy to detect the mode conversion, the attenuation coefficient of shear waves is 0.1dB/cm/MHz for all the tissues, which may be smaller than the standard value of normal tissue. By varying the elastic modulus of the hard tissue, we simulate the shear wave generation via the mode conversion and compare the strength of the shear waves propagating in hard tissue and those in soft tissue. From our initial evaluation, it was determined that a frequency of 3MHz is desirable due to the balance of attenuation and directivity for the layered simulation model used in this study. In actuality, this frequency should be determined by part of the body being interrogated.

Results: In the simulations, a linear array transducer with 32 elements was assumed for transmitting the longitudinal waves. The results of the strength of the shear waves measured near the elasticity boundary, which is proportional to the amplitude of the longitudinal waves, are shown in Table I. It was also found that the strength of shear wave depends on the pulse width of the longitudinal wave. This indicates that continuous waves are suitable for the mode conversion. Additionally, as shown in Figure 1, we confirm that the shear waves are generated at the elasticity boundary of a circular tumor with the radius of 5mm and propagate in the tumor region for a long time, with repeating reflections at the boundary. The material parameters are the same as those of the layered model, i.e. the circular tumor corresponds to the hard tissue in the layered model.

Conclusions: We confirmed that the mode conversion certainly occurs and suitable shear waves can be generated. However, the frequency determined and used in this study may be too high to measure the velocity of the shear wave because of the high attenuation characteristics disregarded in this study. In future, we will construct a mode conversion method by which sufficiently low frequency shear waves are generated from high frequency longitudinal waves using various frequency conversion techniques.

Elastic modulus of hard tissue	**4.0**	**9.0**	**16.0**	**25.0**
Strength of shear wave in soft tissue	0.041	0.047	0.047	0.048
Strength of shear wave in hard tissue	0.276	0.573	1.013	1.566

Table I: Strength of shear waves propagating in soft tissue and hard tissue (kPa).

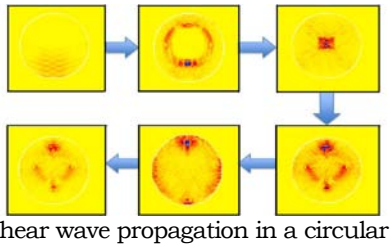

Figure 1: Shear wave propagation in a circular tumor. Time duration of the sequence of images is 1.12ms.

References:

[1] Yagi et al.: Analysis of Transient Shear Wave Generation for Real–Time Elastography. IEEE Int. Ultrasonics Symp., pp. 1356–1359, 2005.
[2] M.L. Palmeri et al.: Quantifying Hepatic Shear Modulus *In Vivo* using Acoustic Radiation Force. Ultrasound Med. Biol. pp. 546–558, 2008.
[3] B.A. Herman et al.: Models and Regulatory Considerations for Transient Temperature Rise During Diagnostic Ultrasound Pulses. Ultrasound Med. Biol., pp. 1217–1224, 2002.

* *indicates Presenter*

017 **ACQUISITION OF HIGH FRAME RATE MOVIES OF SIMULTANEOUS ACOUSTIC RADIATION FORCE IMPULSE (ARFI) AND SHEAR WAVE VELOCITY IMAGES FOR INTRACARDIAC ECHOCARDIOGRAPHY (ICE) APPLICATIONS IN *IN VIVO* MYOCARDIUM.**

PJ Hollender[1], SJ Rosenzweig[1], DP Bradway[1], R Goswami[2], PD Wolf[1], GE Trahey[1].*
[1]Duke University, Durham, NC, USA; [2]Duke University Medical Center, Durham, NC, USA.

Background: Imaging the dynamic elastic properties of the heart may be of significant diagnostic interest, and Acoustic Radiation Force (ARF) imaging methods have been demonstrated as an effective means of interrogating myocardial elasticity. Intracardiac echocardiography (ICE) transducers provide the ability to remotely generate and track ARF excitations in myocardium from within the heart. [1,2] However, conventional imaging sequences for creating ARFI images or Shear Wave Velocity (SWV) images are prohibitively slow for imaging myocardium through periods of high motion.

Aims: This work demonstrates a method of using customized acquisition sequences, which image the on–axis (ARFI) and off–axis (SWV) response to excitations with as few as four simultaneously beamformed lines with ECG triggering to synthesize temporally registered excitation responses through the field of view for creating series of ARFI and SWV images at a high frame rate.

Methods: Custom beam sequences were written for a phased array ICE transducer for use with Siemens' Acuson S2000 and SC2000 ultrasound scanners. Parallel beamforming is used to place up to four beams within the region of excitation and between three and eight beams covering 15 degrees off–axis to one or both sides. ECG triggering gates fixed frame rate and length (approximately one heartbeat) sequences of excitations to the cardiac cycle. Successive trigger events modulate the locations of each excitation–tracking ensemble in the sequence such that, over a number of heartbeats, each azimuthal line in the region of interest is imaged at each point in the cardiac cycle. The synthesized frame rate and number of azimuthal lines can be increased by using more beats. The sequences were tested in phantoms and *in vivo* in a variety of configurations.

Results: Series of images, such as the one shown in Figure 1, were generated, showing good correspondence between the ARFI images and the SWV images. The images formed movies with up to 17 excitation locations and frame rates up to 200fps. ARFI images showed superior resolution and performance through periods of high motion, while SWV images showed greater depth uniformity and provided quantitative estimates of tissue elasticity.

Conclusions: This method was demonstrated to be effective for acquiring series of matched ARFI and SWV images in *in vivo* myocardium. Respiration motion was observed to create artifacts in the multi–beat synthesis of the movies, so holding respiration is important for obtaining quality images. The duration of breath hold imposes a limit on the number of beats that can be used safely and without artifact. The achievable frame rate and number of azimuthal locations that can be imaged are, therefore, limited but sufficient for effectively creating images of the dynamic properties of myocardium.

Acknowledgements: This work is supported by NIH EB001040, NIH 5R37HL096023 and NIHR01EB01248.

References:

[1] Hsu et al.: Challenges and Implementation of Radiation–Force Imaging with an Intracardiac Ultrasound Transducer. IEEE Trans UFFC, 545, pp.996–1009, 2007b.
[2] Hollender et al.: Intracardiac Echocardiography Measurement of Dynamic Myocardial Stiffness with Shear Wave Velocimetry. Ultrasound in Med. and Biol., Vol. 38, No. 7, pp. 1271–1283, 2012.

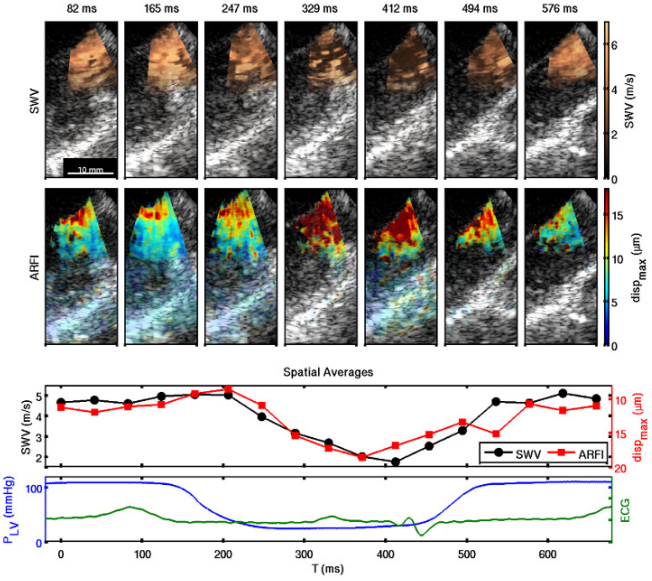

Figure 1: *In Vivo* Shear Wave Velocity Images and ARFI Images of porcine Left Ventricular Free Wall (LVFW). The shear wave speeds are higher in systole (5m/s) than diastole (2m/s), and the peak ARFI displacements are correspondingly lower in systole (11μm) than diastole (18μm).

061 **SINGLE-HEARTBEAT 2–D MYOCARDIAL ELASTOGRAPHY USING AN UNFOCUSED TRANSMIT SEQUENCE: AN *IN VIVO* FEASIBILITY STUDY.**

SJ Okrasinski[1], J Provost[1], D Legrand[1], EE Konofagou[1,2].*
[1]Biomedical Engineering Department, [2]Radiology Department, Columbia University, 622 W 168th St, New York, NY, 10025, USA.

Background: Myocardial Elastography (ME) is a radiofrequency (RF) based modality for myocardial strain imaging. However, the methods previously used required spatial and temporal resolution that could be accomplished through electrocardiogram (ECG) gating over multiple cardiac cycles and long breath–holding times.

Aims: For this study, imaging sequences were developed and applied in an *in vivo* canine model based on a virtual source sequence to image the strain in the entire left ventricle at very high frame rates (2000 fps) during free breathing and over a single heartbeat, in both open– and closed–chest configurations.

Methods: In this study, approved by the Columbia Institutional Animal Care and Use Committee, two male mongrel dogs were anesthetized. Transthoracic images in the short–axis, mid–level view were acquired using a virtual source sequence with a virtual source located behind the transducer with a Verasonics system (Verasonics, Redmond, WA) and a 64–element phased array (ATL P4–2). Images were acquired at 2000fps during 2s, immediately followed by the acquisition of 128–line, 30fps, B–mode frames during 1.5s. ECGs were acquired simultaneously. Their chests were then opened by lateral thoracotomy and images using the same protocol were repeated. RF signals were reconstructed from the element data in a pixel–wise fashion as previously reported [1]. Inter–frame axial and lateral displacements were estimated at 500Hz motion–estimation rate and at 2000Hz motion–sampling rate using normalized cross–correlation (window size: 7mm, 90% overlap) and were then accumulated during systole. Axial and lateral strains were estimated using a least–squares estimator on the axial and lateral displacements (window size: 10.7mm) and then converted to radial and circumferential strains with a previously described principal strain method [2].

Results: The maximum axial and lateral cumulative strains during systole in the open–chest configuration were 35±7% and 30±8%, respectively. The average radial and circumferential strains were found to be 30±10% and -32±9% respectively, which is consistent with previous studies in normal canine hearts using conventional beamforming [3]. In the closed–chest (transthoracic) configuration, the maximum axial and lateral cumulative strains during systole from the open–chest canines were 33±10% and 35±10%, respectively. The average radial and circumferential strains (see Figure) were found to be 33±11% and –36±12%, respectively.

Conclusions: Myocardial Elastography was concluded to be capable of mapping axial and lateral displacement and strain in both transthoracic and closed–chest regimes using unfocused transmit beams over the entire canine left ventricle *in vivo* at very high frame rates during free breathing in a single heartbeat.

Acknowledgements: This study was funded in part by NIH–NHLBI R01EB006042.

References:

[1] Provost et al.: Phys. Med. Biol., 57, pp. 1095–1112. Feb 2012.
[2] Zervantonakis et al.: Phys. Med. Biol., 52, pp. 4063–4080. July 2007.
[3] Lee et al.: Phys. Med. Biol., 56, pp. 1155–1172. Feb 2011.

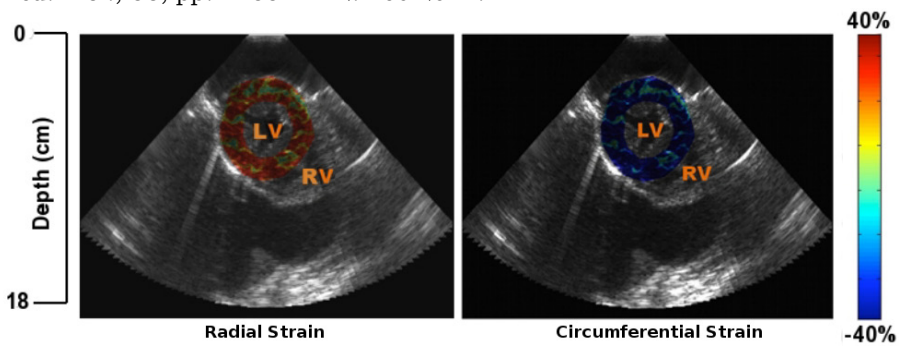

Figure 1: Radial and circumferential strain in a normal, open–chest canine. Strains were estimated using a virtual source sequence with a virtual source located behind the transducer face.

* *indicates Presenter*

066 **COMBINED ULTRASOUND ELASTICITY AND THERMAL STRAIN IMAGING FOR COMPREHENSIVE ASSESSMENT OF ATHEROSCLEROTIC PLAQUE IN A RABBIT MODEL.**

A Mahmoud[1,2], D Dutta[1], L Lavery[1], K Kim[1,3,4] – Presented by JM Rubin.*

[1]Center for Ultrasound Molecular Imaging and Therapeutics, Heart and Vascular Institute, University of Pittsburgh Medical Center, Pittsburgh, PA, USA; [2]Bioengineering Department, Cairo University, Giza, EGYPT; [3]Bioengineering Department, University of Pittsburgh, Pittsburgh, PA, USA; [4]McGowan Institute for Regenerative Medicine, University of Pittsburgh, Pittsburgh, PA, USA.

Background: Atherosclerosis imposes both mechanical and compositional changes in the vascular wall leading to the formation of atherosclerotic plaque (AP) [1]. We hypothesize that ultrasound (US) elasticity imaging (UEI) is able to assess the vascular wall mechanical property changes via measuring local strain distributions, while US thermal strain imaging (TSI) can identify lipids in the vascular wall, and combining these two techniques along with US B–mode morphology imaging can therefore provide more comprehensive information for diagnosis and monitoring of atherosclerosis development and AP vulnerability.

Aims: The aims of this study are: 1) demonstrate *in vivo* feasibility of the combined UEI–TSI technique assessing the mechanical and compositional characteristics of AP using atherosclerotic rabbit model, and 2) correlate the UEI–TSI findings with histology.

Methods: AP was induced to a group of New Zealand white rabbits (n=6) by introducing a balloon injury to the femoral artery while administering high–fat high–cholesterol diet. Optimal US beamforming, imaging–heating sequence, heating US transducer and electronics were designed and integrated to commercial US scanners including a clinical system (SonixTOUCH, Ultrasonix Medical Corp., Canada) and a high–resolution small animal imaging system (Vevo2100, VisualSonics Inc., Canada). US duplex was used to localize atherosclerotic lesions. US radiofrequency (RF) frames were acquired for approximately 2 seconds for UEI, followed by 8 second RF capturing for US–TSI while heating transducer was operated to induce a slight temperature rise (≤2°C) within the safe range according to the American Institute of Ultrasound in Medicine. ECG was used to trigger TSI frame acquisition per the QRS complex and assure eliminating the mechanical strain effect. A 2D phase-sensitive speckle tracking was applied to estimate mechanical strains for UEI due to inter–cardiac pulsation and thermal strains for TSI due to sound speed changes by temperature rise. UEI and TSI strain maps, co–registered to B–mode images, were compared to Oil–Red–O histology.

Results: Lipid–rich lesions exhibited average total compressional strain of approximately -0.44% over the systolic phase, higher than that observed in normal areas in vascular wall. That correlates well with the known elastic characteristics of soft lipid–rich lesions. Whereas in TSI, lipids showed a distinct positive strains (≈+0.18%) in AP upon the slight temperature increase, and negative, or zero, strains in the surrounding water–based tissues. UEI and TSI findings showed good agreement with histology.

Conclusions: The combined UEI–TSI imaging technique was able to assess successfully both mechanical and compositional characteristics of AP in the femoral artery of atherosclerotic rabbit model *in vivo*. The co–registered complete set of morphological, mechanical, and compositional information obtained by the UEI–TSI imaging correlated well with histological findings. This combined UEI–TSI can be relatively easily implemented into commercial US systems with minimal modification to complement other modalities in diagnosing and assessing AP vulnerability in clinics in the future.

Acknowledgements: This study was supported in part by NIH 1R01HL098230–01A1 (PI: Kim). Small animal imaging system (Vevo2100) was supported through NIH 1S10RR027383–01 (PI: Kim).

References:

[1] Virmani R, Narula J, Leon MB, Willerson JT: The Vulnerable Atherosclerotic Plaque: Strategies for Diagnosis and Management. First edition, Wiley–Blackwell, 2006.

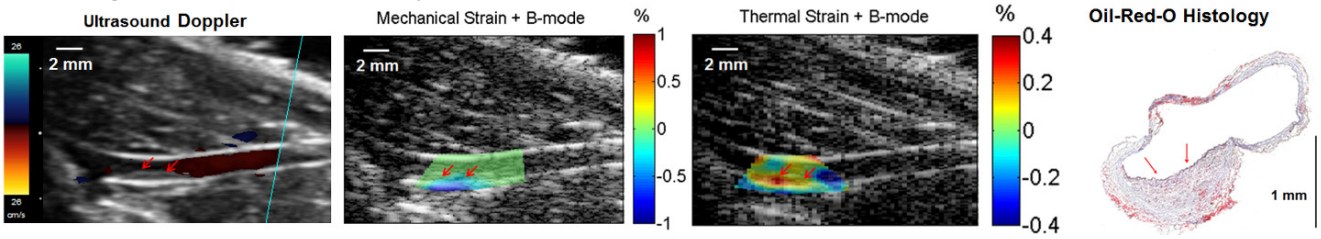

Figure 1: Ultrasound *in vivo* images including Doppler, UEI and TSI compared well with Oil–Red–O histology in assessing atherosclerotic plaque (red arrows) developed in rabbit femoral artery 10 weeks after balloon injury.

* *indicates Presenter*

069 **SHEAR WAVE VELOCITY ACQUIRED BY SHEAR WAVE ELASTICITY IMAGING INCREASES WITH TIME IN NORMAL AND HYPO–PERFUSED LANGENDORFF RABBIT HEARTS.**

M Vejdani–Jahromi[1], DM Dumont[1], A Kiplagat[1], GE Trahey[1], PD Wolf[1] – Presented by Y–J Kim.*
[1]Duke University, Durham, NC, USA.

Background: Heart Failure is a fatal disease in which mechanical properties of the cardiac tissue are affected. Currently, there is no widely used noninvasive technique to evaluate the changes in mechanical properties of cardiac tissue. Shear Wave Elasticity Imaging (SWEI) is an ultrasound technique that can be used to evaluate the stiffness of tissue by acquiring shear wave speed of propagation measurements. It is known that all isolated heart preparations continuously deteriorate and standard measures of cardiac function such as developed pressure or maximum dp/dt can be expected to deteriorate 5–10% per hour [1]. The Langendorff preparation provides valuable information on left ventricular systolic and diastolic pressures and their derivatives in hearts subjected to ischemia or hypoxia [2].

Aims: To evaluate the capability of SWEI in determining changes in functionality and mechanical properties of the cardiac tissue.

Methods: Langendorff preparation is a method by which an isolated heart is kept alive for several hours by retrograde perfusion of the coronaries through the aorta. Three rabbit hearts were isolated on a Langendorff preparation, perfused with Tyrode solution and submerged in a designed bath with acoustic walls suitable for ultrasound imaging to prevent reflections from the wall. Data were acquired using a VF10–5 linear transducer on a Siemens SONOLINE Antares ultrasound system (Siemens Healthcare, Ultrasound Business Unit, Mountain View, CA, USA) with focal point of 1.6cm, transmit frequency of 5.7MHz and F# of 2. The probe was fixed approximately 1cm from the left ventricular free wall along the short axis and acquired data from the same location through time. One rabbit was perfused under normal conditions and two were hypo–perfused by allowing air bubbles to enter the coronaries at the time of cannulation. The ECG and aortic pressure were recorded with PowerLab/Labchart data acquisition system (ADInstruments, Colorado Springs, CO, USA).

Results: Initial results showed that diastolic and systolic stiffness increased over time. This increase was significantly higher in the ischemic hearts compared to the normally perfused heart. Shear wave velocity increased by 56.5±0.71% and 19±1.4% in diastole and systole respectively in the two ischemic hearts and 14% both in systole and diastole in the normally perfused heart. The ratio of systolic stiffness to diastolic stiffness expresses the effectiveness of ventricular function as a balance between its systolic contractility and diastolic stiffness [3]. In our experiments, systolic to diastolic ratio showed 41±12.7% and 4% decrease in the ischemic and normal hearts respectively, indicating decreased functionality in the ischemic hearts.

Conclusions: From this preliminary data, we conclude that shear wave velocity recorded by SWEI shows a decrease in compliance and functionality in an isolated heart similar to the decrease, other researchers have reported in the literature for normal and hypo–perfused hearts, using different methods. This imaging modality can help us better assess and characterize the mechanical properties of the cardiac tissue noninvasively and in real time.

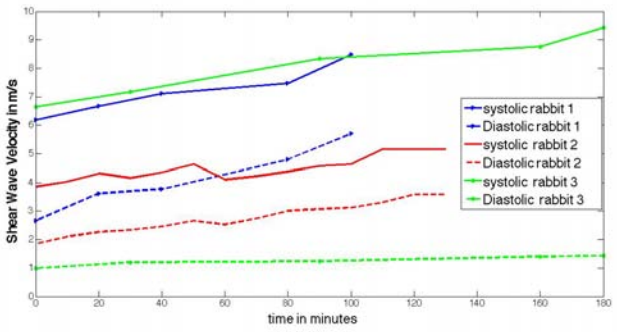

Figure 1: Systolic and Diastolic stiffness versus time in three Langedorff rabbit hearts. Rabbit 1 and 2 were ischemic and rabbit 3 was normal. Solid lines are Systolic shear wave velocity and dashed lines are diastolic values.

Acknowledgements: The authors would like to thank Ellen Dixon Tulloch and Young–Joong Kim for their help in this project. This work was supported by Medtronic Fellowship and NIH Grants R01EB012484 and R01HL096023.

References:

[1] D.R. Gross: Animal Models in Cardiovascular Research. Third edition, p. 123, 2009.
[2] M.Skzypiec–Spring, B. Grotthus: Isolated Heart Perfusion According to Langendorff–Still Viable in the New Millennium. Journal of Pharmacological and Toxicological Methods, 55, pp. 113–126, 2007.
[3] J.N. Amoore: Theoretical Analysis of the Relationship between the Ratio of Ventricular Systolic Elastance to Diastolic Stiffness and Stroke Volume. Med Bio Eng Comput, 30(6); p. 605–12, 1992.

* *indicates Presenter*

073 **ELECTROMECHANICAL WAVE IMAGING OF CANINE AND HUMAN PATHOLOGICAL HEARTS *IN VIVO*.**

Jean Provost[1], Alok Gambhir[1], Alexandre Costet[1], Julien Grondin[1], Stanley J. Okrasinski[1], Hasan Garan[1], Elisa E. Konofagou[1].*
[1]Columbia University, New York, NY, USA.

Background: Although arrhythmia and conduction disorders are a major cause of death and disability, there is no imaging method currently available to the clinician that can map the electrical activation sequence of the heart noninvasively. Electromechanical Wave Imaging (EWI) is an ultrasound–based method that can map the electromechanical wave (EW), i.e., the transient deformations occurring in response to the electrical activation. Recently, we have shown that a direct correlation between the electrical activation sequence and the EW exists in normal canine hearts [1]. For EWI to become useful clinically, it is critical to determine whether this correlation is maintained in presence of disease.

Aims: In this study, we aim at validating that EWI can map the activation sequence of the heart in presence of disease, both in canine and human hearts *in vivo*.

Methods: Four conditions were studied in a total of 12 canine hearts: Progressive ischemia (n=5), left bundle branch block (LBBB) (n=1), ventricular fibrillation (VF) (n=2), atrio–ventricular block (AVB) (n=4). Progressive ischemia was induced by occluding the left–anterior descending coronary artery at 20% flow decrements; LBBB and AVB were induced by radio–frequency (RF) ablation under fluoroscopy, and VF occurred spontaneously. A pacemaker was implanted in the right ventricle (RV) of AVB canines. EWI was performed during progressive ischemia, LBBB, and VF in an acute setting (open–chest) while AVB canines were studied chronically, in a closed–chest setting. A customized acquisition system was used to pace the heart and to map the endocardial electrical activation times using a high–resolution, 64–electrode, basket catheter (Boston Scientific, Nattick, MA). EWI was also performed on three human subjects (n=3) with heart failure undergoing cardiac resynchronization therapy with LBBB, AVB and/or cardiomyopathy, during sinus rhythm, and left–ventricular (LV) or RV pacing. EWI was performed using the automated composite technique (ACT) on a Ultrasonix MDP system with a 3.3MHz phased–array (Ultrasonix, Burnaby, BC) at 500 fps or with virtual–source sequence (VSS) using a Verasonics system (Verasonics, Richmond, WA) at 2000 fps. For the VSS sequence, RF frames were reconstructed using a customized delay–and–sum algorithm implemented on a graphics processing unit (Nvidia, Santa Clara, CA). Strains were estimated using RF cross–correlation and a least–squares estimator. Up to four views were combined in multi-plane 3D EWI representations.

Results: In canines with progressive ischemia, the propagation of the EW was impeded in the ischemic region when the flow occlusion reached 60%. In canines with LBBB, the EW propagation was first observed in the RV and propagated in the LV; a strong correlation (R=0.83) was found between the EW and the electrical activation times measured using the basket catheter. In canines with VF, the EW dominant frequency was in good agreement with the electrical activation dominant frequency. In canines with AVB, the EW was mapped in conscious canines in all four chambers transthoracically; independent activation of the atria and paced ventricles was observed, in agreement with the expected normal (atria) and paced (ventricles) activations.

In patients, EWI could identify the location of the pacing site transmurally. Indeed, during LV pacing only, the EW originated from the epicardium of the LV lateral wall near the base. During RV pacing, the EW originated from the apex of the RV. Both origins were in agreement with the transmural location of the pacing leads. During sinus rhythm with LBBB, the propagation of the EW originated in the RV. In patients with advanced heart failure (NYHA class IV) region in the lateral wall of the LV did not undergo the EW. This phenomenon was not observed in patients with mild heart failure (NYHA class I).

Conclusions: These results demonstrate that EWI can be used to characterize LBBB, AVB, fibrillation and ischemia. Moreover, the results observed in canines were reproduced in the clinical setting. Therefore, EWI has the potential to assist in the diagnosis and treatment monitoring of conduction disorders, and more specifically in patients undergoing CRT.

Acknowledgements: Supported in part by NIH R01EB006042, R21HL096094, and R01HL114358).

References:

[1] J. Provost et al.: Proceedings of the National Academy of Sciences. 108(21), pp. 8565–8570, 2011.

074 **PERFORMANCE ASSESSMENT AND OPTIMIZATION OF PULSE WAVE IMAGING FOR PULSE WAVE ANALYSIS IN *EX VIVO* CANINE AORTAS AND *IN VIVO* NORMAL HUMAN AORTAS.**

Ronny X. Li[1], Danial Shahmirzadi[1], William W. Qaqish[1], Elisa E. Konofagou[1].*
[1]Columbia University, 622 W 168th Street, Vanderbilt Clinic, VC 12–232, New York, NY, USA.

Background: Pulse Wave Imaging (PWI) is an ultrasound–based method [1–3] to noninvasively visualize and map the pulse wave–induced arterial wall motion in normal and pathological (e.g., hypertensive) human arteries [2,3]. Because PWI is capable of acquiring multiple waveforms along an imaged segment over a single cardiac cycle *in vivo*, the regional pulse wave velocity (PWV) can be quantified, and the local morphological changes in the pulse wave can be assessed. Tradeoffs exist between the spatial resolution (i.e. beam density), temporal resolution (i.e. frame rate), and fundamental upper limit on the PWV estimate obtained with PWI.

Aims: The aim of this study was to assess the effects of PWI image acquisition variables (beam density/frame rate and scanning orientation) and signal processing methods (beam sweep compensation and waveform feature tracking) on the PWV measurements in order to validate the optimal parameters.

Methods: A peristaltic pump (Manostat Varistaltic, Barrington, IL) was used to generate pulsatile flow through an *ex vivo* canine aorta embedded in saline. Radiofrequency (RF) signals were acquired using a 10MHz linear array transducer (SonixTouch, Ultrasonix Medical Corp., Burnaby, Canada) at a constant 25x38mm field of view while varying the beam density from 24–128 for both forward (i.e. beam sweeping in the same direction as the fluid flow) and reverse scan orientations. The upper limit on the PWV estimate was derived with respect to the frame rate associated with each beam density, and the inter–frame axial wall displacements were estimated using a 1D cross correlation–based motion estimation method [4] with a 3.5mm window size and 80% overlap. The PWV was estimated, both with and without a previously described scheme to compensate for the beam sweeping–induced time delays [2,3], by tracking the foot (i.e., the beginning of the upstroke) of the consecutive displacement waveforms for all combinations of beam density and transducer orientation. PWI was also performed in six normal human abdominal aortas *in vivo*, and the precisions of the PWVs obtained by tracking different features of the waveform were assessed.

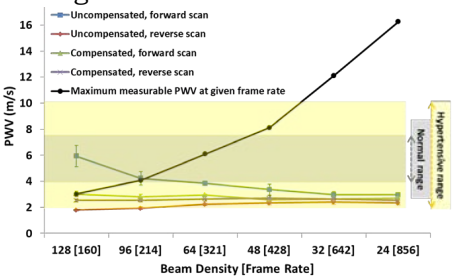

Figure 1: Effects of beam density, scan orientation and beam sweep compensation on the *ex vivo* PWV measurements. The black line represents the upper limit of the measurable PWV given the frame rate associated with each beam density. The shaded areas represent the range of compensated PWVs measured using PWI in normal and hypertensive human aortas obtained from a previous *in vivo* feasibility study [3].

Results: As the beam density decreased (i.e., frame rate increased), the uncompensated forward and reverse scan PWV estimates converged towards a common value, resulting in smaller discrepancies between the uncompensated forward and reverse scan estimates (Figure 1). We can expect the true (i.e. post–beam sweep compensated) PWV to fall in between the uncompensated forward and reverse scan estimates. As expected, the beam sweep compensation adjusted the PWV estimates to a consistent value which fell between the forward and reverse scan estimates. The PWVs obtained using the reverse scan orientation exhibited higher precision and lower deviation from the post–compensated PWVs. For the *in vivo* waveforms, the highest precision PWV measurements were obtained by tracking the 50% upstroke (i.e., the region in each waveform midway between its peak and its foot).

Conclusions: Increasing the frame rate caused the PWVs obtained using the two different scan orientations to converge towards the post–compensated PWV values, despite the reduction in beam density. Thus, the *ex vivo* results indicated that the PWI temporal resolution is more important for accurate PWV estimation than the PWI spatial resolution. Also, the reverse scan orientation is preferable due to its higher precision and underestimation of the PWV relative to the forward scan (Figure 1). If the typical ranges of the PWV measured using PWI in normal and hypertensive aortas [3] (Figure 1) are considered, a beam density of 32 (i.e. frame rate of 642 fps) would be required to reliably measure the PWV in both normal and hypertensive aortas (assuming a 25x38mm field of view). Finally, the *in vivo* results suggest that for clinical PWI on human aortas, tracking the 50% upstroke will yield the most consistent PWV estimates.

Acknowledgements: This work was supported in part by NIH grant R01HL098830.

References:

[1] K Fujikura et al.: Ultrasonic Imaging, 29(3), pp. 137–54, 2007.
[2] J Luo, R Li, E Konofagou: IEEE Trans UFFC, 59(1), pp. 174–181, 2012.
[3] R Li et al.: Conf Proc. IEEE Eng Med Biol Soc, pp. 567–70, 2011.
[4] J Luo, E Konofagou: IEEE Trans UFFC, 57(6), pp. 1347–57, 2010.

* *indicates Presenter*

022 **SHEAR WAVE ELASTOGRAPHY OF PEDIATRIC EPILEPTOGENIC TUMORS: PRELIMINARY RESULTS.**

HW Chan[1,3], A Chakraborty[2], NL Dorward[1], JC Bamber[3], W Harkness[2].*
[1]Neurosurgery Department, Royal Free Hospital, Pond St, London, NW3 2QG, England, UK; [2]Neurosurgery Department, Great Ormond Street Hospital, Great Ormond St, London, WC1N 3JH, England, UK; [3]Joint Department of Physics, Institute of Cancer Research and Royal Marsden Hospital, Sutton, Surrey, SM2 5PT, England, UK.

Background: Almost half of all children with brain tumors have medically intractable epilepsy and therefore are invariably offered surgical therapy with outcomes dependent on the extent of resection. Previous evaluation of adult brain tumor stiffness contrast using preoperative magnetic resonance elastography [1] and intraoperative ultrasound vibrography [2] demonstrated good correlation with the surgeon's opinion of relative stiffness from palpation. We present here our results with shear wave elastography (SWE) of pediatric epileptogenic tumors during resective brain surgery.

Aims: To measure the Young's modulus (YM) of pediatric epileptogenic tumors *in vivo*, to compare tumor YM with surgeon's palpation and to differentiate tumor from normal surrounding brain.

Methods: 11 patients with epileptogenic cerebral tumors were scanned during resective brain surgery. The scans were performed using an Aixplorer® (SuperSonic Imagine, France) scanner equipped with a sector transducer (SE12–3) with a bandwidth of 3–12MHz, using the ShearWave™ Elastography (SWE) mode. YM measurements were made in a region–of–interest (ROI) identified as tumor on the B–mode ultrasound scan using the built–in Q–Box™ function (Figures 1 and 2). The surgeon's opinion of tumor stiffness relative to surrounding brain was scored by palpation during surgery, and tumor diagnosis was obtained from sectional histology. Both were recorded in a manner that was blind to the SWE result.

Results: The patients' ages ranged from 10 months to 15 years and included 8 females and 3 males. One female patient was operated on twice for residual supratentorial primitive neuroectodermal tumor (sPNET). According to the surgeon's opinion, 7 tumors were softer than brain (3 dysembryoplastic neuroepithelial tumor (DNT), 2 astrocytoma grade II, 1 choroid plexus papilloma, 1 sPNET), and 5 were firmer than brain (1 epidermoid cyst, 1 subependymal giant cell astrocytoma (SEGA), 1 sPNET (second operation after radiotherapy), 1 DNT, 1 ganglioglioma). The mean YM ranged from 6.6 to 35.6kPa (mean 19.98kPa; SD 11.5kPa) and 117.2 to 300kPa (mean 186.9kPa; SD 67.9kPa) for tumors that were scored by the surgeon as softer and firmer than brain, respectively. The mean YM for the normal grey and white matter in these patients were 28.5kPa (SD 5.1kPa) and 18.2kPa (SD 5.5kPa), respectively. The tumor that had a mean YM of 300kPa was a SEGA, which was located 5cm from the brain surface (beneath the fluid–filled lateral ventricle), thereby possibly giving inaccurate YM data.

Conclusions: Our preliminary results showed good correlation between YM measurements made with SWE and surgeon's opinion by palpation. Although the YM for tumors that scored softer than brain by the surgeon overlapped with the YM range for normal brain, there was always a YM difference at the tumor–brain boundary (e.g. Figure 1). The YM contrast between tumor and normal brain was much better for tumors that were stiffer than brain (Figure 3), than for tumors that were softer than brain. This is the first intraoperative evaluation of pediatric epileptogenic tumors with shear wave elastography, which seems to show promise for use as an intraoperative adjunct in tumor resection.

Acknowledgements: This work was supported by Engineering and Physical Sciences Research Council, UK. Ethical approval was obtained from the National Research Ethics Service (NRES) Committee London – Queen Square Research Ethics Committee (Ref: 08/H0716/92).

References:

[1] Xu, L., et al.: Magnetic Resonance Elastography of Brain Tumors: Preliminary Results. Acta. Radiol., 48(3), pp. 327–330 2007.
[2] Scholz, M., et al.: Vibrography during Tumor Neurosurgery. J. Ultrasound Med., 24(7), pp. 985–992, 2005.

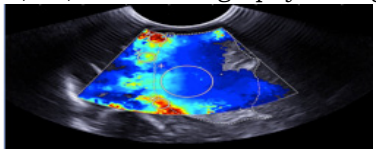

Figure 1: SWE scan of dysembryoplastic neuroepithelial tumor (DNT) outlined by dotted line. The Q–Box™ function was used to measure YM within the tumor (+) and at the peripheries (人,☒,☒).

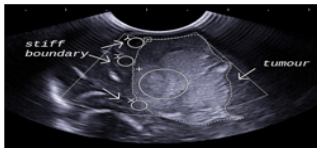

Figure 2: B–mode scan of the corresponding SWE scan in Figure 1.

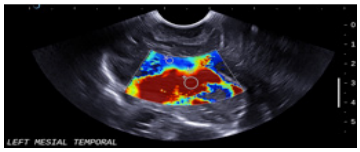

Figure 3: SWE scan of left mesial temporal epidermoid cyst showing a good YM contrast between tumor and brain.

030 **SENSITIVITY OF MAGNETIC RESONANCE ELASTOGRAPHY TO DETECT BRAIN DEVELOPMENT AND MATURATION.**

Katharina Schregel[1,2], Julie Le Faouder[2,3], Eva Würfel[4], Simon Chatelin[2], Pierre Bedossa[2,5], Jens Wüerfel[1], Ralph Sinkus[2].*

[1]Institute of Neuroradiology, University Luebeck, Luebeck, GERMANY; [2] Université Paris Diderot, Sorbonne Paris Cité, INSERM, CRB3 U773, Paris, FRANCE; [3]Institut Fédératif de Recherche Claude Bernard, Université Paris-Diderot, Paris, FRANCE; [4]Neuropediatrics Department, University Goettingen, Goettingen, GERMANY; [5]Pathology Department, Beaujon Hospital, Assistance Publique–Hôpitaux de Paris and Université Paris-Diderot, Paris, FRANCE.

Background: Cerebral tissue structure is altered in many neurodegenerative diseases but also during physiological processes like maturation or aging. It is reasonable to assume that structural changes directly affect the mechanical tissue properties. Magnetic Resonance Elastography (MRE) is an imaging technique capable of assessing biomechanical brain parenchymal properties non–invasively [1]. Viscoelasticity can be quantified by analyzing the propagation of mechanically elicited shear waves in the investigated tissue. Thus, MRE could be a helpful tool to detect physiological or pathological processes influencing the cerebral tissue integrity.

Aims: As previously demonstrated, cerebral viscoelastic properties change during ongoing brain maturation in adolescent mice [2]. However, the underlying cellular or molecular mechanisms responsible for the observed changes have not been elucidated so far. In the present study, we combine full 3D–MRE with MALDI–IMS (Matrix Assisted Laser Desorption Ionization Imaging Mass Spectrometry) in order to (1) prove an age–dependent behavior of cerebral biomechanics and (2) identify the underlying process.

Methods: 20 healthy 4–week-old female C57/BL6 mice were investigated 3–weekly. They were studied for 12 weeks, corresponding to a final age of 16 weeks. High resolution T2–weighted scans in addition to full 3D–MRE were performed on a 7 Tesla rodent scanner. The value of the complex–valued shear modulus |G*| was calculated in a region of interest (ROI) covering the corpus callosum, rendering information on its viscoelasticity. After each scanning period, 5 mice were sacrificed and brains were harvested for further analyses. One part was investigated by MALDI–IMS, the remaining part by immunohistochemistry.

Results: Viscoelasticity shows a triphasic course, matching the time course already observed in former experiments [2]: it decreases from week 0 to 3, then increases up to week 9 and stabilizes afterwards. MALDI–IMS renders matching spectra for all time points. Protein distribution correlates well with anatomical features and peak intensity differs age–dependently.

Conclusions: Viscoelasticity developed during adolescence and reached a plateau at a mean age of 16 weeks, corresponding to the adulthood of the animals. Protein expression assessed with MALDI–IMS seems to be age related as well. As volume fraction of the extra–cellular matrix (ECM) is described to decrease during maturation [3], yet to perform protein identification and immunohistochemistry may help to identify the exact mechanism responsible for the alterations of brain biomechanics during maturation.

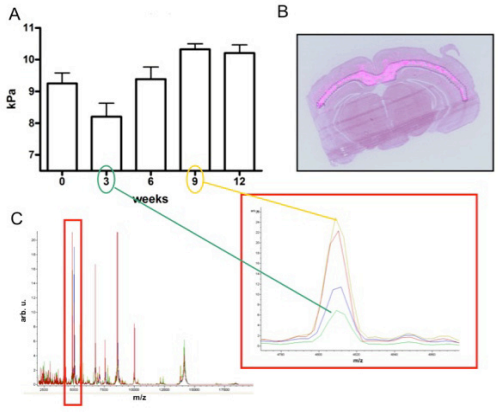

Figure: (A) Quantitative analysis of viscoelasticity |G*| in the corpus callosum (cc). Triphasic timecourse with decrease, then increase and plateau of viscoelasticity. (B) Optical image of the mouse brain with superposed MALDI–MS image (pink). ROI covers the cc. Protein distribution correlates with anatomy. (C) Superposed spectra from different time points. Inlet shows exemplary that peak intensity changes with age.

References:

[1] Green MA et al.: NMR Biomed, 21, pp, 755–764, 2008.
[2] Schregel K et al.: PNAS, 109, pp. 6650–6655, 2012.
[3] Sykova E, Mazel T, Simonova Z: Exp Gerontol., 33, pp. 837–851 1998.

* *indicates Presenter*

037 **ACQUISITON OF FREEHAND ELASTOGRAPHY VOLUMES IN BRAIN TUMOR SURGERY: PRELIMINARY RESULTS.**

Tormod Selbekk[1,2], Frank Lindseth[1,2], Geirmund Unsgård[2,3].*

[1]SINTEF, Trondheim, NORWAY; [2]The Norwegian University of Science and Technology, Trondheim, NORWAY; [3]St. Olav Hospital, Trondheim University Hospital, Trondheim, NORWAY.

Background: Ultrasound imaging is an established method for intraoperative guidance and monitoring in surgery of brain tumors. Some commercial systems also offer the possibility of performing freehand acquisition of ultrasound image volumes. In such systems, an ultrasound scanner is integrated with a navigation system which enables spatial tracking of the ultrasound probe equipped with a position sensor device. The ultrasound volume is generated by tilting and translating the ultrasound probe. After acquisition the ultrasound image volume is stored and subsequently displayed on the navigation system. This enables navigation and simultaneous display of intraoperative ultrasound and preoperative images as, e.g., MRI. Several research groups have explored ultrasound elastography or strain imaging of brain tumors [1–3], and real time 2D ultrasound elastography images have also been compared with co–registered MR–images using a navigation system [4]. Elastography (strain magnitude) images of glial brain tumors have been reported to have higher image contrast than corresponding B–mode images and may, therefore, serve as a complement in distinguishing resectable cancerous tissue from normal brain tissue [5]. It can be speculated that navigation of surgical instruments based on ultrasound elastography image volumes could contribute to detecting and localizing residual tumor tissue during surgery and thereby increase the proportion of gross total resection. We present our initial experience with freehand acquisition of elastography image volumes in brain surgery and neuronavigation based on simultaneous display of intraoperative elastography, B–mode ultrasound and preoperative, registered Magnetic Resonance image volumes.

Aims: The aim of the study was to investigate whether or not it is possible to acquire ultrasound elastography image volumes of brain tumors using a simple freehand technique.

Methods: Data have been acquired using the Ultrasonix MDP scanner (Vancouver, BC, Canada) with a flat linear probe (L14–5/38) and the standard elastography module. The navigation system consisted of the in–house developed CustusX research navigation software and the Polaris tracking system (NDI, Ontario, Canada). So far, data have been acquired in two clinical cases, a glioblastoma and a meningioma.

Results: It was possible to acquire ultrasound elastography volumes of the brain tumor in both cases. Various display techniques like volume rendering and image fusion of ultrasound elastography volumes, conventional ultrasound and preoperative MRI has been explored.

Conclusions: The initial test shows that it is possible to acquire and use ultrasound elastography volumes for neuronavigation purposes. The method must be further developed and refined for further clinical use.

Acknowledgements: This work was financed by the National Centre for Ultrasound and Image Guided Therapy at St. Olav's Hospital, Trondheim, Norway. We acknowledge the work of the CustusX development team: Christian Askeland, Ole Vegard Solberg, Janne B. Bakeng, Lars E. Bø and Erlend Hofstad (all SINTEF).

References:

[1] Selbekk T, Bang J, Unsgaard G: Strain Processing of Intraoperative Ultrasound Images of Brain Tumours: Initial Results. Ultrasound in Medicine and Biology, 31 (1), pp. 45–51, 2005.

[2] Scholz M, Lorenz A et al.: Current Status of intraoperative Real-Time Vibrography in Neurosurgery. Ultraschall Med, 28 (5), pp. 493–497, 2007.

[3] Uff CE, Garcia L, et al.: Real Time Ultrasound Elastography in Neurosurgery. Proceedings of the IEEE International Ultrasonics Symposium, pp. 467–470, 2009.

[4] Chakraborty A, Berry G et al.: Intra–Operative Ultrasound Elastography and Registered Magnetic Resonance Imaging of Brain Tumours: A Feasibility Study. Ultrasound, 14 (1), pp. 43–49, 2006.

[5] Selbekk T, Brekken R, Indergaard M, Solheim O, Unsgård G: Comparison of Contrast in Brightness Mode and Strain Ultrasonography of Glial Brain Tumours. BMC Med Imaging, 12(11), 2012.

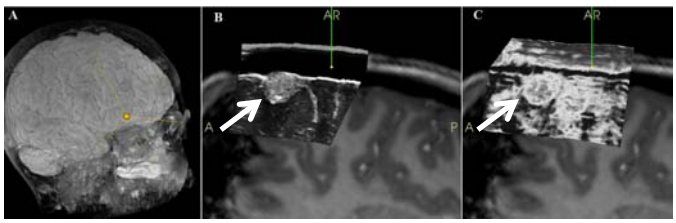

Figure 1: Display from navigation system during surgery of a meningioma showing (A) volume rendering of MR FLAIR;, (B) reformatted ultrasound image slice overlaid on corresponding MR; (C) reformatted ultrasound elastography image slice overlaid on corresponding MR. Tumor is indicated with a bright arrow in (B) and (C).

012 **SUB–VOXEL MICRO-ARCHITECTURE ASSESSMENT BY SCATTERING OF MECHANICAL SHEAR WAVES.**

S. A. Lambert[1], S. Chatelin[1], S. P. Nashölm[2], L. Juge[1], P. Garteiser[1], L. Ter Beek[3], V. Vilgrain[1], B. E. Van Beers[1], L. E. Bilston[4], B. Guzina[5], S. Holm[2] and R. Sinkus[1].*

[1]University Paris Diderot, Sorbonne Paris Cité, INSERM, CRB3, UMR773, 75018, Paris, FRANCE; [2]Informatics Department, University of Oslo, NORWAY; [3]Philips Healthcare, Best, The NETHERLANDS; [4]Neuroscience Research Australia and University of New South Wales, Sydney, NSW, AUSTRALIA; [5]Civil Engineering Department, University of Minnesota, Minneapolis, MN, USA.

Background: Magnetic Resonance Elastography [1] (MRE) is a technique capable of noninvasively assessing the mechanical properties of tissues. It can be hypothesized that the presence of micro–obstacles (similar to effects leading to the apparent diffusion coefficient) changes the dispersion relation of propagating shear waves and, hence, might influence the apparent mechanical properties of the medium at the macroscopic scale [2]. In Diffusion Weighted Imaging, micro–structural information is lost due to the massive averaging that occurs within the imaging voxel and can only be revealed when exploring the tissue using different b–values. Similarly here, where the propagation of a mechanical wave enters into the diffusive regime due to multiple scattering effects, the frequency-dependence of the mechanical properties could allow the assessment of the sub–voxel micro–architecture.

Aims: In this study we investigate the propagation of shear waves in FEM simulations as well as in calibrated phantoms containing accurately controlled size distributions of scattering particles.

Methods: Gel phantoms were fabricated using an agarose solution at 15g/L (BRL, Type 5510UB). In order to create well defined scattering particle size distributions, colloidal suspensions of polystyrene microspheres with precisely known diameter (10µm diameter, Sigma–Aldrich) and concentrations (20–1.25%) were added to the gel before solidification. MRE was performed on a horizontal 7T imaging scanner (Pharmascan, Bruker, Erlangen, Germany) (Figure 1). The MRE (spin echo, 0.4mm thickness, field of view of 30×30mm^2, TE/TR (ms)=13–35/270–505, 8 samples for time encoding, excitation frequencies: 600–1000Hz) sequence was acquired for the three spatial directions of motion in order to obtain volumetric images of the 3D mechanical wave propagating inside the phantom. Data were reconstructed with an isotropic reconstruction technique [3]. Wave propagation has been simulated only in 2D in order to void a time consuming 3D approach using Diffpack finite element code [4]. For both numerical and experimental approaches, power law fit was used to study the influence of micro–particle size concentration on wave scattering frequency dependence.

Results: For the same wavelength over micro–obstacles diameter ratio≈4(00), experimental and numerical results are in good agreement (Figure 2). The maximum of dispersion could be explained by scattering of mechanical wave by fractal systems [5].

Conclusions: For the first time, we demonstrated that the frequency–dependence of mechanical shear wave diffusion can allow probing sub–voxel distributions of scattering structures and as a consequence overcome the spatial resolution limitation relying intrinsically on the MR imaging sensitivity.

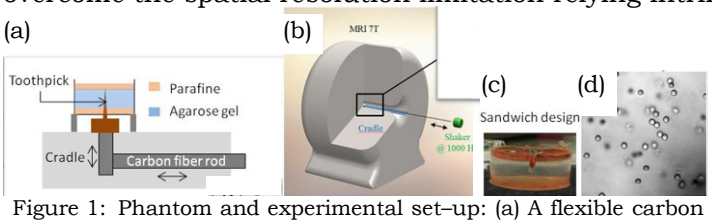

Figure 1: Phantom and experimental set–up: (a) A flexible carbon fiber rod transmits horizontal vibrations from a shaker to a toothpick mechanically coupled to the sandwich design phantoms (c) positioned in (b) a 7T MRI scanner (b). (d) Confocal–microscopy image of the phantom with 1.25% in volume of 10µm diameter microspheres.

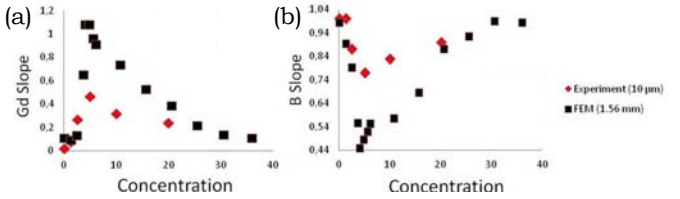

Figure 2: Slopes of the power fit for (a) the elastic–shear modulus (*Gd*) and (b) the propagation coefficient of the wave (β) as a function of microspheres concentration.

References:

[1] Muthupillai, R: Science, p. 269, 1995.
[2] Holm, S: JASA, pp. 542–559, 2010.
[3] Sinkus, R: MRI, pp. 159–165, 2005.
[4] Langtangen, HP: LNCSE, Vol. 2, 1999.
[5] Teixeira, J: J. Appl. Cryst, pp. 781–785, 1988.

* *indicates Presenter*

016 **HYPER–FREQUENCY VISCOELASTIC SPECTROSCOPY OF A VASCULAR–MIMICKING PHANTOM AND A PORCINE AORTA WITH THE RHEOSPECTRIS INSTRUMENT.**

Cédric Schmitt[1], Anis Hadj Henni[1], Simon LeFloc'h[2], Jacques Ohayon[2], Jonathan Vappou[3], Guy Cloutier[4].*
[1]Rheolution Inc., Montréal, Québec, CANADA; [2]Laboratory TIMC–IMAG/DyCTiM, Université Joseph Fourier, Grenoble, FRANCE; [3]IMFS (FRE3240) / LSIIT (UMR 7005) CNRS – University of Strasbourg, Strasbourg, FRANCE; [4]Laboratory of Biorheology and Medical Ultrasonics, University of Montréal Hospital Research Center (CRCHUM), Montréal, Québec, CANADA.

Background: Vascular elastography based on dynamic stress of arterial walls at frequencies typically up to 1500Hz is increasingly developed to monitor the mechanical properties of healthy and pathological vessels. However, available mechanical testing instruments can only measure viscoelastic properties up to 200Hz. Recently, a new instrument, RheoSpectris™ (Rheolution Inc., Canada), has been introduced to perform viscoelastic spectroscopy of biomaterials between 10 and 1000Hz [1]. Thus, there is a great interest for using such an instrument to characterize vascular phantoms and tissues.

Aims: The first objective was to measure the Young's storage (*E'*) and loss (*E''*) moduli of a vascular phantom material and a porcine aorta from 10 to 1000Hz with the hyper–frequency viscoelastic spectroscope RheoSpectris™ C400 using a new beam geometry. The second objective was to compare, on phantom material, the viscoelasticity measurements with those obtained with DMA instruments.

Methods: A standard silicone rubber (Platsil 71–10 silicone, Polytek Development Corp., USA) was first characterized using RheoSpectris™ between 10 and 1000Hz with the bending modality (beam samples). For comparison, cylinders and plates made from the same material were tested using two DMA instruments: the Electroforce 3200 (Bose Corp, USA) using the compression modality and the Eplexor 25N (GABO, Germany) using the compression and tensile modalities. Finally, beam–shaped samples (n=4) of a healthy porcine abdominal aorta were explanted and tested with RheoSpectris™.

Results: Both *E'* and *E''* obtained with the DMA instruments and RheoSpectris™ (Figure 1a) between 10 and 100Hz and the corresponding coefficients of variation (Table 1) are within the same order of magnitude. *E'* and *E"* evolutions at high frequencies indicate a continuous increase of *E''* up to 1000Hz. The low elastic dispersion of the silicone material is also noticeable even at high frequencies. The viscoelastic spectroscopy of fresh beam–shaped specimens (Figures 1b and c) shows a frequency dependence of *E'* (20% increase between 50–800Hz) and of less importance, of *E''*. This behavior is important for developments in elastography to avoid biased estimations of mechanical parameters.

E' and *E''* variability

	E' (%)	E" (%)
GABO Comp.	5.7	6.6
GABO Tensile	6.2	43.5
Electroforce	3.7	3.6
Rheospectris	12.6	23.6

Table 1: Mean measurement variability of the silicone sample between 10–100Hz of *E'* and *E''* for the GABO, the Electroforce and RheoSpectris™.

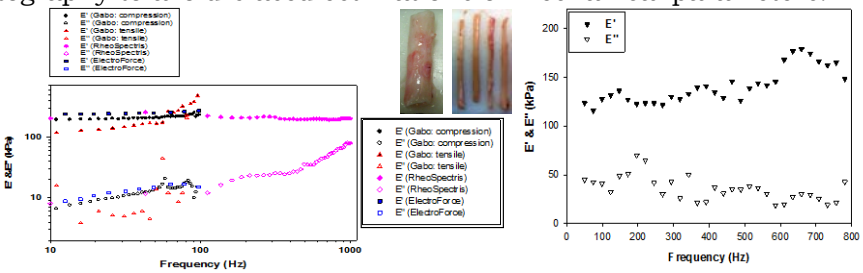

Figure 1: (a) Mean storage (*E'*) and loss (*E''*) moduli of a silicone material measured by two DMA instruments (Gabo and Electroforce) between 10 and 100Hz, and by the RheoSpectris™ C400 spectroscope between 10 and 1000Hz. (b) Pictures of a fresh porcine aorta specimen used to prepare samples tested by RheoSpectris™ C400. (c) Mean *E'* and *E''* of the aorta wall samples obtained by RheoSpectris™ C400 between 50 and 780Hz. The mean variabilities are equal to 12.9% and 48.3% for *E'* and *E''*, respectively.

Conclusions: The use of beam geometry with the RheoSpectris™ instrument has been validated by comparing measurements with those of classical DMA instruments. The same geometry served to successfully characterize the viscoelastic behavior of an artery at high frequencies. These results exhibit an important viscoelastic dispersive effect that may impact *in vivo* quantitative elastographic scanning of arteries with classical methods measuring group velocities over a given frequency bandwidth.

Acknowledgment: Funding was provided by a strategic grant of the Natural Sciences and Engineering Research Council of Canada (#STPGP–381136–09).

References:

[1] Hadj Henni, A., et al.: Hyper–Frequency Viscoelastic Spectroscopy of Biomaterials. J. Mech. Behav. Biom. Mater., Vol. 4, pp. 1115–1122, 2011.

029 ***IN VIVO* TIME HARMONIC MULTIPLE FREQUENCY ELASTOGRAPHY OF HUMAN LIVER.**

H Tzschätzsch[1], J Braun[1], T Fischer[1], R Klaua[2], M Schultz[2], I Sack[1].*
[1]Charité–Univeritätsmedizin Berlin, Berlin, GERMANY; [2]GAMPT mbH, Merseburg, Sachsen–Anhalt, GERMANY.

Background: Noninvasive measurement of tissue stiffness by elastography is increasingly used for the staging of hepatic fibrosis. In particular, the shear–wave based Fibroscan technique has achieved a remarkably high precision for the diagnosis of high grades of fibrosis [1]. The diagnosis of low grades of liver fibrosis remains a major challenge since therapies should be initiated at early stages of the disease. Magnetic resonance elastography (MRE) has been proven most sensitive to early fibrosis [2,3]. In extension to single–frequency time–harmonic MRE, broad–band MRE based on four mechanical excitation frequencies showed an excellent diagnostic power [4]. However, to date MRE has only limited availability and suffers from long scan times.

Aims: We developed a one–dimensional time–harmonic ultrasound elastography (USE) system which adopts the mechanical principle of multifrequency MRE of liver. Due to rapid data acquisition, USE is capable of measuring superimposed multifrequency vibrations in a fraction of the time needed for MRE. The feasibility of the method is demonstrated in healthy volunteers. Results are compared to findings of the literature made by multifrequency MRE [5].

Methods: Three healthy volunteers (male, ages: 26, 35 and 42 years) were scanned after written informed consent was obtained. Superimposed time–harmonic mechanical stimulation of seven frequencies (30–60Hz with 5Hz increments) was achieved by a cradle actuator beneath the right lateral costal arch mounted to a commercial loudspeaker (Figure 1a). The spectral vibration output of the controller is shown in Figure 1b. In addition, the vibration response measured in the liver from the lateral–anterior intercostal position is shown. The mechanical vibrations were captured by a custom designed A–line ultrasonic device, capable of 50MHz data sampling and 1kHz pulse repetition frequency, which was equipped with a single–element 2MHz transducer probe (GAMPT, Merseburg, Germany). Motion estimation was based on a windowed (1.1mm width) phase root seeking algorithm over 10cm depth. The speed of propagating shear waves was detected by a phase gradient method after applying a spatial bandpass filter to the temporal Fourier–transformed vibration signals at each single drive frequency. Total signal acquisition time was one second. The experiment was repeated twenty times in expiration for each volunteer to account for variability in probe positioning.

Results: Group mean shear–wave speed values are plotted in Figure 1c. The apparent dispersion of the wave speed with drive frequency is due to the well–known viscoelastic behavior of liver tissue. The elastic and Kelvin–Voigt (K–V) models were used for fitting experimental wave speed values. The elastic model yields a shear modulus μ=1.93±0.46kPa while the K–V model yields μ=0.64±0.24kPa and η=28±1Pa s. MRE literature values taken from [5] are also shown. Fitting the elastic model yields μ=2.07±0.05 and the K–V model yields μ=1.54±0.23kPa and η=25±5Pa s.

Conclusions: Multifrequency USE is capable to measure the dispersion of the shear wave speed in a total of 5 minutes. Remarkably, the obtained viscoelastic parameters agree well with the values measured by multifrequency MRE which needs about half an hour measure time. A limitation of the method is the high rate of failed scans (ca. 50%) characterized by noise and compression artifacts since probe repositioning and repetitive scans prolong the measure time.

References:

[1] Ziol et al.: C. Hepatology, 41(1), pp. 48–54, 2005.
[2] Yin et al.: Clin Gastroenterol Hepatol, 5(10), pp. 1207–1213, 2007.
[3] Huwart et al.: Radiology, 245(2), pp. 458–466, 2007.
[4] Asbach et al.: Radiology, 257(1), pp. 80–86, 2010.
[5] Klatt et al.: Physics in Medicine and Biology, 52, pp. 7281–7294, 2007.

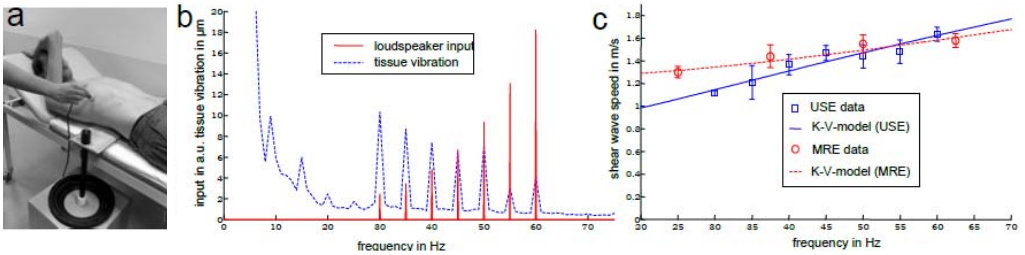

Figure 1: (a) Experimental setup; (b) Spectrum of vibration input and tissue oscillation; (c) Experimental data and model of MRE and USE.

* *indicates Presenter*

049 **SHEAR WAVE SPEED AND DISPERSION MEASUREMENT USING INTERFERENCE PATTERNS FROM A SPECIALLY DESIGNED CHIRP SIGNAL.**

Zaegyoo Hah[1], Alexander Partin[1], Kevin J. Parker[1].*
[1]Electrical and Computer Engineering Department, University of Rochester, Rochester, NY, USA.

Background: There is a growing need to measure not just shear elasticity (or shear speed) but shear speed dispersion. For example, there is a big concern about nonalcoholic fatty liver disease (NAFLD), a major cause of chronic liver disease. It is understood that increasing amounts of fat in the normal liver will increase the dispersion (that is, the frequency dependence or slope) of the shear wave speed [1]. Normally, the dispersion measurements are done separately at several selected frequencies within a range. Shear speeds are then calculated at each frequency, and regressions of the data result in the shear speed dispersion [2]. However, there are inherent problems with this method: signal–to–noise ratio (SNR), measurement time and safety. Therefore, to optimize measurement time and SNR, it would be advantageous to use chirps sweeping over a frequency range.

Aims: A measurement procedure using a chirp scanning over a range of frequency is introduced. Also analysis has been performed to provide a systematic way of measuring the shear speed and dispersion.

Methods: Some biomaterials including a 10% gelatin phantom, a fatty phantom with 10% gelatin and 30% safflower oil, and a fatty phantom with 15% gelatin and 30% castor oil are chosen for this study. All the test biomaterials are assumed to be homogeneous. The biomaterial is vibrated by two mechanical sources (Brüel & Kjaer, Model 2706, Naerum, Denmark) on both ends of the material such that an interference pattern is generated inside the medium. A chirp signal, instead of a fixed frequency signal, is used to drive the sources from 100Hz to 300Hz. The medium is scanned by an ultrasound imaging system (GE Healthcare, Logiq9, Milwaukee, WI, USA), and the movie is saved. The average motion slice image (Figure 1) is dependent on the chirp: the motion slice has a hyperbolic shape as shown in Figure 2a for a linear chirp. A special chirp is designed to produce the fan-shaped motion slice in Figure 2b, thereby providing the advantage of easy smoothing and image processing. Further analysis is performed to provide a closed form solution for the shear speed and dispersion. Measurement results are compared to those obtained by single frequency measurements.

Results: The safflower oil phantom was measured to have (3.5m/s, $2\cdot10^{-4}$ m/s/Hz) of shear speed and dispersion respectively, while the castor oil and the gelatin phantom showed (4.4m/s, $6\cdot10^{-4}$ m/s/Hz) and (3.0m/s, $3\cdot10^{-6}$ m/s/Hz). These results were compared with the conventional methods using either phase map or waveform fitting. Single frequency measurements for the safflower oil, for example, showed some fluctuations: 3.43, 3.62, 3.53, 3.52m/s at 110, 130, 150 and 200Hz respectively.

Conclusions: The developed method of shear speed and dispersion measurement provides advantages over the conventional methods. It is much faster, more robust and easily implemented. The techniques will be further applied to other biomaterials and the liver.

References:

[1] CT Barry, B Mills, Z Hah, RA Mooney, CK Ryan, DJ Rubens, KJ Parker: Shear Wave Dispersion Measures Liver Steatosis. Ultrasound Med Biol, 38(2), pp. 175–182, 2012.
[2] Z. Hah, A. Partin, C.T. Barry, R.A. Mooney, D.J. Rubens, K.J. Parker: Dispersion and Shear–Wave Velocity in a Mouse–Liver Model using Crawling Waves. Ultrasonic Imaging and Tissue Characterization Symposium, Rosslyn, VA, 11–13 June, 2012.

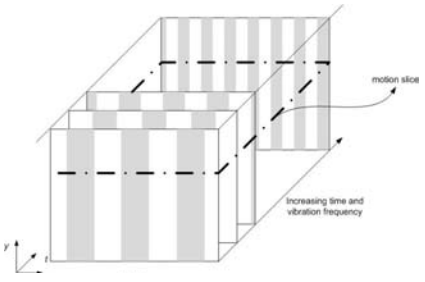

Figure 1

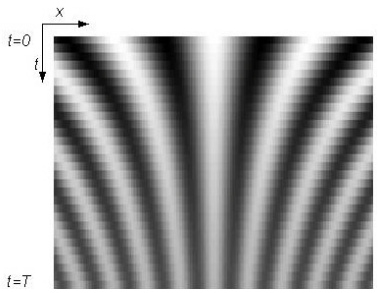

Figure 2a

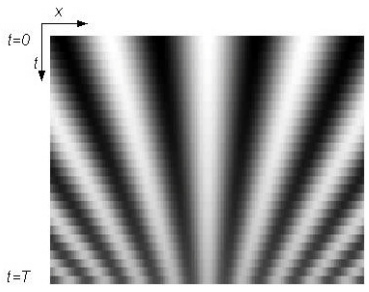

Figure 2b

053 **COMBINED ULTRASOUND AND BIOIMPEDANCE TO ASSESS TISSUE VISCO–ELASTICITY.**

Robert Dodde[1], Grant Kruger[2], Leo Koziol[1], Jonathan Ophir[3], William (Rick) F. Weitzel[1].*
[1]Internal Medicine, [2]Mechanical Engineering Departments, University of Michigan, Ann Arbor, MI 48109, USA; [3]Diagnostic and Interventional Imaging Department, University of Texas Medical School, Houston, TX 77030, USA.

Background: There is an enormous clinical need to manage disease states manifesting fluid overload by edema; these include chronic kidney disease (CKD), congestive heart failure (CHF), liver failure and lymphedema. Current practice entails serial physical examination and is crudely quantitative, rating edema on a scale of zero to 4+. In recent years, bioimpedance measurements have been shown to correlate with hydration status by tracking extracellular resistance over time. While helpful, confounding effects from cellular ionic content, particularly the sequestering of sodium throughout the body, hamper future evolution of this technique. Fortunately, complementary strategies based on ultrasound strain imaging can dynamically quantify and characterize highly non–linear and time dependent changes of a subsurface elastic medium under stress. Combining bio–impedance and ultrasound strain may offer a clinically useful and yet complete analysis of how edematous tissue responds to stimuli.

Methods: Edematous tissue can be contrasted to normal tissue through their time–dependent response to a given stimulus. Physiologically, the removal of excess fluid from the tissue has a time–dependent component as does the reentry of fluid after stimuli are removed. In this manner, tissue can be viewed as a viscoelastic material exhibiting two unique phenomena: creep and relaxation. To test our hypothesis, both creep and relaxation tests were run on phantom materials. Creep was monitored using pulsed–wave ultrasound depth–dependent Doppler in a gelatin–based Metamucil phantom (to provide scattering) under 50g, 100g and 200g constant loads. Relaxation was monitored using bioimpedance in cylindrical blocks of tofu (to mimic poroelastic fluid flow) under 10%, 20% and 30% constant strains. Data were fit to a standard linear solid (SLS) model for creep and relaxation.

Results: Figure 1 below shows the creep measurements made using ultrasound. Fitting the data yielded time constants τ_ε=12s±2s and τ_σ=113s±39s. Figure 2 below shows the relaxation measurements made using bioimpedance. Fitting the data yielded time constants of $\tau_{\varepsilon Z}$=2s±0.4s and $\tau_{\sigma Z}$=40s±8s. Time constants were also obtained by fitting the measured pressure during relaxation. These results compare with the bioimpedance time constants such that $\tau\varepsilon p=3\tau_{\varepsilon p}$ and $\tau_{\sigma p}=0.75\tau_{\sigma Z}$. Standard deviation for the pressure data was 0.7s for $\tau_{\varepsilon p}$ and 3s for $\tau_{\sigma p}$. Time constants between the creep and relaxation experiments are not comparable as different phantom materials were used in each study. Current work also involves integration of bio–impedance and ultrasound phantoms into a single experimental model.

Conclusions: We have begun experiments to develop a one dimensional quantitative edema assessment device and to validate the measurement method. Both bio–impedance relaxation and ultrasound creep measurements demonstrated the time–dependence essential for visco– and poro–elastic detection and monitoring. Targeting future clinical studies, we will seek to perform measurements within one to two minutes (rather than 8 minutes in this study) and expect this to depend on the force used and time constants and time dependent parameters which may be different in future human studies. If successful, changes in τ over time can be used to quantify the amount of edema removed from a tissue in order to guide treatments such as diuretic medications or dialysis. Our work continues directed toward improving the care of patients compared with the centuries old method of pressing on a patient's extremity by providing a convenient, accurate, quantitative assessment of edema.

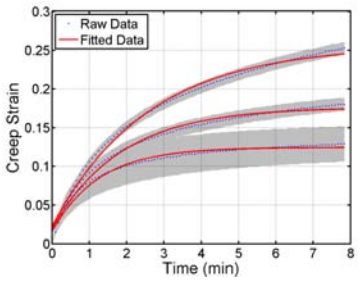

Figure 1: Measured and fitted creep strains. Gray areas are standard deviation limits (n=3).

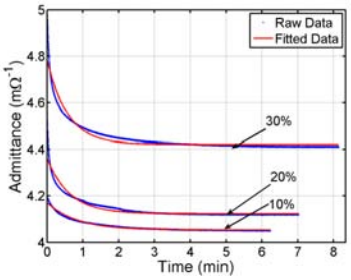

Figure 2: Measured and fitted admittance (1/|Z|) relaxation readings at varying strains.

Amirauté Conference Center Floor Plan

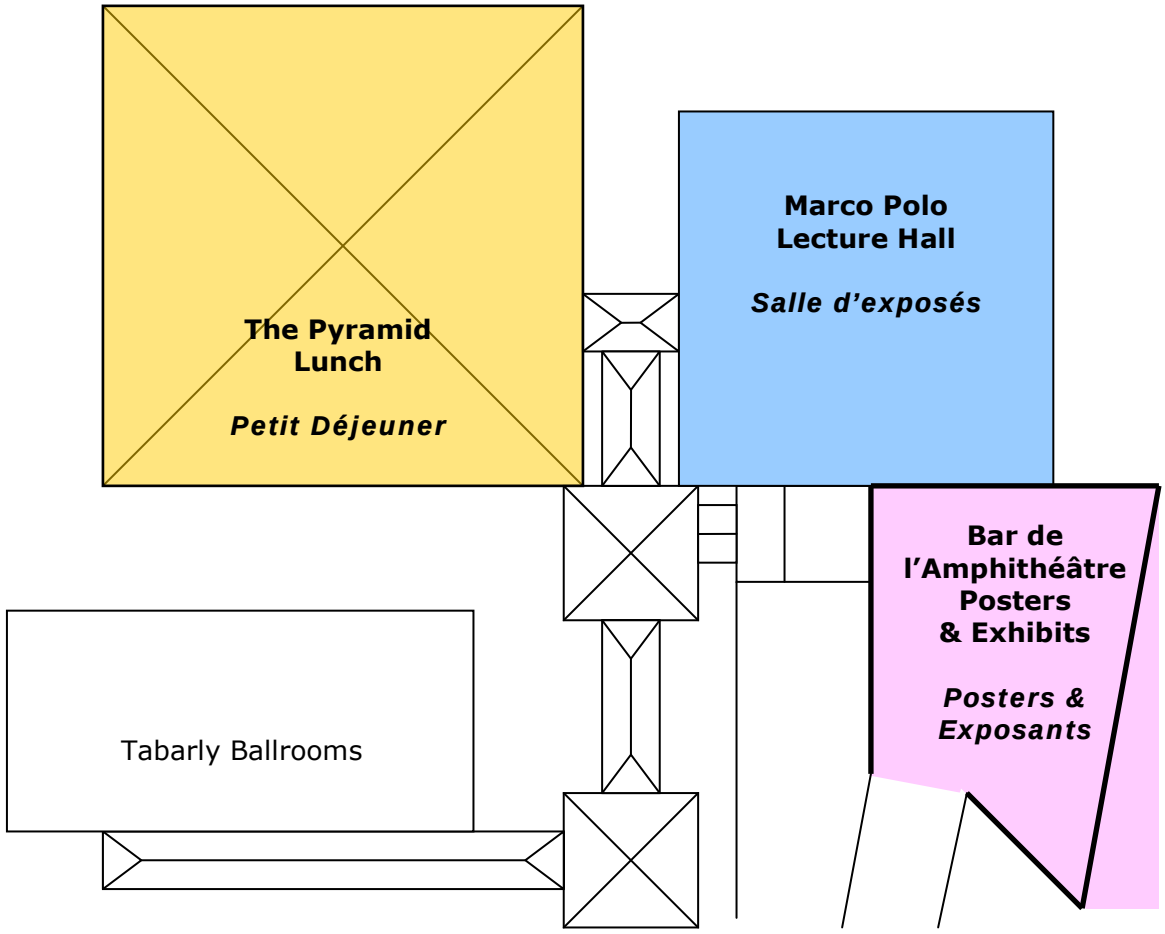

Please Fill Out Both Sides

Conference Evaluation and Questionnaire

OVERALL CONFERENCE

	Poor		Mid		Excellent
Overall Conference Evaluation	1	2	3	4	5
General comments:					

Scientific Program

	Poor		Mid		Excellent
Quality of the Presentations	1	2	3	4	5
Relevance of Presentations to the Conference's Theme	1	2	3	4	5
Time Allotted for Presentations	1	2	3	4	5
Time Allotted for Discussion	1	2	3	4	5
Poster Session	1	2	3	4	5
Tutorials	1	2	3	4	5
Equipment Exhibit	1	2	3	4	5
Student Participation	1	2	3	4	5
Additional comments:					

CONFERENCE MATERIALS

	Poor		Mid		Excellent
Printed Proceedings Book	1	2	3	4	5
CD Proceedings	1	2	3	4	5
Other Registration Materials	1	2	3	4	5
Additional comments:					

CONFERENCE Facilities & Social Program

	Poor		Mid		Excellent
Lecture Hall	1	2	3	4	5
Registration Desk	1	2	3	4	5
Meals: Dining facilities	1	2	3	4	5
Conference Breakfasts and Lunches	1	2	3	4	5
Conference Dinner	1	2	3	4	5
Coffee Breaks	1	2	3	4	5
Opening Dinner Reception	1	2	3	4	5
Closing Pizza Party	1	2	3	4	5
Audio–Visual: Screen Visibility	1	2	3	4	5
Sound Level	1	2	3	4	5
Presentation Transition	1	2	3	4	5
Internet Connectivity:	1	2	3	4	5
Additional comments:					

Please Fill Out Both Sides

Conference Evaluation and Questionnaire

VENUE aND Hotel

	Poor		Mid		**Excellent**
Venue: Amirauté, Deauville, France and Environs	1	2	3	4	5
Would you return to this city?	Yes		Perhaps		No
Area Attractions	1	2	3	4	5
Hotel: Overall	1	2	3	4	5
Reservations	1	2	3	4	5
Transportation and Accessibility	1	2	3	4	5
Reception and Check–In	1	2	3	4	5
Accommodations	1	2	3	4	5
Facilities	1	2	3	4	5
Parking	1	2	3	4	5
Would you return to this hotel?	Yes		Perhaps		No
Additional comments:					

Conference Administration

	Poor		Mid		**Excellent**
Website	1	2	3	4	5
Registration off–site	1	2	3	4	5
Registration on–site	1	2	3	4	5
Administrative staff	1	2	3	4	5
Correspondence	1	2	3	4	5
Additional comments:					

General information

I am a Returning Delegate	Yes		No
I plan to attend the next conference	Yes	Perhaps	No
and present a paper(s) / poster(s)	Yes	Perhaps	No
Other(s) from my lab would attend the next conference	Yes	Perhaps	No
and he/she / they would present a paper(s) / poster(s)	Yes	Perhaps	No
How did you learn of this conference? (Check all that apply)	☐ Email Announcement		
☐ Internet	☐ Website		
☐ Other	☐ Colleague		
Tutorial Topic Suggestions for next year:			
Additional Comments:			

If you would be willing to host the Conference in your city, please give your name to the Conference Staff.

Questions or comments are welcome at any time at <secretariat@elasticityconference.org>

Thank You!